

**TISSUE ENGINEERING OF LYMPHATIC VESSEL
NETWORKS WITH NANOFIBRE REINFORCED
HYDROGEL CONSTRUCTS**

FILIP LACO

M.Sc (Biomedical Engineering) University of Applied Sciences, Aachen

B.Sc (Bioprocess Engineering) Hamburg University of Applied Sciences

A THESIS SUBMITTED

FOR THE DEGREE OF DOCTOR OF PHILOSOPHY

Department of Biomedical Engineering

UNIVERSITY OF STRATHCLYDE

2013

Declaration of Authenticity and Author's Rights

This thesis is the result of the author's original research. It has been composed by the author and has not been previously submitted for examination which has led to the award of a degree.

The copyright of this thesis belongs to the author under the terms of the United Kingdom Copyright Acts as qualified by University of Strathclyde Regulation 3.50. Due acknowledgement must always be made of the use of any material contained in, or derived from, this thesis.

Signed: 

Date: 18th August 2013

Abstract

The lymphatic system comprises tubular vessels which transport lymph back to the blood. Injury to the lymphatic vessels including surgery or radiation therapy during cancer therapy impairs lymphatic fluid transport, with the result that interstitial fluid accumulates causing oedema and inflammation. The lack of effective therapies to address these problems highlights the need to improve understanding of lymphatic vessel development and growth, which is key to the development of novel approaches to treat this debilitating condition.

While regenerative medicine has the potential to resolve lymphoedema through the reconstruction of a functional lymphatic microvasculature, the organisation of endothelial cells into capillaries remains a significant challenge. The interactions between migratory lymphatic endothelial cells (LECs) and surrounding extracellular matrix (ECM) are of central importance to microvessel formation.

In the present study, hydrogels were employed to study lymphatic vessel development and maintenance *in vitro*. Further, a simple electrospinning set up comprising two parallel collectors was used to spin-coat aligned polymer fibres, representing the elastic fibre component of the ECM, over collagen hydrogels. The resulting fibre reinforced collagen gels have been employed here to study the growth, migration and vessel formation of lymphatic endothelial cells *in vitro*, with the aim of elucidating the initial steps of a functional lymphatic tissue, and to serve as a model of lymphedema for use in research.

Acknowledgements

I would like to thank my thesis supervisor, Dr. Richard Black and Prof. Helen Mary Grant, for their patience and guidance throughout the past four years. Richard Black has been very supportive and encouraging to me since the beginning of my studies at Strathclyde University. He secured the funding for my doctoral program, and I was honoured with the University of Strathclyde Scholarship. In this time, he gave me the opportunity to develop a research initiative on my own. I am very thankful that he believed in me and my research quest over the past four years. Helen is a patient advisor and supported me emotionally through my research. In her laboratory, I was given the chance to conduct all my experiments and not become

too frustrated about the results. I will miss the tea breaks and chocolate cakes, which help me greatly to stay focused in my research and with both legs on the ground.

I would like to express special thanks and gratitude to everyone who contributed their wisdom, experience and valuable skills in research. Catharine Henderson who supported me methodologically and technically in the laboratory, and especially for her goodwill and positive attitude during the three years. Liz, who taught me patiently everything about microscopy. Brian Cartlidge who saved my health and safety awareness, and solved my endless IT problems. Kit Mei Tan; who supported me at the atomic force microscope and provided all the jolly moments of my scientific life at Strathclyde. Dr. Simon Milling who shared his animal expertise. Toby Krämer, Ma Kun and Pricilla who provided me with all the literature I desperately needed to write the first scientific review. Nathaniel Jones and Mona John von Freyend who preserved and nurtured most of my scientific conscience and appetite. Chris, Monica, Richard, Emma and all the other guys who stayed with me till midnight in the laboratory.

To all my friends, thank you for being there and for a memorable time; Emily, Amber, Froya, Kenny, Max, Allan, Laurant, Leire, Richard, Hamad, Nick, Vee Han, John Paul, Andre, Nicola and my dancing mates.

Finally to my family the most important group in my life. Thank for your love, patience and unyielding support (emotionally and financially) in so many years. Karmen and Lubo the most loving parents in the world. Betty the best and generously

supporting auntie anyone can wish for. Ivica my brave and enthusiastic sister. David who convinced me to take up the PhD offer. Jonathan my best friend, partner and editor.

Table of Contents

Declaration of Authenticity and Author's Rights	i
Abstract	ii
Acknowledgements	iii
Table of Contents	v
Index	viii
Figure legends	viii
Table legends	ix
Abbreviations.....	ix
Publications	x
Chapter I	1
1.1 Introduction	2
1.2.1 Background Lymphatic System	5
1.2.1 Background Electrospinning	10
1.3 Motivation	11
1.4 Thesis Objectives	12
1.4.1 Objectives Chapter 2	13
1.4.2 Objectives Chapter 3	14
1.4.3 Objectives Chapter 4	14
1.4.4 Objectives Chapter 5	15
1.5 Thesis organization	16
Chapter II	18
Lymphatic Endothelial Cell Culture, Characterisation and Tube Formation in Hydrogels	19
2.1 Introduction	19
2.1.1 Lymphatic Tissue Identification and Characterisation	19
2.1.2 Lymphatic endothelial cell culture	22
2.2 Methods	31
2.2.1 Tissue isolation from rat and mouse	31
2.2.2 Hydrogel Gel Preparations	32
2.2.3 Cell Culture	33
2.2.4 Collagen type I delivery systems for LEC growth and tube formations ...	33
2.2.5 Immunostaining of cell monolayers, collagen gel cultures and tissue dissections	34
2.2.6 Real-time microscopy of tube-like formations in collagen-gel constructs	35
2.2.7 Biomaterial coating of Tissue Culture Plates	36
2.2.8 MTT formazan assay for Lymphatic Endothelial Cells	36
2.2.9 Tube forming degradation assay	37

2.2.10 Calculation of cellular population doubling time and half life	38
2.2.11 Cell viability staining and cell count	39
2.2.12 Co-Culture Assay with 3T3 Mouse Fibroblasts	40
2.2.13 Experimental design and statistics	42
2.3 Results	45
2.3.1 LEC characterisation of tissue and cells	45
2.3.2 LEC growth and tube formation in hydrogels	48
2.3.3 LEC co-culture with fibroblasts	61
2.4 Discussion	69
2.4.1 LEC characterisation <i>in vivo</i> and <i>in vitro</i>	69
2.4.2 LECs growth and tube formation in hydrogels	70
2.4.3 LEC co-culture with fibroblast.....	73
2.5 Conclusions.....	75
Chapter III	78
Electrospinning and polymer nanofibre properties	79
3.1 Introduction	79
3.2 Methods	84
3.2.1 Polymer preparation	84
3.2.2 Electrospinning Set Up	84
3.2.3 Electrospun Polymer Degradation	86
3.2.4 Surface Scanning Electron Microscopy	86
3.2.5 Experimental design and statistics	87
3.3 Results	88
3.3.1 Electrospinning properties of fibre diameter and morphology	88
3.3.2 Correlation of pore size and fibre diameter	84
3.3.3 Influence of the relative humidity on electrospun polymer fibres	87
3.3.5 Polymer degradation	87
3.4 Discussion	91
3.5 Conclusion	95
Chapter IV	97
Alignment of Nanofibres with dual field electrospinning	98
4.1 Introduction	98
4.2 Method	102
4.2.1 Dual Field Electrospinning	102
4.2.2 Characterisation of fibre distance, diameter and orientation	106
4.3 Results	111
4.3.1 Dual Field Electrospinning Design and Fibre Deposition	111

4.3.2 Dual Oscillating Field Electrospinning and Fibre Alignment	113
4.4 Discussion	118
4.4.1 Dual field electrospinning and electrostatic field strength	118
4.4.2 Dual oscillating field electrospinning and fibre alignment	122
4.5 Conclusion	125
Chapter V	126
Interactions of polymer nanofibres with lymphatic endothelial cells	127
5.1 Introduction	127
5.2 Methods	132
5.2.1 Electrospinning and Polymer Casting over Glass Slides	132
5.2.2 Polymer Fibre, Film and Collagen Matrix Analyses	133
5.2.3 Lymphatic endothelial cell attachment assay	134
5.2.4 Lymphatic endothelial cells growth assay on nanofibre mats	136
5.2.5 Lymphatic endothelial cells migration assay	136
5.2.6 Tube forming assay	137
5.2.7 Cell staining: Viability, Cytoskeleton and Morphology	138
5.2.8 Experimental design and statistical analyses	139
5.3 Results	140
5.3.1 Attachment and Growth of LECs on polymer films and fibres	140
5.3.2 Topography of aligned fibres influences cellular tube-like formations and morphology	142
5.3.3 Migration of LECs on aligned nanofibres	150
5.4 Discussion	155
5.5 Conclusion	159
Chapter VI	161
Summary	162
Discussion and Future Recommendations	167
References	179
Annex	I
SOP Electrospinning	I
Polymer fibre alignment quantification	V
Calculation of Decay / Half life of Cell populations	IX

Index

Figure legends

Figure 1: Lymphatic Anatomy	6
Figure 2: Lymphatic System	8
Figure 3 Immunostaining of rodent tissue with Lymphatic markers	46
Figure 4 Evaluation of lymphatic markers	47
Figure 5 Growth analyses of LECs with different media	49
Figure 7 LEC viability in collagen type I hydrogel matrix	52
Figure 8 Immunostaining of LECs in 2D and 3D collagen matrix conditions	54
Figure 9 LEC tube formations on various biomaterial surfaces with collagen type I hydrogels	57
Figure 10 LEC tube formations on various biomaterial surfaces with fibrin hydrogels	58
Figure 11 LEC attachment to Hyaluronate hydrogels	59
Figure 12 Population doubling time and half life of LECs on various surfaces in collagen type I and fibrin matrix	60
Figure 13 Mouse 3T3 fibroblast culture under endothelial conditions	62
Figure 14 LECs and 3T3 mouse fibroblast co-culture growth and attachment	64
Figure 15 Tube forming LECs in direct co-culture with 3T3 mouse fibroblasts	66
Figure 16 Tube forming LECs in 3D co-culture with 3T3 mouse fibroblasts	68
Figure 16 Chemical structure of poly(lactic- <i>co</i> -glycolic acid) PLGA	80
Figure 17 Set up and Measurements	85
Figure 18 Polymer flow rate and Morphology	82
Figure 19 Polymer viscosity and concentration	83
Figure 20 Interspatial fibre distance	85
Figure 21 Applied Voltage	86
Figure 22 Humidity	87
Figure 23 Degradation Chart	88
Figure 24 Degradation of polymer fibres SEM Images	90
Figure 25 Collector Geometries	99
Figure 26 Dual electric field electrospinning method	99
Figure 27 Dual field electrospinning of aligned fibres	103
Figure 28 Dual oscillating field electrospinning	104
Figure 29 Labview® control	105
Figure 30 Fibre alignment evaluation Part I.....	109

Figure 31 Fibre alignment evaluation Part II	110
Figure 32 Initial Set Up	111
Figure 33 Polymer fibre distribution pattern	115
Figure 34 Time controlled fibre distance and deposition	113
Figure 35 Dual oscillating field electrospinning	116
Figure 36 Electrostatic field	119
Figure 37 Different types of filopodia	129
Figure 38 LECs attachment and growth on randomly oriented nanofibres	141
Figure 39 Tube formation of LECs on nanofibres in 3D collagen gels	143
Figure 40 Actin filament of LECs	145
Figure 41 Atomic force microscopy of collagen-nanofibre constructs with LECs ..	146
Figure 42 Determination of aspect ratio of tube forming LECs	149
Figure 43 Morphology and actin staining of LECs on aligned nanofibres	152
Figure 44 Growth and migration of LECs on 2D aligned nanofibre surfaces	154

Table legends

Table 1 Key markers for lymphatic differentiation and development	22
Table 2 Overview experimental designs	43
Table 3 Variations of collagen type I delivery systems inducing LEC tubular-like formations.	51
Table 4 Effects of changing electrospinning process parameters on the resultant fibre diameter and morphology	82
Table 5 Properties of the polylactide-co-polymers	84
Table 6 Setting range for the electrospinning procedure	86
Table 7 Setting range and examples for the dual field electrospinning process	106
Table 8 Fibre alignment under various conditions	117

Abbreviations

3-(4,5-Dimethylthiazol-2-yl)-2,5-diphenyltetrazolium bromide (MTT)
4',6-diamidino-2-phenylindole (DAPI)
Arginine-Glycine-Aspartic acid (RGD)
Atomic Force Microscope (AFM)
Basic Media for Endothelial Cells (BME)
Blood Endothelial Cell (BEC)

Dulbecco's Modified Eagles Medium (DMEM)
Extra Cellular Matrix (ECM)
Endothelial Cell Basal Medium fully supplemented (EMB-2)
Extra Cellular Matrix (ECM)
Fast Fourier Transformation (FFT)
Fluorescein isothiocyanate (FITC)
Hertz or frequency per second (Hz)
Kilo Voltage (kV)
Lymphatic Endothelial Cells (LEC)
polycaprolactone (PCL) poly(glycolic acid) (PGA) poly(lactic acid) (PLA)
polylactic-co-glycolic acid (PLGA)
poly(L-lactic)-co-(D-lactic acid) (PLDL)
Scanning surface electron microscope (SEM)
Standard operating procedure (SOP)
Tetramethylrhodamine-5-(and 6)-isothiocyanate (TRITC)
Tissue Culture Plate (TCP)
Vascular Endothelial Growth Factor (VEGF)

Publications

Cellular trans-differentiation and morphogenesis toward the lymphatic lineage in regenerative medicine.

Laco F, Grant MH, Flint DJ, Black RA.
Stem Cells Dev. 2011 Feb;20(2):181-95

Collagen-nanofibre hydrogel composites promote contact guidance of human microvascular endothelial cells and directed capillary tube formation

Laco F, Grant MH, Black RA.
Journal of Biomedical Research A 2013 (ahead of print)

Dual Fied Electrospinning Parameters and Applications

Laco F, Grant MH, Black RA.
Macromolecular Materials and Engineering (in submission)

Chapter I

Thesis Introduction

1.1 Introduction

The human body is exposed to environmental damage over the course of time, as are all living things. Damage occurs in many ways to a living system; radiation, diseases, physical impact, heat and intoxication are only a few examples of environmental damage. Such damage accumulates over time and leads to inevitable cell death (necrosis) followed by tissue death and organ failure. Although we cannot avoid damage to our body as it is part of our daily life, the human body is able to avoid tissue and organ failure to some extent through self renewal. A living system, such as our body, constantly reconstructs itself, replacing necrotic tissues and cells with newly formed ones. Living organisms use two methods to reconstruct themselves. Regeneration, in which the necrotic cells are replaced by new cells that reform the original tissue; or repair, in which injured tissue is replaced with scar tissue. Depending on the extent of the damaged area, tissues will heal using a mixture of both mechanisms. Severe damage (i.e. heavy physical injuries such as large burns and cuts, progressive liver damage due to high alcohol consumption, aggressive bacterial or parasitic infections and other sorts of extensively prolonged immunological inflammation) will result mostly in scar tissue. Scar tissue is only a structural replacement without tissue and organ functionality. In general, scar tissue does not re-form into functional tissue without external medical intervention.

Regenerative medicine is the process of creating living, functional tissues to a) support the regenerative healing within the living organism, and b) to reconstruct impaired and scarred tissues or organs to their functional state. The principle of regenerating medicine is to regenerate damaged tissues and organs in the body by stimulating previously irreparable organs to heal themselves. Regenerative medicine

also includes tissue engineering, which describes the growth of tissues and organs in the laboratory and their safe implantation when the body cannot heal itself. Scar tissue can be prevented and replaced with tissue engineered products. Moreover, tissue engineering attempts to generate specific physiological functional tissues as well as dysfunctional diseased tissue models in the laboratory. Such physiological tissues and disease models are contributing to our understanding of contemporary biological issues such as wound healing, cancer or embryonic development. Cells used in tissue engineering are mostly obtained by biopsy from a donor. These are either somatic cells or stem cells which are expanded in tissue culture and re-grown to form functional tissue. The standard approach to generate a tissue from single cells is to stimulate cell growth and differentiation with bio-molecules on 3D constructs, which mimic closely the body's own environment [1]. Cells, bio-molecules and a 3D scaffold are the three fundamental requirements of tissue engineering state-of-the-art products.

The primary objective of a 3D constructs or scaffolds is simply to provide a 3D surface for cell growth. Advanced structures provide mechanical, structural and biological cues for specific tissue generation. There are various methods to produce scaffolds. Mostly, 3D porous material is produced for tissue engineering applications with simple techniques such as solvent casting, gas foaming or phase separation. The products provide a good surface for efficient cell growth, but the solid porous structures are very different from the native cellular environment limiting essential cues for soft tissue generation. A 3D scaffold structure can be also generated with electrospun polymer nanofibres; a method to produce mats of nonwoven nano and micro sized fibres [2]. The advantage of electrospun scaffolds is that its unique fibre

properties mimic the fibre network of the extracellular matrix (ECM). It is already possible to create such a scaffold that can provide the topographical cues and contact guidance for alignment and growth direction of cells [3]. However, properties of electrospun scaffolds are unique to every tissue and little is known about lymphatic endothelial cells behaviour with electrospun polymer fibres.

The development of tissue engineered implants has already contributed to patients' well-being in several areas. Simple tissue engineered grafts for cartilage, urinary bladder tissue, cornea and cardio-vascular tissue are used in experimental medical procedures. For instance, vascular grafts of the body's own (autologous) bone marrow cells seeded onto biodegradable polymer conduits or patches have been implanted in children with congenital heart defects. The tissue engineered vessels remained functional and adapted to the body environment [4]. In the past 20 years, tissue engineering applications and models with electrospun scaffolds have been extensively explored in the areas of vascular diseases, but very little attention has been devoted to the closely related lymphatic system, which originates from the blood vessel system. In this thesis I will focus towards the lymphatic system and develop a tissue engineered model with electrospun material. My approach aims towards a structured and biologically functional scaffold seeded with engineered lymphatic cells, which could be implanted post-surgically in order to support the injured tissue area with a functional network, cell guidance and accelerated wound healing.

1.2.1 Background Lymphatic System

The lymphatic system is a closed network originating from the interstitial tissue (interstitium) as small lymphatic capillaries [5]. Lymphatic capillaries are

blindended vessels formed by a single layer of overlapping endothelial cells (Figure 1). It is important to point out that the basement membrane of lymphatic capillaries is often absent or discontinuous. This specific morphology allows particles, fluids, macromolecules and cells to enter the vessels easily [6]. Whereas vascular endothelium consists of a solid basement membrane, lymphatic vessels present thin fibrillar structures, called anchoring filaments. The anchoring filament connects the abluminal surface of lymphatic endothelial cells (LECs) to the extracellular matrix of the interstitium, providing a way to sense the expansion of the interstitium [7]. Under physiological conditions, most lymphatic capillaries remain collapsed. However, when interstitial pressure increases due to enhanced fluid leakage from hyper-permeable blood vessels (oedema), the anchoring filaments exert tension on the LEC to pull open the overlapping cell junctions so that fluids are able to flow into the lymphatic capillaries [8]. Lymphatic capillaries (~50 μm in diameter) join to form collecting lymphatic vessels (80-200 μm in diameter) [9]. A distinguishing feature of collecting lymphatic vessels is intraluminal valves [5,9]. Large collective vessels or lymphatic ducts are surrounded with smooth muscle cells. The spontaneous contraction of smooth muscle cells, and surrounding skeletal muscles, as well as arterial pulsations, contribute to active lymph fluid propulsion, and valves prevent backflow [9]. Collecting lymphatic vessels closely follow the veins from the legs and release their lymph into the thoracic duct that drains into the great blood vessels (brachiocephalic vein) in the chest (Figure 2). Moreover, the lymphatic vessel system includes specific lymphoid organs, such as lymph nodes, tonsils and Peyer's patches.

Lymphatic capillaries are present in the skin and in most internal organs, with the exception of the central nervous system, retina, bone marrow and avascular tissues such as cartilage, cornea and epidermis. The lymphatic vascular system is a characteristic feature of higher vertebrates, whose complex cardiovascular system and large body size require the presence of a secondary vascular system for the maintenance of fluid balance [10]

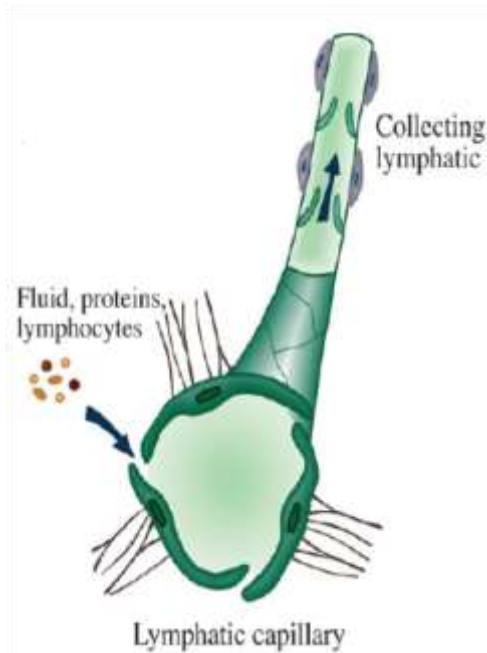


Figure 1: Lymphatic Anatomy

Lymphatic capillaries are blind-ended tubes with thin endothelial walls (only a single cell in thickness). They are arranged in an overlapping pattern, so that pressure from the surrounding capillary forces at these cells allows fluid and protein to enter the capillary. The capillaries are fixed with a fine anchoring filament within the ECM. The lymphatic capillaries grow progressively larger and form collective vessel and lymphatic ducts. Collective vessel and lymphatic ducts vessels have one way valves to prevent any backflow. The pressure gradients that move lymph through the vessels come from skeletal muscle action, smooth muscle contraction within the smooth muscle wall, and respiratory movement; Image adapted from

Alitalo et al. 2005 [10]

The main function of the lymphatic system is to control tissue fluid homeostasis, which means it maintains the interstitial tissue fluid balance by draining protein rich lymph from tissues and organs and transporting it back to the blood vascular system for recirculation [11]. It is still not clear how much fluid from the interstitium is transported via the lymphatic system; various sources claim up to 5%-20% of the total fluid circulation in the human body [12]. Oxygen, nutrients and hormones are delivered to tissues by blood vessels, and capillaries are involved in the molecular

exchange of these compounds with the surrounding tissues. Blood pressure causes plasma to leak continuously from the capillaries into the interstitial space. The main function of the lymphatic vasculature is to return a lipid- and protein-rich fluid back to the circulating blood (Figure 2). For example, the absorption of dietary fat, which is secreted by enterocytes in the form of lipid particles, is facilitated by the lymphatics [7]. The lymphatic system transports fluid and macromolecules, also cells, such as white blood cells - monocytes, dendritic cells and leucocytes [6]. Some cells (lymphocytes) are generated at the lymph node directly. White blood cells exit and enter through the blind-ended lymphatic capillaries or initial lymphatics. From the initial lymphatics, lymph fluid is transported towards collecting lymphatic vessels and is returned to the blood circulation through the lymphatico-venous junctions in the jugular area. On its way, lymph is filtered through the lymph nodes, where it responds to foreign particles, cells and cancer cells. Foreign particles, taken up by antigen presenting cells, are used to initiate specific immune responses in the lymph node; reviewed by Alitalio et al. 2005 [10]. All together the lymphatic system has three main functions: fluid homeostasis, macromolecular transport, in particular lipid circulation and metabolism, and an immunological response system

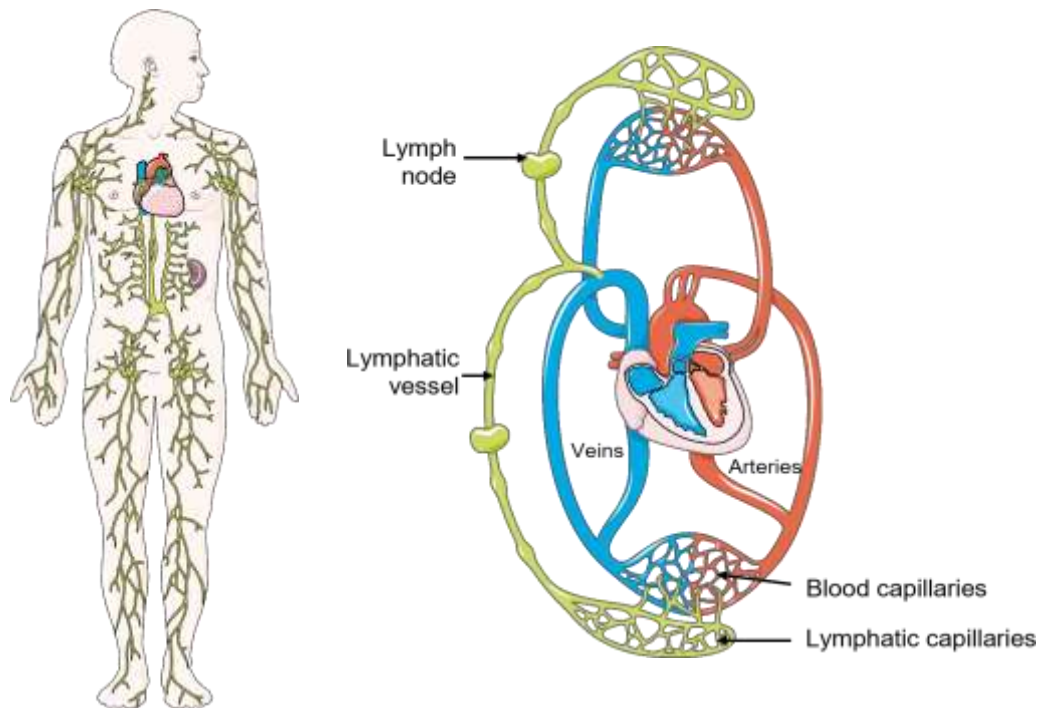


Figure 2: Lymphatic System

Left image shows the lymphatic network in the human body. The lymphatic system parallels the cardiovascular system. Right image shows the connection between lymphatic and vascular network. Lymph is a fluid derived from blood plasma. It is pushed out through the capillary wall by pressure exerted by the heart or by osmotic pressure at the cellular level. Lymph contains nutrients, oxygen, and hormones, as well as toxins and cellular waste products generated by the cells. As the interstitial fluid accumulates, it is picked up and removed by lymphatic vessels that pass through lymph nodes, which return the fluid to the venous system. Image source with permission from, Les Laboratoires Servier Medical Art © 2006

Lymphatic regeneration and healing: Wound healing is essential for lymphatic regeneration. Should the healing process be impaired, large areas of scar tissue can be formed. Lymph vessels cannot grow through the dense collagen fibre formations of scar tissue and the area will be without functional lymphatic vessels, which can cause major physiological problems such as oedema [13].

Generally, lymphatic regeneration during wound healing is driven strongly by vascular endothelial growth factor A and C (VEGF-A and C). Immunological cells such as macrophages infiltrate the injured area excreting various bio-molecules,

including VEGF-A and C which chemo-attract the invasion of vascular and initial lymphatic capillary sprouts from non-damaged areas [14]. A nascent lymphatic network is only visible after vascular networks are established [11]. Therefore, biomolecules excreted by vascular endothelial cells might be a key factor for lymphatic vessel re-growth during wound healing. Further, vascular endothelial cells and other reconstructing cells such as fibroblasts deposit collagen type I loosely during wound healing. This is thought to be a structural attractant for lymphatic vessel reformation. Actually, the full spectrum of lymphatic chemical and structural attractants is unknown. Moreover, regeneration is a process of constant tissue reformation in an orchestrated manner. It is not known how many key factors contribute to morphological and functional changes in the lymphatics during this process. However, functional lymphatic tissue is different compared to the transient state of the tissue achieved during wound healing. Mature lymphatic vessels are surrounded by a fibronectin based ECM [7]. Areas are populated by different cell types excreting different sets of growth factors and the lymphatic vessel itself matures to a collective vessel structure with a functional valve system.

The complexity of the dynamic regeneration process with its transient morphological and environmental stages in comparison to our current knowledge about lymphatic vessels makes it hard to establish a functional model. Currently, chemokines such as VEGFs, structural proteins such as collagen and a 3D environment have been proposed to be key factors in lymphatic morphogenesis. The challenge in this thesis is to find an environment which provides supporting factors for lymphatic re-growth. I will focus in this thesis on structural proteins and polymers that can influence growth, survival and morphology of LECs.

1.2.1 Background Electrospinning

Electrospinning is the most versatile, simple, cost-effective and scalable method to fabricate micro- and nano- fibres. The merit of this technique is that it can produce scaffolds with most of the structural features required for cell growth and subsequent tissue organization. It also offers many advantages over conventional scaffold methodologies. For example, it can produce ultra-fine fibres with spatial orientation and a high surface-to-volume ratio; the process provides control over fibre diameter and gives flexibility for surface modification [15]. This technique was first introduced by Zelency in 1914 [16]. Later, Formhals contributed much to the development of electrospinning and obtained several patents in the 1930s and 1940s. In those days it was called electrostatic spray or electrostatic spinning and then renamed as electrospinning in the 1990s.

The advantage of electrospinning is that ultra-fine polymer fibres can be prepared from almost any polymer with a sufficiently high molecular weight that forms a solution. Synthetic and natural polymers, polymer blends, nanoparticles or drug impregnated polymers as well as ceramic precursors have been successfully electrospun into nanofibres. Different fibre morphologies such as beaded fibres, ribbon fibres, porous fibres and fibres with a core-shell structure have also been electrospun [17].

The technique of electrospinning is simple: a syringe is loaded with a polymer solution, which is forced out by the application of a high voltage of the order of 5-30 kV between the syringe tip and a collector. The polymer melt or solution is pumped out of the spinneret at a controlled rate. Under the high voltage field the

polymer solution is drawn from the needle tip towards the collector with the opposite charge. A thin jet of the polymer liquid flies towards the collector plate. As the charged jet accelerates toward the collector with opposite charge, entanglements of the polymer chain will prevent the jet from breaking up, while the solvent evaporates resulting in the formation of randomly oriented micro and nanofibres. Fibre diameter and morphology is controlled mainly by the polymer composition, flow rate and applied voltage and fibre alignment can be generated by different collector arrangements (see Chapter 3 and 4). Electrospun nanofibres can be further biologically functionalized, reinforced and integrated with other materials for applications including enzymatic catalysts, filters, textiles, optics, electronics, sensors, medical dressings and tissue engineering scaffolds [18].

In the field of tissue engineering, electrospun nanofibre scaffolds have been actively explored for different applications such as skin [19], cartilage [20], bone [21], blood vessel [22], heart [23], and nerve [24]. In this thesis electrospun fibres of defined alignment and diameter will be generated and incorporated within hydrogels to regrow lymphatic vessel structure. Our main focus (Chapter 5) is to evaluate the relationship between the LECs growth and the nanofibre environment.

1.3 Motivation

Lymphatic disorders are quite common and impairment of the lymphatic system leads in most cases to lymphedema. Lymphedema is the development of lymph fluid in soft tissues, interstitial spaces, and subcutaneous fat due to inadequate drainage. While the exact cause of lymphedema is still unknown in some diseases, it generally occurs due to poorly developed or missing lymph nodes and/or channels in the body.

Lymphedema can be of various origins such as parasitic infestation by filariasis [25], hereditary diseases such as Milroy's disease [26] and most commonly in western countries during the treatment of cancer, particularly gastric and breast cancer. It occurs in 20-30% of breast cancer patients, who have undergone lymph node removal [27]. The great challenge of post surgical lymphedema is the reconstruction of the interrupted lymphatic vessel with a regenerative approach. Currently, there have been only a few significant approaches to address this medical condition. Four different approaches demonstrated amelioration of lymphedema; microsurgical lymphatic transplantation and lymphatic anastomosis in human trials [28,29], mesenchymal stem cell injection with animal models [30], growth factor stimulation with vascular endothelial growth factor (VEGF-C) [31], biomaterials and hydrogels such as collagen hydrogels [13] and a combinatory approach with a hyaluronan hydrogel based drug delivery system [32]. The tissue engineering approach in lymphatics is still under developed. Although lymphatic capillaries have been engineered in the past [33], laboratory approaches have not improved further than simple 3D lymphatic endothelial cell (LEC) cultures. Physiological vessels have not been developed, and neither have been scaffolds and biomaterials generated to support lymphatic growth in 3D hydrogels or scaffolds. This thesis set out to explore the possibility of generating tissue engineered lymphatic vessels in hydrogels and elucidate biomaterial and matrix mechanism(s) by which lymphatics can be sustained

in vitro.

1.4 Thesis Objectives

The work of this thesis describes the development of a novel tissue scaffold for lymphatic regeneration based on collagen type I hydrogels which are first reinforced by electrospun nanofibres to mimic structural features and matrix organisation of native tissue. The properties and dimensions of the polymer fibre materials which influence lymphatic growth, attachment and organisation were determined. Prior to that, the electrospinning technology was modified and a new electrospinning procedure was developed to produce aligned nanofibres specifically on hydrogels. Moreover, lymphatic growth and tube formation was analysed in various hydrogel and biomaterial conditions. The research aim was to generate a scaffold that would support lymphatic development and provide topographical cues to direct lymphatic migration and growth for applications in regenerative medicine.

1.4.1 Objectives Chapter 2

LECs have shown to express a unique set of antibody markers which set them apart from other cell types, especially from vascular endothelial cells [34,35]. These markers are important in identifying LECs in co-culture and tissues. However, their expression can change with origin and age, especially after *in vitro* culture [36]. Therefore, a set of LECs markers was evaluated in *in vitro* culture and from fresh specimens. The aim was to establish a reliable set of markers for further experiment with co-culture and animals.

LECs growth ex-vivo has been shown to be dependent on VEGF-C [37]. Growth factor supplementation is very costly and delivery can be difficult in tissue engineered scaffolds. Further, it has been postulated that structural proteins contribute to cell growth, differentiation and maintenance in combination with

growth factors [34]. However, structural key factors have not been evaluated yet for LEC *in vitro* culture and tissue culture. Therefore, the effect of growth, morphology, tube formation and decay of LECs on ECM proteins (e.g. collagen) was investigated. An objective of this thesis was to identify a structural protein which supports LEC growth with limited supplementation of VEGF-C *in vitro* culture.

Another strategy to reduce VEGF-C supplementation in LECs culture was implemented by using fibroblast co-culture. Fibroblasts are known to support various cells in culture (e.g. skin keratinocytes, skin models), by excreting vascular growth factors and basic fibroblast growth factor (FGF-2). Therefore, it was an objective to support lymphatic vessel functionality *in vitro* with a fibroblast co-culture. Together these approaches with growth factors, biomaterials and co-cultures targeted a tissue engineering approach to develop functional lymphatic vessels *in vitro*.

1.4.2 Objectives Chapter 3

Electrospinning of polymer fibres is an established procedure. Although properties of electrospun material have been evaluated for most biomedical grade polymer types [38], there are strong differences between laboratories and electrospinning set ups due to surrounding environmental conditions and “home made” equipment. Therefore, electrospun polymer materials were evaluated with regard to morphology, diameter, porosity and biodegradation. A set goal was to establish the specific laboratory electrospinning parameters in order to generate reproducible materials for further cell culture experiments.

1.4.3 Objectives Chapter 4

Electrospinning technology produces random meshes of polymer nanofibre. In order to spin nanofibres with a specific direction or alignment the electrospinning set up

had to be modified. Modifications have been carried out at the electrospinning collectors, which can direct a relatively orderly deposition of fibres [39]. In addition, manipulations of the electrostatic field (e.g. applying alternate current or dividing collectors with an individual electrostatic field “dual field”) are known to support the alignment of the electrospun material [40]. “Dual field” electrospinning technology has been poorly investigated and applications in cell culture or surface coating have not been established yet. Therefore, control of fibre quality and its dependence on several electrospinning parameters (eg. voltage, collector distances, humidity, collecting surfaces...) were evaluated. Further, the electrostatic field of the electrospinning process was manipulated and switched to an alternating electric field between two parallel positioned collectors in order to produce higher alignment and better reproducibility. The technology was utilized to electrospin fibres over surfaces such as hydrogels, or tissue culture plastics/glass for tissue engineering applications. The aim was to produce highly aligned single, and/or sheets of, polymer fibres with a specific fibre to fibre distance, orientation and fibre diameter which could be collected over various surfaces in the form of a surface coat.

1.4.4 Objectives Chapter 5

Cells growing on nanofibre constructs have been shown to recognize the nanofibre features via surface chemistry and topography. The interactions of cells are different from one cell type to another [41]. Specific fibre diameter and fibre alignment can provide the cells with environmental cues to organize in a specific manner and grow and differentiate accordingly [42]. Although there have been many approaches to growing endothelial cells on nanofibre sheets [41], it has been technologically impossible to produce 3D scaffolds with organized fibres. A 3D environment is

crucial for LECs to generate vessel like structures (Chapter 2) which resemble the native state of lymphatic vessels. Therefore, hydrogel nanofibre constructs with specific dimensions were generated to investigate tube formation and growth of LECs. The aim was to determine the quality and quantity of topographical cues in the form of nanofibre alignment and density to organize LECs in collagen hydrogels. The overall objective was to establish a lymphatic tissue model that satisfies the tissue engineering approach.

1.5 Thesis organization

The thesis is composed of 6 chapters.

Chapter 2, 3, 4 and 5 are designed in the form of research papers. The chapters are conclusive and can be read without knowing or referring to the previous or following chapters. However, Chapter 5 builds upon the acquired knowledge from previous chapters and combines their achievements in a final study.

Each chapter has an individual introduction, which provides a literature review giving an extensive background with respect to the technology, biological or bioengineering application of that chapter. The introduction is followed by a methodological section, which describes the experimental designs, materials and the mathematical models used as well statistical evaluations of the experimental data. The results section lists the findings of the conducted experiments in the form of images, charts and tables. The experimental results are described and evaluated in this section. The discussion section places the results and methods in context with current

research reports and weighs them against correlating, as well as controversial, publications. Directions and recommendations for future research are provided in this section. The conclusion section summarizes key findings and their importance.

Chapter 1 describes the general background about lymphatic biology and electrospinning. Further it portrays the motivation and objectives of this research. Chapter 2 presents a study on the significance of lymphatic endothelial cell culture within hydrogels and variations of biomaterials. The chapter explains also the difficulty in lymphatic characterization and sets out a new approach in developing a lymphatic endothelial cell co-culture system.

Chapter 3 documents the generation of electrospun nano- and micro- fibres with various biodegradable polymers. Polymer fibre properties and biodegradability are illustrated in this chapter.

Chapter 4 describes a new electrospinning design and methodology to produce aligned polymer fibres over metallic, inert solid materials and hydrogel surfaces. The fibre alignment properties and electrospinning process parameters are evaluated and discussed in this chapter.

Chapter 5 sets out to combine lymphatic hydrogel culture with the application of electrospun aligned polymer fibres to guide cellular growth and migration. This chapter shows how fibre parameters such as diameter, alignment degree and hydrophilicity influence lymphatic migration and tube formation in hydrogels.

Chapter 6 concludes with a summary of the findings of this research thesis and discusses prospects for future research and development in the field of lymphatic tissue engineering.

Chapter II

Lymphatic Endothelial Cell Culture, Characterisation and Tube Formation in Hydrogels

**Lymphatic Endothelial Cell Culture, Characterisation
and Tube Formation in Hydrogels**

2.1 Introduction

2.1.1 Lymphatic Tissue Identification and Characterisation

The lymphatic tissue can be visualized and mapped in human and animal bodies with new non-invasive methods [43]. However, identification and characterization of the

lymphatic system is still carried out with invasive (surgical) methods [44]. The latter methods have contributed to the understanding of the lymphatic vessel anatomy.[45,46]. The collective lymphatic vessels in the body appear translucent or white in colour after fat digestion. Animals are given an oil gavage 1h before dissection, which helps to identify the lymphatics [44]. However, lymphatic vessels collapse within a few minutes after physiological death. A fine transparent vessel structure is left behind, which makes it difficult to identify the structure from surrounding tissue. Hence, lymphatic dissection is often performed under anaesthesia. Moreover, small initial lymphatic vessels within the connective tissue are not detectable without strong magnification and staining with Evans Blue [44] or by fluorescence microlymphography [47].

Dissected lymphatic tissues such as the initial lymphatics of the interstitium or collective vessels of the mesentery were often analysed by electron microscopy [48]. Significant progress in lymphatic vessel identification has emerged with the development of a specific antibody marker in the late 1990s. The discovery and development of Prospero-related homeobox transcription factor (Prox-1) in 1998 by Wigle and Oliver [49] has made identification of lymphatic vessels available for science and medicine. Prox-1 is mostly applied with other markers for lymphatic identification such as the endothelial hyaluronan receptor (Lve-1), Podoplanin and vascular endothelial growth factor receptor -3 (VEGFR-3).

Prox-1 is expressed at an early stage in embryonic development, and represents the first cell commitment towards the lymphatic lineage [49]; promoting the organization of sprouting LECs [50]. In adulthood it controls the on/off set of lymphatic genes related to morphogenesis [51]. Hence, Prox-1 has been established

as the master control gene in lymphatic endothelial cells. Prox-1 is a nuclear transcription factor whose appearance, unlike other markers such as LYVE-1 and VEGFR-C, is

exclusive to cells of committed lymphatic lineage [52].

Other bio-markers commonly used to demonstrate lymphatic competence (Table 1) are VEGFR-3/*Flt4*, the lymphatic endothelium-specific hyaluronan receptor (LYVE1) and Podoplanin. VEGFR-3, and its associated growth factor, initiate migration from the anterior cardinal vein [53]; it is required for migration and proliferation, but not for vessel tubulogenesis in adults [54]. LYVE-1 represents a major component of the extracellular matrix binding to hyaluronan, although it is expressed during embryonic development in early lymphatic and blood vessels [55-57], it is absent in mature blood endothelial cells (BECs) [58]. The complete functions of LYVE-1 in lymphatics remain largely unknown. Podoplanin expression is maintained by Prox-1 positive cells [59]. Moreover, podoplanin is an essential part of the motile/adhesive apparatus in the plasma membrane of the lymphatic vessel wall [59-61], which promotes adhesion, migration [59], and is essential for vessel formation [62].

Lymphatic endothelial cells express several additional bio-markers during their development, which are mostly shared with blood endothelial cells (BECs). In general, a sufficient number of bio-markers must be examined in order to minimise the risk of misinterpretation, and to conclude, without doubt, a true lymphatic commitment. In addition, most lymphatic markers such as Prox-1, LYVE-1, and VEGFR are thought to be expressed to a lesser extent on mature lymphatic endothelial cells (LECs) [63]. Moreover, transfer from *in vivo* to *in vitro* condition

reduces lymphatic specific gene expression by more than 80% [64]. Hence, antibody markers might be expressed differently under experimental conditions. It is therefore essential to apply a broad, analytical approach to immunological markers including morphological appearance to identify correctly lymphatic tissues and isolated cells. In the immunofluorescence staining experiment podoplanin, Lyve-1 and Prox-1 antibody markers were used to characterise lymphatic tissue and cells as well as nonlymphatic tissue and mouse 3T3 fibroblasts in order to establish a protocol for reliable markers in future co-culture experiments.

Table 1 Key markers for lymphatic differentiation and development

(adapted from Laco et al. 2011 [34])

Lymphatic Bio-marker and Function	Co-expression on other tissues and cell types
Prox-1 Initiation of lymphatic cell commitment	In germ layers: neural tube, bile duct, pancreatic epithelium, trigeminal, spinal, sympathetic ganglia, retina, placodal structures, hepatoblast, cardiomyocytes [65]; In adult tissue: hippocampus, cerebellum [66], hepatocytes [67]
VEGFR-3 Initiation of lymphatic cell migration and proliferation; maintaining cell survival	Several organs: fenestrated capillaries, bone marrow, splenic, hepatic sinusoids, kidney glomeruli, adenohypophysis, thyroid gland, adrenals, choroid plexus [68]; tumour-, inflamed or wound-associated blood vessels [68,69]; circulating endothelial precursor cells or endothelial progenitor cells [70]
LYVE-1 Complete function unknown, Extra cellular matrix communication, hyaluronan metabolism	During embryogenesis in lung endothelial cells, arterial and venous endothelium and endocardium [56]. In adult cells and tissue: circulating endothelial precursor cells or endothelial progenitor cells [70], adipocytes and macrophages [71], especially activated tissue macrophages, lung sinusoidal endothelium of the liver and the spleen [72] dendriform cells in the eye [73]
Podoplanin Initiation of LEC migration, tubulogenesis, maintaining separation from blood vessels	choroid plexus, ciliary epithelium of the eye, intestine, kidney, thyroid and oesophagus of the fetal rat [74], trabecular cells of the eye [73], type I alveolar cells of the lung [75], salivary glands [76], basal keratinocytes [59] and a variety of tumour cells [77-79]

2.1.2 Lymphatic endothelial cell culture

Cell isolation and cell culture of LECs has been established for more than 20 years.

Successful dissection, cell isolation and pioneering experiments with lymphatic endothelial cell *in vitro* culture have been performed by Leak and Jones in 1993 [80].

LECs can be isolated from collecting vessels and ducts as well from the microvasculature in skin and connective tissues. In this thesis human lymphatic microvascular endothelial cells of dermal origin were used during experimental conditions. Dermal LECs are less mature than cells from collective vessels. They form mostly an initial capillary network without functional valves for passive lymph

transport. During tissue repair, in the dermis, lymphatic capillaries have been shown to sprout and reform a functional network in the healing area (see Chapter 1). The cells were shown to be adaptable to *in vitro* culture conditions and assemble in tube like formations with appropriate stimulation (Lonza, communication). Therefore, they are a good model to observe initial lymphatic tissue formation *in vitro*.

Although LECs show a broad heterogeneity and response to markers, and cell culture depends on tissue origin and vessel maturation [36], most culture techniques are the same for all endothelial cell types. Culture conditions for LECs have been adapted from microvascular blood endothelial cell (BEC) culture. LECs and BECs also show a similar growth factor dependency; whereas vascular endothelial growth factor A essentially contributes to BECs growth, - vascular endothelial growth factors, C and D, are key players for LECs survival and growth [54]. However, as soon as LECs are cultured on tissue culture plastics many lymphatic genes are down regulated [81] and cells lose their morphological tubular structure. In 2D *in vitro* culture, lymphatic endothelial cells adopt a cobblestone morphology similar to vascular endothelial cells [80,82,83]. The junctions between adjacent LECs form a characteristic wavy outline giving them the appearance of an oak-leaf in profile. While this renders the monolayer relatively impermeable, it is nevertheless selective to fluid and cell trafficking by formation of open junctions and flap valves [82,84,85]. LECs form typical junctional complexes with adherens, tight and occasionally gap junctions [86]. Unlike mature lymphatics, immature and initial lymphatic cells are connected by zipper-like junctions, which develop to form discontinuous, button-like tight junctions and zona occludens consisting of linear segments of Platelet Endothelial Cell Adhesion Molecule (PECAM)-1, VE-cadherin, and occludin in addition to claudin-5, T-

cadherin and plakophilin 2 [82,84]. Therefore, the phenotype of initial lymphatics can be determined by the expression of cell-cell adhesion markers, and the oak-leaf morphology characteristics of mature cells.

Leak and Jones's early experiments established cells in culture and first showed tube forming cells in native collagen cultures [80]. Their collagen cell culture experiment demonstrated how essential the understanding of the surrounding lymphatic extracellular matrix is to generate functional vessels *in vitro*.

Native lymphatic vessels are embedded in the extracellular matrix (ECM) of the interstitium. The amount of interstitium as defined above, varies from up to 50% of the wet weight in skin to 10% in skeletal muscle [87]. The ECM consists of collagens and other glycoproteins such as proteoglycans, glycosaminoglycans and elastins. Their distribution and organization differs from tissue to tissue [88]. Ultrastructural analyses and immunostaining of the LEC ECM revealed the presence of Collagen type I, III, IV, laminin, fibronectin and tenascin [89]. The ECM structure and deposition is specific to the vessel maturation. *In vivo* lymphatic vessels anchor via fibronectin, fibrillin and other structural glycoproteins to a fibrillar elastic apparatus of immature elastic fibres of 0.5-2 μ m such as oxytalan, elaunin, and mature elastic fibres [90]. Single elastin fibres of 1 μ m in bovine samples [91] and 24 μ m in human samples [90] run closely along the vessel wall. Some fibres branched into two or four fibres of equal size. They are strongly aligned with the vessel at a distance of 40 μ m from each other. These fibres interconnect from time to time with non aligned elastin fibres to form a greater network. Mature collective vessels are overlaid by a layer of muscle cells, which are connected by occasional elastin fibres following a tortuous path between the cells [91]. The elastin network around the vessels connects further

to collagen fibres. In bovine samples, the collagen matrix around the vessel shows two types of bundles: close to the endothelial cell wall collagen fibres present an interwoven network of 15 μ m-25 μ m thick, which orients at 45° along the vessel axis under physical pressure. On top of this layer smaller collagen fibres of 2-5 μ m are densely packed in a wavy pattern orientated in direction of the vessel. Adipose cells can be embedded into this wavy collagen structure and the elastin network. The whole structure is part of the interstitium which consists of further structural proteins such as proteoglycans, hyaluronan and resident cells such as adipose cells and fibroblasts [92], which generate most of the interstitial matrix. Moreover, motile cells such as dendrites and monocytes enter and travel within lymphatic vessel system. The environment of the lymphatics is a complex organisation of structural proteins and cell-cell interactions. The communication between the structural proteins of the ECM and the cell is mediated by specific proteins, cytoskeleton components and a family of cell surface transmembrane receptors called integrins. LECs are known to express various integrin forms such as α 1 β 1, α 2 β 1, α 4 β 1, α 5 β 1, α 6 β 1, α 9 β 1 and α v β 3, [93-97]. Cells have the ability to bind a ligand of the extracellular matrix via a specific integrin. The integrins expressed in LECs can bind among other ligands such as fibronectin, fibrinogens, collagens, and laminin [98]. However, LECs express very little ECM matrix proteins by themselves [99], so they might depend on other cells for structural protein excretion.

Structural proteins for lymphatic in vitro culture are based on lymphatic ECM and integrin expressions, and examination of their native extracellular matrix. Fibronectin, fibrillin, collagens, elastin, glycosaminoglycans and hyaluronan are therefore the building blocks for lymphatic tissue engineering. Five structural

proteins have been investigated for lymphatic tissue engineering in form of coats and 3D hydrogels:

Collagen: Collagen accounts for 30% of all vertebrate protein. The basic structure of collagen is composed of three polypeptide chains with high glycine content, building up a three-stranded rope structure. It consists of a helical structure with non-helical ends for intermolecular cross linking which is regulated partially by the glycine content. These structures self assembly into arrays of fibrils. Fibrils in turn aggregate into larger fibres. Their structure is specific to cells and tissue. Different collagen types have significant variation in their polypeptide chains and glycine content. Collagen type I is the most abundant form of collagen. It is synthesized by fibroblasts in the interstitium especially in the skin, where lymphatic vessels are located. Collagen fibres in skin and in fabricated hydrogels from rat tendon are about 280nm in diameter and randomly orientated, but can vary in polymer length (reviewed by Smith 2009 [100]). Another type of collagen used in the experiments is collagen IV. It varies in the glycine content from collagen type I and is part of the LEC basement membrane. Collagen is biologically active and certain collagens of animal origin can provoke a foreign-tissue response. The origin of the collagen is therefore crucial to implantation. Bovine collagen type I is FDA approved and a reliable source for medical applications. The mechanical properties of collagen based hydrogels scaffolds are very low, but they are useful for soft tissue applications [101].

Hyaluronan: Hyaluronan is the simplest glycosaminoglycan. Glycosaminoglycans are polysaccharide chains. Hyaluronan is a polymer of disaccharides, themselves composed of D-glucuronic acid and D-N-acetylglucosamine, ranging in size from 104 to 107 Dalton. It is a randomly coiled structure and its large size exhibits a range

of physiochemical properties [102]. Hyaluronan is synthesized by fibroblasts in the interstitium. One third of hyaluronan is replaced daily in tissues. LECs capture hyaluronan from the interstitium by binding it to the LYVE-1 protein structure. Hyaluronan is transported by the lymphatic vessels and/or degraded by lymphatic cells in the lymph nodes [102]. Hyaluronan biomedical products are FDA approved for use in eye surgery and ophthalmic surgery. It is supplied as a highly viscous salt solution of sodium hyaluronate 10mg for direct injections. Moreover, sodium hyaluronate has found application in tissue engineering, cosmetics and wound healing.

Fibrin and fibrinogen: Fibrinogen is a glycoprotein 45 nm in length and made up of three pairs of polypeptide chains. Fibrin polymerization is initiated by the action of the proteolytic enzyme, thrombin. Thrombin cleaves the fibrinopeptides from the middle of fibrinogen and converts the structure into a fibrin monomer. Monomers assemble into 200 nm thick fibrin fibres. The detailed structure and function of fibrin and fibrinogen was reviewed by Mosseson in 2005 [103]. Fibrin has two pairs of Arginine-Glycine-Aspartic acid (RGD) sequences through which it can interact with the integrins (see below) of LECs [104]. Fibrin hydrogels (or fibrin glues) are generated by blending human fibrinogen and thrombin in the presence of calcium chloride. Aprotinin is added to prevent clotting (premature fibrinolysis) of the fibrin polymer [101]. Current clinical and bioengineering applications feature drug delivery, wound healing, soft tissue engineering and cell differentiation [105].

Fibronectin and the Arginine-Glycine-Aspartic acid (RGD) sequence:

Fibronectin is a dimeric extracellular matrix glycoprotein consisting of two polypeptide chains that are disulfide bonded at their carboxy termini. Fibronectin

monomers are composed of a number of repeating homologous sequences termed type I, II, and III. Only type III modules contain an RGD sequence forming an integrin binding loop with adherent cells [106]. Monomers of fibronectin form stable fibronectin fibrils during the cellular attachment process. Fibril formation is regulated through RGD within fibronectin and the specific integrins of the cell [107]. Fibronectin surrounds LECs and lymphatic organs [89,92]. Tissue engineering approaches with biological active surfaces for vascular endothelial cells with fibronectin [107] and RGD [108] peptides have shown promising results, pointing towards a beneficial application in the lymphatic field.

Laminin: Laminins are a major ECM protein component of the basal lamina. In general, laminins are heterotrimeric glycoproteins. Laminins are trimeric proteins that contain an α -chain, a β -chain, and a γ -chain, with genetic variants, which are specific to cell and tissue. The laminin heterotrimers are assembled inside the cell, but further extracellular proteolytic processing may occur in various chains before the laminins reach their final form to fit their environment [109]. The laminin types which are known to be expressed within LECs are 511, 521 and 421 [110]. Laminin is generally used to improve cellular attachment in culture conditions. The commercially available Laminin-111 extracted from mouse sarcomas was used in the experiments. It is found mostly in developing and embryonic tissue [109]. The Laminin type is crucial for maintaining attachment and growth of most cells and tissue. Unfortunately, there is less information available in this respect for the lymphatics compared to other tissues.

The extracellular matrix triggers different cellular responses in LECs from migration to proliferation and apoptosis [98,111]. Although matrix dependent effects have been

observed *in vivo*, many have not been evaluated yet in *in vitro*. Hence, the best matrix for LEC networks *in vitro* is yet to be determined. Under experimental conditions matrices are supplied as 2D surface coats or in form of 3D hydrogels (def.: hydrophilic polymer network dispersed in water, which is similar to soft tissue). Unlike the native ECM, matrices in experimental conditions consist of a homogeneous structural protein of random arrangement. A homogeneous matrix allows us to study the interaction of one cell type with one biomaterial. However, *in vivo* cells are seldom exposed to a single structural protein. Further, lymphatic cells transferred from *in vivo* to *in vitro* down regulate many of their specific lymphatic genes due to a reduced cell-cell, and cell-matrix communication [64,81]. As a result, collagen hydrogel cultures with LECs are not self sustainable by nutrition alone and require further VEGF-C or basic fibroblast growth factor supplementation [112]. Recent studies with collagen and fibrin hydrogels and analyses of the expressed integrins of LECs point towards collagen as well as fibronectin/fibrin based matrices [34]. Therefore, a combination of cellular relevant biomaterials is supposed to mimic native ECM better than a single structural protein matrix. In this regard, the present work questions whether one of, or combinations of, the LEC relevant biomaterials can maintain lymphatic vessel networks *in vitro* without the attribution of additional growth factors. In this thesis I show how to perform LEC 3D cultures with functional vessel networks, and demonstrate their dependency on VEGF-C during maintenance. Further, I have investigated the effect of growth, morphology, tube formation and decay of lymphatic endothelial cells on surfaces such as RGD, fibronectin, collagen I, IV and laminin, and in hydrogels such as fibrin gels, collagen type I gels and hyaluronan hydrogels. Combinations of these biomaterials were tested as well. In

this way, I address the complexity of the lymphatic matrix environment and bring *in vitro* culture closer to mimic the *in vivo* environment.

Moreover, I have taken the first steps to establish a LEC co-culture without additional growth factor contribution. For co-culture experiments mouse feeder cells were chosen. Mouse feeder cells are generally used in combination with multiple cell types of human origin to support growth and cell maintenance *in vitro* [113]. Established protocols for mouse feeder 3T3 fibroblast were developed among other cells for human epithelial cells [113], and skin organ culture [114] and embryonic stem cell maintenance [115]. However, lymphatics have not been yet cultured with feeder support.

2.2 Methods

2.2.1 Tissue isolation from rat and mouse

Lymphatic tissue was removed from a freshly killed male Sprague Dawley rat and a male Balb/c mouse. The protocol was adapted from Gashev and colleagues [116]. Briefly, an initial incision was performed under the rib cage of the rodents. The abdominal incision was made through the skin, underlying fascia and muscle layers (incision length: 4cm rats; 2cm mouse). A part of the intestine was exteriorised through the incision. A section of the mesentery containing lymphatic vessels was positioned in a sterile petri dish within the field of view of a dissecting microscope. The tissue was kept moist during the procedure with a few drop of sterile Phosphatebuffered saline (PBS) (Invitrogen, UK). The lymphatic vessel network was easily identified against the darker background of the intestine. In contrast to the blood vessels the lymphatic tissue differed in size and colour. A white coloured fine vascular network was dissected with the surrounding connective tissue. Tissue was washed in PBS and suitable vessel structures were roughly cleared of surrounding tissue, mostly fat tissue. Sections of mesenteric lymphatic vessels 1-2 cm (rat) and <1 cm (mouse) in length were collected and immediately transferred into an ice-cold PBS or cell culture medium DMEM (Lonza, UK) prior to fixation. Moreover, tissue samples were taken from the underlying smooth muscle layers which covered the abdomen. Also, a major blood vessel was dissected and used for the subsequent staining protocol.

All freshly isolated segments of rat and mouse mesenteric lymphatic vessels and blood vessels were gently double-rinsed in ice-cold sterile PBS and freed from excess fat tissue as much as possible. This procedure was performed in two sterile

35-mm plastic Petri dishes under a dissecting microscope with sterilized forceps, to minimize possible contamination. The dissected smooth muscle tissue was washed in sterile PBS and cut into thin strips of about 1cm x 0.5cm. All tissues were transferred into 4% para-formaldehyde for 30min at room temperature, washed once with sterile PBS and stored in sterile PBS at 4°C.

2.2.2 Hydrogel Gel Preparations

Acid soluble collagen type I was isolated from rat tail tendons according to the method of Elsdale and Bard (1972) [117]. Collagen gels were cast by mixing cold collagen solution, a mixture of 10X Minimum Essential Medium (Lonza, UK) and 0.4M NaOH (2:1), and 1/1000 (v/v) acetic acid at a ratio of 7:1:2 to a final concentration of 0.3% (w/v). The pH was adjusted to ~8 with 1 M NaOH. The gels were allowed to set for 15-30min before endothelial cell culture medium was added. Generation of fibrin gels was adapted from various sources [118-120]. Fibrin gel was prepared by mixing solution A (Fibrogen 50mg/ml (Sigma, UK) and 50U/ml Aprotinin (Sigma, UK) in sterile PBS 1:1) with solution B (10U/ml Thrombin and 2.5mg/ml Heparin (Sigma, UK) in sterile 40mM CaCl₂ solution). In order to produce an evenly solid gel solution A and B was blended in the culture well using a pipette for 5-15 seconds. The solution gelled within 1-2min. The casting time can be adjusted by the thrombin amount. Culture medium was added very carefully after 1530 min to prevent the fibrin gels from being dislodged.

Sodium Hyaluronate (10mg/ml, Ophthalin®, Switzerland) is a commercially available hyaluronate gel was used directly without preparation according to manufacturer. In two cases hyaluronate hydrogels were blended with freshly cast collagen gels at 1:1 and 1:20.

2.2.3 Cell Culture

Immortalised mouse feeder 3T3 fibroblasts were cultured in DMEM (Lonza, UK) supplemented with 10% fetal bovine serum (Gibco, UK) and penicillin (100units/ml) - streptomycin (0.1mg/ml) solution (Gibco, UK) in T-25 flasks. Cells were passaged at 90% confluence. Cells were washed with sterile PBS and incubated with 1ml trypsin (Gibco, UK) for 3-5min. Thereafter, the enzymatic reaction was stopped with 5ml of culture medium. Cells were split in a 1:10 ratio into a new T-25 flask with fresh culture medium. Medium was replaced the next day with frequent media changes every 3 days.

Adult human lymphatic microvascular endothelial cells (LECs, Lonza, UK) were cultured in a) basic medium for endothelial cells (BME) (MCDB131, Gibco, UK) medium with 1µg/ml hydrocortisone (Sigma, UK) and Dibutyl cAMP 50µmol (Sigma, UK) b) in fully supplemented endothelial cell culture medium (EMB-2, Lonza, UK) with 5% (v/v) fetal bovine serum at 37 °C in a humidified 5% CO₂/air atmosphere. Additionally, c) VEGF-C (Reliatech, Germany) was supplemented at a concentration between 50-200ng/ml to BME and EMB-2 media - refer to experiment and Table 2. The culture medium was changed every 2-3 days and cells were passaged at 70% density (see above 3T3 fibroblasts). The cells used in this study were of passage 3-5.

2.2.4 Collagen type I delivery systems for LEC growth and tube formations

Hydrogel matrices were prepared for LECs growth, maintenance and tube formation. In the experimental designs Table 2 hydrogel matrices and coatings were delivered in many forms to demonstrate growth, tube formation and morphological differences of LECs in experimental conditions. 2D collagen type I matrices were either prepared

by a) coating 2-50ng/cm² collagen type I (ApCol, Devro Medical Ltd., UK) on tissue culture plastics (TCP) (see below 2.2.7) or by b) seeding LECs on top of 0.5-5mg/ml collagen type I hydrogels (see above 2.2.2). LECs were seeded at 100000 cells per well (24-well plates). 3D collagen type I matrices were prepared by c) seeding LECs onto TCP or collagen type I hydrogels, which were layered after 24h attachment with freshly cast collagen type I hydrogel. Alternatively, 3D suspension culture was performed by suspending LECs in collagen type I solution prior to gel casting. LECs in suspension culture were seeded at 1x10⁶ cells/ml.

2.2.5 Immunostaining of cell monolayers, collagen gel cultures and tissue dissections

Freshly prepared samples were washed in PBS, fixed with 4% para-formaldehyde at room temperature for 30-45 min, and washed with PBS again. Samples were incubated with blocking-permeabilisation solution (PBS, 3% w/v BSA, 0.1% v/v Triton-X100) at room temperature for 1h on a shaking plate. Primary antibodies including rabbit anti-human/rat/mouse Prox-1 (Reliatech, Germany) at 1, 10 µg/ml, mouse anti-rat/human Podoplanin at 2 µg/ml and rabbit anti-mouse Lyve-1 at 2 µg/ml were added to the samples incubated in blocking buffer; PBS, 3% Bovine Serum Albumin (BSA, Sigma UK) a) for 4h, b) overnight at 4°C and then washed 35 times for 15 min each in PBS. Respectively, collagen gel cultures and tissue dissections were incubated for up to 48h. Corresponding secondary antibodies conjugated with goat anti-rabbit FITC (1:160) (Sigma, UK) and goat anti-mouse TRITC (1:64) (Sigma, UK) were incubated in blocking buffer for 1h at room temperature and washed as described above. Respectively, collagen cell cultures and tissue dissections were incubated for up to 24h at 4°C and then washed 5 times for

15 min each in PBS. Subsequently, DAPI staining was performed. Tissues samples were placed between glass slides and cover slips in mounting medium. Samples were examined by fluorescence microscopy (Zeiss Axio Imager) and the images captured were analysed using proprietary image-analysis software (AxioVision, version 4.7, Zeiss Ltd. UK).

2.2.6 Real-time microscopy of tube-like formations in collagen-gel constructs

LECs were cultured on a microaqueduct slide of a Focht micro-environmental control chamber for upright microscopes (model FCS3, Bioptechs Inc., Butler, PA) in BME or EMB-2 medium (Lonza, UK) until LECs reached confluence in the form of a dense monolayer. The FCS3 chamber was loaded and assembled according to the manufacturer's protocol. Briefly, the base, upper gasket, tubing, microaqueduct slide and singular lower gasket (14x22mm rectangle) were assembled under sterile conditions. About 400µl freshly prepared rat collagen type I gel (3mg/ml) (preparation see chapter 2.2.2) was poured onto the microaqueduct slide filling the lower gasket gap and left for up to 20min to set the gel in sterile conditions. Thereafter, the chamber was filled with BME or EMB-2 medium supplemented with 20mM HEPES buffer and the 40mm cover slip was placed on top, avoiding bubbles in tubing and chamber. Pressure plate and top were assembled and the whole chamber was mounted onto the Universal Upright Stage Adapter (Bioptechs, Butler, PA). The FCS3 controller was set to 37°C. Flow of media through the chamber was adjusted to 5ml/24h. The entire device was mounted onto the Zeiss Axio Vision microscope. Phase-contrast images were captured once every 20min at 5 different

positions over a 24h period. An AVI format video was generated from 167 image stack with ImageJ® software at a rate of 7 frames per second.

2.2.7 Biomaterial coating of Tissue Culture Plates

Cell culture plates (24-Well and 96-Well plates) and 13mm ϕ glass slides were coated with 5 different biomaterials. Cell culture plates were coated with a PBS solution of either fibronectin (Sigma, #F1141, UK), RGD (fibronectin analogue) (Sigma, #G1269), collagen type IV (Sigma, #C0543, UK), collagen type I (APColl, Devro, UK) or laminin (Sigma, #C2020) at a final concentration of $2\mu\text{g}/\text{cm}^2$. 96-well plates were incubated with 100 μl and 24-well plates were incubated with 0.9ml volume. All biomaterials except Laminin were air dried over 3 days in the laminar flow hood. Laminin was incubated for 2h at 37°C on tissue culture plates and washed once with PBS. Plates were stored at 4°C for up to one month and washed once with PBS prior to cell culture.

2.2.8 MTT formazan assay for Lymphatic Endothelial Cells

LECs at 90% confluence were harvested and seeded in triplicates at a density range from 1×10^3 – 1×10^6 cell per well in 24-well plates. LECs were cultured overnight in EMB-2 medium to allow complete cell attachment. A yellow coloured 3-(4,5Dimethylthiazol-2-yl)-2,5-diphenyltetrazolium bromide (MTT) (Sigma, UK) stock solution (0.4143g of MTT/ 100ml of PBS, pH 6.75) was prepared, filter sterilized and kept for no more than 2 weeks at 4°C. LECs cultured in 24-well plates were washed with PBS prior to the MTT assay. To start the reaction, 200 μl of warm MTT stock solution was added to growing cultures in 24-well plates. The cells were incubated with MTT for different time periods to estimate the saturation of formazan

production. Incubation time was tested with 3hr and 4hr in a humidified incubator at 37°C. Thereafter, MTT solution was aspirated and 100µl of Dimethyl sulfoxide (DMSO) was added to the cells. The DMSO solution was pipetted up and down until all cells and purple formazan were dissolved in the solution. 80 µl of the DMSO solution was transferred into a 96-well plate. The absorbance was measured with a spectrophotometer (BioRad, UK) at 520 nm. A blank well with DMSO alone was measured and subtracted from all values. The results were used to generate a calibration curve, to calculate the number of proliferating cells under experimental conditions. LECs were seeded at 40000-55000 cells per 24-well and cultured with different endothelial cell culture media and on different substrates (see above experimental designs Table 2). Samples for the MTT assay were taken every day up to a week. 24-wells were washed with PBS and the number of proliferating cells was determined from the linear equation generated from the calibration curve. Moreover, the population doubling time was calculated with the exponential growth function (equation 1) from the incremental LEC number over time (see below 2.2.10).

2.2.9 Tube forming degradation assay

LECs were seeded and cultured in 100µl EMB-2 under cell culture conditions at a density of 2×10^4 cells/well (96-Well plates) on seven different biomaterial surfaces; a) fibronectin b) RGD (fibronectin analogue), c) laminin, d) collagen type I, e) collagen type IV, f) freshly cast rat collagen type I gel and on g) tissue culture plastic as control. Cells were allowed to attach to the surface overnight in EMB-2. Thereafter, medium was renewed and supplemented either with 100µg/ml collagen type I (ApColl®, Devro Medical Ltd., UK) in 100µl EMB-2 medium or a fibrin gel

of 25µl was cast above the cells (see above 2.2.2). LECs were cultured for up to five days in EMB-2 medium. Daily cell culture samples were stained with acridine orange and visualised by fluorescence microscopy (Zeiss Axio Imager). Images were analysed using proprietary image-analysis software (AxioVision, version 4.7, Zeiss Ltd. UK). The viable cell count was performed with the ImageJ® cell counter plugin. The decrease of the number of the acridine orange stained nuclei per day was calculated with the exponential growth function (equation 1) and evaluated as population half life (see below 2.2.10).

2.2.10 Calculation of cellular population doubling time and half life

Growth and decay of cells describes a typical function which is segmented into lag phase, exponential phase and plateau phase. The growth/decay behaviour was analysed with the values of the exponential phase. Values were fitted with an exponential function with excel curve fit (Microsoft Excel®). The resulting equation represents the exponential growth or decay of one specific cell population (equation 1)

$$(1) \quad x(t) = x_0 \cdot e^{kt} = x_0 \cdot e^{t/\tau} = x_0 \cdot 2^{t/T}$$

k is the growth frequency described as time/unit. T is the time it takes to grow by a factor e . T is the doubling time. Setting the time to 1 ($t=1$) the growth frequency k can be easily translated into doubling time T (time needed for a population to double its size or number) with the application of the natural logarithms (equation 2).

$$(2) \quad k = \frac{1}{\tau} = \frac{\ln 2}{T}$$

The resulting values show the exponential behaviour of the cell population in either growth or decay and are displayed as the number of days needed to double or halve the cell population. The calculation of the doubling time allows comparison of results from growth or decay studies despite the differences in acquisition such as MTT or nuclei counts. An example for the growth calculation is given in the results section 2.3.2, and an example for decay calculation is presented in the Annex.

2.2.11 Cell viability staining and cell count

Cells were stained with Acridine Orange (Molecular Probes, US) for live cells (identified by green nucleus stain) and Propidium Iodide (Invitrogen, UK) for dead cells (identified by red nuclear stain).

Samples were incubated with 1-2ml Propidium Iodide (20 μ g/ml in PBS) and Acridine Orange (100 μ g/ml in PBS) at a 1:1 ratio at room temperature for 1-2min in the dark. Samples were washed 3-5 times with PBS and viewed immediately with a fluorescence microscope. Representative images of viable cells and morphology during attachment, growth, tube forming and migration were captured with an epifluorescence microscope (Zeiss Axio Imager, Zeiss Ltd, UK).

Nuclear staining was performed with DAPI (Sigma, UK). After sample fixation in 4% para-formaldehyde (10-15min for monolayer cell culture, up to 45min for 3D gel culture or tissue) at room temperature, samples were washed with PBS. Samples were then incubated with DAPI (1 μ g/ml in PBS) at room temperature for 5-10min in dark. Thereafter, samples were washed 3-5 times with PBS. DAPI stained cell nuclei blue. Representative images of cells in hydrogels on tissue culture plastic or in dissected tissues were captured with an epifluorescence microscope (Zeiss Axio Imager, Zeiss Ltd, UK).

Images were evaluated with ImageJ® cell counter plug-in for total, viable and dead cell count. ImageJ software and plug-in are freeware downloaded from the National Health Institute, available at <http://rsbweb.nih.gov/ij/>. Resources and manuals are available at the integrated microscopy core facility at the University of Chicago. <http://digital.bsd.uchicago.edu/resources.html>

2.2.12 Co-Culture Assay with 3T3 Mouse Fibroblasts **Fibroblast growth under LEC culture conditions**

Viability of mouse 3T3 fibroblasts in endothelial cell medium was tested prior to coculture. Mouse 3T3 fibroblasts were seeded at 1.5×10^5 per well (24-well plate, Greiner). Cells were cultured for 3 days in DMEM, BME and EMB-2 media, and additionally, samples were supplemented with 100µg/ml collagen type I solution (APColl®, UK). Cells were stained with Acridine Orange and Propidium Iodide.

Viability calculations were performed with the ImageJ cell counter plug-in.

LEC growth in co-culture with 3T3 fibroblasts

Prior to co-culture LECs were stained with a long lasting fluorophore in order to distinguish the two cell populations from each other in co-culture. LECs were incubated in BME medium with 20µM Cell Tracker Green (Invitrogen, UK) at 37°C under cell culture conditions. They were washed with PBS 3 times prior to co-culture. Several co-culture experiments were performed as shown in Table 2 with the experimental designs.

LECs and 3T3 fibroblasts were enzymatically dissociated from their culture flasks and seeded together into 24-well plates at a total concentration of 5×10^4 cell/well. LECs and fibroblasts are seeded in close proximity allowing paracrine and juxtacrine signalling between them. In this “juxtacrine co-culture system” 3T3 fibroblast to

LEC ratios were a) 1:1, b) 1:4, c). 1:10 and d) LECs only as control group. Additionally, LECs and fibroblasts were seeded separately, spatially divided from each other allowing only paracrine signalling between them. In this “paracrine coculture system” 3T3 fibroblasts were seeded at 5×10^4 cells/well into 24-well plates and cultured for 24h in EMB-2 medium. Thereafter, 3mg/ml type I collagen was cast onto the cells as a hydrogel and 5×10^4 LECs were seeded on top. Cells were cultured up to 48h hour. Samples were washed in PBS and fixed in 4% para-formaldehyde after 24h and 48h. Nucleus staining was performed with DAPI. Cells were viewed with an epifluorescence microscope and total cell count evaluations were performed with the help of ImageJ, cell counter plug-in software.

Tube formation of LECs in co-culture with 3T3 fibroblasts

Co-culture collagen assays with tube forming LECs were performed similar to the previous juxtacrine co-culture experiment system. Cell Tracker Green (Invitrogen, UK) stained LECs, and 3T3 fibroblasts were seeded simultaneously at a 4:1 ratio and cultured in EMB-2 medium supplemented with collagen solution $100 \mu\text{g/ml}$ (APColl, UK) to initiate tube forming of LECs. Cells were cultured for up to 8 days.

Additionally, a paracrine co-culture system was performed with either a) high (4:1) LEC to fibroblast cell ratio or b) low (1:8) LEC to fibroblast cell ratio. 3T3 fibroblasts at a) 3×10^4 or b) 1.2×10^5 cells/well were seeded into 24-well plates and cultured for 24h in a) BME and b) EMB-2 medium. Thereafter, a thin layer of 3mg/ml rat type I collagen hydrogel was cast onto the cells and LECs were seeded on top and cultured further in a) BME and b) EMB-2. After 24h in culture a second layer of collagen type I gel (3mg/ml) was cast on top of the attached LECs to induce tube formations. Cells were cultured up to 7 days with a) BME and b) EMB-2 medium under cell

culture conditions. (In this particular experiment LECs were not treated with Cell Tracker Green, due to the distinctive separate locations of the two cells types).

Prior to staining, samples were washed with PBS. Experiments with Cell Tracker Green stained LECs were fixed in 4% para-formaldehyde. Nucleus staining was performed with DAPI. Samples of 3T3 fibroblast and LECs in collagen matrices were also stained directly with acridine orange and propidium iodine without fixatives (see above 2.2.11). Cells were viewed with an epifluorescence microscope, cell 3D stacks and images were produced with Zeiss Axio Imager and software (AxioVision, version 4.7, Zeiss Ltd. UK). 3D image compilation was performed with ImageJ software.

2.2.13 Experimental design and statistical analyses

All conducted experiments of Chapter 2 are summarized in Table 2. The experiments are explained briefly, and list the tested groups and parameters. Further, the table links the used methods of (Chapter 2.2) and finding (images and tables) of the result section (Chapter 2.3).

In general, all experiments with qualitative value (images) and statistical value were performed at least 3 times.

In addition, MTT assays were performed with a minimum of 3 replicates. MTT assay with 3 replicates computes to one doubling time value. Therefore, a minimum of 3 MTT assays, each with 3 individual replicates were performed to generate sufficient statistical data, with one exception; the data in Figure 5 represents a single experiment with 3 replicates. Therefore, the data shown in Figure 5 demonstrates proof of concept/methodology only.

Image evaluation, nuclei counts after DAPI, Acridine Orange or Propidium Iodide staining, was performed from 3-5 Images per replicate. An experiment consists of a minimum of 3 replicates. All experiments were conducted at least 3 times to generate sufficient statistical data. With one exception; the data in Figure 12 represents a single experiment with 3 replicates. The data shown in Figure 12 therefore demonstrate proof of concept/methodology only.

Data were grouped and analysed using Student's T-test or ANOVA, and statistical significance assigned to results where is $p < 0.05$ if not stated differently in the figure caption. ANOVA data were computed with tools for science <http://www.physics.csbsju.edu/>. Full sample data and ANOVA calculation for Figure 11 and Figure 13 are attached with the CD/ANNEX.

Table 2 Overview experimental designs

Experiments	Description	Method section	Tested Parameters	Result section
LECs characterisation				
Evaluation of different LECs antibody markers <i>in vivo</i>	LEC antibody markers (LYVE-1, Podoplanin and Prox-1) were tested on three different tissue dissections. Further, the expression of primary antibody markers was optimized in terms of incubation time in co-culture with 3T3 fibroblasts.	2.2.1, 2.2.3, 2.2.5	Tissues: a) Lymphatics b) Smooth muscles c) Vascular vessel Antibody incubation time: 1) 4h 2) 24h	2.3.1 Figure 3, Figure 4
Characterisation of tube forming LECs in 3D collagen matrices	Tube formation of LECs was induced with collagen type I on different 2D and 3D matrices with two different media, Immunocytohistology of Prox-1 was performed to verify lymphatic phenotype after 24h.	2.2.2, 2.2.3, 2.2.4, 2.2.5	a) delivery systems: 2D b) collagen coatings 2D c) collagen hydrogel 3D Media: 1) collagen hydrogel 2) EMB-2 EMB-2 + VEGF-C (200ng/ml)	2.3.2 Figure 7
Growth Studies				

LECs growth in different media	LEC growth was studied in different media over 7 days; growth curves and cell division rates were produced with MTT assay	2.2.3, 2.2.8, 2.2.10	Media: a) BME b) EMB-2 c) BME + 50ng/ml VEGF-3	2.3.2 Figure 5
LECs growth on different surfaces	LEC growth was studied on different surfaces in EMB-2 media over 7 days; growth curves and cell division rates were produced with MTT assay	2.2.3, 2.2.8, 2.2.7, 2.2.10	Surface coatings: a) Fibronectin b) RGD c) Collagen type IV d) Collagen type I e) Laminin	2.3.2 Figure 11

Tubular Formation Studies				
Assembly of LEC tubular formation with different collagen delivery systems	Tube formation of LECs was induced with different amounts of collagen type I in different 2D and 3D matrices, 24h image analyses was performed and captured in real time.	2.2.2, 2.2.3, 2.2.4, 2.2.6	&collage delivery systems a) concentrations: 2D collagen coatings (2-5ng/cm ²) b) 2D collagen hydrogel (0.5-5mg/ml) c) 3D collagen hydrogel (0.5-5mg/ml) d) Collagen supplemented media (10-100ng/ml)	2.3.2 Table 3 Annex CD (Videos)
LEC tube formation maintained with different media	LEC tube formation was induced in 3D collagen type I hydrogels in different media. The LEC growth/decline in growth was evaluated over 3 days with visual imaging of live cell stains	2.2.2, 2.2.3, 2.2.11	Media: a) BME b) EMB-2 c) EMB-2 + VEGF-C (125ng/ml)	2.3.2 Figure 6
LEC tube formation assembly with different hydrogels	LEC tube formations were induced with different hydrogels in EMB-2 medium. Development of tube formation was assessed with visual imaging of live stains	2.2.2, 2.2.3, 2.2.11	Hydrogels: a) Collagen type I b) Fibrin c) Hyaluronan d) Hyaluronan blended with Collagen type I	2.3.2 Figure 8 Figure 9 Figure 10
LEC tube formation and degradation on different surfaces	LEC tube formations were induced with a layer of two different hydrogels on different surface coatings in EMB-2 medium. The LEC decline was evaluated over 3 days with visual imaging of live cell stains	2.2.2, 2.2.3, 2.2.7, 2.2.9, 2.2.10, 2.2.11	Surface coatings: a) Fibronectin b) RGD c) Collagen type IV d) Collagen type I e) Laminin f) Collagen type I hydrogels Hydrogels: 1) Collagen type I 2) Fibrin	2.3.2 Figure 8 Figure 9 Figure 11

Co-Culture studies with LECs and 3T3 Fibroblast				
Fibroblast growth under LEC conditions	3T3 fibroblast growth was studied in different endothelial media with collagen type I hydrogel	2.2.2, 2.2.3	Media; a) DMEM b) EMB-2 c) BME	2.3.3 Figure 12
LEC growth in coculture with fibroblasts	LECs and fibroblast were cocultured in two different systems and in different cell number ratios. LEC growth was assessed with visual imaging of Cell Tracker® and DAPI staining	2.2.3, 2.2.5, 2.2.11, 2.2.12	Co-culture systems: a) Juxtacrine distance b) Paracrine distance LECs to Fibroblast ratio: 1) 1:1 2) 4:1 3) 10:1	2.3.3 Figure 13
Tube formation of LECs in co-culture with fibroblasts	LECs were co-cultured with fibroblast in two different culture systems with different cell ratios and in two different media. LEC tube formation was induced with 3D collagen type I hydrogels. Tube assembly and maintenance over 7 days was assessed with visual imaging of Cell Tracker® and live stains	2.2.3, 2.2.5, 2.2.11, 2.2.12	Co-culture systems: a) Juxtacrine distance b) Paracrine distance LEC to Fibroblast ratio: 1) 3:1 2) 1:8 Media: I) BME II) EMB-2	2.3.3 Figure 14 Figure 15

2.3 Results

2.3.1 LEC characterisation of tissue and cells

The tissue segments of a collecting lymphatic vessel in rodents showed positive staining results for all three lymphatic markers (Figure 3). However, LYVE-1 was weakly expressed compared to Prox-1 and Podoplanin. LYVE-1 was also expressed in the surrounding connective and/or fat tissue (Figure 3, arrow). Moreover, LYVE-1 was strongly expressed between the smooth muscle fibres. It remains questionable whether these were lymphatic cells. Podoplanin was strongly expressed in the cytoplasm of the lymphatic tissue and co-stains with the nuclear expression of Prox-1. Podoplanin antibody stained the inter-cellular connections of blood vessel endothelia cells, but was not expressed on smooth muscle tissue. Prox-1 was exclusively expressed in the lymphatic vessel endothelial cell nuclei and was not expressed in the surrounding tissue, such as smooth muscle, connective tissue, fat tissue and blood vessel endothelial cells.

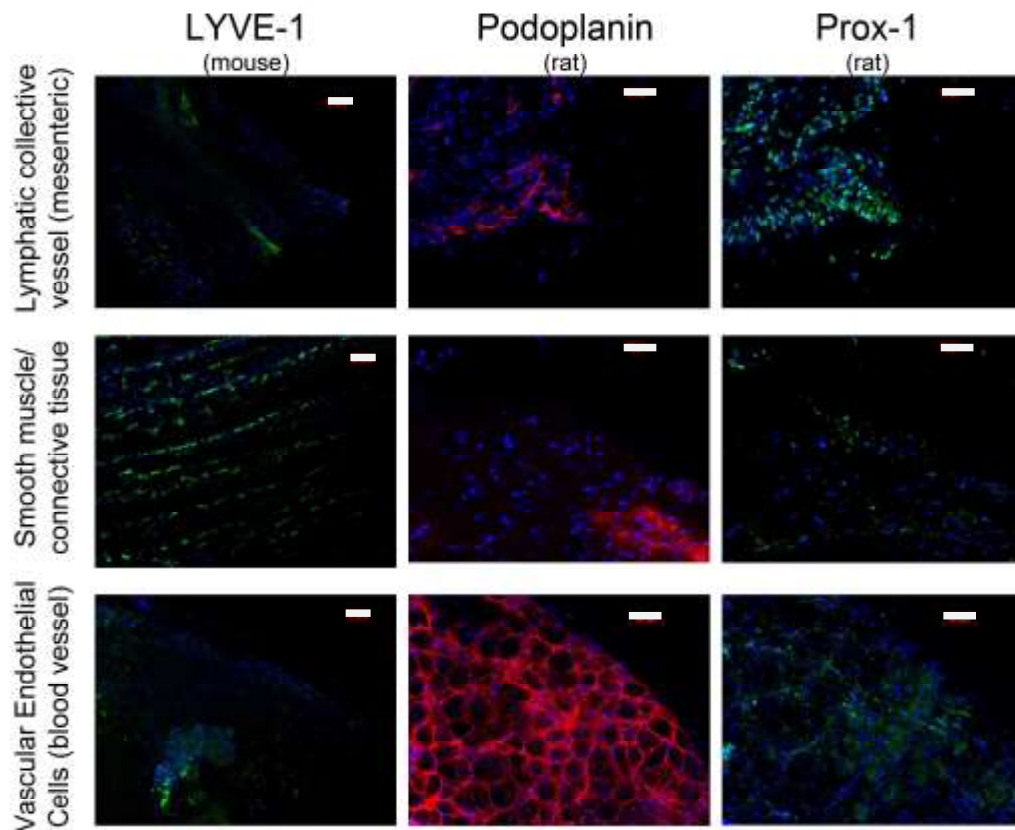
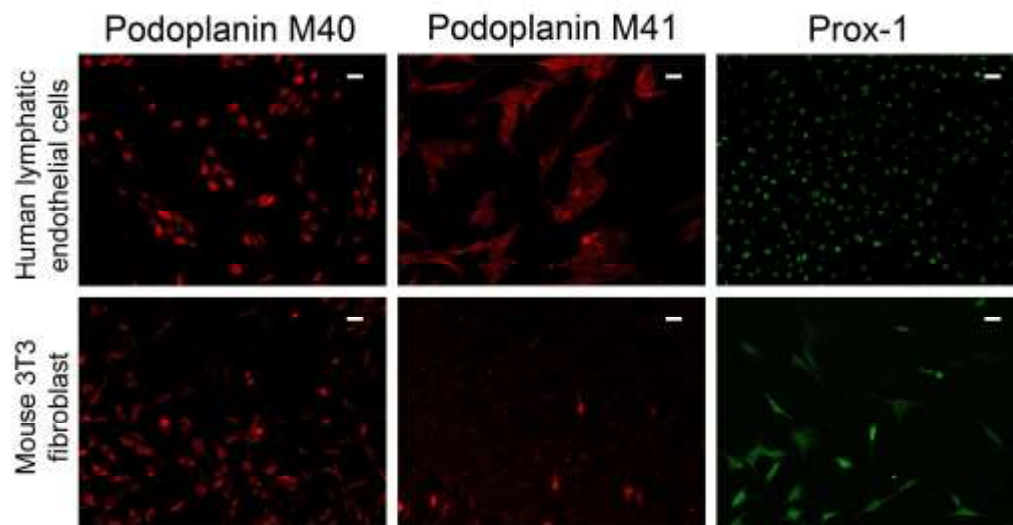


Figure 3 Immunostaining of rodent tissue with Lymphatic markers

The images show staining of three different rodent tissues (lymphatic vessel at the mesentery, smooth muscle tissue and blood vessel) with the three most common lymphatic markers LYVE-1 (green), Podoplanin (red) and Prox-1 (green) with a nucleus DAPI co-stain (blue). Lyve-1 was stained on mouse tissue. Podoplanin was co-stained with Prox-1 on rat tissue. White scale bar = 50µm

In vitro staining of LECs and mouse 3T3 fibroblasts with human anti-podoplanin showed similar expression profiles (Figure 4). Podoplanin marker (M40) was expressed in the cytoplasm whereas podoplanin marker (M41) stained the cell surface. From the excitation table (Figure 4, Table) it is obvious that podoplanin (M41) was not significantly differently expressed within mouse 3T3 fibroblasts and human LECs, which indicated unspecific binding to the cell membranes on both cell types. Nevertheless, podoplanin (M40) showed weak unspecific binding to mouse

3T3 fibroblast nuclei. Prox-1 was expressed in the nucleus of the human LECs only. 3T3 fibroblasts were not stained by the lower concentrations of Prox-1 antibodies, however, 24h at a 10x higher concentration of Prox-1 antibody introduced a background staining to the whole cells as shown with the mouse 3T3 fibroblast (Figure 4). Prox-1 staining is as effective *in vivo* as *in vitro* and produces reproducible results. Moreover, in our experiments it did not show cross staining of other cell types and tissues at a concentration of 1 μ g/ml.



	2ug/4h (M40)	2ug/24h (M40)	2ug/4h (M41)	2ug/24h (M41)
Podoplanin				
3T3 Mouse Fibroblast	18223ms	9315ms	18222ms	15213ms
Human LECs	5818ms	5778ms	15792ms	15354ms
	1ug/4h (PA30)	10ug/24h (PA30)		
Prox-1				
3T3 Mouse Fibroblast	-	12357ms		
Human LECs	8460ms	7527ms		

Figure 4 Evaluation of lymphatic markers

Expression of immunostaining with two human podoplanin markers and a prox-1 marker was tested on 3T3 mouse fibroblasts and LECs. Differences in fluorescence excitation (ms = milliseconds) are shown in the table. An incubation time between

4h at room temperature and 24h at 4°C was compared with a primary antibody concentration between 1 and 10µg. Black background highlights the staining parameters which showed significant differences between the 3T3 mouse fibroblast and LECs. Scalbar = 10µm.

2.3.2 LEC growth and tube formation in hydrogels

Lymphatic endothelial cells were tested in titrations from 1×10^3 to 2.5×10^5 cell with an MTT assay for 3 and 4h. The MTT assay was applied to attached cells. LECs incubation with MTT in PBS for more than 3h led to cell dissociation. Therefore, all assays were performed with a maximum of 3h incubation time. The cell titration shows a linear absorbance profile at 520nm between 4×10^4 to 2.5×10^5 cells (Figure 5, a). LEC growth was analysed in three different culture media (Figure 5, b). Growth was strongly induced by the EMB-2 medium, whereas BME medium showed almost no growth. Addition of 50ng/ml VEGF-C to the BME medium significantly stimulated cellular metabolism and growth. In order to analyse the differences in proliferation by means of doubling time and fold increase, exponential values from Figure 5, b were fitted with an exponential growth function equation (1), (Figure 5, c). Solving the function via the logarithmic function (equation (2)) resulted in the doubling time of the LEC population (Figure 5, d). The doubling time of the LECs in the three different media showed the differences in fold increase between the groups, where LEC growth in EMB-2 media was approximately 5 fold higher than in BME and 3 fold higher than in BME supplemented with VEGF-C. These results represent the methodological approach and analyses for further experiments with the MTT assay. Moreover; it re-confirmed the importance of VEGF-C as a single additive in basal media for LEC growth and metabolism.

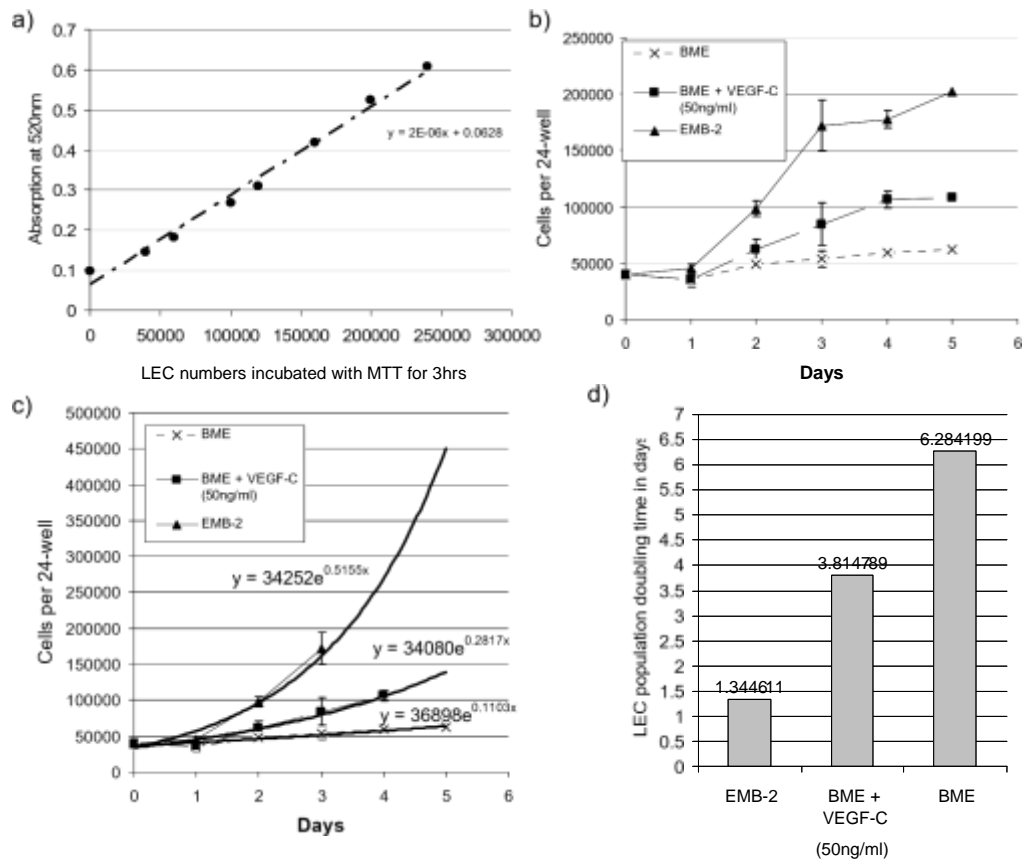


Figure 5 Growth analyses of LECs with different media

An example of one calibration curve of the MTT assay is shown in chart (a). Cells seeded between 40000 to 250000 show a linear absorption profile after 3h incubation in Thiazolyl Blue Tetrazolium Bromide. Chart (b) shows the growth of LECs seeded at 40000 Cell/Well (24-Wellplate) in BME, EMB-2 and in supplemented BME medium with 50ng/ml VEGF-C. Cell numbers were calculated from the MTT absorption with the linear equation formula shown on graph (a). The exponential values (BME= day 0-5, EMB-2 = day 0-3, BME + VEGF-C = day 0-4) of the growth the chart (b) where plotted with an exponential curve fit (c). Values of the exponential equation (c) were solved with formula (1) and (2) resulting in the doubling time of the LEC population shown on (d)

LECs were seeded and cultured in various conditions with collagen type I matrices (Table 2 and Table 3). LECs develop tubular-like structures only under 3D collagen matrix conditions. The assembly of LECs into tubular-like structures was observed on plastic surfaces when covered with 1-5mg/ml collagen gel or media supplemented

with a minimum of 50 μ g/ml collagen. Further, LECs formed tube-like structures when embedded between layers of collagen hydrogels. Surprisingly, LECs suspended in collagen type I hydrogels showed tube like structures only in very few experiments (1 out of 20). However, an additional supplementation of 200ng/ml VEGF-C lead easily to tube forming cells in all experiments. It seems the presence of collagen type I was essential to initiate and maintain tubular structures in all experiments. Once the collagen hydrogel is removed or peeled off, tube-like LECs reorganise back to a cobblestone formation within a few hours (observations during experiments). The real time video footage shows the development of LEC tubular like structures when layered with 3mg/ml collagen gels over 24h (Video 1 and 2, Annex/CD). In the beginning LECs showed a typical endothelial cobblestone formation (0h). After attachment to collagen type I hydrogel, LECs started to migrate and detach from each other within a few hours (4-12h). Thereafter, they re-organised into new formations of tubular like structures (>12h). The cobblestone morphology of the LECs converted within a few hours after attachment to the collagen matrix into a tube-like network resembling a honeycomb pattern. Unlike the static monolayer, LECs actively migrated between these network structures and reorganised the pattern all over within the first 24h. It was observed that LECs generated a lot of cell debris during tubular assembly (24h), especially when cultured in non-supplemented medium such as BME (Video 2, Annex/CD). Tube formations were observed with BME (growth factor free basal medium) and EMB-2 medium (Video 1/ Annex/CD). Thus initial migration and tube formation is not dependent on medium growth factors.

Table 3 Variations of collagen type I delivery systems inducing LEC tubularlike formations.

X = no tubular structures observed. √ = tubular structures visible after 24-48h

Collagen type I concentrations/ Collagen delivery system	10 μg/ml	50 μg/ml	100 μg/ml	500 μg/ml	1 mg/ml	2 mg/ml	3 mg/ml	4 mg/ml	5 mg/ml	Tubular like formations
(2D) Collagen coated surface	X	X	X	n.a.	n.a.	n.a.	n.a.	n.a.	n.a.	X
(3D) Collagen supplemented Media	X	√	√	n.a.	n.a.	n.a.	n.a.	n.a.	n.a.	√
(2D) Collagen hydrogel surface	n.a.	n.a.	n.a.	X	X	X	X	X	X	X
(3D) Collagen hydrogel matrix	n.a.	n.a.	n.a.	√	√	√	√	√	√	√ [#]
√ [#] in suspension collagen type I culture conditions (see 2.2.4); LECs required mostly an additionally supplementation with 200ng/ml VEGF-C, n.a. = not available										

Collagen type I induced cellular migration and tube like formation of LECs. However, the tube like formations of LECs degenerated over a time span of 4-5days in all commercial media (Figure 6). Growth factor free basal medium such as BME led to an accelerated cellular death of LECs after 24h compared to growth factor supplemented basal medium such as EMB-2 which showed a significant decline after 96h. However, EMB-2 medium supplemented with 125ng/ml VEGF-C showed an increase in the viable cell number in addition to cellular migration and tube formation in collagen type I matrix. In this experiment LECs were viable for at least 4 days in supplemented EMB-2 medium with VEGF-C (100ng/ml-200ng/ml). There was no indication of a viability or proliferation decline after day 4. Hence, LEC viability was secured with supplementation of VEGF-C 125ng/ml in *in vitro* long term culture within a collagen type I hydrogel. Without supplementation of VEGF-C LEC tubular formations were viable for at least 24-48h in EMB-2 medium.

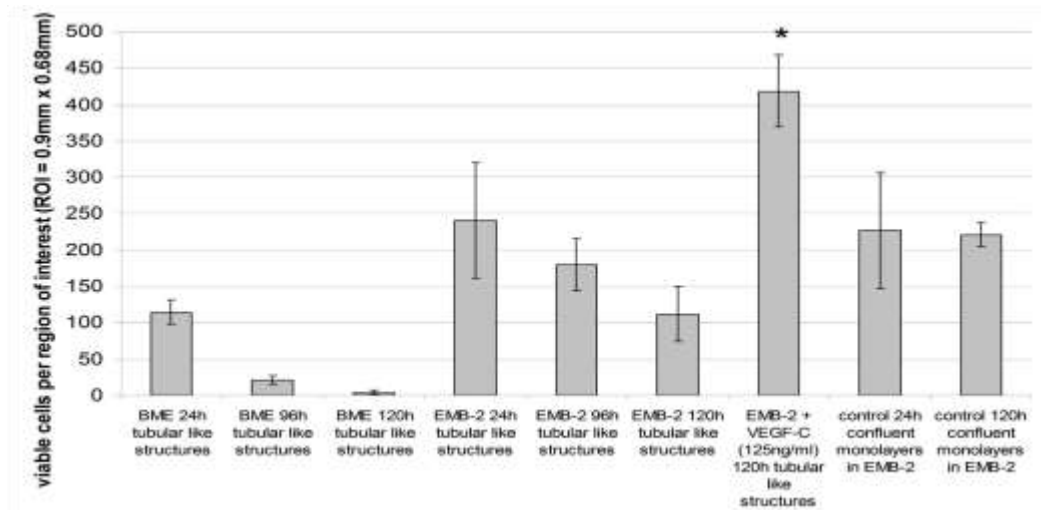
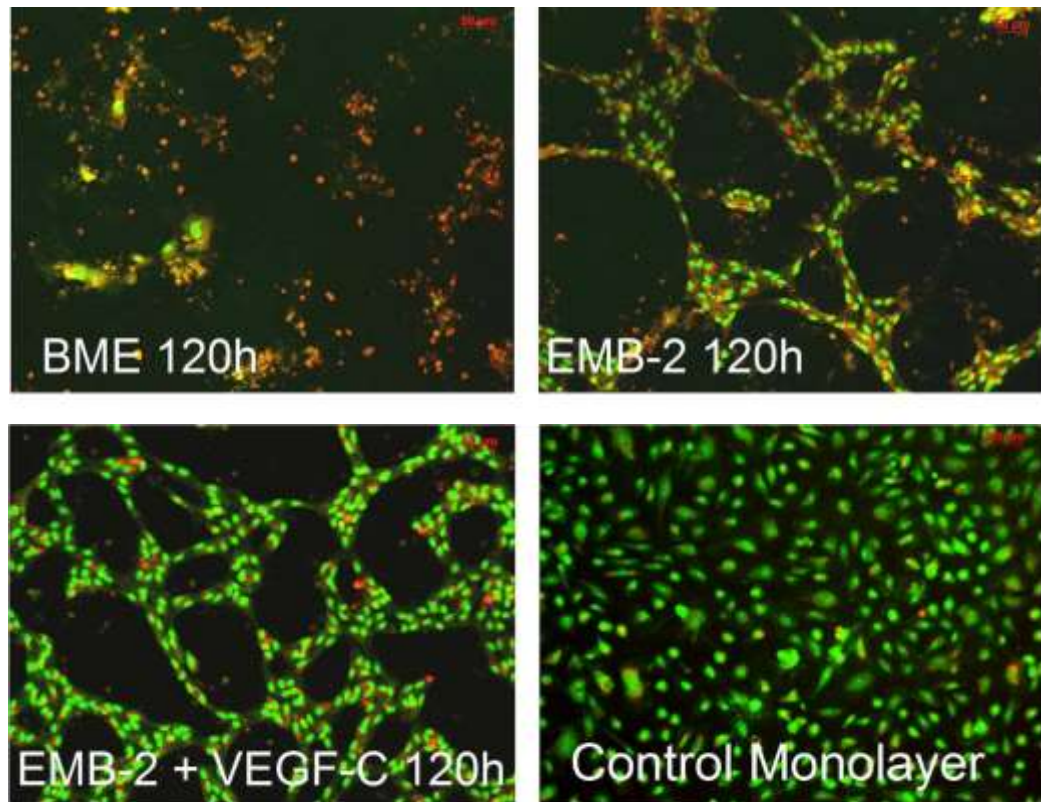


Figure 6 LEC viability in collagen type I hydrogel matrix

Images show LEC nuclei stained with Acridine Orange (viable population, green) and Propidium Iodine (dead population, red) in collagen type I hydrogels after 120h. Cells displaying a green cell nucleus stained for Acridine Orange indicating viable cells, whereas a red cell nucleus and debris stained for Propidium Iodine indicating dead and dying cells. Images were taken with a Zeiss fluorescence microscope at 10x magnification. The chart shows the viable cell nucleus count between 24h and 120h in three different media conditions (BME, EMB-2 and EMB-2 + VEGF-C 125ng/ml).

LECs in 3D collagen type I matrix conditions formed tube-like structures within 24h (Figure 7). Previously, the assumption was that LECs are sustainable in EMB-2 medium for at least 24h before onset of cell death. However, immunocyto-histochemistry staining of the lymphatic master control gene Prox-1 showed differences in LECs within different collagen delivery systems (Figure 7). LECs cells were Prox-1 positive and viable within the first 24h when seeded onto or covered with collagen type I hydrogels. LECs were also Prox-1 positive and viable when embedded between two collagen hydrogels (collagen gel sandwich) and supplemented with 200ng/ml VEGF-C. However, without the growth factor supplementation LECs lost most of their Prox-1 expression in less than 24h. Loss of Prox-1 indicates the loss of function and cellular specificity of lymphatic cells. LECs in 3D matrix (collagen gel sandwich) were surrounded with collagen type I compared to the other experiments where LECs could adhere to the culture plastic surface. Hence, this indicates that the binding capacity towards collagen might be a crucial factor for LECs accelerated cellular death, which could be avoided by VEGF-C supplementation.

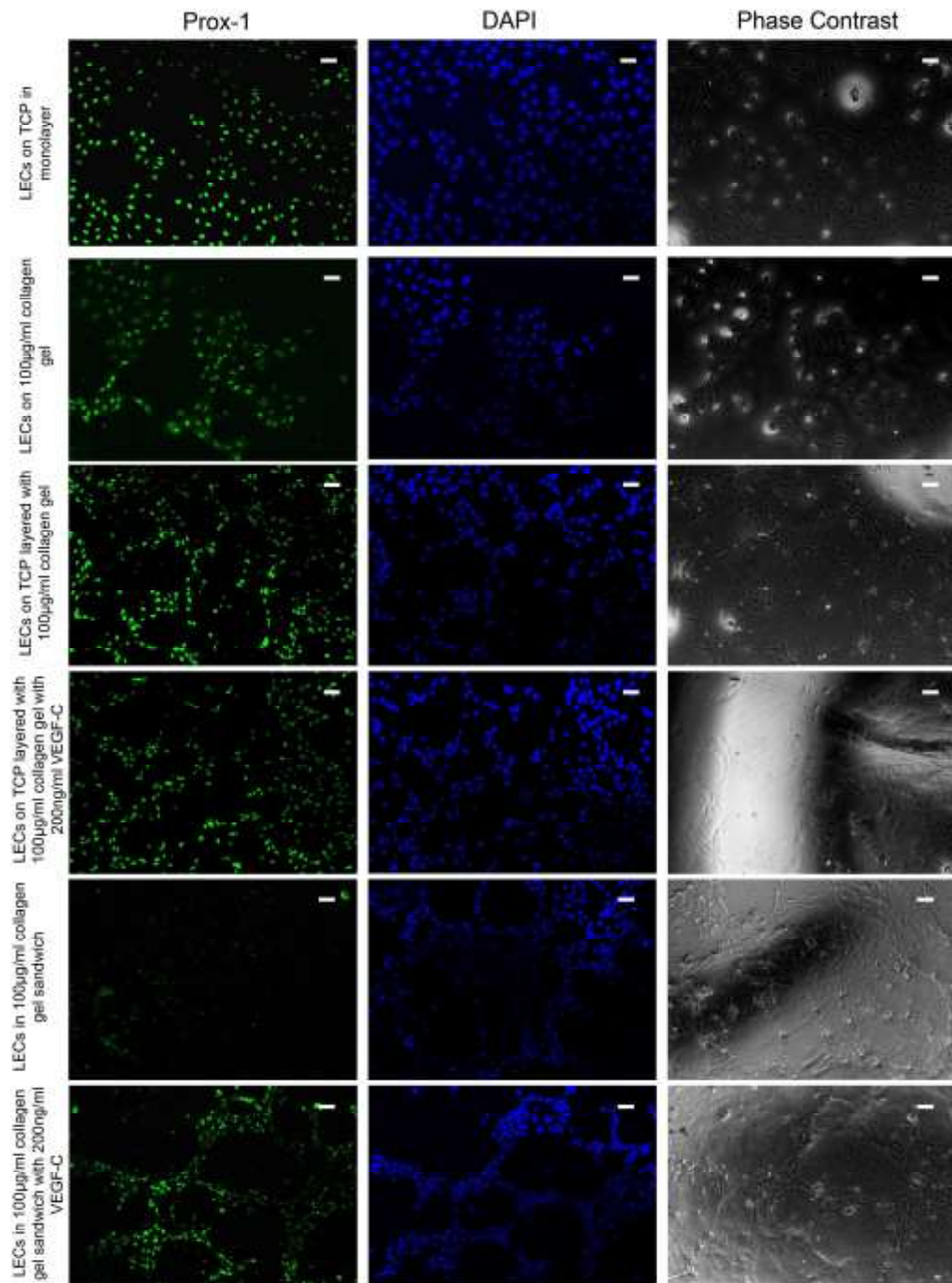


Figure 7 Immunostaining of LECs in 2D and 3D collagen matrix conditions
 Images show Prox-1 expression, DAPI staining as well as phase contrast image of LECs after 24h in culture. Phase contrast images revealed that tube forming structures formed more readily in collagen-covered samples whereas cells seeded directly on collagen gels do not form tubular networks to the same extent. Immunofluorescence images showed that the lymphatic master control gene Prox-1 (green) overlaps with the nuclei stain DAPI (blue). Prox-1 was expressed in all

samples, except in “collagen gel sandwiches” without the appropriate VEGF-C supplementation. Bar equals 50µm.

As shown previously LEC’s physiological functional loss *in vitro* was reduced either by addition of VEGF-C or by changing the surface matrix from collagen to tissue culture plastic. It is therefore questionable whether bioactive substrates can contribute to LEC survival in tube-like structures. In order to answer this question LECs were seeded onto surfaces such as fibronectin, RGD, Laminin, Collagen type I or IV and tube -like formation was induced either by deposition of collagen type I hydrogels (Figure 8), fibrin hydrogels (Figure 9), sodium hyaluronate hydrogels or hyaluronate blended with collagen type I hydrogels (Figure 10). LEC viable cell number decreased on all surfaces and in all matrices within 5 days when cultured within EMB-2 medium (Figure 8 and Figure 9) LECs formed tube- like structures only in fibrin and in collagen matrices. Surprisingly, the morphology between tube forming LECs in fibrin and collagen type matrices was different. In collagen type I matrices cells formed a wide honeycomb structured network with multiple closely attached cells (Figure 8), whereas in fibrin matrices cells did not cluster together. The tube forming cells in the fibrin matrix displayed a narrow irregularly shaped network of blind-ended tubes mostly composed of strings of single cells (Figure 9). In sodium hyaluronate hydrogels LECs failed to form tube like structures. LECs do not attach to sodium hyaluronate hydrogels. In 1:1 blends with collagen and sodium hyaluronate cells attached poorly. In blends with a 20 times higher collagen type I solution cells attached in 3D clusters. The formation of a network could not be evaluated from the images. Moreover, in all sodium hyaluronate hydrogel experiments the gel structures were completely dissociated in the culture dish within the first 24h.

Seeding cells on different surfaces such as fibronectin, RGD, laminin, collagen type I or IV compared to tissue culture plastic shows different proliferation rates or LEC population doubling times (Figure 11, a). On surfaces such as tissue culture plastic and collagen type I and IV cells displayed a lower doubling time compared to laminin and RGD. Fibronectin showed a significantly higher doubling time than collagen type I, but not to collagen type IV. The degradation or half life of LECs on the same surfaces within collagen type I or fibrin matrices were accelerated by collagen surfaces in general (Figure 11, b). Fibrin matrices, in combination with either fibronectin or RGD have a 75% to 50% extended half life compared to collagen type surfaces. Collagen matrices in combination with laminin, RGD, and fibronectin show a 50%-30% higher half life compared to collagen type I surfaces. Collagen type I hydrogel surfaces were not evaluated due to image acquisition difficulties but images showed a very high degree of LEC death within the first 48h.

(An example of the calculation of the decay rate is given in the Annex)

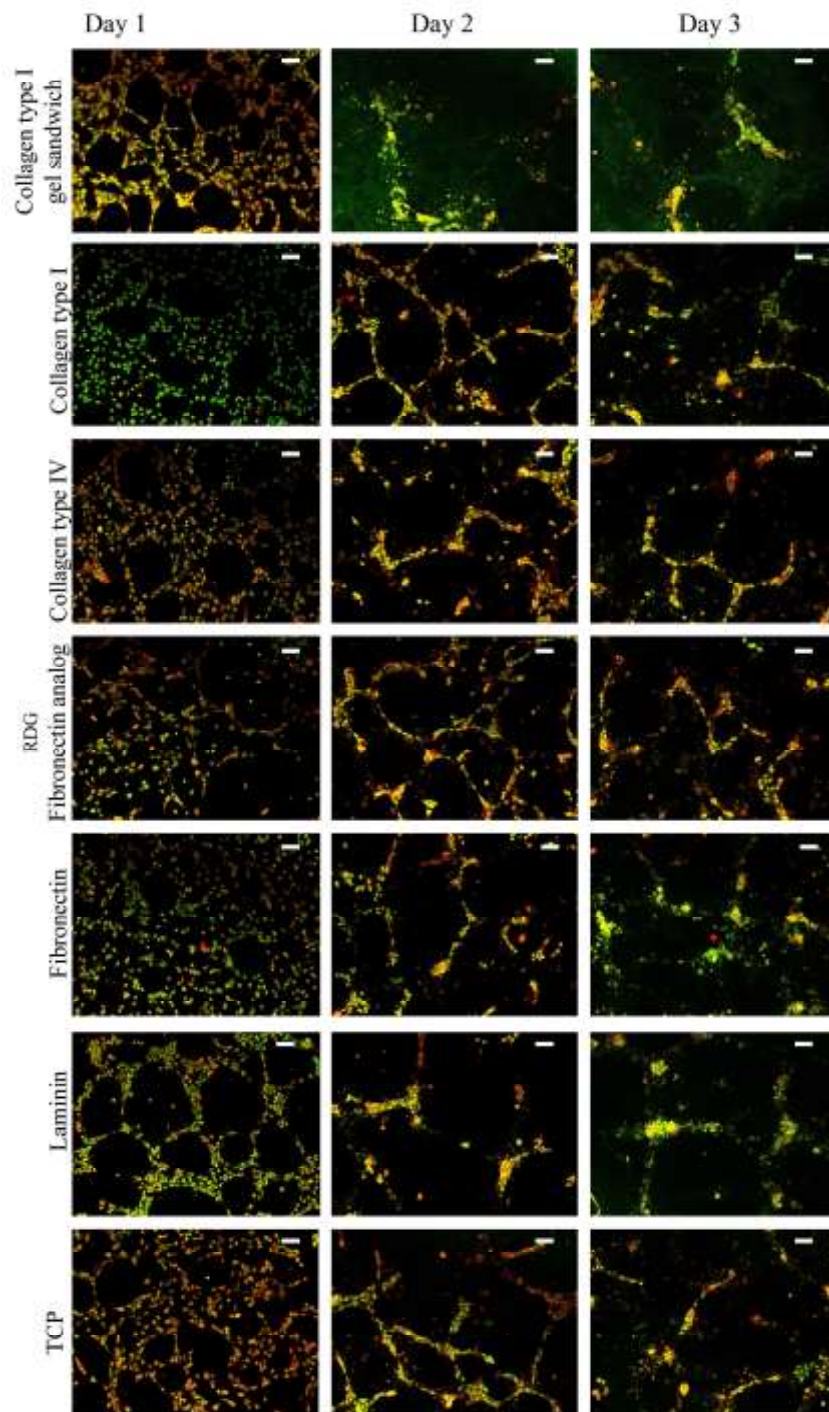


Figure 8 LEC tube formations on various biomaterial surfaces with collagen type I hydrogels

Images show tube formation of LECs on different biomaterial substrates layered with collagen type I hydrogel. LECs were stained with Acridine Orange. Viable cells display a green nucleus. Their morphology and viability was observed over 3 days. Images were taken with a Zeiss fluorescence microscope at 10x magnification, scale bar = 50 μ m.

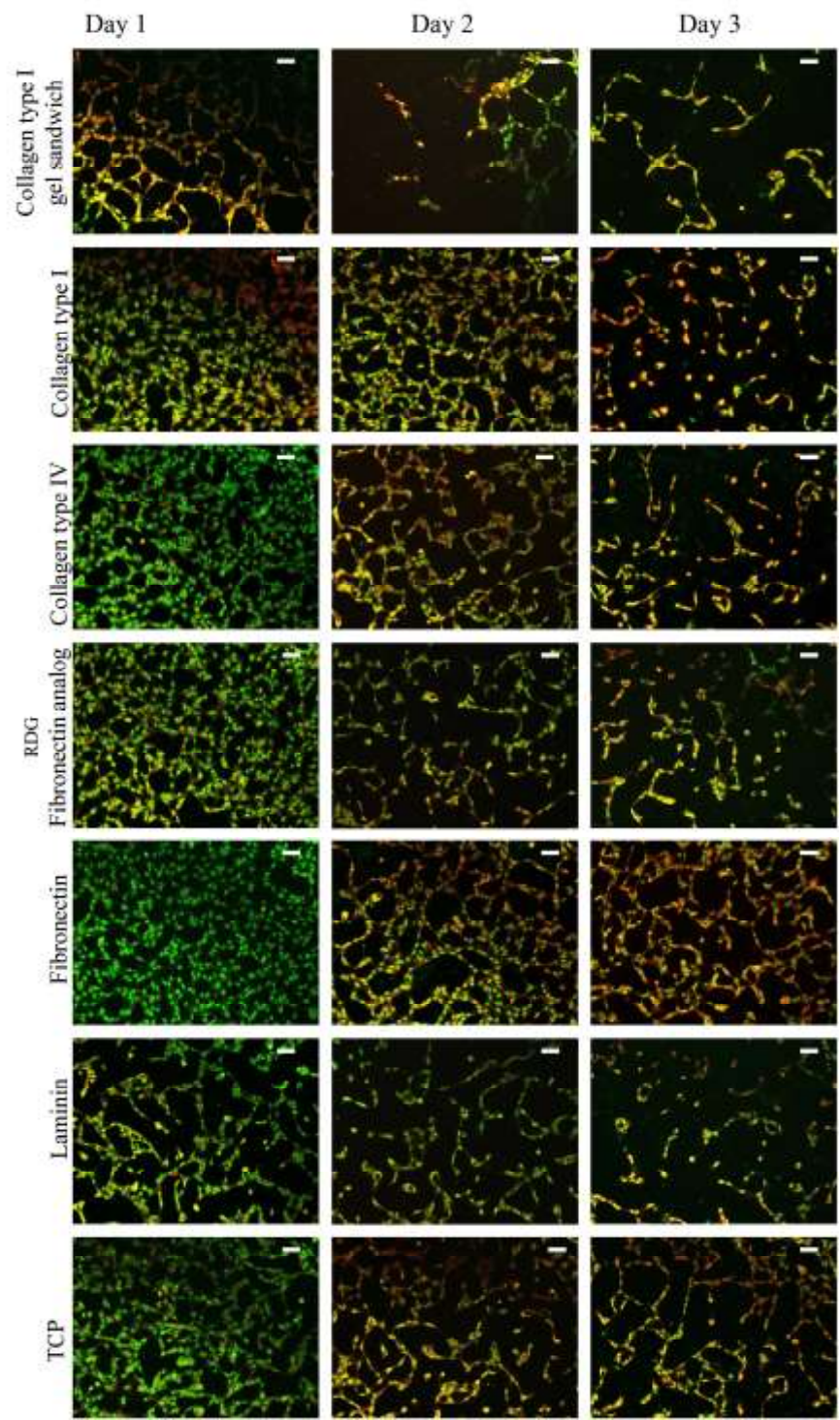


Figure 9 LEC tube formations on various biomaterial surfaces with fibrin hydrogels

Images show tube formation of LECs on different substrates layered with fibrin hydrogel. LECs were stained with Acridine Orange. Viable cells display a green

nucleus. Their morphology and viability was observed over 3 days. Images were taken with a Zeiss fluorescence microscope at 10x magnification, scale bar = 50 μ m.

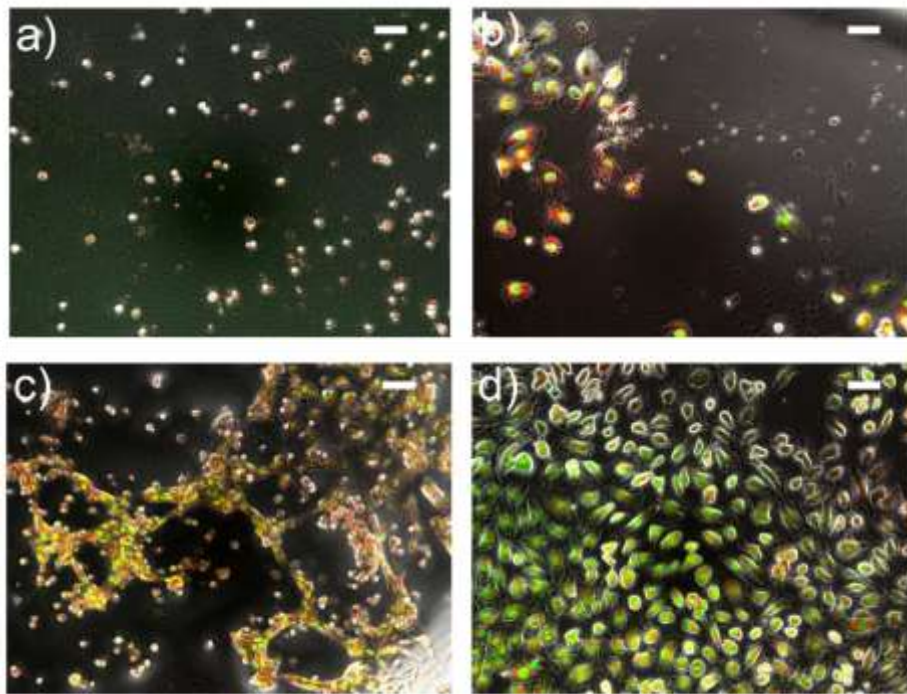
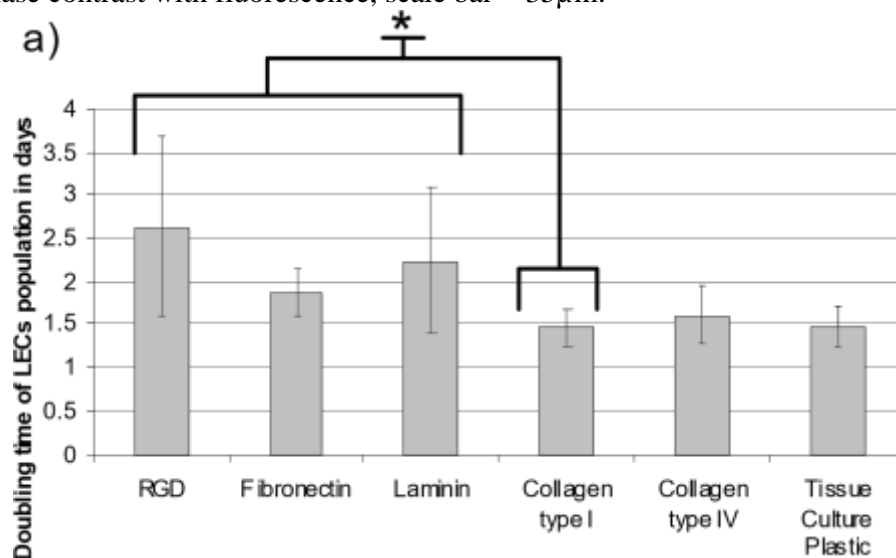


Figure 10 LEC attachment to Hyaluronate hydrogels

Images show LECs stained with Acridine Orange 24h after seeding onto Hyaluronate hydrogels (a), Hyaluronate hydrogels blended collagen type I at 1:1 ratio (b) and hyaluronate hydrogel blended with collagen type I 1:20 (c). Image (d) shows LECs covered with hyaluronate hydrogels after 24h (d). Images are combined images of phase contrast with fluorescence, scale bar = 35 μ m.



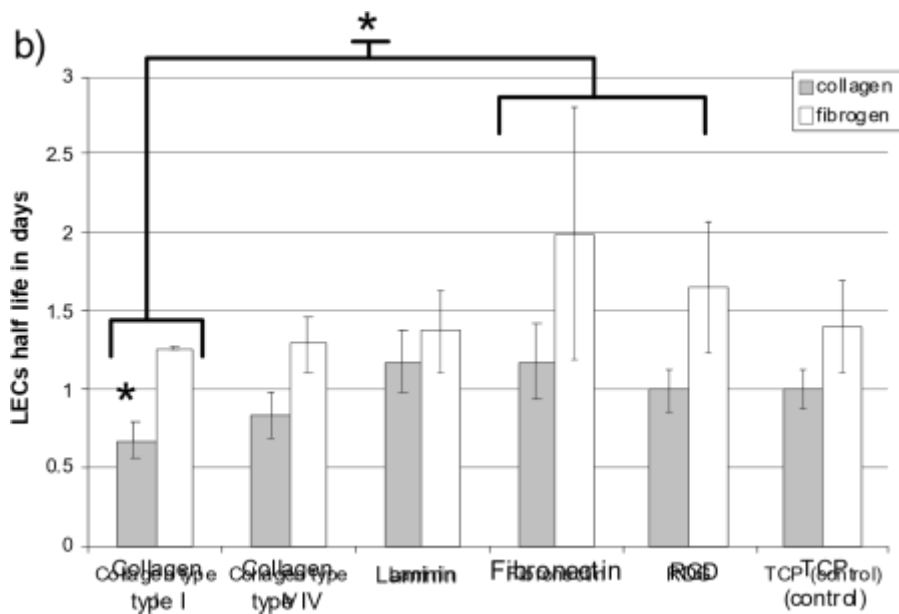


Figure 11 Population doubling time and half life of LECs on various surfaces in collagen type I and fibrin matrix

Chart (a) shows the population doubling time in days of LECs on RGD, fibronectin, laminin, collagen type I and IV. Significant differences between RGD, fibronectin and collagen type I ($p < 0.05$). The difference between laminin and collagen type I is $p < 0.15$. Chart (b) shows the half life in days of LECs on the same biomaterial surfaces when covered with collagen type I and fibrin hydrogels. Half life is significantly decreased with collagen type I hydrogels, especially on collagen type I surfaces when compared to the other groups ($p < 0.05$). Half life with fibrin hydrogels is more stable across the groups. Fibronectin, RGD surfaces are significantly slower decaying compared to collagen type I surfaces ($p < 0.05$).

2.3.3 LEC co-culture with fibroblasts

3T3 Fibroblasts of mouse origin were tested in BME and EMB-2 media with and without collagen type I matrix. Fibroblasts were apoptotic after 5 days in culture in BME medium, whereas EMB-2 medium provided cell growth and high viability similar to control (Figure 12 a, b). Addition of a collagen type I hydrogel layer onto the fibroblasts in BME medium rescued cells from cellular death (Figure 12 b). However, the cell growth remained significantly below the DMEM control (Figure 12 a). It has been shown here that mouse 3T3 fibroblasts in EMB-2 medium

with/without collagen type I hydrogel are viable and functional. Hence, LECs in coculture with 3T3 mouse fibroblasts with collagen matrices and basal media provide a suitable condition to co-sustain both cell populations.

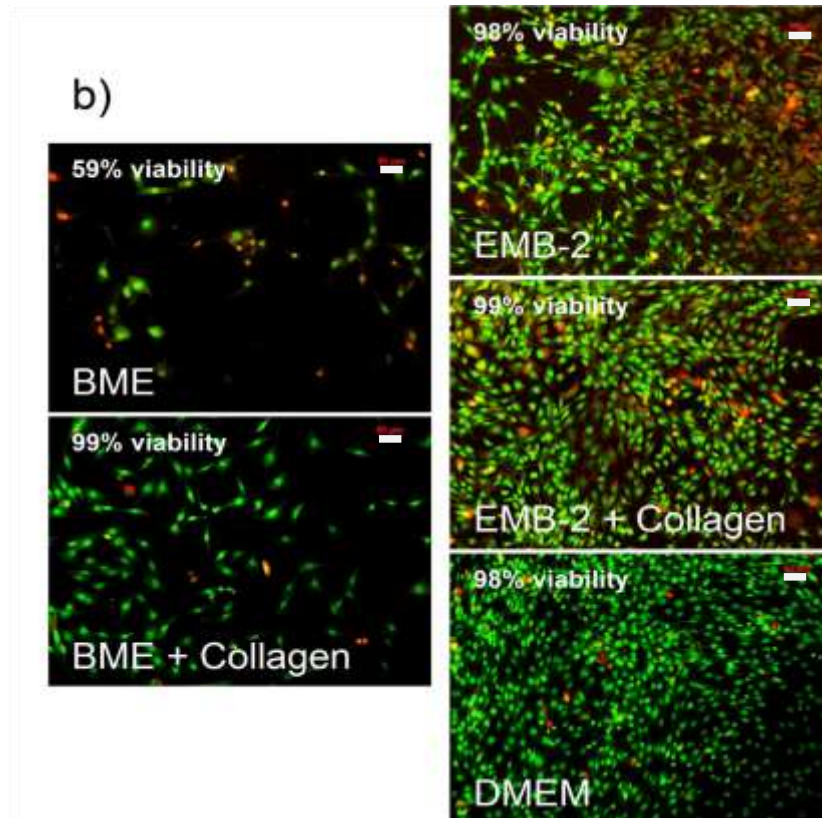
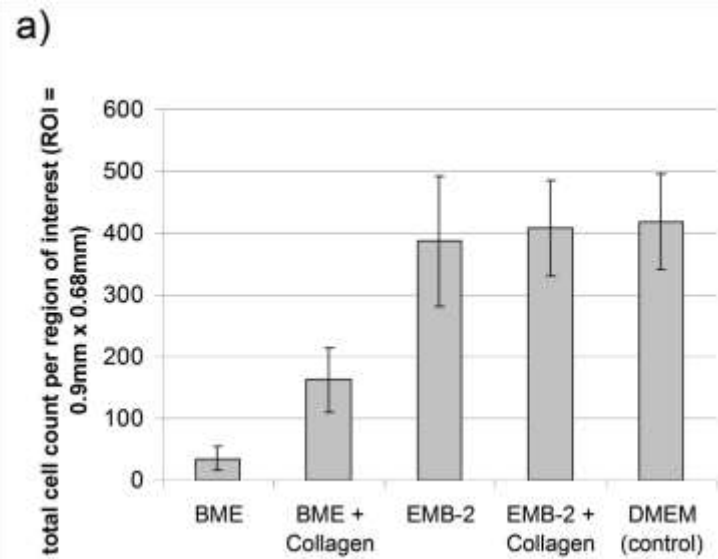
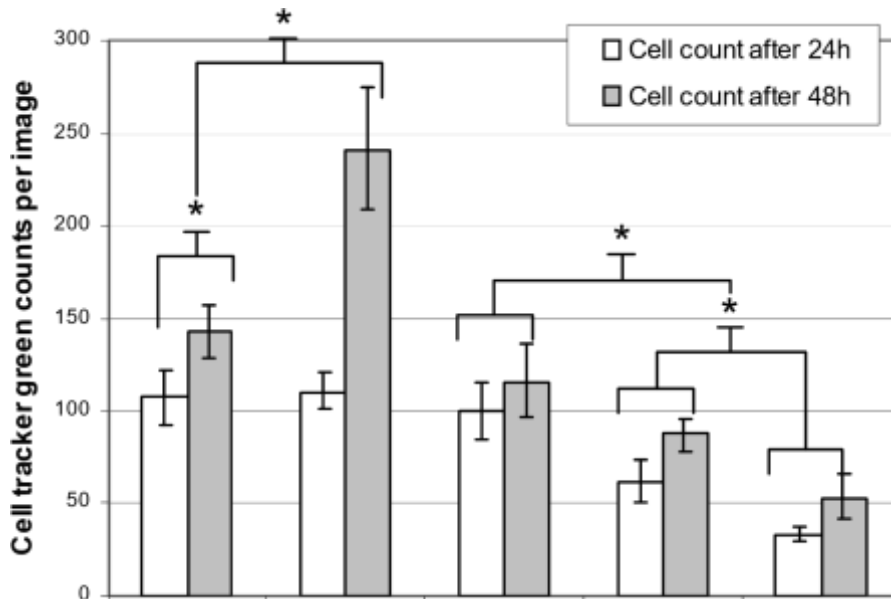
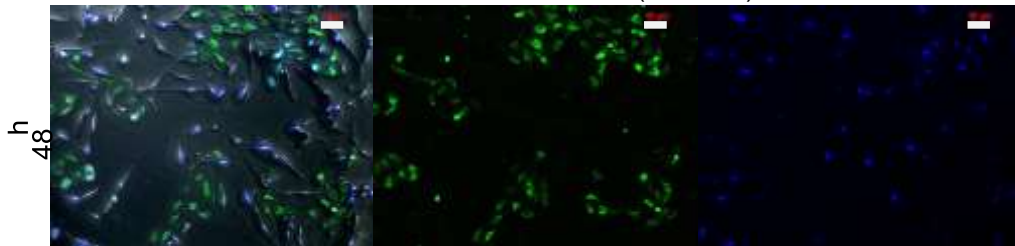


Figure 12 Mouse 3T3 fibroblast culture under endothelial conditions

The chart shows the viable cell count of 3T3 mouse fibroblasts in BME, DMEM and EMB-2 medium with and without 100 μ g/ml collagen supplementation after 3 days in culture. Cells were stained with Acridine Orange and Propidium Iodide staining. Images were taken with an epifluorescence microscope. Viable cells are indicated by green cell nucleus, whereas dead cells are indicated by red cell nucleus. Bar = 50 μ m

Cell Tracker Green labelled LECs and 3T3 mouse fibroblasts were cultured together for up to 48 h. Both cell types attached and grew in co-culture together expressing their unique morphology; LECs showed colonies and cobblestone morphology, whereas fibroblasts were spindly shaped with elongated filopodia (Figure 13, images). Interestingly, DAPI staining is always present in fibroblasts, but rarely in LECs. Fibroblasts and LECs were seeded in 3 ratios: 1:10, 1:4 and 1:1. The experiments showed that the more fibroblasts were present the fewer LECs cells attached to the surface (Figure 13, chart). LEC growth did not seem to be either significantly inhibited or significantly increased in direct co-culture within the first 48h compared to control. However, separation of LECs from direct contact with 3T3 fibroblasts with a 3mg/ml collagen type I gel layer resulted in a growth boost (Figure 13, chart) after 48h. Collagen itself did not increase LEC growth when compared to tissue plastic surfaces (Figure 11, a). The result might indicate a paracrine contribution from fibroblasts stimulating the LEC growth. The collagen type I matrix supported survival growth of fibroblasts in endothelial cell media. Hence, growth factors excreted by fibroblasts would increase and affect LECs more strongly. It remains questionable whether juxtacrine factors would have the same effect on LECs in the presence of a collagen type I matrix, or whether fibroblast-endothelial cell contact would restrict the LEC growth.

Co-culture of LECs with 3T3 mouse fibroblast (ratio 4:1)



Control (LECs)	LECs separated from fibroblast collagen gel	Co-culture 10% fibroblast by seeding	Co-culture 25% fibroblast seeding	Co-culture 50% fibroblast seeding
-------------------	---	---	--	--

Figure 13 LECs and 3T3 mouse fibroblast co-culture growth and attachment

Top images centre row show LECs (green) stained with Cell Tracker Green cocultured with 25% fibroblasts after 48h. Images left column show cell nuclei stained with DAPI for all fibroblasts and a few LECs. Images right column are combined images of phase contrast with fluorescence green and blue. Scale bar equals 50µm. The chart shows the total cell count of Cell Tracker Green positive LECs after 24h and 48h. Cells were seeded in different ratios in direct co-culture as well as in coculture where LECs and 3T3 mouse fibroblasts were physically separated by a collagen type I gel layer. Statistical significance is indicated with $p < 0.05$

In a further experiment Cell Tracker Green labelled LECs were seeded with 3T3 mouse fibroblasts at a ratio of 1:4 together in co-culture. Tube formations of LECs were induced with a collagen type I solution (100µg/ml) in EMB-2 medium. LECs formed tube-like formations within 24h (Figure 14). Again fibroblasts stained strongly for DAPI compared to LECs, and after 48 DAPI staining was missing with LECs. Thereafter, LECs number decreased whereas 3T3 mouse fibroblasts grew increasingly to fully confluent within 6 days. On day seven, tube forming LECs were missing. 3T3 mouse fibroblasts in direct co-culture with LECs did not arrest LECs from apoptosis when cultured in EMB-2 medium with a collagen type I matrix.

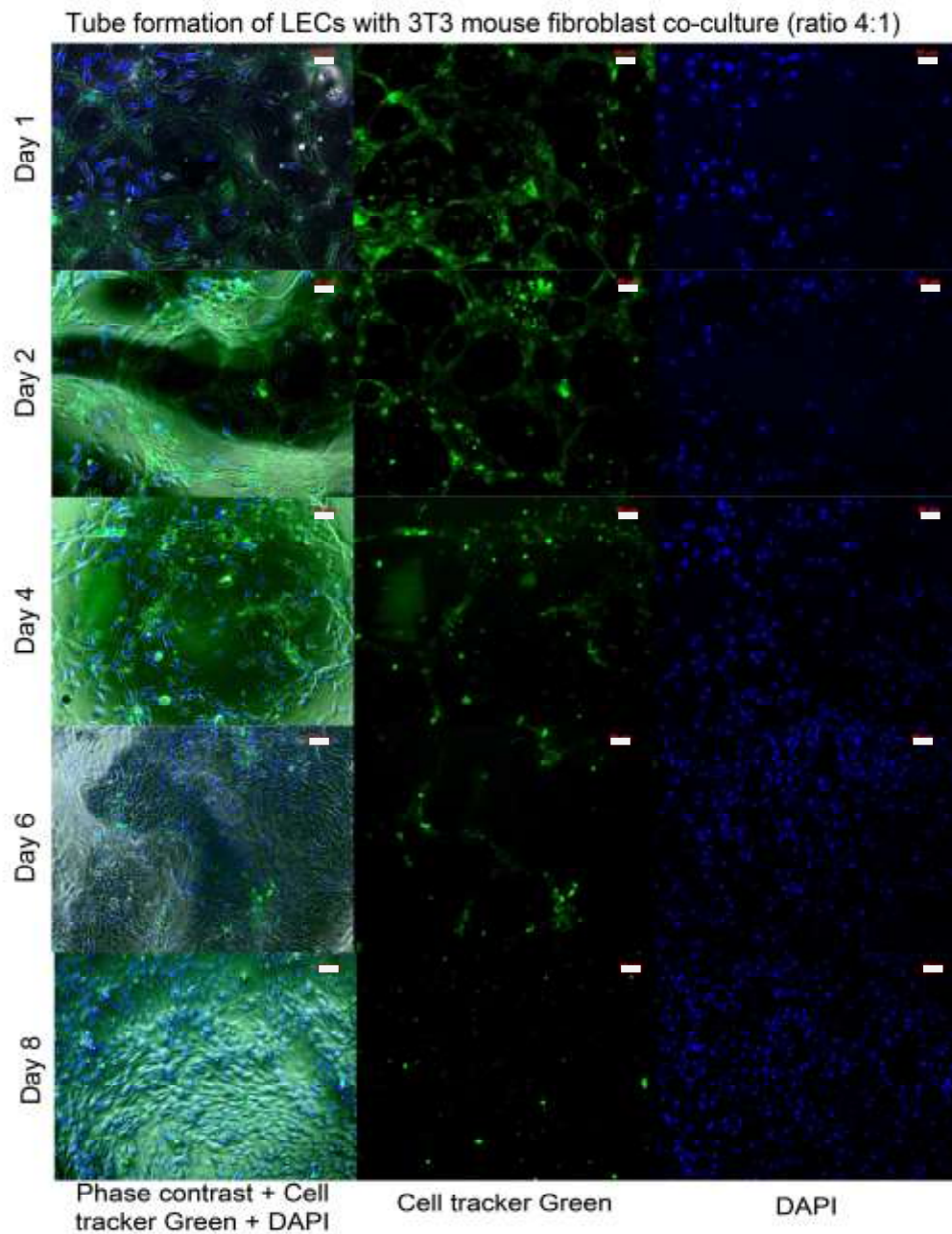


Figure 14 Tube forming LECs in direct co-culture with 3T3 mouse fibroblasts
 The centre row shows fluorescence images of LECs (green) stained with Cell Tracker Green co-cultured with 25% fibroblasts after 48h. The right column shows the fluorescence images of cell nuclei stained with DAPI (blue). Images of the left column are combined images of phase contrast with fluorescence stains green and blue. Bar equals 50µm
 In the next experiment LECs and 3T3 fibroblasts were co-cultured together, but separated from direct physical contact by a thin collagen layer. Tube-like formations

of LECs were induced by a second layer of collagen type I gel. It was observed that at low fibroblast (3×10^4 Cells) to LEC (1.2×10^5 cells) concentration (1:4) a growth in 3T3 fibroblasts (Figure 15, a) and a decay of LECs (Figure 15, b) occurred. On day seven, tube-like structures of LECs were degraded. Raising the fibroblast concentration to 1×10^6 cells by blending fibroblasts into the collagen matrix showed viable tubular LEC formation at day 7 (Figure 15, c). Although a high number of propidium iodine stained cells were observed in the LEC layers (Figure 15, c), the remaining structures were not degraded and seemed to proliferate slowly (Figure 15, d). This experiment could not be repeated in BME medium, but was observed only in EMB-2 medium.

Although this experiments indicates that LECs require a growth factor contribution in addition to co-culture in order to maintain tubular structures, it remains unclear at which fibroblast concentration LECs can be supported most efficiently.

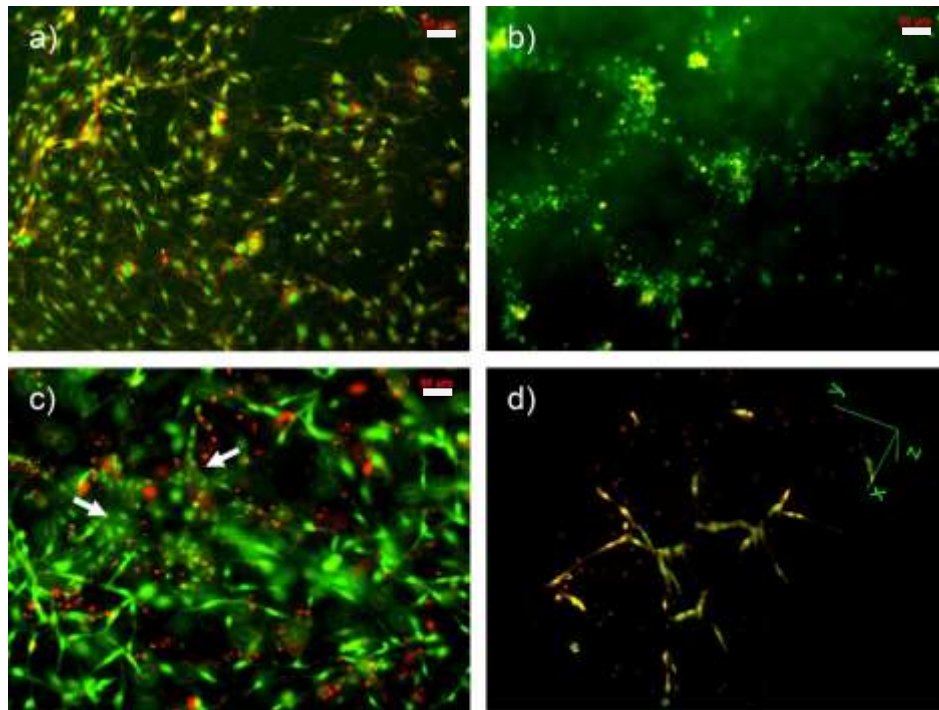


Figure 15 Tube forming LECs in 3D co-culture with 3T3 mouse fibroblasts

Images show collagen type I hydrogel co-culture of fibroblasts(a) and (c) and LECs (b) and (c) after 7 days culture in EMB-2 medium. Upper images were cultured with a low fibroblast and high LEC concentration (1:4). Bottom images were cultured with a high fibroblast and low LEC concentration (8:1). Images were stained with Acridine Orange (green) and Propidium Iodide (red). Fluorescence images show live (green) and dead cells nuclei (red). Image (c) shows LECs (arrow) in close proximity to fibroblasts. Image (d) shows the intersection of tube-forming LECs in collagen type I hydrogel in a 3D fluorescence image stack. Bar equals 50µm.

2.4 Discussion

2.4.1 LEC characterisation *in vivo* and *in vitro*

Characterisation of the lymphatic endothelium has been challenging in the past. With the establishment of Prox-1 as a general marker for the lymphatic lineage, research in lymphatic tissue progressed. Prox-1 was verified against podoplanin and LYVE-1 as the only specific marker for lymphatic tissue and endothelial cells *in vitro*. Nevertheless, markers such as Podoplanin and Lyve-1 can be used as co-stains to support lymphatic characterisation. However, neither podoplanin nor Lyve-1 has the capability to identify lymphatics exclusively. Not only are these markers expressed on other cells (Table 1) but it has been shown that expression profiles change during maturation of lymphatic vessels. Expression of Lyve-1 on mature vessels is generally less [121], and was nearly undetectable in stained vessel tissues. Prox-1 is an early indicator of lymphatic commitment during development. Although it is expressed to a lesser extent on mature cells [63], its expression remains throughout the entire lymphatics. The importance of Prox-1 was demonstrated in experiments by Petrova and colleagues (2002), where blood vascular endothelial cells (BEC) were reprogrammed with Prox-1 to express a lymphatic phenotype [122]. Their results demonstrated that Prox-1 not only revealed lymphatic identity but also its physiologically important aspect. The loss of Prox-1 therefore correlates with the

loss of lymphatic phenotype and functionality. The experiments reported in this thesis showed that LECs embedded in collagen type I lost their Prox-1 expression within 24h, followed by a slow cellular degeneration over 3 to 5 days, indicated by decline of viable LECs and cell debris accumulation. It can be theorised that Prox-1 predicts a loss of lymphatic functionality prior to morphological changes and most likely prior cell death and apoptotic signalling. Hence, Prox-1 could be used as a tool to predict early onset of lymphatic apoptosis. Further experiments would be required to verify whether prox-1 deactivation is linked to the apoptosis signalling pathway. If that is the case, Prox-1 could be used as diagnostic tool in tissue engineering and medicine. Further manipulations of Prox-1 expression might reveal a possibility to increase the robustness of LECs in 3D *in vitro* culture.

2.4.2 LECs growth and tube formation in hydrogels

The *in vitro* culture of LEC monolayers does not represent the native state of functional lymphatic vessel. It is known that the surrounding ECM is essential for LECs, because they generate relatively little matrix compared to other endothelial cell types [82]. Therefore, it was proposed that the provision of ECM proteins *in vitro* would provide the basis for a functional morphology resembling the native state of initial lymphatics. LECs have been shown to assemble into tubular like structures once exposed to collagen type I hydrogels, matrigel[®] or fibrin hydrogels [33]. The mechanism of new tube or vessel formation, tubulogenesis, is initiated by integrin attachment to the ECM structural proteins such as collagen type I [52]. Moreover, LECs need to overcome the restriction imposed by a two-dimensional environment, - on coated surfaces with collagen type I, VI, laminin and fibronectin LECs do not form tube like formations. A 3D matrix, which surrounds LECs providing the

necessary binding cues, is thought to induce tubular assembly of LECs. However, without the appropriate growth factors, such as VEGF-C, LECs become apoptotic, or are incapable of infiltrating hydrogels. It has been shown that addition of FGF-2 (10ng/ml), VEGF-A and -C (>100ng/ml) supports LECs tube formation and neof ormation of vessel-like structures in various 2D and 3D collagen type I hydrogel culture models [123]. Neo lymphatic vessel formation is described as lymphangiogenesis. Lymphangiogenesis is induced by the ligands of vascular endothelial growth factor receptor-3 (VEGFR-3) [124]. However, simple tube formations *in vitro* do not require VEGF-C supplementation, although VEGFR-3 activation via VEGF-C is required for cellular survival and functional maintenance [54]. Commercially available endothelial expansion medium does not include VEGF-C, only 2-4ng/ml VEGF-A and <8ng/ml FGF-2 (Lonza, communication), therefore, it seems not appropriate for 3D collagen type I culture of LECs. Conditions to form tubular structures were tested mostly in collagen type I hydrogels. The different effects of other ECM structural proteins on tube formation induction and maintenance have not been tested intensively.

Hyaluronan is a network of hydrophilic polymer chains consisting of non-ionic glycosaminoglycans. Unlike collagen and fibrin, most cell-hyaluronan functions require binding to non-integrin cellular receptors such as LYVE-1, RHAMM or ICAM-1 [125]. Hyaluronan function is associated with increased cellular migration and metabolism. Receptors, such as ICAM-1 which are expressed by lymphatic cells mediate migration via integrin binding sites [126]. However, LEC on hyaluronan hydrogels showed impaired attachment and tube formation. Similar results have been shown earlier, where outgrowth of LECs was impaired by hyaluronan surfaces [127].

Hyaluronan is metabolised quickly by LECs via Lyve-1 receptor [98], therefore it can be assumed that attachment to this structural glycoprotein is reduced over time as it is metabolised by lymphatic endothelial cells. Cellular tube formation, migration and attachment are regulated via specific integrins. The amount of integrin attachment sites towards a surface matrix is critical to cellular survival. Loss of attachment leads to cellular death. Lymphatic endothelial cells degrade hyaluronan. Therefore, hyaluronan hydrogels fail as a suitable matrix for LECs as they lose their functions to provide a structural matrix for attachment and migration.

Fibrin hydrogels provided a suitable matrix for lymphatic tube formation under the experimental conditions used. The integrin binding towards the RGD sequences in the fibrin matrix is thought to induce lymphatic tube formation in a similar mechanism to collagen induced tube formations. However, the outcome differed from the structures observed with collagen type I matrices. In the experiments, the resulting structures in fibrin hydrogels displayed a morphological change of an irregular network and visually narrowed lumen of partially blind-ended tubes. The observed vessel network morphology was similar to the native structure of initial lymphatic vessels illustrated in literature [128]. LECs express ECM components such as laminin [110], fibronectin [95], and are enclosed in a matrix structure mainly composed of collagens [128]. This demonstrates that LECs are not exposed directly to collagen type I and recognise laminin and fibronectin as their native basal matrix. Moreover, it was shown earlier that lymphatics organize best in soft fibrin rich matrices compared to collagen matrices [33]. In this study growth and decay of LECs was examined on biomaterials with and without 3D matrices. Collagen type I matrices increased proliferation and cellular metabolism, but reduced the half life of

cells in 3D structures. Integrins for collagen type I are expressed during cellular processes of inflammation and wound healing [94]. This process coincides with the presence of VEGF-C excreting monocytes [14]. VEGF-C attracts LEC migration, promotes growth and supports their invasion into collagen rich matrices. Therefore, collagen type I matrices might be suitable for rapid formation of LECs neo-vessels, accelerated migration and high metabolism/proliferation. However, these matrices fail without the necessary growth factor support.

Fibrin hydrogels extended LECs survival in tubular structures compared to collagen type I hydrogels. It has been shown here that the native ECM of lymphatic vessels may provide better survival cues for LECs in 3D hydrogel culture. Although, fibronectin/fibrin matrices had the greatest potential to support LECs tubular structures, all matrices failed to support lymphatic tubular structures in vitro without the presence of additional growth factors. This indicates a central role for growth factors contribution in lymphatic tissue engineering, but the dynamics between matrix and growth factors are yet to be understood.

The work in this thesis correlates with similar findings by Helm et al. 2007 [33].

Moreover, the experiments show exclusively that the morphological differences of LEC tubes in collagen type I and fibrin matrices resemble a native like phenotype and morphology in fibrin/fibronectin matrices only.

2.4.3 LEC co-culture with fibroblast

The lymphatics share their microenvironment with adjacent cells such as smooth muscle cells, monocytes and dendritic cells. These cells are in direct cell-cell communication via juxtacrine and paracrine exchange. Moreover, LECs are

influenced via paracrine exchange by other cells such as fibroblasts, adipose cells and vascular endothelial cells in the distal ECM, as reviewed by various authors [34,98]. The complex structural and cellular environment is essential and supports functionality of most tissues including the lymphatics via growth factor excretions of adjacent and proximal cells (juxtacrine and paracrine) and EMC deposition [8,129]. It is known that monocytes support growth and invasion of LECs by VEGF-C excretion [14]. Vascular endothelial cells also contribute by matrix deposition and growth factor release to lymphangiogenesis during wound healing [130]. The influence of fibroblasts has not been studied within lymphatics. Fibroblasts supplied as a feeder layer support many cell types in their physiological aspects during cell culture (e.g. epithelium). However, direct co-culture with fibroblasts restricts LECs in their attachment as shown in the experiments. Further, survival of LEC tube-like formations was not supported by fibroblasts. Although direct co-culture seems not to be beneficial in creating an environment for lymphatics in in vitro culture, the development of non penetratable layers by LECs with fibroblast-collagen type I sheets can become a useful tool in advanced tissue engineering.

A different co-culture approach has shown beneficial properties for LECs in 3D collagen type I matrices. LECs co-cultured with fibroblasts with physical separation by a collagen type I hydrogel layer showed growth increase and survival in collagen type I matrices. 3T3 mouse fibroblasts excrete FGF-2 among other growth factors and have been shown to support vascular growth in collagen type I matrices [131], therefore it is possible that paracrine signalling by fibroblasts provided beneficial support for the lymphatic structures in the collagen type I culture. Nevertheless, fibroblasts seem not to be an appropriate cell type to support LECs in co-culture by

paracrine stimulation. First, a high number of fibroblasts is required to support LECs in endothelial cell expansion medium EMB-2. Although these cells survive for 7 days, large quantities of cell debris and death cell are observed in the proximity of LECs. Further, EMB-2 provides additional growth factors for lymphatic expansion, which were essential for LECs survival. It seems that fibroblasts have a minor effect on physiological stability of LECs in collagen type I culture. Therefore, other proximal cell types such as monocytes or adipose cells are suggested as appropriate to develop and maintain LEC tubular structures *in vitro* without additional growth factor supplementation. Moreover, the introduction and combination of matrices such as fibronectin/fibrin with proximal cells types and collagen might be a promising approach to address LEC survival in 3D hydrogels on many different levels; juxtacrine, paracrine and stimulation by multiple ECM cues.

2.5 Conclusions

The results presented here suggest how LECs can be characterised with immunofluorescence markers LYVE-1, Podoplanin and Prox-1 on tissue sections and in cell culture. Further, the influence of biomaterials and hydrogels in lymphatic cell *in vitro* culture was evaluated with regard to cellular growth, tube formations and morphological changes. Last, an approach to generate a co-culture was demonstrated with LECs and fibroblasts.

Characterisation has shown that Prox-1 is a reliable marker for lymphatic vessel tissues as well as a cellular marker during LEC culture. Podoplanin co-stained fibroblasts *in vitro*, and vascular endothelial cells in tissue sections. Co-staining with Podoplanin and Prox-1 was sufficient to identify lymphatic tissue. LYVE-1 was very weakly expressed on lymphatic vessels tissue sections and stained for other cell types

in various tissues such as muscle, fat and interstitium. Thus, Prox-1 is the most relevant of the markers used in lymphatic identification. Moreover, Prox-1 not only identifies LECs on tissue and in cell culture as a single marker, but it also indicates cellular vitality of LECs.

Cell culture of lymphatics is non-physiological, where LECs develop a monolayer of cells instead of a tubular network as observed with the initial lymphatics *in vivo*. In order to convert LECs into a more physiological state *in vitro*, LECs have to be cultured in 3D conditions, within appropriate biomaterials such as fibronectin, fibrin or collagen hydrogels and nourished with appropriate growth factors such as VEGFC to maintain their physiological and functional aspects. A three dimensional matrix is essential for LECs to form tube like structures *in vitro*. The supplied matrix, either collagen type I or fibrin (fibrinogen, fibronectin, RDG based matrices), initiates LECs migration and reorganisation into tubular like structures. Collagen matrices increase the metabolism and growth of LECs compared to fibronectin, fibrin or laminin matrices. Due to a higher metabolism in collagen type I matrices LECs decay rapidly within 4 days if not supplied with a high doses of VEGF-C. Although, fibronectin surfaces do reduce LEC growth slightly when compared to collagen type I surfaces, the decay of LECs in fibronectin/fibrin matrices is significantly reduced. Hence, fibrin/fibronectin matrices are proposed as potential tools for LEC tissue engineering. Nevertheless, none of the tested biomaterials and hydrogel matrices was shown to support LEC maintenance *in vitro* solely. A supplementation of appropriate growth factors such as VEGF-C was always required.

The need to support LEC functionality with growth factors lead to the initial coculture experiments. One aim was to replace growth factors with the help of

growth factor excreting fibroblasts. Fibroblasts are shown to maintain LEC tubular formations for at least 7 days in collagen type hydrogels. Fibroblasts need to be supplied in a high ratio to LECs in order to provide the beneficial paracrine factors. Further, LECs were restricted in their attachment when seeded in close proximity to fibroblasts, growth seems to be reduced and LECs needed an additional minimum supplementation of growth factors to maintain their tubular structures in collagen type I matrices. Accordingly, fibroblasts in combination with collagen type I hydrogels were not suitable to support the LECs functionality sufficiently. Further experiments, which introduce fibrin hydrogel and other growth factor expressing cells, potentially may have a higher success to create an *in vitro* environment where LECs cells can be sustained physiologically and functionally without addition of external growth factors.

Chapter III

Electrospinning and polymer nanofibre properties

Electrospinning and polymer nanofibre properties

3.1 Introduction

A wide variety of materials can be electrospun into nanofibre scaffolds. Biomaterials used for this purpose are either natural polymers such as collagen networks, alginate, chitosan, fibrin and hyaluronic acids or synthetic polymers such as polyglycolic acid (PGA), poly(L)-lactic acid (PLA), poly(DL)lactic-co-glycolic acid (PLGA), polyvinyl alcohol (PVA) and polyhydroxyethylmethacrylate [18]. In this research medical grade PLGA was utilised to generate electrospun scaffolds.

PGA is a biodegradable, thermoplastic polymer and the simplest linear, aliphatic polyester. PLA is also a biodegradable, thermoplastic, aliphatic polyester. Both lactic acid and glycolic acid are polymerized to generate PLGA copolymer. During polymerization, successive monomeric units (of glycolic or lactic acid) are linked together in PLGA by ester linkages, thus yielding a linear, aliphatic polyester as a product (Figure 16). Depending on the ratio of lactide to glycolide, different forms of PLGA can be obtained: these are usually identified with regard to the monomer ratio used (e.g. PLGA 75:25 identifies a copolymer whose composition is 75% lactic acid and 25% glycolic acid. All PLGAs are amorphous rather than crystalline and show a glass transition temperature in the range of 40-60 °C. Unlike the homopolymers of lactic acid (PLA) and glycolic acid (PGA) which show poor solubility, PLGA can be dissolved by a wide range of common solvents, including chlorinated solvents, tetrahydrofuran, acetone, ethyl acetate or hexafluoro-2-propanol (HFIP). Moreover, PLGA has been widely used in various biomedical applications due to its biodegradability, biocompatibility and good mechanical properties [132]. The aliphatic polyesters such as PGA, PLA, polycaprolactone

(PCL), and their copolymers have been approved by the FDA for certain human clinical use such as surgical sutures and some implantable devices.

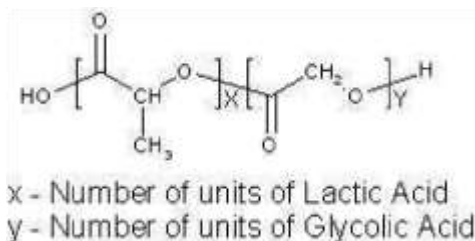


Figure 16 Chemical structure of poly(lactic-co-glycolic acid) PLGA

Controlled biodegradability of the polymer is a welcome if not an essential feature in soft tissue engineering. Biodegradable synthetic polymers include polyesters, polyanhydride, polyorthoester, polycarbonate, and polyfumarate [133]. PLA and PGA co-polymers degrade mainly via enzymatic and/or chemical hydrolysis of the hydrolytically unstable ester bonds into lactic acids and glycolic acids, which are non-toxic and can be removed from the body by normal metabolic pathways. The degradation behaviour depends on the polymer structure and surface properties (e.g. molecular weight, co-polymer composition, crystallinity, and overall material surface) and environmental conditions such as temperature, pH, interstitial flow and polymer/host interactions [101]. Rapid degradation can lead to cell death in culture due to the accumulation of lactic acids [134]. Therefore, the extent of the lactide incorporation in PLGA cannot be too high, as it can produce a highly acidic environment that is not suitable for cellular growth. It has been reported that the maximum amount of the lactide that can be incorporated into the electrospun scaffold without damaging fibroblast cell viability *in vitro* varies around 20 mg per ml cell culture medium [134]. The degradation rate of polyhydroxy acids can be adjusted by changes of the PLA:PGA ratio, the molecular weight of each component, the

crystallinity and other factors in order to slow down the degradation rate [101]. Moreover, hydrophobicity and a low surface roughness of these polymers are critical factors for cellular attachment and growth [135]. However, most of their negative physical properties for cell culture can be adjusted by blends with other (natural) polymers, and physical or chemical treatments [39,135]. PLGAs have limited resistance to loading, as well as limited deformability and elasticity [136]. They do not fully satisfy the scaffold requirements of native soft tissues [136], however, as temporary scaffolds they are a useful tool to administer cells or bio-molecules and are easy to implant compared to hydrogels.

Standard electrospinning is based on a polymer solvent system. The solvent performs two crucial roles in electrospinning. One is to solvate the polymer molecules, ready to form the electrified jet. The other is to carry the solvated polymer molecules towards the collector, then evaporate to allow polymerization towards nanofibres. The right solvent system is important for successful electrospinning.[137]. HFIP is a solvent which fits electrospinning criteria. Polymers once dissolved with HFIP are easier to electrospun than with other solvents (i.e. acetic acid) due to its high conductivity (based on acidity), volatility and good solubility with ionic and non ionic polymers. It was shown that solutions with HFIP lead to a successful electrospinning with nanofibres of PLGA [38]. A drawback of this solvent is its hazardous potential for cells as traces can remain in electrospun fibres.

The properties of the scaffold are controllable via the following process parameters: viscosity of the solvent, the dielectric constant of the solvent conductivity, surface tension of the polymer, polymer molecular weight, the distance between tip and

collector, the flow rate and the strength of the electric field (Table 4). Fibre diameter and morphology is controlled mainly by the polymer composition, flow rate and applied voltage (Table 4) and fibre alignment can be generated by different collector arrangements (see Chapter 4). Electrospinning adjustments can generate synthetic polymers in diameters varying from 3 nm to greater than 5 μm [38]. Although, PLGA has been electrospun in the past, electrospinning settings from other laboratories are not easily transferable, due to equipment changes, environmental influences, especially humidity, and differences in the molecular weight of the polymers. Therefore, all polymers have to be re-evaluated.

Chapter III demonstrates the generation of PLGA polymer fibres between 100nm and 2000nm in diameter. The electrospinning process parameters required for PLGA polymers were evaluated to show the electrospinning limitations of these polymers. Further, the degradation of these polymer fibres with different diameters and PLG-PGA composition was investigated.

Table 4 Effects of changing electrospinning process parameters on the resultant fibre diameter and morphology

Electrospinning Process Parameters	Effect on Fibre Diameter and Fibre Morphology	Reference
Viscosity/ Concentration	Low concentrations/viscosities yielded defects in the form of beads and junctions; increasing concentration/viscosity reduced the defects	[138,139]
	Fibre diameters and fibre uniformity increased with increasing concentration/viscosity	[139-141]
Conductivity/ solution, charge density	Increasing the conductivity aided in the production of uniform bead-free fibres	[140,142]
	Higher conductivities yielded smaller fibres in general	[143]
	Higher conductivities yielded smaller mesh pore sizes	[143]

Surface tension	In general, no conclusive link was established between surface tension and fibre morphology, however, bead formation can be affected by surface tension	[142]
Polymer molecular weight	Increasing molecular weight reduced the number of beads and droplets	[144]
	High molecular weights of the same polymer can produce thinner fibres compared with low molecular weight polymers	[144]
Dipole moment and dielectric constant	Successful spinning occurred in solvents only with a high dielectric constant	[39]
Flow rate	Lower flow rates yielded fibres with smaller diameters in general	[141]
	the opposite effects (high flow rate; smaller fibre diameter) can be observed with some polymers	[18]
	In some cases flow rates did not influence fibre diameter at all	[39]
	Very high flow rates produced fibres that were not dry upon reaching the collector resulting in interconnected nanofibre mats fibres	[140,145]
	High flow rates can also lead to beaded fibre morphologies	[18,141]
Field strength/ voltage	At too high voltage, beading was observed; the polymer jet can split into multiple jets at high voltages which results in beaded and non uniform fibres	[138,140]
	Correlation between voltage and fibre diameter was ambiguous. In general, a voltage decrease led to uniform thick fibres, but some polymers such as PVA showed the opposite behaviour	[139-141]
Distance between tip and collector	A minimum distance was required to obtain dried fibres	[140]
	At distances either too close or too far, beading could be observed	[38]
	Narrow distances produced flat fibres, longer distances generated round fibres	[38]
	The further away the needle was positioned the smaller the fibre diameter in general	[39]

Needle tip design	Using a co-axial, two-capillary spinneret, hollow fibres were produced	[146]
	A smaller needle orifice decreased the fibre diameter	[146]
Collector composition	Smooth fibres resulted from metal collectors, water and methanol surfaces	[140,145]
Ambient parameters	Increased temperature caused a decrease in solution viscosity, resulting in smaller fibres	[140]
	Increasing humidity above 30% can lead to nano structured pores on the fibre surface which increased in size, number and shape	[147]

3.2 Methods

3.2.1 Polymer preparation

Three different polylactide-co-polymer solutions were dissolved in hexafluoroisopropanol (HFIP) (Sigma,UK); a) PLGA (10:90), b) PLGA (50:50) and c) poly(L-lactic)-co-(D-lactic acid) (PLDL) (Purasorb, NL) (Table 5). The solutions were prepared in 10ml glass containers in the exhaust fume cabinet, sealed and agitated with a magnetic stirrer on a magnetic stirring plate for up to 3 days at room temperature prior to the electrospinning process. Properties of the polymers used in these experiments are summarized in Table 5.

Table 5 Properties of the polylactide-co-polymers

Thesis Identity	PURASORB identity	L-Lactide	D-Lactide	Glycolide	inherent Viscosity	Concentrations. (w/v) in HFIP	MW [g/mol] x1000	glass transition temp [C°]	melting temp. [C°]	Degradation times in PBS
PLDL	PLDL 7060	70%	30%		6.0dl/g	5%-2.5%	1,523	55-60	115-125	12-16mth
PLGA (50:50)	PDLG 5010	50%		50%	1.0dl/g	15%-10%	153	45-50	amorphous	1-2mth
PLGA (10:90)	PLG 1017	10%		90%	1.7dl/g	15%-10%	200,	35-45	200-210	6-12mth

3.2.2 Electrospinning Set Up

The electrospinning apparatus consisted of a syringe pump (Harvard Apparatus PHD 2000 infusion, US) and two 30kV high-voltage power supplies (Brandenburg, UK).

The solutions to be electrospun were added to a 5.0 ml plastic syringe (BD Syringe, UK) fitted with a 18 gauge needle (BD Microlance, UK), and loaded into the speed syringe pump. In the standard set up a positive terminal (ground) of the power supply was connected to the syringe needle. The negative terminal of the power supply was connected to a single plate collector assembled from an aluminium plate to collect random fibres (Figure 17, a). The collector was covered with standard aluminium foil, on which the polymer fibres deposited. The electrospinning time was flow rate dependent and varied between 15sec and a few minutes. The electrospinning process was terminated as soon as a white polymer spot appeared on the aluminium sheet. A detailed description of the laboratory set up is included as standard operating procedure (SOP) for the Electrospinning process in the Annex. The three polymers were electrospun under various settings of voltage, flow rate and viscosity (Electrospinning parameters and electrospinning examples: Table 6). After each electrospinning process the aluminium foil was changed and the sample was vacuum dried at 37°C degree for 24h and stored in desiccators under vacuum. A set of 3 to 5 samples were generated per electrospinning setting for the analyses.

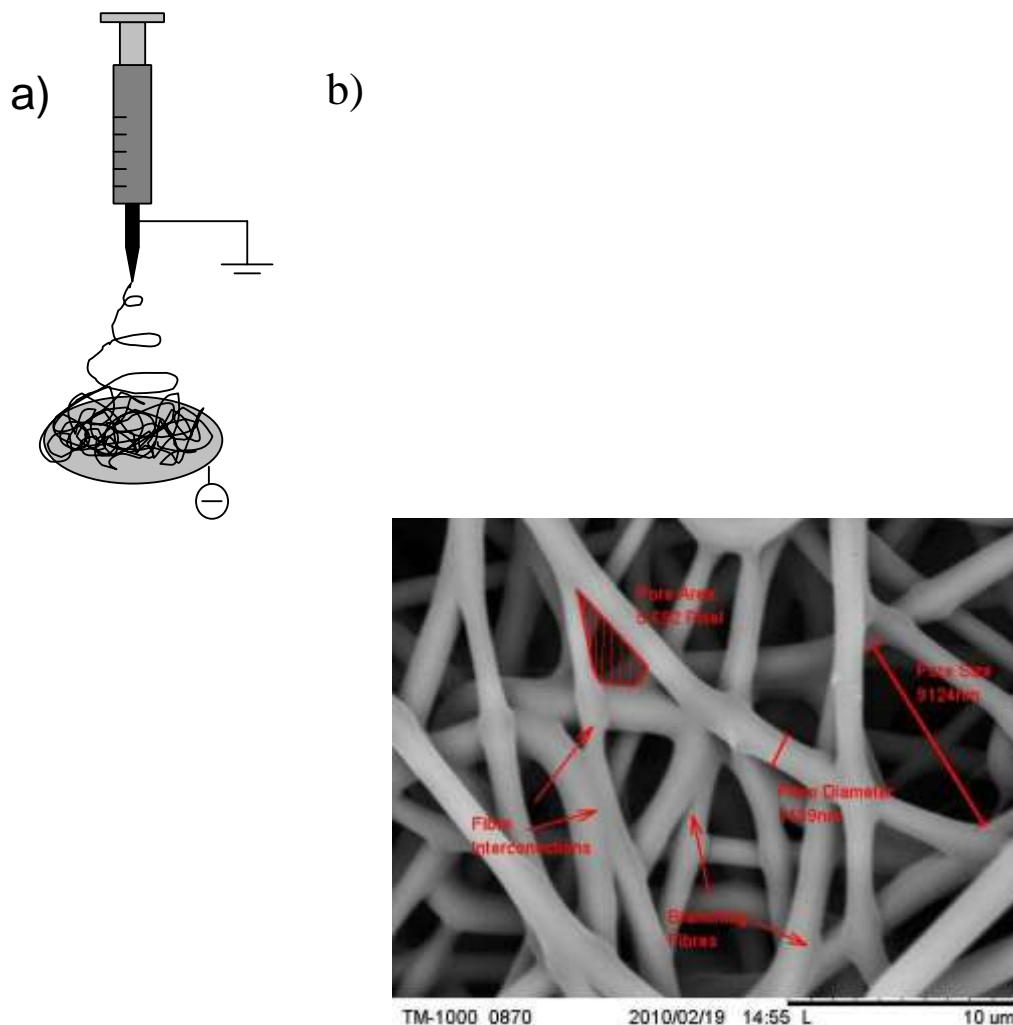


Figure 17 Set up and Measurements

Image (a) shows the schematic of the electrospinning process. A polymer solution was extruded in the presence of an electrostatic field from the needle tip to the negatively charged collector plate. The polymer jet was pulled by the electrostatic field in a whipping fashion towards the negative pole. The solvent evaporated and fibres deposit randomly on the collector plate. Image (b) shows a sample of a SEM image of smooth PLGA (50:50) polymer fibres, which have accumulated on the collector. The measuring parameters (fibre diameter, widest gap between two fibres (pore size), pore pixel area) and morphological specifications are indicated in red.

3.2.3 Electrospun Polymer Degradation

Nanofibre mats of various nano-dimensions were generated with the electrospinning process (Table 6). PLDL, PLGA (10:90) and PLGA (50:50) electrospun samples were peeled off the aluminium foil and cut into rectangles for *in vitro* degradation testing. The samples were dried in a vacuum oven at 37°C, weighed, placed in a

closed containers containing 20 ml of a phosphate buffer solution (PBS; pH 7.4) and incubated *in vitro* at 37°C for 15, (30), 45 and 90 days. After each degradation period, the samples were washed with PBS, dried in a vacuum oven at room temperature for 48 h, and weighed. The weight-loss percentages of the samples were calculated from the dried weights obtained before, and after, degradation. In addition, samples taken on day 15 and 90 were dried and prepared for morphological analyses with surface scanning electron microscopy.

Table 6 Setting range for the electrospinning procedure

Polymer types	Polymer Concentration	Polymer Flow Rate	Voltage	Needle Collector Distance	Humidity (18°)	Fibre Diameter analysed by SEM
Poly(lactide)co-polymers	2.5% - 20% (w/v)	0.005-8ml/h	9-24kV	14 cm	23-35%	50nm - 1800nm
Examples of settings used in degradation experiments:						
PLGA (50:50)	10% (w/v)	1.5ml/h	18kV	14 cm	25%	431nm (+/- 140nm)
PLDL	3.75% (w/v)	0.1ml/h	12kV	14 cm	23%	522nm (+/-68nm)
PLGA (10:90)	10% (w/v)	4ml/h	18kV	14 cm	25%	541nm (+/- 172nm)
PLGA (10:90)	8% (w/v)	0.25ml/h	15kV	14 cm	26%	189nm (+/-88nm)

3.2.4 Surface Scanning Electron Microscopy

The aluminium foil with the deposited electrospun nanofibres was glued to a doubleface carbon adhesive sample holder. The sample was gold sputtered with a sputter coater (Quorum Technologies, UK) for 1.5min at 1.2kV, 40mA under vacuum of 0.1 torr (13.33 Pa). Thereafter samples were analyzed using a bench top scanning surface electron microscope (SEM): Hitachi Analytical TableTop Microscope TM3000 (Hitachi, Japan). The average polymer fibre diameter (vertical diameter across a single fibre), pore size/interspatial fibre distance (widest gap distance between two fibres in the same plane) and its distribution were calculated using the ImageJ® software (Figure 17).

3.2.5 Experimental design and statistical analyses

The fibre diameters of electrospun scaffolds were determined from the SEM images, using ImageJ® software (National Institutes of Health, USA). During the electrospinning process 3 to 5 samples were generated. From each sample 5 random areas of the deposited polymer material were selected and scanned with the surface scanning electron microscope. A total of 15 images were generated for each electrospinning setting. From each image a minimum of 20 fibres were measured. The final fibre diameters and interspatial fibre distances were evaluated from a sample size of 150 to 200 fibres per electrospinning setting, (Figure 17, b). Pore area was measured parallel to pore size as a second reference value. The sample size for pore area and pore size was calculated from the same set of images consisting of 50 to 100 measurements per electrospinning settings. T-test was performed between groups and a p-value below 0.01 was considered significant.

The degradation experiments were performed from 3 individual electrospun samples per group. A triplicate of 3 samples represents polymer group or fibre diameter group. Samples were weighed every 24h over the drying period. Only consecutive constant weights were logged. Statistical tests were performed between several groups with ANOVA or between two groups with Student's t-test. A p-value below 0.05 was considered significant.

3.3 Results

3.3.1 Electrospinning properties of fibre diameter and morphology

Polymer fibres were electrospun over a single collector (Figure 17, a) at 18kV with increasing polymer flow rates. PLGA (90:10), and PLGA (50:50) at 10% weight per volume (w/v) and PLDL at 3.5% (w/v) showed that the higher the flow rate the

thicker the resulting fibre diameter and the wider the nanofibre mesh (Figure 18, a,b). PLGA fibres had a similar fibre diameter increment to each other, whereas PLDL formed thicker fibre diameters at comparable flow rates. PLDL could not be electrospun in micrometer dimensions and showed a fibre diameter maximum of $<1\mu\text{m}$. At flow rates above 0.75ml/h fibres merged together, but PLDL was electrospun to nanofibre dimensions below 50nm (maximal resolution) at flow rates of 0.01ml/h and below. Both PLGA polymers were electrospun to fibres of several micrometers in diameter. PLGA (50:50) with (10% w/v) was limited at the nanoscale dimension at about 250nm fibre diameter and could not be electrospun at very low flow rates below 0.1ml/h compared to PLGA (10:90) which was electrospun to fibre dimensions of under 100nm in diameter. However, PLGA (10:90) did not produce uniform nanofibres at lower flow rates (Figure 18, b). Two fibre populations of very fine fibres below $<200\text{nm}$ diameter and thicker fibres above $>500\text{nm}$ diameter accumulated at the same time during the spinning process. Finer fibres were attached and branched from thicker ones. The population of fine fibres increased with a lower flow rate, whereas the thicker fibres diminished. The overall fibre morphology was smooth and round. Fibres appeared to deposit as a non woven mesh, however, fibre branches and fibre interconnections were observed within all polymers. Fibre branches and interconnections were missing at low flow rates and were shown to increase at higher flow rates. PLDL showed mostly uniform fibres without interconnections of branches at flow rate between 0.01ml/h and 0.1 ml/h compared to the two PLGA polymers.

Polymer viscosity was changed by increasing or decreasing the polymer concentration in the solvent. Increments of 2.5% polymer concentration had huge

effects on the viscous behaviour of the fluids and their processing. PLDL concentrations above 5% (w/v) increased the viscosity to such an extent that it could not be extruded from the needle tip. A higher polymer concentration and viscosity produced thicker polymer fibres in general. Doubling of the PLDL polymer concentration from 2.5% to 5% w/v showed an 80% increase in fibre diameter from 387nm (+/- 52nm) to 696nm (+/-109nm) at the same flow rate of 0.5ml/h. PLGA (50:50) was concentrated at 10% to 15% w/v and showed a 60% increase in fibre thickness from 636nm (+/-140nm) to 1024nm (+/- 148nm) at a flow rate of 0.5ml/h (Figure 19). It was not possible to electrospun PLDL at concentrations higher than 5% w/v, whereas PLGA (90:10) and PLGA (50:50) were spinable at concentrations between 8-20% w/v (Table 6). An increase in fibre diameter of PLDL 2.5% w/v and PLDL 5% w/v was observed at flow rates between 0.01ml to 0.75ml, and showed similar fibre diameter increments to PLGA (50:50) 10% w/v and 15% w/v at flow rates between 0.1ml to 1ml. Fibre diameter increased strongly with high polymer concentration, especially at low flow rates. Electrospun PLDL at 2.5% w/v and 5% w/v showed a 4 fold fibre diameter increase from 101nm (+/- 48nm) to 411nm (+/- 247nm) at a flow rate of 0.01ml/h compared to 0.5 fold increase from 696nm (+/- 109nm) to 917nm (+/- 161nm) at a flow rate of 0.75ml/h. Similar results were observed for PLGA (50:50) (Figure 19).

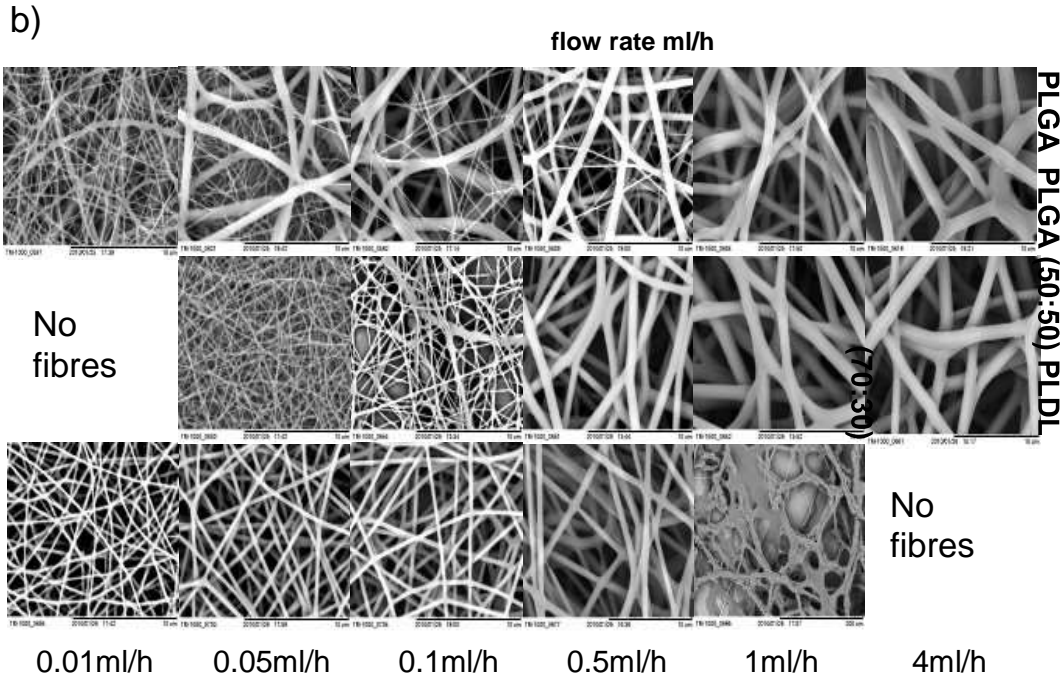
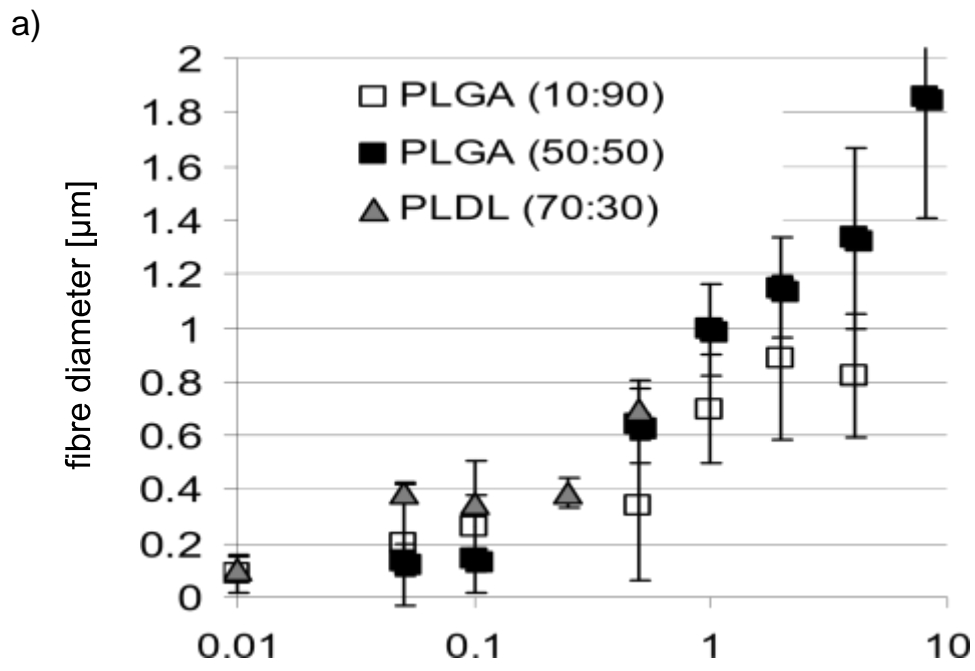
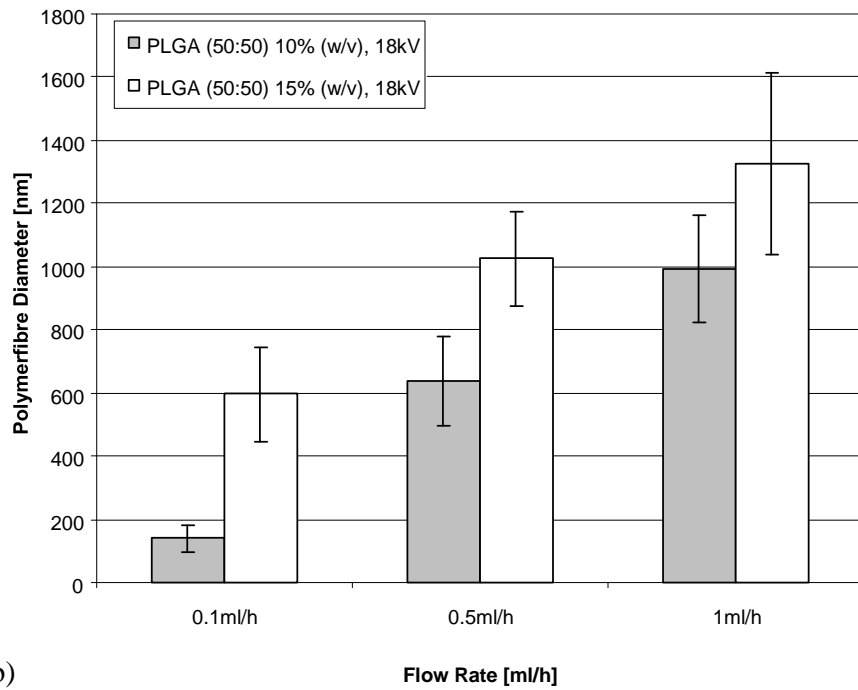


Figure 18 Polymer flow rate and Morphology

PLGA (50:50) 10% w/v, PLGA (10:90) 10% w/v and PLDL (70:30) 3.5% w/v were electrospun at 18kV with different flow rates (a), showed a decrease in fibre diameter with reduced flow rate. The log x-axis for the flow rate shows a exponential correlation between fibre diameter and the increase in flow rate. The scanning electron microscopy images show a round and smooth polymer fibre morphology (b). PLGL (50:50) and PLDL show a uniformly fibre distribution. PLGA (10:90) shows variable

fibre diameters at low flow rates. PLDL shows merged/wet polymer fibre deposition at high flow rates. Scale bar on images is 10 μ m.

a)



b)

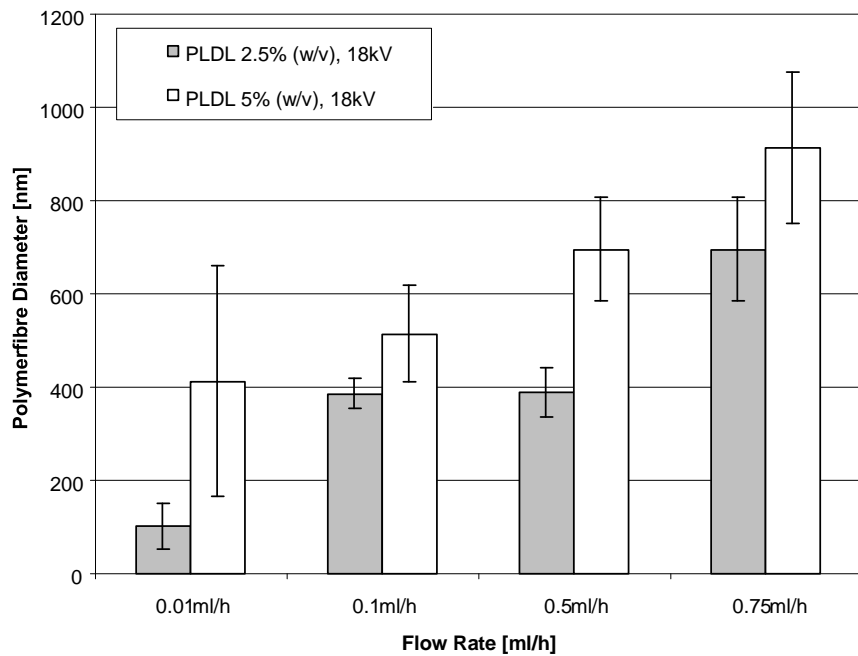


Figure 19 Polymer viscosity and concentration

PLGA (50:50) 10% w/v and PLGA (50:50) 15% w/v electrospun at 18kV with different flow rates (a), showed a decrease in fibre diameter with reduced flow rate

and lower polymer % concentration (a). PLDL 2.5% w/v with a low viscosity and PLDL 5% w/v with a high viscosity electrospun at 18kV with different flow rates showed an increase of fibre diameter with high flow rates (b).

3.3.2 Correlation of pore size and fibre diameter

The polymer pore size or the interspatial distance between fibres was measured at various flow rates. Pore size increased with higher flow rates (Figure 20, a). The interspatial fibre distance increments of electrospun PLGA (50:50) correlated with the increments in fibre diameter. PLGA (50:50) showed an average fibre diameter of 636nm (+/- 140) and an interspatial fibre distance of 2.94 μ m (+/- 1.01 μ m) at set polymer concentration (10% w/v), flow rate (0.5ml/h) and applied voltage (18kV) (Figure 20, b). An increase of the PLGA (50:50) polymer concentration at the same flow rate and voltage from 10% w/v to 15% w/v increased not only the fibre diameter, but also the interspatial fibre distance in the same ratio to each other (Figure 20, b). PLGA (90:10) showed an average fibre diameter of 337nm (+/- 275nm) and an interspatial fibre distance of 2.17 μ m (+/- 0.48 μ m), but correlations between fibre diameter and interspatial fibre distance were difficult to evaluate due to the non-uniform fibre distribution. The broad variations of PLGA (90:10) multiple fibre diameter are shown in Figure 18 (b) and it is also evident that the error bar for the PLGA (90:10) fibre diameter is twice as high as that of the other polymers in Figure 20 (b).

a)

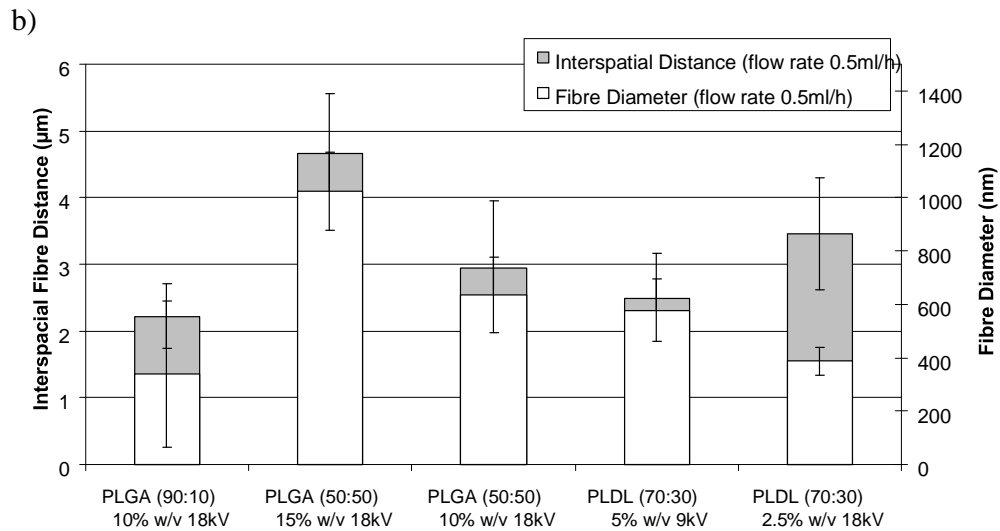
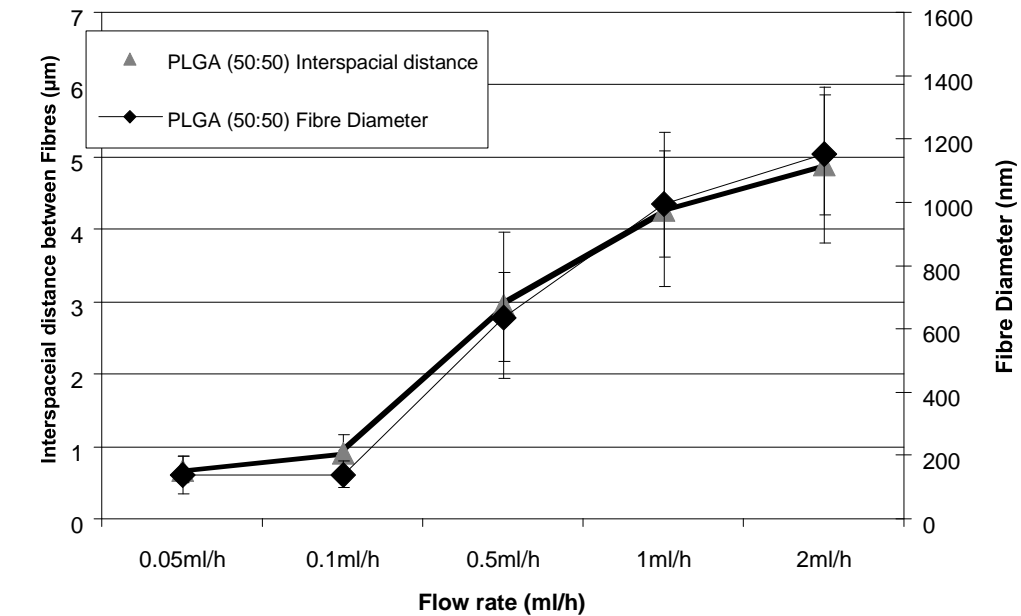


Figure 20 Interspatial fibre distance

Chart (a) shows the increase of fibre diameter and interspatial fibre distance with increasing flow rate. Chart (b) shows the variation of interspatial fibre distance and fibre diameter when the polymer type, polymer concentration and voltage were adjusted.

Applied voltages between 9kV and 18kV affected the fibre diameter (Figure 21). A decrease in voltage from 18kV to 9kV at a flow rate of 2ml/h increased the fibre diameter of PLGA (90:10) in a linear fashion from 606nm (+/- 203nm) to 1066nm (+/-346). In contrast, interspatial fibre distance was reduced at lower voltage (Figure

20, b). PLDL electrospun at 18kV showed an average fibre diameter of 577nm (+/- 117nm) and an interspatial fibre distance of 2.49 μ m (+/- 0.69 μ m). Voltage reduction of 50% to 9kV of the same electrospinning process resulted in an average fibre diameter of 387nm (+/- 52nm) and an interspatial fibre distance of 3.45 μ m (+/- 0.84 μ m).

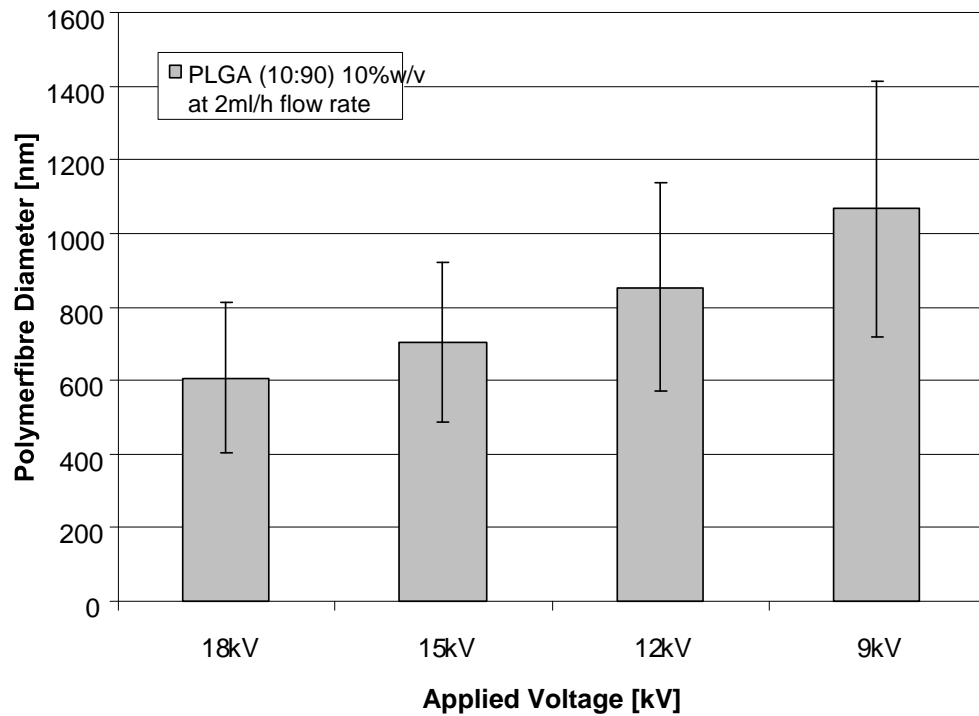


Figure 21 Applied Voltage

The chart shows the fibre diameter increment of electrospun PLGA (90:10) at a stable flow rate of 2ml/h with a decreasing voltage from 18kV to 9kV. The diameter increase is linear with an average increment of ~150nm per 3kV.

3.3.3 Influence of the relative humidity on electrospun polymer fibres

The electrospinning process was strongly influenced by the relative humidity.

Electrospun PLDL fibres at 23% relative humidity showed a rounded and smooth morphology with a fibre diameter below 1 μ m and recognizable interspatial fibre distance (Figure 22, a). At a relative humidity of 35% PLDL fibres were ribbon shaped and mostly flat (Figure 22, b). Their fibre diameter was increased and pore

size was reduced compared to fibres spun at lower humidity. b)

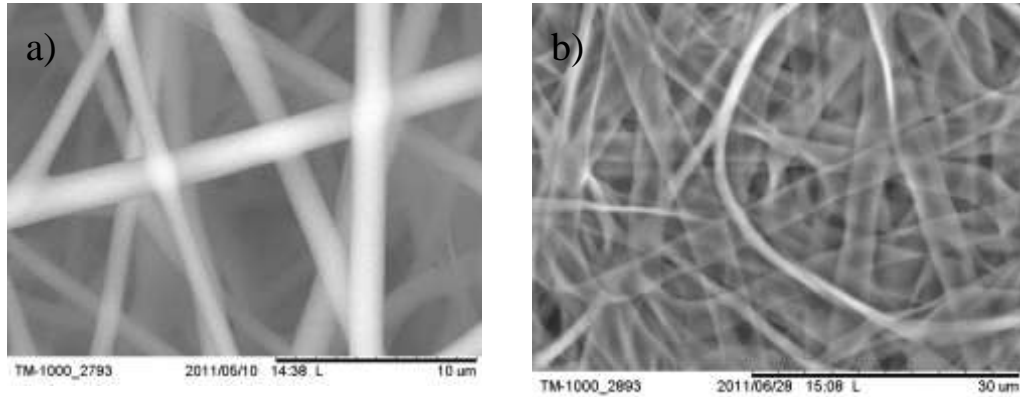


Figure 22 Humidity

The SEM images show PLDL 5% (w/v) fibres electrospun at 12kV with a flow rate of 0.5ml/h at 23% (a) and 35% (b) relative humidity. Polymer fibres show differences in size and morphology; rounded (a) and ribbon like shape (b).

3.3.5 Polymer degradation

PLGA and PLDL degradation properties varied according to the polymer type, molecular weight and fibre thickness (Table 5 and Table 6). Figure 23 shows the weight loss of electrospun PLGA (50:50), PLGA (10:90), and PLDL nanofibre mats with a fibre diameter range of 300-700nm in PBS at 37°C. Additionally the weight loss of PLGA (10:90) with comparable smaller fibre diameters was monitored. The degradation rate of PLGA was higher than that of PLDL. PLDL had no significant weight loss during the first 90 days. During the first 15 days of degradation, PLGA (50:50) exhibited a very slow weight-loss rate. The weight loss of PLGA (50:50) was accelerated after this period. PLGA (10:90) showed a rapid degradation rate without a delayed degradation onset. After 45 days, the residual weight of PLGA (50:50) and PLGA (10:90) was similar to each other. After 90% both polymers had lost more than 50% of their initial weight.

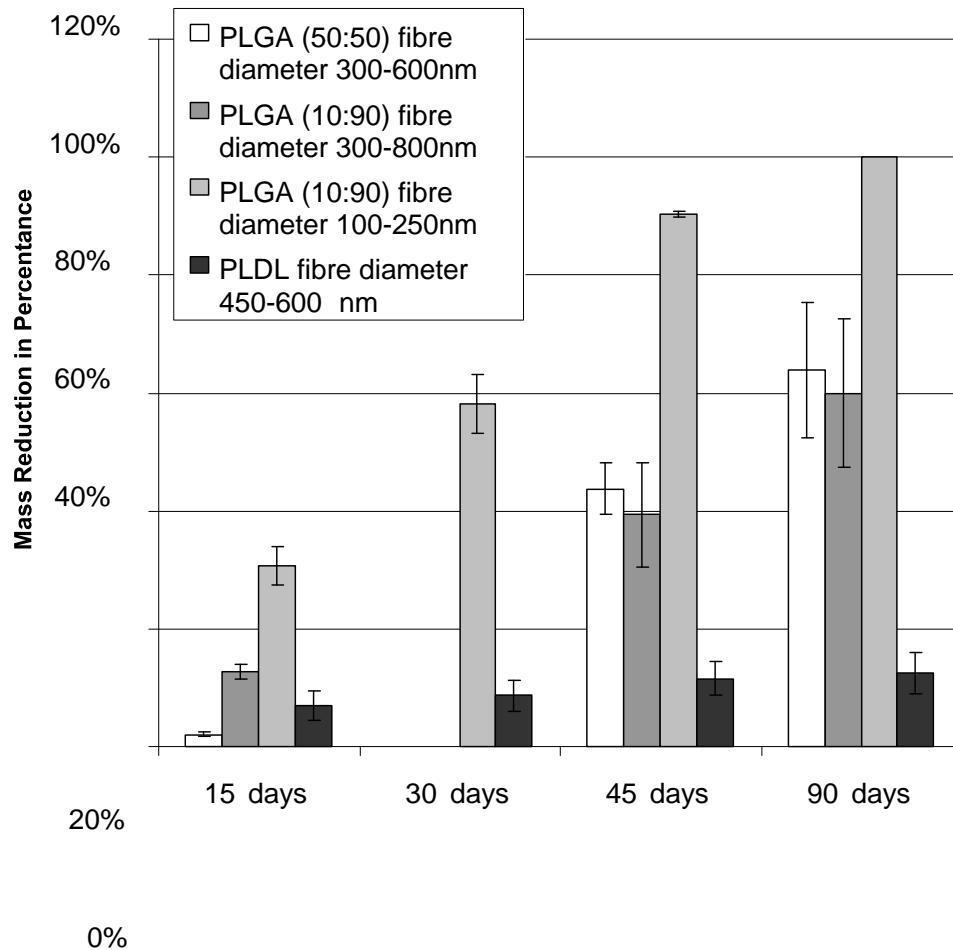


Figure 23 Degradation Chart

The chart shows the mass reduction of electrospun polymer mats with different fibre diameter and polymer type. Polymers were incubated at 37°C in PBS over a period of 90 days. Sample showed a significant faster mass reduction with small fibre diameter. No significant mass reductions were observed with purely polylactic polymers (PLDL).

Figure 24 shows the morphological changes of the polymers on day 15 and 90.

During *in vitro* degradation period, the fibre mats contracted a little and some fibres started to swell significantly within the first 15 days. PLGA (50:50) and PLGA (10:90) fibres started adhering to one another and the fibrous structure of the PLGA (10:90) swelled partially into agglomerations of fragmented polymer chunks.

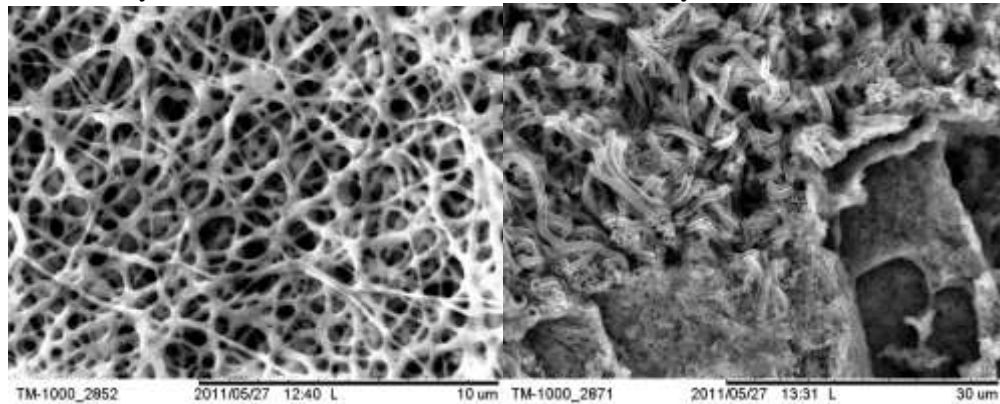
Observation on day 90 showed surface defects which led to fibre rupture of PLGA (10:90) and changed into chunks consisting of the short fibre fragments. Degradation of PLGA (10:90) was different from the porous, membrane-like structure of PLGA (50:50). On day 90 the fibre structures of PLGA (50:50) were less segmented but hollow or porous. No fibre break-down was observed with PLDL during the degradation. However, a fibre mat contraction on day 15 and a strong swelling on day 90 showed that fibre mat had changed its properties showing the loss of porosity and ability to be perfused.

Figure 24 Degradation of polymer fibres SEM Images

Electrospun PLGA (50:50) with a fibre diameter of 300-600 nm in PBS

After 15 days

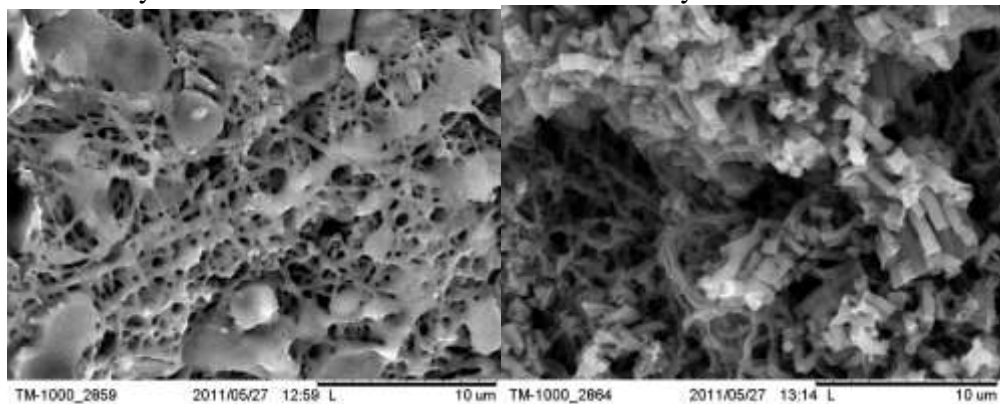
After 90 days



Electrospun PLGA (10:90) with a fibre diameter of 300-800nm in PBS

After 15 days

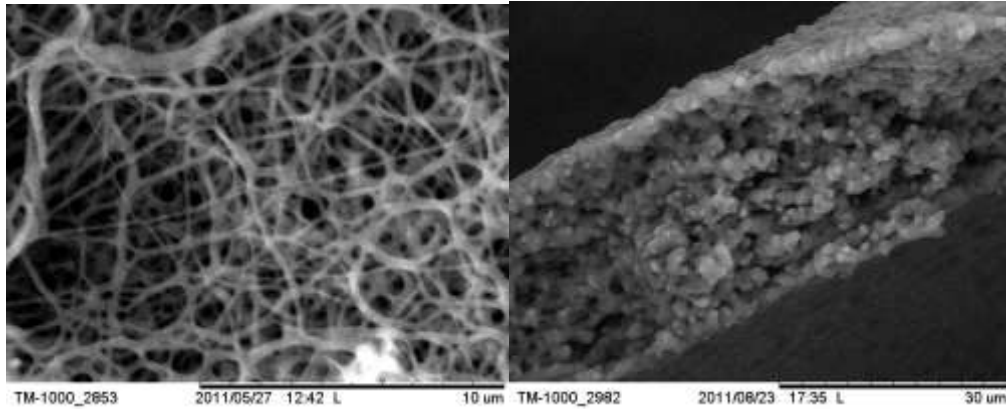
After 90 days



Electrospun PLDL with a fibre diameter of 450 to 600nm in PBS

After 15 days

After 90 days



3.4 Discussion

Electrospinning of PLGA and PLDL has been widely demonstrated in the past and much of the body of this electrospinning work has been summarized and discussed in several books [38,39,148]. The presented findings are comparable to those in the literature, which show a linear increase in diameter with increasing flow rate, polymer concentration and decreasing voltage. The differences in the diameter are subject mostly to the inherent viscosity, which is lowest for PLGA (50:50) and highest for PLDL. Fibre diameter is dependent on the viscosity of the solution [148]. Therefore it is just plausible that PLDL shows a 1.5 fold thicker fibre diameter at similar low flow rate compared to PLGA. Although PLGA (50:50) has a lower molecular weight than PLGA (10:90), the latter has a slightly lower fibre diameter. The difference between PLGA (10:90) and PLGA (50:50) is the percentage of glycolic acids. A shift in the balance between glycolic- and lactic acids could result in a higher conductivity of PLGA (10:90). Solutions of higher conductivity yield nanofibres smaller in average diameter due to the transfer of electric charge from the electrode to the spinning solution [39]. Moreover, PLGA (10:90) produced two fibre diameter populations at the same time. Similar PLGA (10:90) blends have been electrospun previously [23], but two distinctive fibre diameter populations have not

been observed so far. One possibility could be that a multi-jet occurs due to high voltage and high surface charge of PLGA (10:90). Applied voltage provides the surface charge on the electrospinning jet. Charges in the jet accelerate the polymer solution in the direction of the electric field towards the collector, thereby closing the electrical circuit. The jet while moving towards the collector undergoes a chaotic motion or bending instability. Instability and stretching of the jet correlates with the increase of the applied voltage [149]. It has been discovered that high instabilities causes a single rapidly whipping jet to generate multiple fibre diameters [150]. The whipping phenomena occurs so fast that the jet appears to be splitting into smaller fibre jets, resulting in ultra fine fibres as observed with PLGA (90:10). There are in total three models of jet instabilities and for further reading refer to Hohman and colleagues (2001) [151]

Electrospun nanofibrous membranes consist of specific pores sizes. The pore size is measured by the interspatial distance between fibres. Interspatial fibre distance correlates with the fibre diameter as long the applied voltage is not changed. Flow rate and polymer concentration influences the average pore size in a similar manner as the average fibre diameter. It has been found that pore dimensions vary with the volume density of nanofibres in the mat and therefore also with the yield and collection time [152], but are not directly related to the average fibre dimensions. Porosity tests with indirect methods such as bubble point or mercury intrusion measurements showed that there is no relationship between the average fibre distance and porosity [39,152-154]. However, the pressure required to form a bubble point test relates to the maximum pore size (range) [154]. Thus it can be suggested that increments in polymer concentration and flow rate reduced the porosity of the

electrospun material. Nevertheless, porosity is a factor for intrusion of material, drugs or cells. Coatings or cellular attachment will not be affected by it as much, because these act more in a 2 dimensional way. For this reason, interspatial fibre distance and fibre diameter were selected over porosity as the essential parameters for this research.

Electrospinning at higher humidity influences fibre morphology. Nanopores generally occur on polymer fibres when electrospun at high humidity as reviewed by [38,140,155]. These pores were not evidenced, because of the limitation of scanning surface microscope resolution. However, the generated fibres showed ribbon morphology. Ribbon fibre morphologies are created with higher molecular weight and higher polymer concentration at times where water solvent evaporation reduces with higher solution viscosity. The solvent system volatility is reduced. As a result wet fibres are generated which then accumulate flattened on the collector [38]. It is questionable whether enough water is adsorbed by the solvent system during the electrospinning process at a high relative humidity or whether it is more likely that water contamination of the solvent system caused the ribbon effect. Nevertheless, the effect of water during the electrospinning process is critical to the electrospinning product.

The electrospinning process of PLGA blends generates highly biodegradable nanofibres. These will lose complete structural integrity between 15 to 45 days and start to shrink, swell and break down after a few days in water based solutions. The process is described by Dong and colleagues [156] and factors which affect the polymer degradation included hydrophobicity, surface to volume ratio, nanofibre shrinkage, hydrolysis of crystalline polymers and surface erosion. The degradation

rates of the nanofibre matrices are reported in the order of $PGA < PLGA \ll PLA$ [157]. PLDL fibres did not degrade significantly, but showed shrinkage due to thermally induced relaxation on day 15 and strong swelling on day 90. A possible explanation is that the high molecular weight, and a difference in amorphous and crystalline properties, slowed down the degradation process; the degradation of the polymer scaffolds being initiated in the amorphous regions. The water molecules easily diffuse into the amorphous chain segments. Temperature crystallisation and crystalline properties of the polymer lead rapidly to hydrolytic degradation through polymer chain scission [156,158]. In the early stage PGA-rich matrices degrade quickly because they are more crystalline leading to a hydrolytic degradation and a gradual degradation over time [156,157]. After the initial phase of 15 days, PLGA (10:90) and PLGA (50:50) show similar mass losses. Firstly, the amorphous region of PLGA (50:50) allows a faster access of water to the inner crystalline region of the polymer, accelerating the degradation process after the initial phase of 15 days. This process leads to further crystallization and a rapid degradation [156]. Secondly, the higher molecular weight of PLGA (10:90) slows down the hydrolysis of water to the polymer backbone under aqueous conditions. A faster degradation of PLGA (10:90) can be achieved with higher surface area or lower fibre diameter. The degradation of PGA-rich matrices shows fibre breakages and polymer chunks, which is typical for a crystalline polymer such as PLGA (10:90), whereas hollow or porous fibres are observed with semi-crystalline polymers such as PLGA (50:50). Crystalline rich fibres are segmented through hydrolysis from outside. Amorphous polymers are dissolved from inside by water intrusion through the amorphous polymer chains, which allows crystalline hydrolysis from the inside of the fibre. Polylactic polymers

can consist of isomers of D- and L-lactic acids (Table 5). The percentage of L-lactic acids represents the crystalline fraction of the polymer and D-lactide the amorphous fraction of the polylactic polymers [156]. Hence, nanofibre stability can be adjusted by polymer composition and blends to achieve desirable degradation properties. Polymer fibres with a small diameter degrade faster. Water can easily access the inner core of polymers with a lower diameter, which accelerates the degradation process, and a higher amount of lactic acid is released within a shorter time. The amount of lactic acid released limits the amount of polymer that can be used *in vitro* or *in vivo*. The incorporated amount (mass) of PLGA (10:90) with a low diameter fibre (100-250nm) *in vitro* would be 50% less when compared to larger fibres (300-800nm) because these show a 50% reduced degradation rate. However, degradation *in vivo* is thought to act even faster. In this situation enzymatic degradation, erosion, friction, diffusion, temperature and pH will influence the degradation process further. Therefore, tissue models with cell culture would be a more accurate tool to predict degradation behaviour of polymer nanofibre mats, whereas *in vitro* studies can provide a guideline for polymer amount with regard to fibre diameter and porosity.

3.5 Conclusion

Electrospinning settings have a strong impact on fibre diameter and interspatial fibre distance. Adjustments of the main three electrospinning properties: flow rate, polymer concentration/viscosity and applied voltage increases and/or decreases fibre and mesh dimensions. The highest impact on fibre diameter and interspatial fibre distance can be achieved with flow regulation and polymer viscosity. In addition, environmental properties such as the relative humidity should be controlled during the electrospinning process to avoid severe product differences.

Equal fibre qualities are not achievable with all tested polymers. All polymers behave uniquely in the electrospinning process and generate distinctive fibre products. However, individual electrospinning settings can generate similar fibre and mesh properties. Nevertheless, PLGA (50:50) is the most versatile polymer tested compared to the PLGA (10:90) or PLDL. Although, it is technically more difficult to electrospin PLGA (50:50) fibres of 100nm diameter and below, there are no limitations to electrospinning fibres of several micrometers in diameter. PLGA (50:50) shows uniform fibre distribution and stable interspatial fibre properties, which are not achievable with PLGA (10:90) solutions. Degradation properties *in vitro* were shown to be fast for PLGA (10:90) and PLGA (50:50) making these fibres attractive for soft tissue engineering and wound healing. Although, PLDL showed excellent properties to generate uniform fibre below 100nm its degradation ability is questionably low. It is therefore preferable that PLGA (50:50) is used in further studies with cellular interactions.

Chapter IV

Alignment of Nanofibres
with dual field
electrospinning

Alignment of Nanofibres with dual field electrospinning

4.1 Introduction

An alignment of the fibres is difficult to achieve with a conventional electrospinning set up, because the polymer jet performs a whipping movement and is deposited randomly on the opposite collector. There is no effective way to overcome the whipping effect of the polymer jet, however, changes in the collector geometry can lead to different fibre deposition from random to highly aligned nanofibres (Figure 25). The commercial method to achieve highly aligned fibres mats is to spin over a rotating mandrel [159]. However, this method cannot be used to coat fragile or gelatinous material because of the high rotation speed of the mandrel. Only a few electrospinning methods are able to spin highly aligned fibres at static conditions, rotating jet electrospinning [160], dual magnetic field electrospinning [161] or dual electric field electrospinning [162].

The collectors describing a dual electric field or magnetic field electrospinning are positioned opposite each other allowing fibres to align over the narrow gap or a static target (Figure 26). A variant of this approach involves the use of a static (or rotating) grounded metal frame as collector which is described as rotating jet electrospinning. In the vicinity of such collectors, the electromagnetic field is split into two and runs in straight parallel lines between the collector segments. The whipping jet is attracted first to the collector closest to the jet segment and is then stretched rapidly to the adjacent collector. Fibres are placed along the electromagnetic field in the vicinity perpendicular to the collectors [39] (Figure 26). Polymer fibres in between the collectors charge up slowly and tend to repel each other. Their tautness as well as

their strongly parallel placement with respect to each other is believed to be due, partially to the surface charge [162].

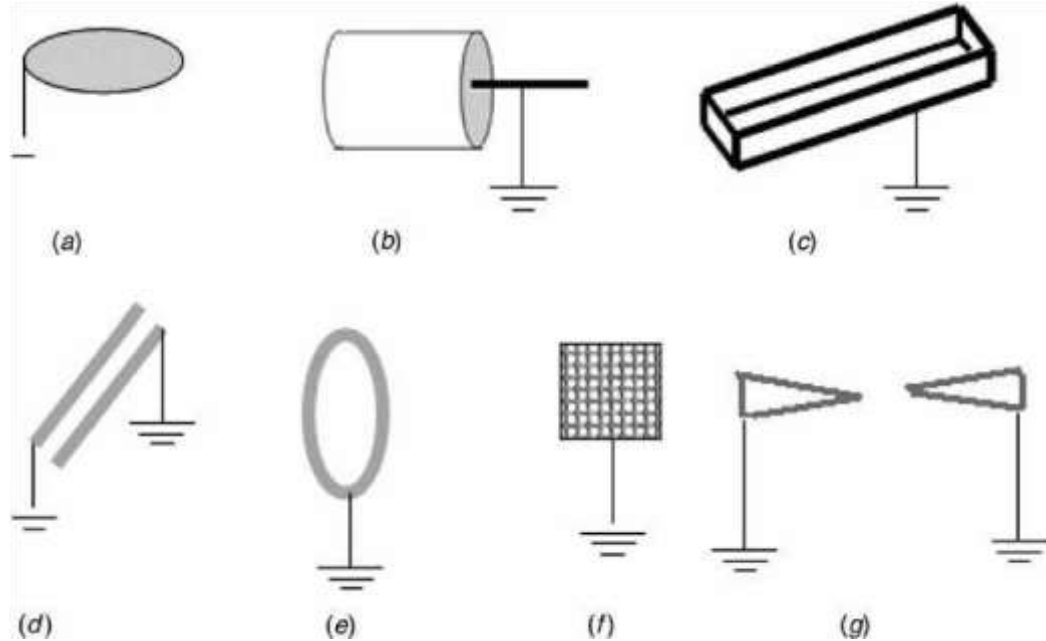


Figure 25 Collector Geometries

Adapted from Anthony Andrady, *Science and Technology of Polymers*, p.99 [39]
 Different types of collectors used in electrospinning: (a) flat plate collector produces random nanofibre mats (b) rotating drum, mandrel, rotating disc produces thick aligned nanofibre mats and strings at high rotations; (c) rectangular, triangular, or wire cylinder frame produces aligned nanofibres; (d) electrode pair arrangements or dual electric field electrospinning produce highly aligned nanofibres; (e) single or multiple ring electrodes or rotating jet electrospinning produces aligned nanofibres; (f) mesh electrode produces horizontally and vertically poorly aligned nanofibres; (g) pair of cone-shaped collectors, a different type of dual electric field electrospinning which produces strings of highly aligned nanofibres.

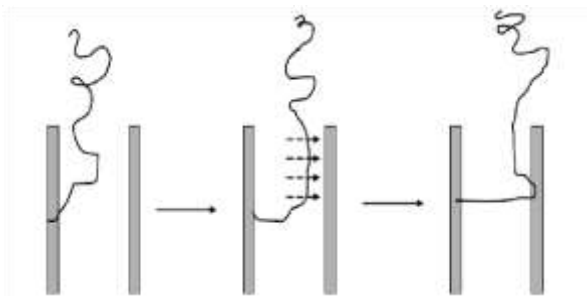


Figure 26 Dual electric field electrospinning method (adapted from Anthony Andrady,

Science and Technology of Polymers, p.267 [39])

Method shows the stretching of a charged jet segment across a pair of parallel electrodes.

Li and colleagues first showed that nanofibres of diameter exceeding >150 nm could be deposited as a highly aligned mat in the void space between a pair of electrodes [162]. Thinner nanofibres (less than diameter < 150 nm) were too fragile to be oriented in this manner. In recent studies it has been found that dual field electrospinning can generate higher fibre alignments comparable to those electrospun over a rotating mandrel at 300rpm [163]. Initially during the development of dual field electrospinning, alignment was achieved only with very narrow collector distances of between a few millimetres up to 3-4 cm [163,164]. This has changed recently; new large scale dual field electrospinning methods achieved alignment of fibres over a 60cm gap distance with a tip collector [165]. This progress moves the dual field electrospinning technology closer to a commercial application. There are still some technical issues to be addressed before this technology will be ready for industrial production of aligned polymer fibre material. Foremost, the fibre alignment varies and accumulation of random or “stray” fibres reduces the quality of the product. The resulting fibres from dual field electrospinning depend on parameters in addition to collector distance, such as electric field voltage, feeding rate and polymer concentration. Recently, a few approaches have been started to improve the electrospinning conditions. The fibre distance and deposition can be enhanced with auxiliary electrodes which narrows the whipping of high speed jet down [163]. Further “stray” fibres have been reduced with the combination of dual field and magnetic field electrospinning [166].

Once the technical problems are resolved and reproducibility of high polymer fibre alignment is guaranteed; products of dual field electrospun material have a broad application spectrum. These electrospun polymers with high fibre alignment are

desirable in regenerative medicine, as they greatly affect cell fate and morphology [167], extracellular matrix formation [168] and direction of cell growth [169]. Further they have great potential applications in the fields of catalysts [170] and photonics [171].

In this Chapter, I evaluate the process parameters to spin highly aligned fibres with defined interspatial fibre distance across the dual collectors. I investigate the effects of static and low oscillating electromagnetic fields, voltage strength, spinning duration as well as needle and collector positions. I will use the advantage of dual field electrospinning to coat flat surfaces such as aluminium and glass. Further I will demonstrate that fragile surfaces such as collagen hydrogels can be coated with defined fibre amounts and alignments in preparation for cell culture experiments.

4.2 Method

4.2.1 Dual Field Electrospinning

The electrospinning apparatus consisted of a syringe pump (Harvard Apparatus PHD 2000 infusion, US) and two 30kV high-voltage power supplies (Brandenburg, UK) as described in chapter 3.2. Either a PLGA (50:50) 10% (w/v) in HFIP or a PLDL 2.5% (w/v) in HFIP highly viscose solution was placed in a 5.0 ml plastic syringe (BD Syringe, UK) fitted with a 18 gauge needle (BD Microlance, UK), and loaded into the syringe pump. The polymer solution controlled by a syringe pump was extruded with a flow rate of 0.05ml/h to 1ml/h. The tip of a blunt 18 gauge needle was attached to the ground of a high voltage source and positioned in the middle between the collector and 8cm to 14cm above the two parallel collector rods. The high-voltage source was used to apply an electrostatic field of 9-24 kV to both collectors (Figure 27, a and b and Figure 28). In addition, an oscillating transverse electric field was applied with the help of a second power voltage supply (Brandenburg, UK) to each collector. A square function at frequencies between 0.5-2 Hz with maximum amplitude between 9-24 kV was fed to one of the power supplies. Simultaneously, a 180° phase shifted copy of the former function was fed to the other power supply (Figure 28). Both functions are fed with an offset which is 3kV below the amplitude settings. The oscillating amplitude is restricted to maximum of 3kV above the offset. Amplitude and frequency operations were controlled with the help of a multifunction data acquisition (DAQ) device and programmed with Labview® (National Instruments). An example of the Labview® program and the control panel are shown in Figure 29, b and c. Signal and measurements were fed to power supplies via a 21 pole socket according to the manufacturer's manual.

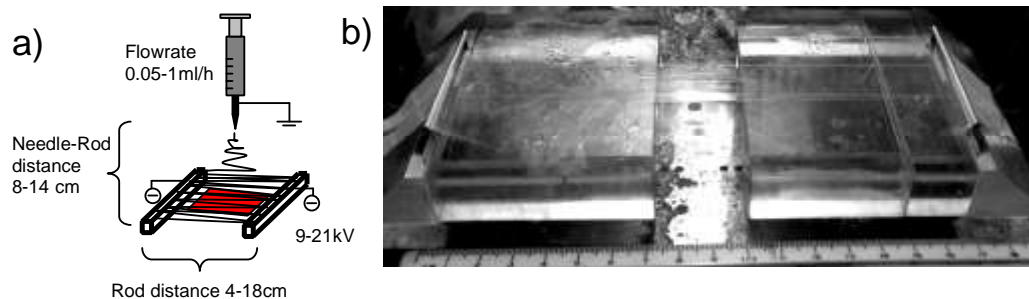


Figure 27 Dual field electrospinning of aligned fibres

Schematic dual field electrospinning set up with parallel bar collectors, a centrally positioned syringe and coated glass sheet (a). Image (b) shows electrospun dual field fibres at a gap distance of 18cm. The glass slide is positioned on two strings 1mm below the collectors. Aligned polymer nanofibres were covering the whole area between the 7cm long collector rods. The collector rods are half covered with polymer fibres and form a sharp edge from which the fibres transverse over the gap. The arrow head indicates the edge effect at the collector bar end where fibre direction changes due to the changes in the electrostatic field.

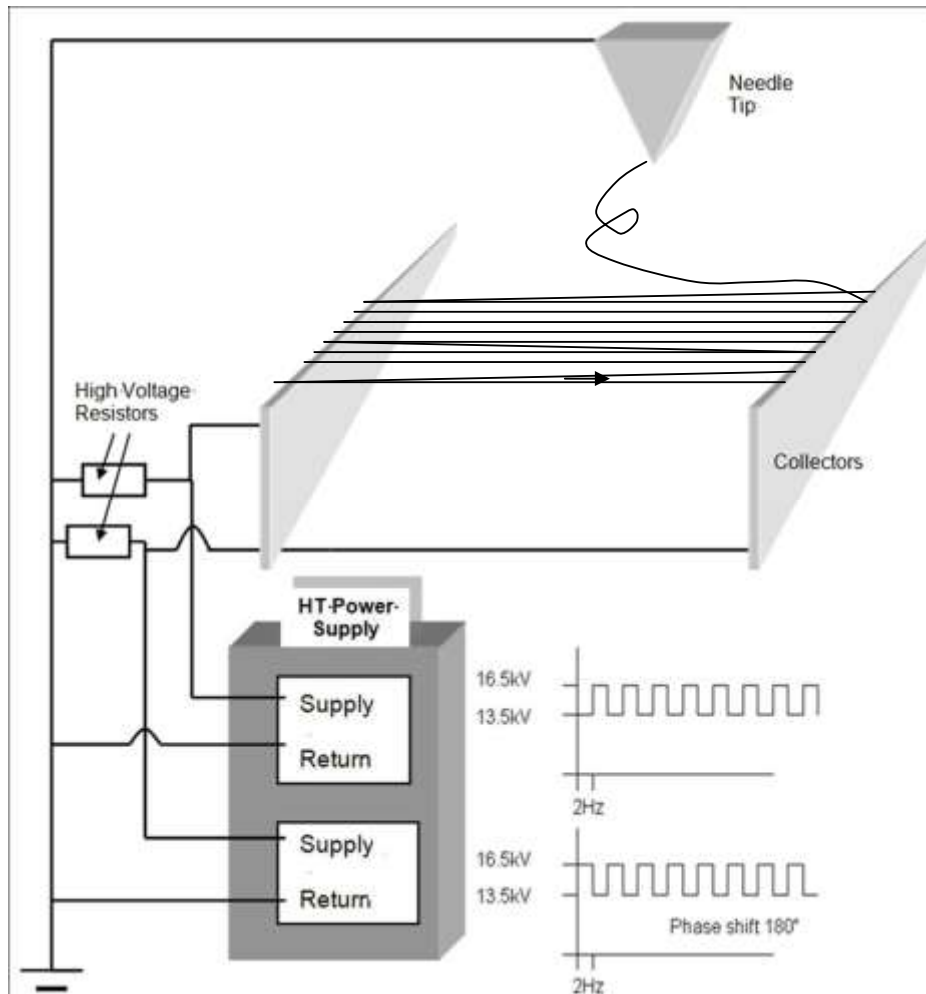


Figure 28 Dual oscillating field electrospinning

The image shows the schematic set up of the transverse oscillating electric field electrospinning system. Two high voltage power supplies were fed with a square function of 0.5-2 Hz. Offset was set at 13.5kV. Amplitude was 3kV. The square function was delayed by 180 degrees from the other voltage supply. Polymer solution was extruded from the grounded needle tip and the resulting polymer fibres deposit in an aligned manner between the collectors.

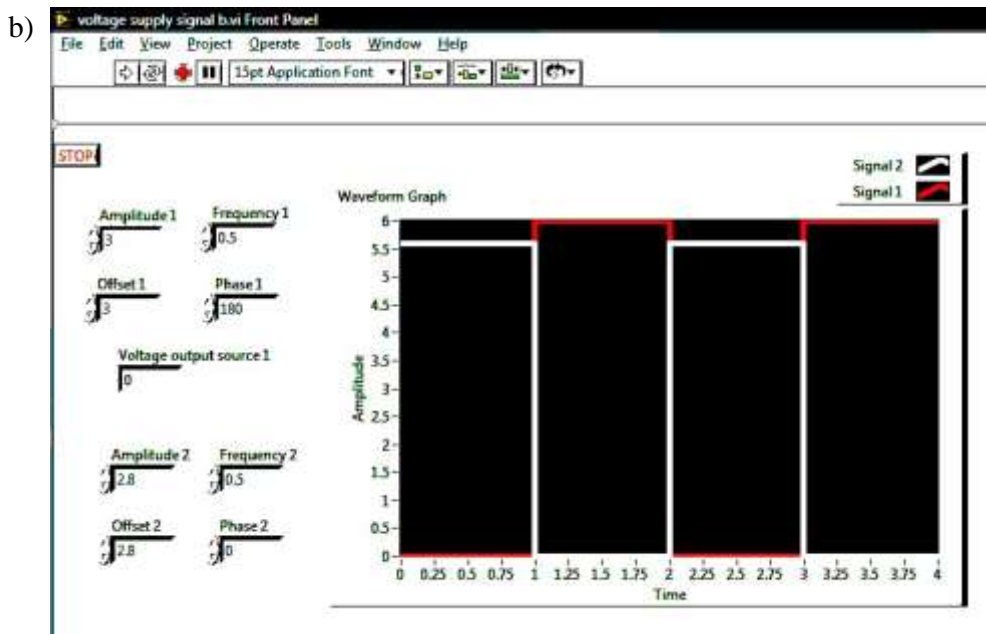
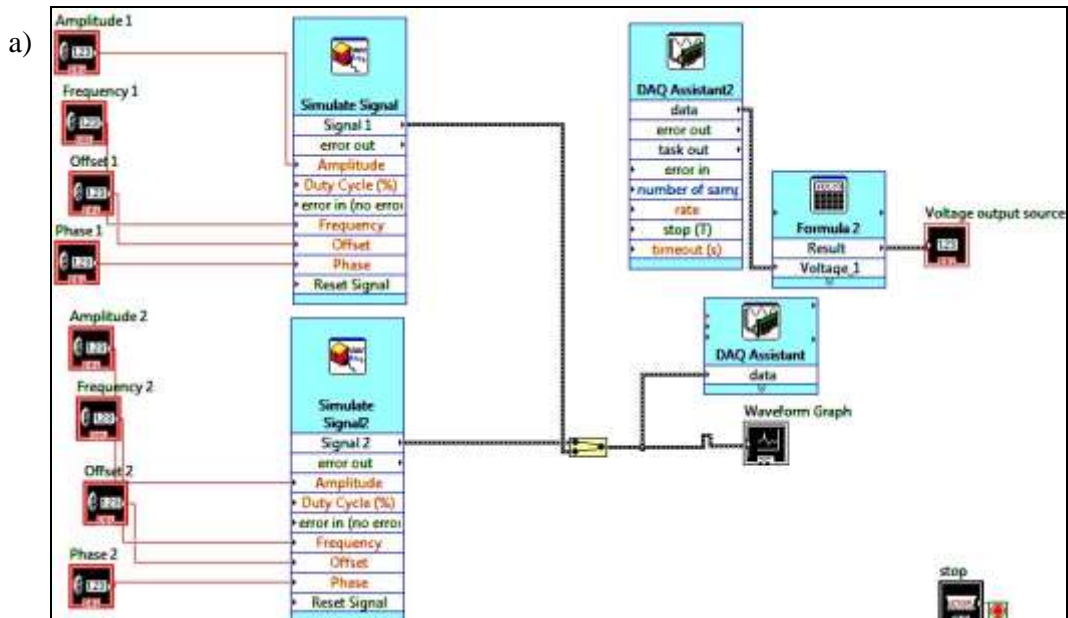


Figure 29 Labview® control

The Labview program in image (a) simulates two signals, which were fed via the multifunction data acquisition device to the power supplies. Voltage amplitude, frequency, voltage off set and phase were adjusted individually for both power supplies. Data output of the voltage was measured in return to control the input. The Labview Front Panel (b) displays the square functions and the voltage output (Amplitude 1 and 2 differs in order to visualize the square function in the image, experimental setting of amplitude 1 and 2 were set between 3 and 7 digit). The input for voltage and off set: 1 = 3000V, and the frequency: 1 = 1Hz.

Polymer solution was extruded from the grounded needle tip and the resulting polymer fibres were deposited in an aligned manner between the collectors. Collectors consisted of 2mm diameter steel rods and vary in length between 7cm and 2cm. Electrospun fibres were collected between a 4cm to 18cm wide gap. A glass slide (2.5cm x 5cm) was positioned slightly below (1-2mm) the collector rod level. Electrospun fibres were collected over glass slides for 30sec to 30min. In addition fibres were collected over glass slides which have been covered with aluminium foil or 0.1-1ml collagen gel (method for collagen preparation, Chapter 2). Electrospuncoated samples were cut free from the collector rods prior to characterization. A set of 5 samples (n=5) were electrospun for each electrospinning setting. Setting and range of the dual field electrospinning process are summarized in Table 7.

Table 7 Setting range and examples for the dual field electrospinning process

Polymer*	Flow Rate	Needle Collector Distance	Collector Gap Distance	Applied Voltage	Spinning Duration	Oscillating Frequency	Relative Humidity	Fibre to Fibre Distance	Fibre Diameter range	Average Fibre Orientation
PLDL /PLGA	0.05ml/h - 1ml/h	8cm - 14cm	4cm - 18cm	9kV - 21kV	30sec - 30min	0Hz - 2Hz	23% to 35%	1.5µm - 80µm	200nm - 1500nm	0° - 45°
Examples of dual field electrospinning										
PLDL	0.05ml	14cm	7cm	14kV	0.5min	2Hz	23%	45-60µm	<350nm	0°-15°
PLDL	0.1ml/h	14cm	7cm	12kV	5min	2Hz	26%	1.5-3µm	350-650nm	5° - 12°
PLDL	0.25ml/h	14cm	7cm	14kV	10min	2Hz	26%	2-4µm	300-500nm	22° - 30°
PLGA	0.5ml/h	14cm	7cm	14kV	2min	-	25%	7-16 µm	0.7-1.1µm	10° - 17°
PLGA	0.5ml/h	14cm	7cm	12kV	3min	2Hz	35%	50-70µm	0.7-1.2µm	5° - 10°
PLGA	0.25ml/h	14cm	18cm	15kV	10min	2Hz	23%	5-35µm	500-900nm	15° - 25°

* PLGA = PLGA (50:50) with a polymer concentration of 10% (w/v) and PLDL = PLDL with a polymer concentration of 2.5% (w/v)

4.2.2 Characterisation of fibre distance, diameter and orientation

Glass slides and collagen gels with fibre deposition were visualised with a Zeiss Axio Vision Microscope in bright field. Fibres deposited on aluminium strips were visualised with scanning surface electron microscopy. The number of fibres per cm² and the average interspatial fibre distance per image was calculated from the Zeiss

Axio Vision Microscope brightfield images. Images of a 2.5 cm deposition area were taken with the Zeiss Axio Vision Microscope. Fibre distance between aligned fibres (interspatial distance) per microscopy image (2.2 mm) was counted with ImageJ® length measurement tool from 5 images of the glass slide centre (0.9-1.3cm). Fibre deposition was calculated from 32 images (equal to 2.5cm) of 5 individual experiments with ImageJ®. Images were transformed into binary (black/white images) and the amount of fibre deposition calculated by its pixel value for every frame. As an internal control, fibres were also counted directly from the bright field images and the average fibre to fibre distance and the number of fibres per cm² was calculated by dividing fibre amount through frame length (78.125µm). Both described methods were compared to each other to minimize evaluation errors.

Alignment was evaluated with Fast Fourier Transformation (FFT) of the microscope bright field images. The method was adapted from Ayres and colleagues [172]. The initial bright field microscope image was cropped to 1036 by 1036 pixel or 6.91 by 6.91 inches, thereafter FFT was performed with ImageJ software. A circular selection was placed over the whole FFT image (Figure 30, b row 3). An oval profile plug-in (authored by William O' Connell) downloaded from <http://rsb.info.nih.gov/ij/plugin> was used to determine the radial summation of intensities from 0° to 355° degree on the FFT image. The pixel/light intensity value was measured every 5° resulting in 72 values per image (Figure 30, c). Values from 270° degree to 85° and 275° degree to 90° representing top and bottom half of the FFT images. The upper and lower half of the images is similar to each other. Thus, the evaluation was simplified and the alignment was compared and evaluated by the pixel intensity over a 180° degree spectrum from 270° degree to 85°. At 90° FFT

images generate at “fake” intensity measurement shown as a horizontal line (Figure 30, b row 1, 2, 4). The pixel line results from the noise or background in the picture. The background value of every image was subtracted from each measured intensity value. Resulting negative values were excluded and set to zero. Values were normalized to the control (random fibres) and results were shown as a percentage over the whole spectrum of 180° . The results showed that fibre alignment is concentrated around 0° ($\pm 45^\circ$), therefore further charts and tables displayed values at a reduced range. In some cases the background was too high to generate comparable data (i.e. SEM images of fibres over aluminium foil). This led to an incorrect percentage evaluation of the actual fibre alignment. The values were similar to those of random fibres (Figure 31). For this reason the evaluation of SEM images was excluded in this study. Only images taken from bright field microscopy were evaluated and compared to each other. A protocol for alignment quantification is attached with this work (Annex).

The statistical image evaluation in terms of measurement replicates and analyses methods for fibre alignment, diameter and interspatial distances were the same as in Chapter 3.

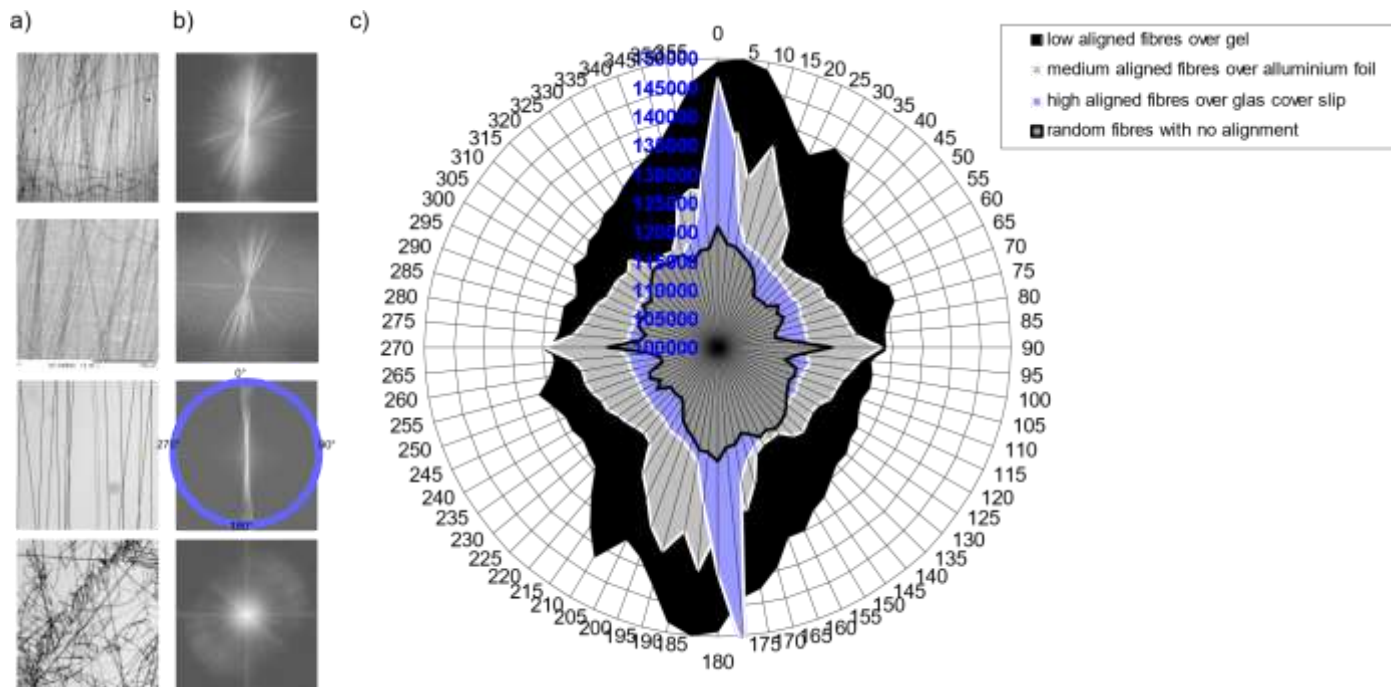


Figure 30 Fibre alignment evaluation Part I

Production of varied alignment and fibre density on three different materials- collagen gel (image (a) top) aluminium sheet (image (a) second row) or glass slide (image (a) bottom two). Fibres on aluminium sheets were analyzed with scanning surface electron microscopy (TM-1000, Table top microscope, Hitachi) and the bright field and/or phase contrast images of the glass slides and gels were visualized with Zeiss Axio Vision Microscope. Nanofibres produced with dual electrostatic field electrospinning showed variations of alignments from 0-90 degrees and can be electrospun in low and high densities as seen on the bright field images (a). Fast Fourier transformation (FFT) of the bright field images showed orientation of the fibres in radial direction (b, row 3). Background is displayed a horizontal line at 90° (b, row 2). Acquisition of the radial pixel light intensity of the FFT images allows translation of the alignment to real values, which are illustrated on a rotation graph of 360° on the x-axes and the pixel intensity on the y-axes (c).

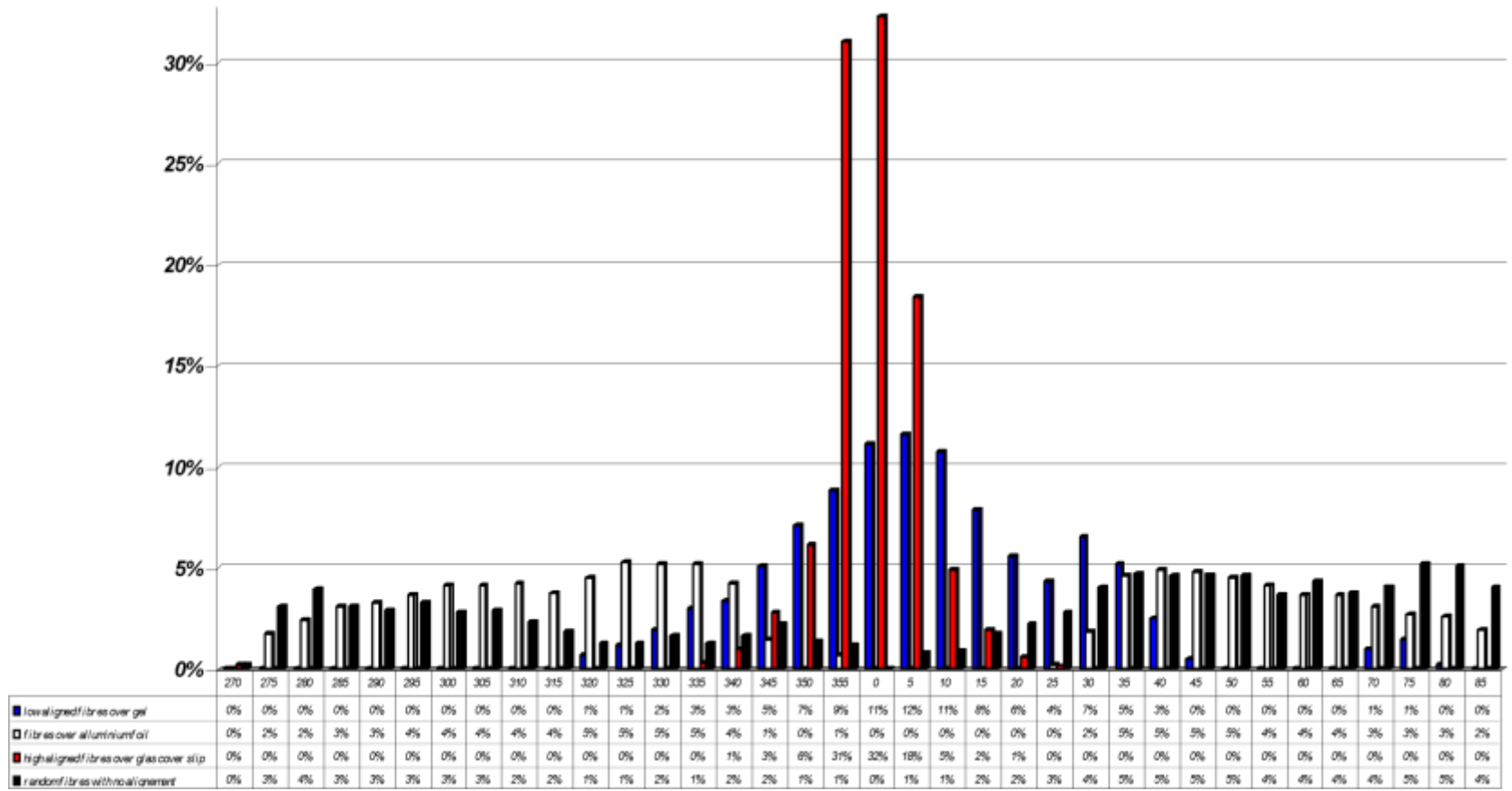


Figure 31 Fibre alignment evaluation Part II

Image shows the percentage of aligned fibres from 270° to 90° with 5° intervals after background reduction and pixel value normalization from Figure 30 c). A higher percentage around 0° indicates alignment of the electrospun polymer fibres, whereas an increase at $305^\circ/45^\circ$ and below indicated random orientation and stray fibre accumulation.

4.3 Results

4.3.1 Dual Field Electrospinning Design and Fibre Deposition

The standard set up to coat aligned nanofibres over various materials is shown in Figure 27. The materials such as glass slides, and glass slides covered with aluminium foil or collagen gels were mounted on two non-conductive strings 1-mm below the collector rods, which were isolated from surrounding connective material.

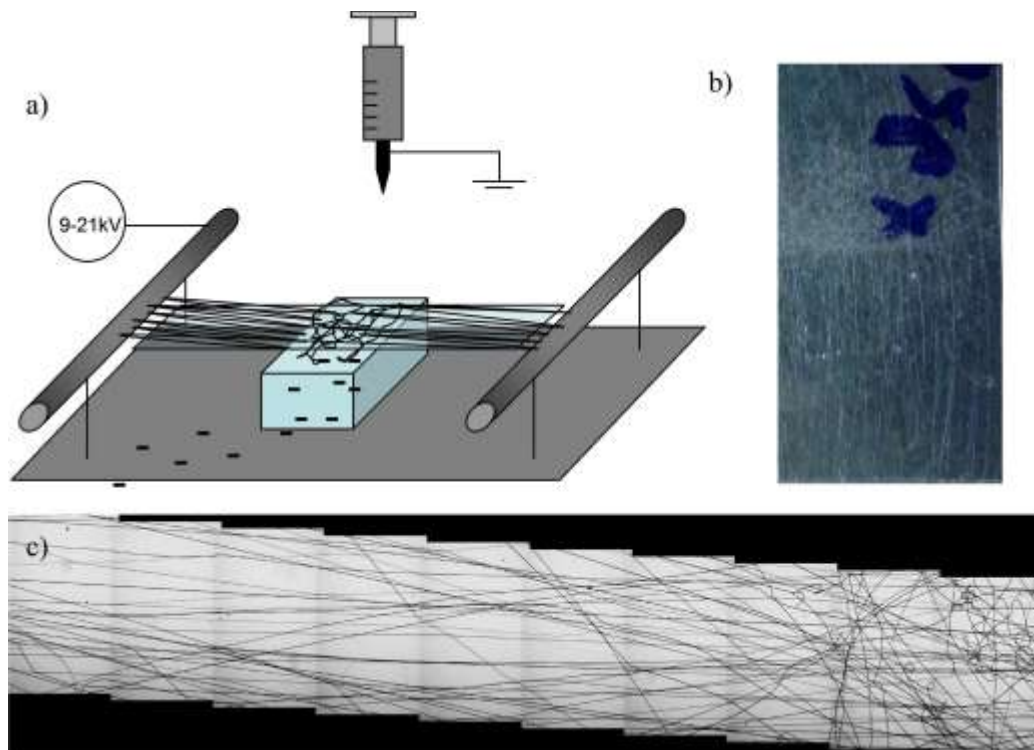


Figure 32 Initial Set Up

Image (a) shows the electrospinning set up of two negatively charged parallel rods 7cm distance from each other. Electrospinning solution was extruded from the positively charged needle tip, generating parallel fibres between the rods. Fibres were collected over a glass slide which had been positioned on an inert plastic stand. Negative charges (leaking charges), were able to transfer over the surfaces onto the stand and changed the electrostatic field below the glass slide, which was attracting random fibres. Image of a 5cm x 2.5cm glass slide (b) shows the aligned fibres in air isolated part of the glass slide and a random mesh in the position of the plastic stand. The (x10) magnification under the microscope showed a mosaic bightfield image of

ten frames each 2.2mm in width (c) where aligned fibres merged with random fibres in the surface contact area with the plastic stand.

Initially, several mounting methods were tried out. The glass slide was placed on an inert polystyrene block (Figure 32, a). However, aligned fibres could only be collected outside the contact area of the glass slide and plastic stand (Figure 32, b).

The (x10) magnification under the microscope showed a mosaic brightfield image where aligned fibres merged with random fibres in the surface contact area with the plastic stand (Figure 32, c). The accumulation of random fibres was significantly reduced once the glass slide was detached from the larger surface area.

Fibre accumulation over the glass slide was shown to be influenced by the position of the syringe. A syringe was placed in the centre between the collector system to distribute fibres evenly over the surface. A shift to one or other side of the collectors led to an accumulation of fibres on one collector only. However, dual field electrospinning supported with oscillating frequency at 2Hz was able to transfer polymer fibre between the collectors. When the syringe was placed in the centre between collector rods, the fibre deposition occurred first in the centre below the needle tip and slowly spread out over the full bar length. The deposition pattern showed a Gaussian distribution in the central area of 2.5 cm at 12kV (Figure 33). At higher voltages (18kV) a Gaussian distribution could not be observed at the same central area, the fibres were distributed uniformly over the glass slide. At the end of the collector rods an “edge effect” was observed which changed the deposition pattern. The edges of the rods attract most of the fibres in a point to point dual field electrospinning process. In cases where the needle was positioned centrally most of the fibers were electrospun along the rod length. It was observed that the collector

rods were coated with nanofibres prior to the actual fibre transfer between the collectors. Nanofibre transfer between the collectors was set in motion from a sharp polymer edge at the rods (Figure 27, b).

Polymer types such as PLDL, PLGA and flow rates between 0.1-1ml/h did not influence the spinning process; however, high polymer viscosity coated the collectors without transferring fibres over the collector gap. After a short spinning time it led to a Taylor Cone deformation at the needle tip, and polymer solution was dropping from needle tip instead of being electrospun. Hence, all consecutive experiments were conducted with a medium polymer concentration of PLDL 2.5% (w/v) and PLGA (50:50) 10% (w/v). Although the flow rates were restricted between 0.1 and 1ml/h a wide range (200nm-1500nm) of fibre diameter has been electrospun with the dual field electrospinning set up (Table 7). Generation of specific fibre diameter followed the same electrospinning principles as illustrated in Chapter 3; mostly adjustment to flow rate was used to produce fibres of specific diameters.

The duration of the electrospinning process not only increased the fibre deposition but also had an effect on the interspatial fibre distance. Interspatial fibre distance decreased over time. PLDL fibres electrospun at a stable gap distance (7cm), flow rate of 0.1ml/h and 12kV showed an average of 13 μ m interspatial fibre distance after 1 minute of electrospinning (Figure 34). In the experiments the deposition was saturated after 5min of electrospinning time. The interspatial fibre distance was limited to 2.5 μ m or 400fibres/mm in these samples. An extended electrospinning period showed no significant changes in deposition of the fibre amounts at the described setting of 12kV and 7cm gap distance. Dual field electrospinning was

mostly stable for up to 10min at 9-12kV. Thereafter, the transversal electrospinning effect declined and a dropping needle tip was observed. The longest electrospinning process which lasted for about 30min was generated at 12kV with 7cm rod length, a rod needle distance of 14cm and the lowest humidity of 23% (Table 7). At this point the entire bar length was coated fully and evenly with polymer fibres and a dense single layer matt of fibres was observed between the collectors before the electrospinning process self terminated. In general high fibre depositions were achieved at low (< 26%) relative humidity (Table 8).

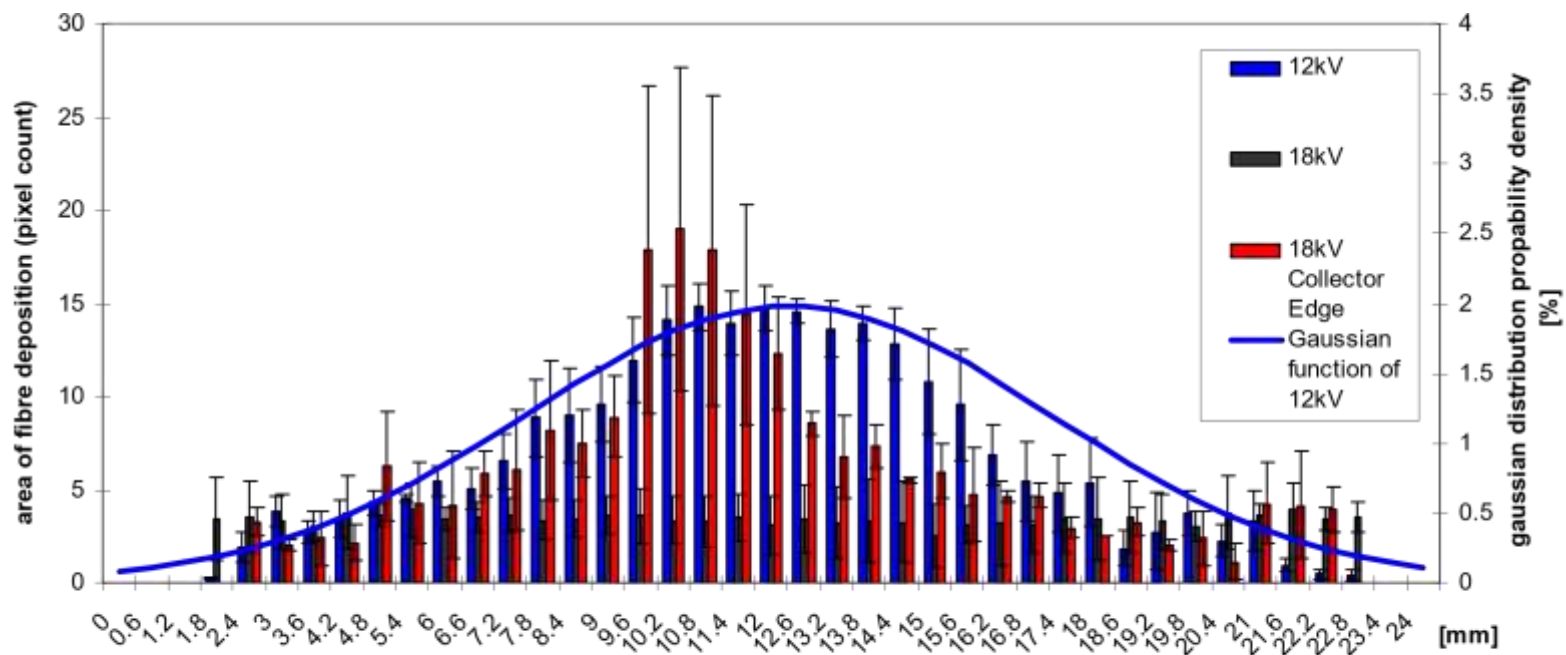


Figure 33 Polymer fibre distribution pattern

The Chart shows the distribution pattern of dual field electrospun polymer fibres at 12kV and 18kV after 2min of spinning duration. The position of the needle was at the centre of the image row. Fibres electrospun at 12kV show a Gaussian distribution. Fibres at 18kV are uniformly distributed. The highest amount of fibres accumulated at the tip ends of the collector rods. Bright field image below the chart shows the 12kV sample of the actual polymer fibre deposition over a length of 2.5cm. The evaluation of the fibre deposition for each group was conducted from 3-5 individual experiments; the average and standard deviation is represented in the chart.

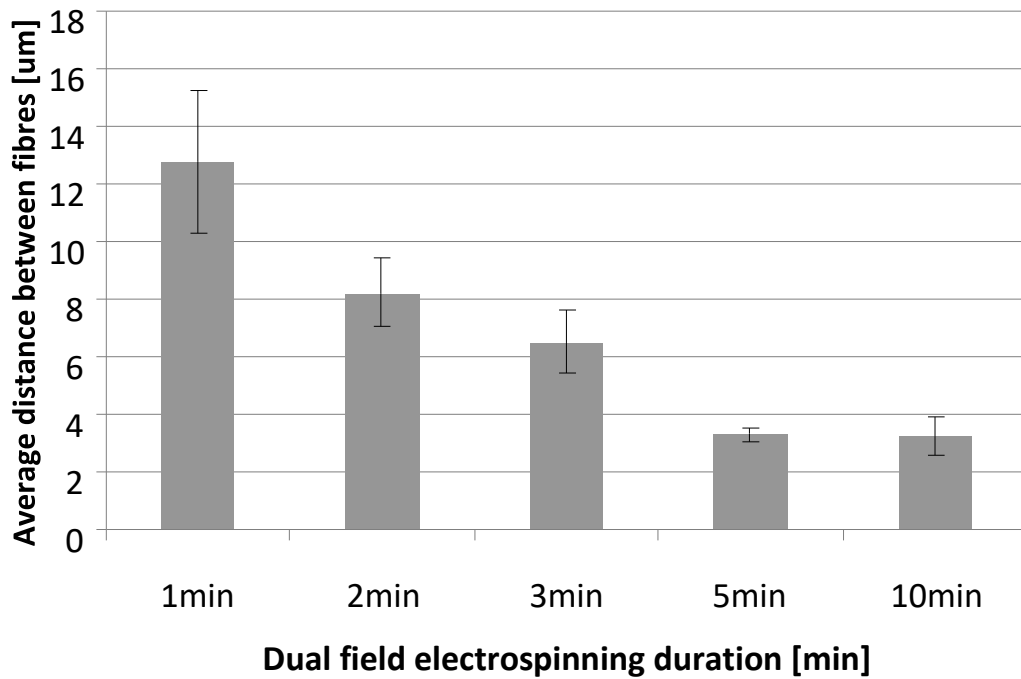


Figure 34 Time controlled fibre distance and deposition

Accumulation of polymer fibres over time shows the fibre to fibre distance in micrometers between 1 and 10 minutes. PLDL fibre distribution was measured at the central area below the needle tip at 14cm needle collector distance, 7cm gap distance and 12kV applied voltage. The evaluation of the interspatial fibre distance was based on 3 individual experiments per time frame and the average and standard deviation is displayed in the chart.

4.3.2 Dual Oscillating Field Electrospinning and Fibre Alignment

As previously mentioned oscillating field electrospinning was able to stabilize the transversal electrospinning process between the two collector bars. In general it reduced stray fibre accumulation at high voltage (Table 8, Figure 35, a). Further, an electrostatic field imbalance either by needle position or voltage impaired the fibre quality. A voltage difference of over >1000kV reduced the alignment quality and increased the accumulation of stray fibres (Table 8). The negative effect of a voltage imbalance towards the fibre alignment quality was resolved by a low oscillating electric field. The frequency of the oscillating field had to be higher than 1Hz to reduce the accumulation of random fibres or “stray fibres” (Figure 35, a). Accumulation of stray fibres is indicated with a fibre degree at 35° and above. These

were significantly reduced at 2Hz frequency. Moreover, at 12kV amplitude a higher alignment was produced with oscillating field (Figure 35, b). Nevertheless, an electrostatic field showed a better fibre yield compared to a 2Hz oscillating field (Figure 35, b). The difference between fibre deposition with and without an oscillation support is in average 20% at 18kV and increased with a lower voltage (Figure 35, c).

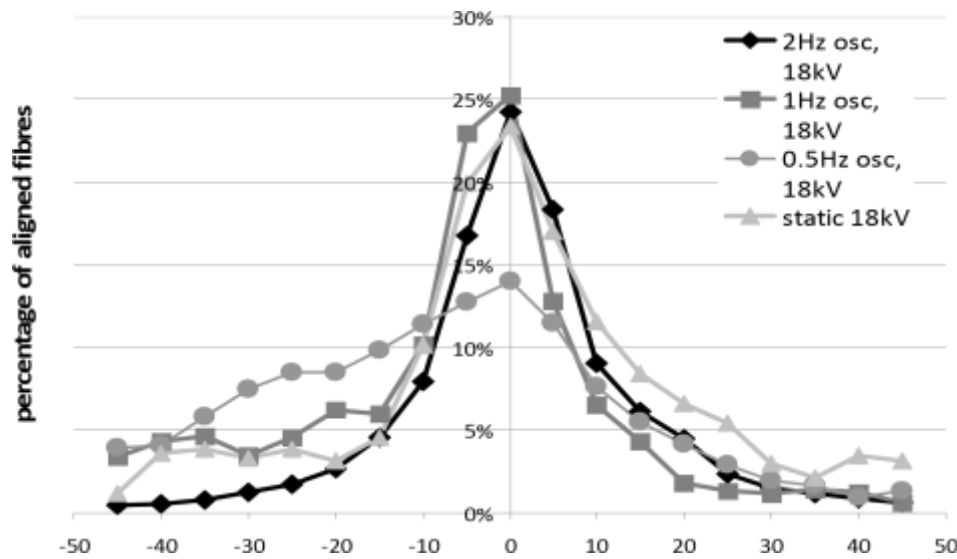
The fibre alignment during dual oscillating field electrospinning was strongly influenced by the applied voltage. High voltages attracted many stray fibres and reduced the overall alignment, whereas low voltages produced a high fibre alignment with no stray fibres (Table 8). More than 75% of the electrospun fibres were aligned below 20° degrees when electrospun at 9kV. The accumulation of stray fibres was highest at 18 and 21kV with every 10th fibre depositing in a random pattern.

Another factor that led strongly to the accumulation of stray fibres was humidity. A rise from 25% to 35% relative humidity tripled the stray fibre percentage and lowered the overall alignment (Table 8). In this regard, dual electric field electrospinning over surfaces such as hydrogels showed a similar effect. Small amounts of gel or small areas of gels did not influence the fibre alignment significantly compared to a glass surface, but 1ml of gel distributed over 2cm x 3cm area showed accumulation of stray fibres and an overall reduced fibre alignment profile (Table 8).

Minor effects of stray fibre accumulation were observed with spinning duration and collector/needle arrangements. Accumulation of stray fibres did not increase over

114 time, but the overall alignment decreased with extended electrospinning durations (Table 8). Accumulations of stray fibres were not influenced by collector to collector distance or needle to collector distance (Table 8). However, the overall alignment was influenced by the gap distance in a voltage dependent way, whereas needle-bar distance between 8-14cm did not influence the alignment. At 15kV the highest alignment was observed at an 11cm gap distance, whereas at 18kV alignment it peaked at 7cm.

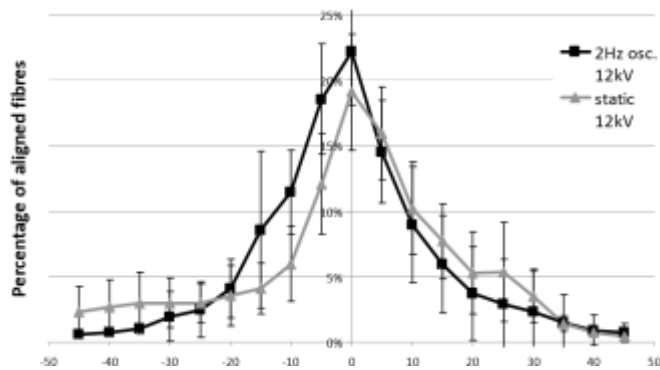
The results suggest a high polymer fibre alignment with dual oscillating field electrospinning at following parameter setting: a minimum voltage 9kV (or lower if possible), a low humidity <23%, an anticipated gap distance of >7cm, and an oscillating frequency of 2Hz (potentially >2Hz).



a) **Figure 35 Dual oscillating field electrospinning**

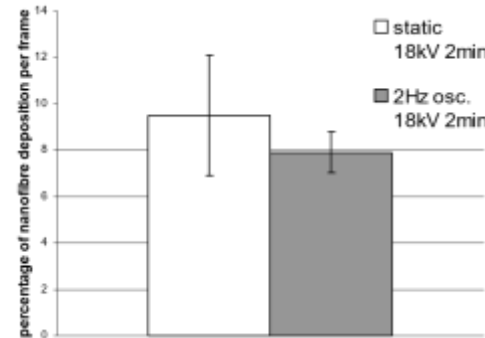
Chart (a) shows the alignment of PLGA (50:50) fibres at 2Hz, 1Hz, 0.5Hz and electrostatic conditions at 18kV, gap distance 7cm and a flow rate of 0.5ml/h. The percentage of aligned PLDL fibres between an oscillating field of 2Hz and an electrostatic field at 12kV, with a gap distance of 7cm and a flow rate of 0.1ml/h is compared in chart (b). Alignment was evaluated from 3 individual experiments per group. 35 images per experiment were quantified. The alignment average

Alignment angle and standard deviation is represented in the chart.



b) c) The deposition of fibre material

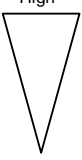
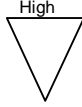

after

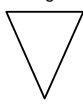


2 minutes dual field electrospinning with a 2Hz oscillating field and an electrostatic field at 18kV has been compared in chart (c). The evaluation of the fibre deposition for each group was conducted from 3-5 individual experiments and the average and standard deviation is represented in the chart.

Table 8 Fibre alignment under various conditions

(**Bold** letters indicate optimal setting, whereas **red** indicates 2-3 fold increase of stray fibres when compared to samples for the same group). Alignment was evaluated from 3 individual experiments per group. 3-5 images per experiment were quantified. The alignment average per 5° is shown in the table.

		0°	-5°-5°	-10°10°	-15°15°	-20°20°	-25°25°	-30°30°	-35°35°	>-40°40°	Alignment
Degree:											
Alignment over time											
electrospinning duration [min]	1min	30.8%	24.8%	16.9%	10.9%	5.4%	3.9%	3.4%	2.4%	2.0%	High  Low
	2min	26.3%	21.4%	17.5%	13.8%	7.9%	4.2%	3.2%	2.7%	3.1%	
	3min	26.6%	22.6%	17.8%	12.0%	7.9%	5.9%	5.0%	2.1%	1.3%	
	5min	27.4%	20.4%	14.1%	11.0%	8.0%	7.0%	5.5%	4.0%	3.0%	
	7min	24.2%	22.8%	18.3%	15.9%	6.6%	4.4%	5.6%	2.5%	2.5%	
	10min	22.8%	21.6%	19.9%	15.8%	8.8%	5.6%	3.8%	2.7%	1.8%	
	30min	22.1%	20.6%	18.6%	12.2%	8.8%	5.6%	4.7%	3.9%	3.3%	
Alignment with different Voltages											
electro-spinning with applied Voltage [kV]	9kV	37.1%	27.5%	16.0%	10.1%	3.7%	2.1%	1.2%	0.9%	1.2%	High  Low
	12kV	34.9%	25.9%	13.6%	8.8%	5.0%	4.6%	3.3%	1.8%	2.1%	
	15kV	26.0%	21.5%	16.4%	13.7%	9.8%	6.2%	3.0%	1.5%	2.0%	
	18kV	23.8%	19.1%	11.7%	9.0%	8.4%	7.5%	4.6%	6.1%	9.8%	
	21kV	26.0%	18.0%	8.6%	9.2%	10.5%	7.8%	5.3%	4.4%	10.2%	
Alignment with voltage imbalance											
Voltage imbalance [kV] at electrostatic and oscillating dual field condition	Static 18kV/18kV	24.2%	20.5%	14.7%	11.5%	9.7%	6%	4.5%	3.4%	7.8%	Low Lowest Highest High
	18kV/16.5kV	23.4%	19.4%	14.1%	10.3%	7.9%	8.1%	5.5%	4.6%	9.3%	
	18kV/15kV	19.0%	15.0%	11.5%	10.4%	8.4%	9.2%	8.2%	7.6%	15.1%	
	Oscillating 2Hz 18kV/18kV	29.3%	24.2%	18.2%	12.4%	6.2%	4.2%	3.1%	2.1%	2.8%	
	18kV/16.5kV	26.3%	25.0%	20.8%	11.8%	5.9%	3.0%	2.4%	1.9%	4.7%	
18kV/15kV	26.1%	20.5%	16.9%	10.7%	7.7%	4.8%	3.5%	3.8%	6.3%		
Needle to collector distances											
Needle distance	14cm	30.8%	24.8%	16.9%	10.9%	5.4%	3.9%	3.4%	2.4%	2.0%	Indifferent
	8cm	32.3%	26.0%	16.1%	9.4%	5.9%	3.5%	2.7%	2.8%	1.3%	
Gap distance											
Collector distance [cm] at high voltage	4cm	31.8%	24.7%	15.6%	9.7%	4.0%	4.2%	3.9%	3.0%	3.1%	small gap  wide gap
	7cm	42.4%	27.2%	13.4%	8.6%	3.5%	1.9%	1.2%	0.9%	0.6%	
	11cm	28.6%	23.9%	18.1%	11.8%	6.1%	4.4%	2.7%	2.1%	2.3%	
Collector distance [cm] at medium voltage	7cm	26.0%	21.5%	16.4%	13.7%	9.8%	6.2%	3.0%	1.5%	1.2%	
	11cm	36.4%	24.0%	12.1%	6.7%	5.8%	4.2%	3.0%	2.5%	2.4%	
	18cm	25.6%	22.7%	15.9%	12.2%	9.9%	4.4%	3.4%	3.2%	2.7%	
Environmental Humidity											
	25%	31.9%	27.4%	16.9%	8.6%	5.3%	3.6%	3.2%	1.5%	1.7%	

relative humidity												High
	35%	23.1%	20.2%	15.6%	13.1%	8.2%	6.0%	4.8%	3.8%	5.3%	Low	
Alignment over Gels												
Collagen gel amount [ml] and distribution [cm ² over glass slide]	1x1cm (0.25ml)	38.4%	29.2%	16.9%	8.7%	3.2%	1.9%	0.5%	0.4%	0.9%	High 	
	1.5x1.5 (0.5ml)	35.3%	28.2%	16.5%	8.8%	5.1%	3.2%	1.6%	0.7%	0.4%		
	2x3cm (1ml)	27.7%	23.3%	16.5%	11.0%	6.4%	5.6%	3.6%	2.9%	3.0%	Low	
	glass slide control	41.9%	27.0%	13.6%	8.5%	3.3%	2.4%	1.2%	0.8%	1.0%		

4.4 Discussion

4.4.1 Dual field electrospinning and electrostatic field strength

Polymer nanofibres between 250nm and 1.2µm have been electrospun in alignment between two parallel rods of 2mm diameter with a gap distance between 4cm and 18cm. The variation in fibre diameter observed is consistent with previous reports, where fibres of 150nm to several micrometers were successfully electrospun over a variety of collector gaps [165,173,174]. So far, most techniques transfer the mat of electrospun aligned nanofibre onto the designated surfaces. A simple dual field electrospinning set up can spin directly onto a variety of surfaces such as glass slides, aluminium surfaces or hydrogels with polymer fibres. Surfaces which are selected for the coating process are placed ~1mm below the collector rod level. For the set up it is important that surfaces such as glass slides are positioned below the level of the collector rod so that they do not disturb the electrostatic field, which would terminate the fibre transfer between the two collectors. Aligned fibres will deposit onto those surfaces as long as these are isolated from any negative voltage source. Non-isolated parts can be charged up by leaking charges from the collector and changing the electrostatic field below the glass slide, which will attract random fibres (Figure 32, a). Fibres along the rods are electrospun according to the electro magnetic field

direction (Figure 36). The driving force for the fibre alignment is the electrostatic field between the two collectors and it is important that this electrostatic field remains undisturbed during the electrospinning process [162,174]. Further, it has been shown that support of the electromagnetic field increases the fibre quality [166]. However, the field strength is not equally distributed. The fibre accumulation shows two distinctive patterns, which can be related to the field strength. Fibres accumulate at the edge of the collector. The electrostatic field is strongest, at the sharp parts of the conductor, which are the edges of the rods. This phenomenon has been described earlier as a “point to point” electrospinning method and has been further investigated by Teo and Ramakrishna in 2005 [175]. In this regard it has been also postulated that rather than rods, collectors such as razors would provide better platform for direct fibre transfer [39].

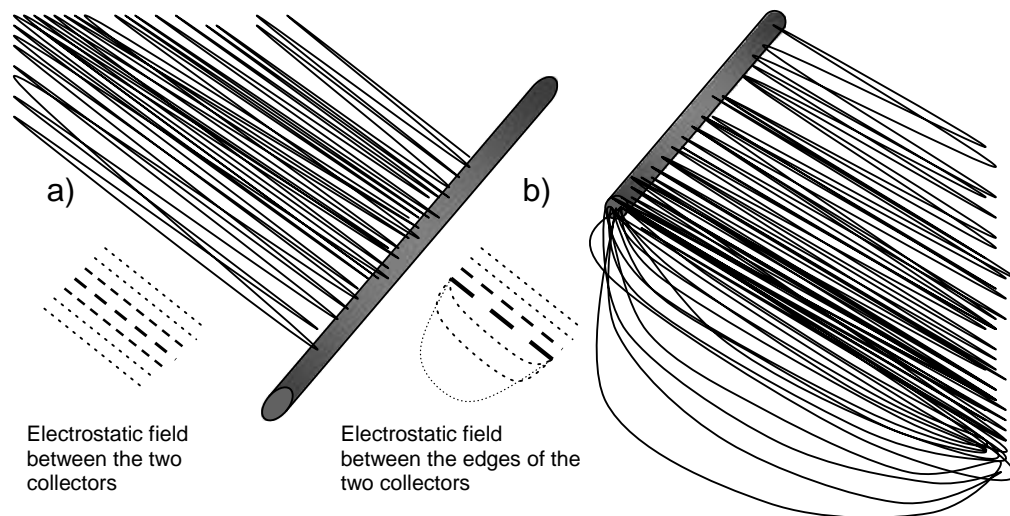


Figure 36 Electrostatic field

The Schematic (a) shows the general fibre position between two collectors, forming central distribution of fibres parallel to each other. The second schematic (b) shows the edge effect. Fibre deposition concentrates at the tip and creates concave fibre deposition in accordance to the expected electrostatic field lines (indicated by the dashed lines).

Although the electrostatic field has not been visualized in the experiments, the distribution pattern of the polymer fibres over the glass slide is specific to the electrostatic field strength. Higher voltages (i.e. 18kV) provide a stable electrostatic field strength, which is less affected by distance than a low voltage electrostatic field <12kV. Fibres are distributed more evenly over the coated area at high voltages. No significant changes in the electrostatic field were observed. At low voltage the magnitude of electrostatic field is concentrated in the centre below the needle tip.

The distance between needle and collector is closest in the centre, and the electrostatic field the strongest in that particular area. Hence, the fibre deposition occurs first at this point and distributes slowly to the periphery of the collectors. A Gaussian fibre deposition pattern was observed. Fibre accumulation first increased and then decreased until it reached a deposition maximum and interspatial fibre distance minimum. A similar effect has been demonstrated by Park and Yang 2011 [173]. The effect can be explained in that the deposited fibres carry a positive charge which is repulsive to other freshly ejected fibres [39,174]. Therefore, successive fibre deposition occurs at a certain distance from previously deposited fibres. Fibres maintain a specific distance to each other, which has been described earlier by the deposition analysis model [176]. Moreover, it was observed that deposition was influenced by humidity. High humidity allows fibres to carry a higher charge via water molecules at the polymer fibre surface. Also the air isolated glass slide accumulated more charges due to the electrostatic charge up of water particles in the air, which deposit onto the spin coated surface. Thus, accumulation of stray fibres and wider interspatial fibre distances are observed. In order to reduce this effect of residual charge, a dischargeable surface could be anticipated. The dual

electrospinning process coats surfaces with fibres, but is not able to spin aligned fibre mats, without first clearing the rods from the accumulated polymer or by discharging previously deposited fibres. The dual field electrospinning process was shown to be self terminating at low voltages. The termination of the spinning process was most likely due to a drop in electrostatic field strength. As the electrospinning process continued, the collectors were covered with polymer solution and positively charged fibres spun over the gap, which reduced the field strength. These two effects drive newly ejected fibres to the periphery of the rods. At a critical point, where the polymer insulates most of the collector, the electrostatic field strength diminishes and becomes insufficient to generate a stable Taylor Cone formation. I believe for this reason, that the attenuation in the electrostatic field strength self-terminates the electrospinning process and is also responsible for the Gaussian patterned deposition of fibres per area.

Alterations of the electrostatic field strength to one or the other collector side, either through needle position, different collector size- and geometry or voltage imbalance play an important part in the spinning. All these parameters can impair the electrospinning process and the fibre alignment and deposition pattern. Some of these parameters such as voltage imbalance between the two collectors can be stabilized by low frequency oscillation. It is reasonable to theorise that the low frequency forces the fibres to transverse from one to the other collector. Frequencies of 1Hz and above are beneficial to the transversal electrospinning process. Moreover, oscillating dual field electrospinning generates highly aligned fibres, despite changes in the electrostatic field strength or environmental factors such as humidity. In a different approach by Liu and colleagues, the alignment of electrospun fibres has

been improved at low voltages ($<6\text{kV}$), but with a high frequency (4-7kHz) auxiliary oscillating transverse electric field [176]. The mechanism is not known. However, it is known that the electrostatic charge on the insulating material such as rubber, plastics and polymer fibres is unequally distributed in comparison to a conductive material which provides an equal distribution of charges. Therefore residual charges of the electrospun fibre material deposit unequally over the surface. Further, the experiments in this work support the theory that addition of charge to the fibre coated surface via “leaking charges” from the collector itself can contribute to stray fibre accumulation (Figure 32). It has been described earlier (Chapter 3) that instability and stretching of the jet correlates with the increase of the applied voltage; hence it would be plausible that the jet instability is affected by charge differences as well. Therefore, I believe that an unequal charge distribution forces new electrospun fibres to deposit randomly on surfaces over time. An oscillating field might harmonize the charge distribution by actively shifting residual charges over the electrospun material to generate a rather equal charge distribution minimizing stray fibre accumulation. It is debatable to hypothesise whether higher frequencies will show greater benefits for the alignment and the reduction of stray fibres. However, due to technical limitations it was not possible to explore this phenomenon further.

4.4.2 Dual oscillating field electrospinning and fibre alignment

The alignment and accumulation of stray fibres of the polymer are influenced by a) the applied voltage b) gap distance of the collectors, c) spinning duration d) humidity and e) surface.

The principle of narrow alignment depends on residual charges in the electrospun nanofibre. As nanofibres accumulate on non-conductive material such as glass slides, the nanofibres retain mostly their charge. This has two effects. One mentioned earlier separates the fibres from each other due to electric repulsion. The other effects the orientation of the deposited nanofibre, due to differences between residual charges causing jet instability followed by less aligned fibres. In simulation it has been shown that this effect reduces the orientation by 10-15% [177]. Firstly, the more fibres deposited, the higher the residual charge, the more instable the jet becomes and the lower the alignment. Secondly, the stronger the electrostatic field the more residual charge is carried over by each nanofibre transfer. The residual charges can be controlled through the electrostatic field strength or voltage by maintaining a low humidity. However, there are more parameters which influence the electrostatic field strength of the dual field electrospinning process. For further research it would be beneficial to describe the influence of voltage and conductivity of the electrospun material, collector geometry and the changes of the electrostatic field strength during the electrospinning process.

Electrostatic field strength and residual charges are not the only factors that affect the dual field electrospinning process. Further alignment and gap distance converge at a specific voltage towards an optimum. In this regard Park and Yang [173] reported a higher alignment at increased gap width and Liu and Dzenis [177] simulated and experimentally demonstrated the benefit of collector to collector distance of about

7cm and wider collector distances for fibre alignment at low voltages of <12kV [177].

Controversially, Pokorny and colleagues showed the opposite effect for high voltage (20-25kV) dual field electrospinning [164]. Moreover, they showed that high voltages produced a peak alignment at 1mm distance and this declined at wider or narrower gap size. However, it was technically impossible to produce an electrostatic field of 12kV or less over a gap distance of more than 10cm. Therefore, data cannot be compared to those of Park and Liu who showed theoretically an “infinite” improvement of alignment with wider gap size at low voltages. Further investigations are required to determine whether gap size and voltage complement each other to produce a favourable higher alignment.

Other factors such as collector geometry have been not considered in this work, but further improvement of the fibre alignment has been shown with an inclined gap method at either high 25-30kV [178] or lower voltages 9-15kV [173] and with a tip collector instead of razors, bars or rods [165]. These electrospinning modifications can be applied to achieve higher alignment results and would be transferable to coat surfaces such as gels, metals, plastics and glass.

4.5 Conclusion

Dual field electrospinning generates narrow fibre alignment over surfaces. It produces a monolayer of aligned fibres over various surfaces such as glass, plastics, metals and hydrogels. Interspatial fibre distance is dependent on several parameters such as gap distance, collector geometry, electrospinning duration and voltage. The mechanism behind narrow alignment and deposition pattern is subject to residual charges of the electrospun fibres and underlying surfaces. On the one hand it is necessary to maintain residual charge of freshly electrospun fibre to separate one fibre from another, on the other hand charge accumulation and unequal distribution reduces the quality and alignment of the fibres. The initial charge of the fibres as well as the accumulation and distribution of charge over time on the fibre coated surface is crucial to the outcome. Therefore electrospinning duration and the applied voltage are identified key regulators to control the deposition process and fibre alignment quality. Moreover the distance between the collectors and humidity has to be evaluated appropriately for the process. Application of a low oscillating field compared to electrostatic field stabilizes the electrospinning process, reduces stray fibres and improves alignment. There is certainly room for improvement in the dual field electrospinning design and >80% fibre alignment has not been achieved so far. Dual field electrospinning technology is the only technology so far able to coat any desired surface with a monolayer of polymer nano/- microfibres. Therefore it would be advisable to further investigate in the electrostatic and oscillating mechanics and improve dual field electrospinning technology.

Chapter V

Interactions of polymer
nanofibres with
lymphatic endothelial
cells

Interactions of polymer nanofibres with lymphatic endothelial cells

5.1 Introduction

A long-standing challenge for tissue engineers is the rapid organisation of endothelial cells into a network of capillaries and their directed growth through an acellular tissue or scaffolds to reconnect with the native vasculature. The interactions between migratory endothelial cells and the surrounding environment are of central importance to this process, with cell orientation being achieved to a degree through the use of structured scaffolds. Studies with endothelial cells on aligned fibrous materials, for example, have shown that these cells recognise and respond to their topographical microenvironment, aligning and elongating, and eventually migrating in the direction of the fibre alignment [179]. In a process known as contact guidance, topographical features on the surface of the biomaterial substratum regulate the spatial distribution of adhesive contacts and thereby determine how a cell spreads. In general, vascular endothelial cells prefer smoother surfaces for adhesion and migration [180], nevertheless, they require a structured surface for cellular orientation. These principles have been used in practice to grow endothelial cells within hydrogels [181,182] and to direct cell proliferation and division on solid surfaces [183]. Thus surface topography plays an essential role during attachment and migration of endothelial cells equal in importance to that of surface chemistry [184]. Contact guidance is subject to hydrophilic surface chemistry for cellular attachment. ECM compounds, protein and growth factors in cell culture media are adsorbed by these surfaces providing a substrate for cellular attachment. Depending on the hydrophilicity of the underlying surface material cellular attachment can be

accelerated or strongly reduced. Contact guidance is subject to either attachment or repulsion to parts of the surface substrate. Therefore contact guidance can be provided and manipulated by either hydrophilic or hydrophobic material. The use of hydrophobic surfaces to promote cell guidance has been less investigated. The fabrication of guiding structures of hydrophobic and hydrophilic surface chemistry on two-dimensional surfaces and in three dimensional environments such as hydrogels has been a challenge so far. Approaches with nano-imprinting [184,185] have produced structured micro- and nano- surfaces for cellular contact guidance, but have not demonstrated a feasible three-dimensional scaffold. Nanofibrous scaffolds of random fibre meshes have a high porosity and the fibers provide a high surfacearea-to-volume ratio. The topographical features can encourage cellular adhesion, migration, proliferation and differentiation. Moreover, electrospun polymer fibre scaffolds demonstrate a 3 dimensional surface and as shown in this thesis they can be incorporated in hydrogels. These 3D hydrogel based scaffolds with highly aligned polymer fibers may be useful to replicate the ECM of specific tissue with topographic cues for “cellular guidance”.

Topographical cues translate into cellular growth directions, orientations and many other cell functions via the “cellular fingers”, the filopodia. Filopodia are thin membrane protrusions of 60-200 nm diameter with the parallel bundles of 10-30 actin filaments, the “cellular muscles”. Filopodia are oriented with the end of their actin filaments towards the protruding membrane (Figure 37). Filopodia sense the extracellular environment at their tips using cell surface receptors [186]. Filopodia are prominent in fibroblasts and neurites as growth cones but specialized endothelial cells show also growth cones at the tip of sprouting capillaries [187]. Filopodia,

especially during formation of growth cones, cyclically penetrate into the ECM, searching for inhibitory or stimulatory cues. It has been found that different cell types react to topographical cues from a few nanometers to several 100nm depending on shape and surface chemistry. Endothelial cells have been shown to respond to larger structures >200nm in terms of attachment and contact guidance [188,189].

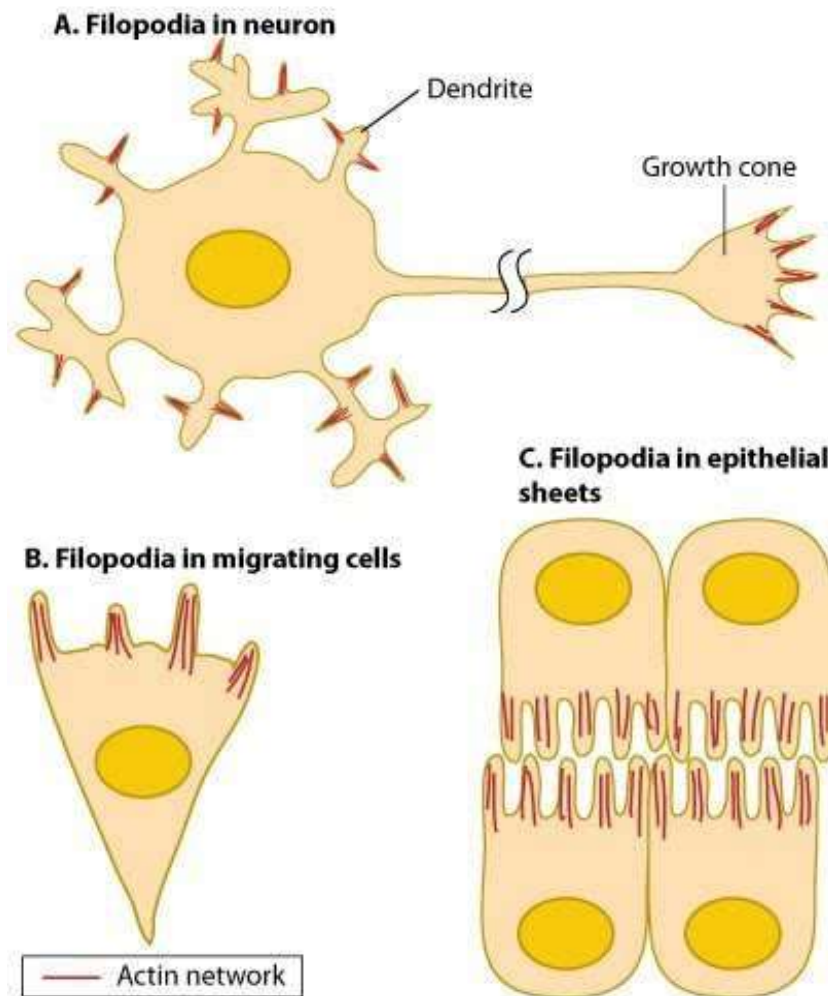


Figure 37 Different types of filopodia

Filopodia are prominent at the tips of neural dendrites and growth cones (A), the front edge of migrating cells (B), and at the interface between epithelial cells (C). (© by *Manual of Cellular and Molecular Function*, National University of Singapore, by Pham Thi Phuong Thao, 2010)

The model of contact guidance with topographical cues is well established for endothelial cell and neural cells [190]. Guidance cues may be diffusible chemicals such as growth factor gradients or contact of the physical structure of the surface [180]. Contact with the environment promotes the coupling of membrane-bound proteins to the backward (retrograde) flow of actin; this coupling produces the pulling forces needed for cell migration processes such as wound healing or capillary sprouting [191]. In contrast to hydrogel scaffolds which provide no directional cues, polymer nanofibres can interact directly with the growth cone providing contact guidance cues allowing for directed cellular growth; as reviewed by Nisbet [180].

It is already possible for skin [168], tendons [167], muscular tissue [3] and neural tissue [169] to create scaffolds which provide the topographical cues and contact guidance for alignment and growth direction, while providing an elastic substrate for cellular differentiation. Vascular endothelial cells have been proven to attach proliferate and migrate on electrospun fibre scaffolds [192], as well as to orientate along microstructure patterned surfaces [41]. Little is known about the lymphatic endothelial vasculature in comparison to the extended knowledge of vascular endothelial cell behaviour on surfaces and in hydrogels. Especially, research on the interaction between tube forming lymphatic endothelial cells and electrospun material has not been carried out yet.

The objective of this thesis was to determine how diameter, density and orientation of PLGA (50:50), PLGA (10:90) and PLDL (30:70), electrospun fibres affect morphology, attachment, proliferation, migration, cell elongation and tube formation of human lymphatic microvascular endothelial cells in collagen hydrogels and on flat surfaces. Fibre diameter varied between 100 nanometers to a few micrometers and

was oriented by the dual electrostatic field electrospinning procedure, which allows the coating of surface and hydrogels with precise fibre distribution, diameter and alignment. Tube formation of endothelial cells was induced by seeding of cells between layers of collagen. In addition various biomaterial coatings and hydrogels were evaluated for their ability to maintain lymphatic endothelial cells in three dimensional cultures. This chapter describes a systematic study the aim of which was to identify the parameters for directed growth of endothelial cells in two- and threedimensional culture environments, in particular the influence of fibre size, orientation, density and hydrophobicity.

5.2 Methods

5.2.1 Electrospinning and Polymer Casting over Glass Slides

The electrospinning set up, process and generation of random fibres is documented in chapter 3 and 4. In this study we used four solvent systems from which fibres were electrospun with different diameters. Moreover, we used the same materials to cast polymer film for cell culture. The materials are polylactide-co-polymers dissolved in HFIP: a) PLGA (10:90) at 10% (w/v), b) PLGA (50:50) 10% (w/v) c) PLDL (70:30) 5% (w/v) and d) PLGA (50:50) 6% (w/v) blended with 2% (w/v) collagen type I from rat tendon (Sigma, UK). The polymer solutions were electrospun at flow rates in the range 0.01 to 8ml/h and at applied voltages of between 12kV and 18 kV. Electrospun PLGA (50:50) (fibre diameters in the range 150-1000nm), and PLGA (50:50) / Collagen type I blends (fibre diameters in the range 100-250nm) were collected over 13 mm diameter glass cover slips (Figure 27). Glass cover slips were placed onto the aluminium foil of the collector plate and 3-5 ml of the polymer and polymer blend solutions were electrospun for 1-3h until the entire surfaces was covered with polymer fibres. The fibre material was dried for at least 24h in the fume cabinet. Thereafter, the fibre coated coverslips were cut out from the aluminium foil, vacuum air-dried for at least 24h and stored in desiccators under vacuum.

Polymer solutions of PLGA (50:50) and (10:90), and PLDL (30:70) in HFIP were cast over glass cover slips to produce polymer film. Glass cover slips were placed in a 10cm petri dish and layered with 2ml polymer solvent solution. The solvent solutions were air dried in a fume cabinet for 3 days and vacuum air-dried for additional 24h to generate a solid polymer film above the glass slides. The coated

glass cover slips were chipped off the petri dish and stored in a desiccator under vacuum.

Glass cover slips coated with polymer fibres or cast polymer films were fixed in 24well plates with medical silicone glue and dried for 3 days in a vacuum oven at room temperature. Prior to cell culture usage, the prepared 24-well plates were sterilized for two hours under UV light.

The previously described dual field electrospinning method in Chapter 4 was used to generate surfaces and hydrogels with aligned polymer fibres. The settings are comparable to the method in Chapter 4. Here we used 2 parallel orientated collector rods of 7 cm length which were separated by a gap distance of 5-8 cm. The needle was placed 14cm above and at the centre between the two collector rods. Fibres were electrospun onto a thin glass slide (Ultima, UK) or onto the surface of freshly cast collagen gels for periods of 1-10 min. The solvent system and flow rates were PLGA (50:50) 10% w/v and PLGA (10:90) 10% w/v at a flow rate of 1ml/h, and PLLA (70:30) at 3.5%, and 5% w/v at 0.25-0.5ml/h. The applied voltage was set between 9kV and 15kV. The electrospinning process was run at room temperature and environmental humidity. Prior to cell culture experiments the polymer nanofibres were sterilized for 2h under UV light.

5.2.2 Polymer Fibre, Film and Collagen Matrix Analyses

Electrospun samples were visualised by scanning electron microscopy (TM-1000, Tabletopmicroscope, Hitachi) and the diameter and morphology of individual fibres quantified with ImageJ® software. Bright field, dark field or phase-contrast images were captured with an upright microscope (Axio Imager Z1, Carl Zeiss Ltd, UK).

These images were used to calculate interspatial fibre distance as well fibre alignment as described in Chapter 3.

The topography of the collagen-nanofibre constructs was quantified by Atomic Force Microscopy (MFP-3D, Asylum Research, UK) in contact mode and fitted with an Olympus silicon-nitride micro-cantilever probe (TR400PB). Samples on glass cover slips were washed with deionised water to remove salt crystals. The air dried samples were mounted onto the scanning stage and fixed with two magnetic strips. The cantilever was lowered close to the surface. The laser light is focused with the manual wheels at the tip of the cantilever. The resulting SUM of the laser adjustment was around 3. The deflection was set manually with the hand wheel between -0.2 and -.0.22. Prior to engaging the tip of the cantilever to the surface the Z Voltage was adjusted to 70 and the surface scanning mode options were set: Set point was adjusted to -0.200V and gain was fixed between 6.5-7V. The scan angle was set to 90°C, initial scan size was 40µm. Scan size was lowered to 10-5µm after the first image was processed. Scan lines vertically and horizontally were set initially to 64 and increased to 1024 lines per scan to achieve higher image resolutions. Scan speed was 10µm/s and below. After engaging the cantilever with the surface, adjustment of gain and set point were carried out to optimize the image quality. Resulting readouts were processed with Asylum Software to evaluate fibre diameter, material depth and fibre surface morphology.

5.2.3 Lymphatic endothelial cell attachment assay

Electrospun PLGA (50:50) (fibre diameters in the range 150-1000nm), PLGA (50:50) / Collagen type I blends (fibre diameters in the range 100-250nm) and PLGA

(50:50), PLGA (10:90) and PLDL films were prepared and used as attachment surface in this experiments. Nanofibre diameter was assessed with the same method as described in Chapter 3 and 4.

In the first experiment the influence of different surface chemistries of nanofibres and polymer films on cellular attachment was investigated. Polymer films and nanofibres were not pre-equilibrated in cell culture media in order to show the effect of surface hydrophobicity and protein adsorption as a factor for cellular attachment.

PLGL (50:50) polymer nanofibres (with a diameter of 800-1000nm), PLGA (50:50) /

Collagen type I blends (with a diameter of 150-250nm) and the three polymer films (PLGA (10:90), (50:50) and PLDL) were seeded at a density of 150,000 cells per well after surface sterilization. LECs on non-equilibrated polymer films and nanofibres surfaces were cultured for 18h. Thereafter, surfaces were washed twice with PBS, and the number of attached cells was determined using a colorimetric MTT formazan assay (MTT assay, chapter 2). A few samples were fixed with 4% para-formaldehyde and stained with acridine orange (see below). These samples were visualized with a fluorescence microscope (Axio Imager Z1, Carl Zeiss Ltd, UK) to demonstrate the morphology of LECs attached to nanofibre mats.

In the second experiment the effect of fibre diameter on cellular attachment was investigated. PLGL electrospun (50:50) mats with an average fibre diameter of 250nm, 500nm, 1000nm and tissue culture plastic as control surfaces were equilibrated for 24-48h in endothelial culture medium (EMB-2, Lonza) prior to cell seeding in order to allow proteins to adsorb and to minimize the effect of surface chemistry dependent cell attachment. Thereafter, LECs were seeded at 100,000 cells

per well. LECs on equilibrated PLDL (50:50) nanofibre mats were cultured for 30min, 1h and 3h (LECs culture method, Chapter 2). Thereafter, surfaces were washed twice with PBS, and the number of attached cells was determined using a colorimetric MTT formazan assay (MTT assay, Chapter 2).

5.2.4 Lymphatic endothelial cells growth assay on nanofibre mats

Electrospun PLGA (50:50) fibre mats with a diameter between 750nm-1000nm were prepared on glass coverslips, mounted into 24-well plates and sterilized (detailed description see 5.2.1). Prior to cell seeding the electrospun mats were equilibrated for 48h in endothelial culture medium (EMB-2, Lonza). LEC were seeded at 65,000 cells per well and cultured in endothelial cell culture medium (LECs culture method, Chapter 2). Every 24h wells were washed with PBS and the number of proliferating cells over 5 days was determined using a colorimetric MTT formazan assay (MTT assay, Chapter 2).

5.2.5 Lymphatic endothelial cells migration assay

PLGA (50:50) nanofibres (with a diameter of 400-1000nm) and PLDL (70:30) nanofibres (with a diameter of 300-500nm) had been deposited on glass microscope slides and were sterilized with the method above (4.2.1). The interspatial fibre distance varied from sample to sample. Samples with an interspatial fibre distance of <math><4\mu\text{m}</math>, 4-8 $\mu\text{m}</math>, 8-19 $\mu\text{m}</math> and 20-50 $\mu\text{m}</math> were grouped and used in this experiment. The slides were immersed in endothelial cell culture medium for 24h, after which a previously autoclaved heavy stainless steel ring, i.d. 11mm, was mounted in the middle of the glass slide. LECs were seeded inside the ring at a density of 150,000 cells. After 24h culture in endothelial cell culture medium the ring was removed and$$$

slides washed in PBS. Slides were cultured for an additional 10-14 days in endothelial culture medium and then fixed in 4% para-formaldehyde, stained with DAPI and visualized with fluorescence microscopy. Images were taken of the whole glass slide in a mosaic pattern with 12 x 9 frames at 5x magnification. Images were stitched together with the Axio Vision software and exported as a single image. Cell migration and outgrowth from the seeding point was quantified with ImageJ® software (Figure 43) and the aspect ratio of the cellular growth area in the horizontal versus vertical directions calculated in each case. LEC growth was estimated by subtracting the initial seeding area, and expressing the results as growth (area) per day. The distance between the cell frontier and the position of the initial ring barrier was measured and expressed as migration in microns per day. Morphology of the actin cytoskeleton was visualized with phalloidin staining (see below 5.2.8).

5.2.6 Tube forming assay

PLGA (50:50), (10:90) or PLDL (70:30) polymer nanofibres were deposited on glass slides via electrospinning and sterilized for 2h under UV light (see above 5.2.1). The electrospun polymer fibres were between 100-1500nm in diameter and showed an interspatial distance of between 2 and 50 micrometer. A stainless steel metal ring (11mm i.d.) was placed on the surface to define the cell culture area, and LECs seeded into the ring well at a density of 1×10^5 cells/ring area. Cells were cultured in endothelial cell medium for 24h. Thereafter, medium was renewed and supplemented with 100mg/ml collagen type I (ApColl®, Devro Medical Ltd., UK). Cells were cultured for additional 24h. Samples were stained with acridine orange and propidium iodide (see below 5.2.8) to demonstrate cell viability, migration and

tube formation. Images of the vacuoles that formed between the cells in the horizontal versus vertical direction were captured and the aspect ratios quantified with ImageJ® software (Figure 39, a and b). The samples were visualized at 10 x magnifications with a fluorescence microscope (Axio Imager Z1, Carl Zeiss Ltd, UK). Several images were taken to quantify a sufficiently large area per sample. The images were combined of in a mosaic of 3x3 frames and stitched together with Axio Vison software.

5.2.7 Cell staining: Viability, Cytoskeleton and Morphology

LECs from growth, migration and tube forming assays were stained with Acridine Orange (Molecular Probes,US) for live cells and Propidium Iodide (Invitrogen, UK) for dead cells. Nuclear staining was performed with DAPI (Sigma, UK) after fixation in 4% para-formaldehyde. For the detailed protocol see chapter 2.

Actin filaments of the cytoskeleton were stained with Phalloidin-FITC conjugate (Molecular Probes, US). Cells or cell-gel-nanofibre constructs were rinsed with PBS to remove media components. LECs and gel constructs were fixed in 4% paraformaldehyde in PBS (freshly prepared) for 15-45 min at room temperature. The time and concentration of fixative varied, depending on the thickness of the specimen (time for fixative to diffuse into the sample).

Phalloidin binding requires the F-actin to have a protein structure which is nearly native. The methanol or acetone used to fix and / or permeabilize essentially abolishes phalloidin binding. Preparation of Phalloidin solutions require methanol. However, the amounts of methanol used do not inhibit the binding totally.

Nevertheless, fixation is the critical step in the procedure.

The phalloidin vial content was dissolved in 1mL methanol to yield a final concentration of 200 units/mL, which is equivalent to approximately 6.6 μ M. This stock solution was diluted further with 4 ml solution of 1% BSA in PBS. Aliquots can be stored at -20°C. Working solution was diluted further 1:10 with PBS.

After fixation, cells were washed with PBS 3 times in PBS, 5 min/wash and incubated in FITC conjugated-phalloidin solution for 15-30 min in darkness at room temperature. Thereafter, samples were rinsed 3 times in PBS, 5 min/wash. No mounting medium was used; samples were visualized immediately after staining. A few samples were further stained with DAPI (for DAPI staining refers to Chapter 2). Representative images of cell viability and morphology, and the cell cytoskeleton during attachment, growth, tube forming and migration assays, were captured with an epifluorescence microscope (Zeiss Axio Imager, Zeiss Ltd, UK).

5.2.8 Experimental design and statistical analyses

Experimental results are expressed as mean +/- standard deviation. The analyses of fibre diameter and interspatial fibre distances were evaluated from 3-6 images, which were captured from 3 to 5 independent samples, each with a minimum of 100 fibres; likewise the analysis of fibre orientation was based on measurements made on a minimum of n=3-6 images each from 3-5 individual samples. Tube formation pattern from 3 individual samples were evaluated from 9-27 images with n>150 measurements of length and width of cell elongation patterns. Cellular migration on fibres was performed with a minimum of n=3 experiments and the MTT tests on polymer films and fibres were designed with n=3-6 replicates to ensure experimental reproducibility. Data were grouped and analysed using Student's T-test between two

groups and ANOVA for comparison between several groups. Statistical significance was assigned to results where $p < 0.05$. Data analyses with ANOVA were performed with <http://www.physics.csbsju.edu/stats/anova.html>. As an example complete analyses reports and box plot of Figure 38, a, and Figure 42, b and d are part of the supplemented material annex.

5.3 Results

5.3.1 Attachment and Growth of LECs on polymer films and fibres

LECs showed superior attachment to PLGA (10:90) films than to other materials used (Figure 38, a). LECs attached less well to PLDL and PLGA (50:50) after 18h than to PLGA (10:90) and tissue culture plastic. Cells seeded on electrospun PLGA (50:50) nanofibres with a diameter of $\sim 1\mu\text{m}$ showed a similar attachment to PLGA (50:50) films. Blending PLGA (50:50) polymer with 2% collagen type I increased the cellular attachment significantly though not on fine fibres of $\sim 150\text{nm}$, which again emphasises the importance of surface topography. Immersion of the electrospun polymer nanofibre and polystyrene tissue culture plates for at least 48h in culture medium prior to cell seeding allowed the cells to attach to the surfaces within a few hours (Figure 38, b). Moreover, attachment was significantly greater on microfibrinous mats with average fibre diameters of about $1\mu\text{m}$ compared to mats comprising nanofibres less than 500nm in diameter; however the initial attachment of cells onto $1\mu\text{m}$ thick fibres was poor compared to the attachment on flat surfaces. Cell growth on PLGA (50:50) nanofibres compared to flat surfaces was slower by more than 1.5 fold (Figure 38, c). A confluent monolayer on flat surfaces was observed at day 4, whereas cells on $700\text{-}1000\text{nm}$ diameter nanofibre mats remained

non-confluent after 7 days (Figure 38, d). LECs exhibited a cobblestone morphology on random nanofibre mats and their viability was confirmed by live/dead staining.

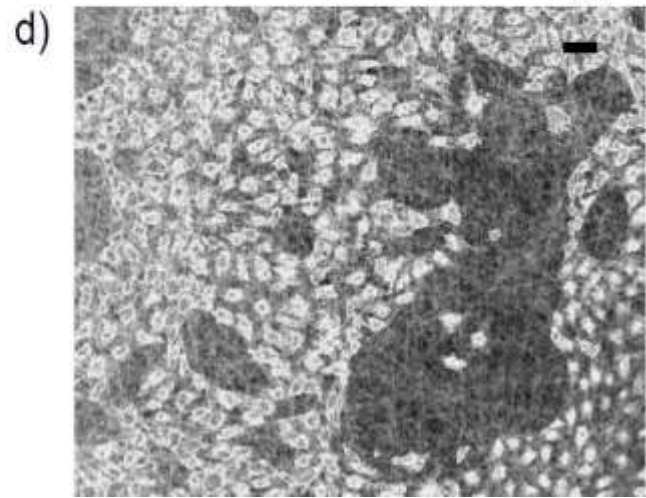
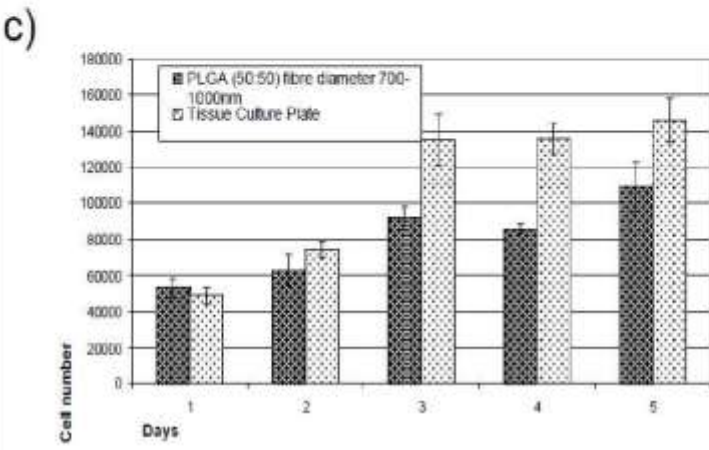
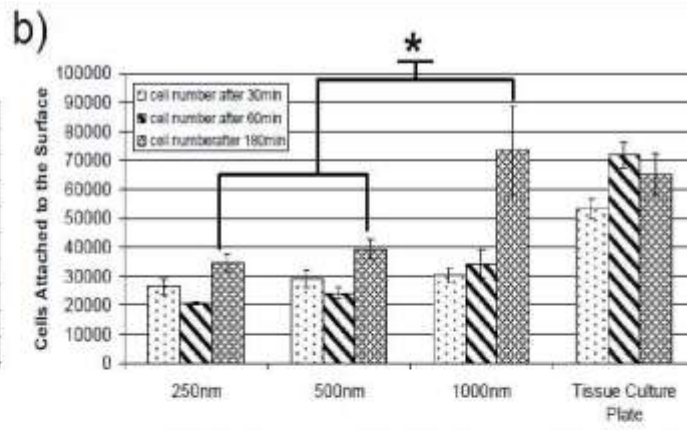
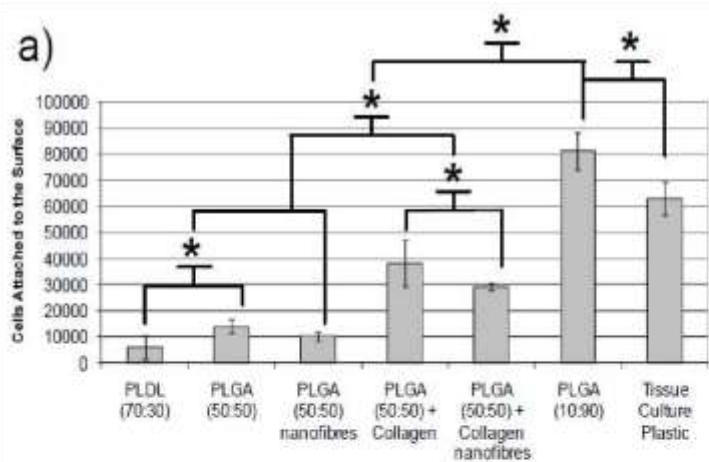


Figure 38 LECs attachment and growth on randomly oriented nanofibres

Attachment of LECs on non-equilibrated polymer films and nanofibres of PLGA (10:90), PLGA (50:50), PLDL (30:70) and PLGA (50:50) / collagen type I blends after 18h (a). Nanofibres of PLGA (50:50) are 800-1200nm.

Nanofibres of PLGA (50:50) collagen blend are 100200nm. Attachment of LECs on culture medium equilibrated PLGA (50:50) of different fibre diameters (250nm - 1000nm) after 30-180min (b). Growth of LECs on culture medium equilibrated PLGA

(50:50) nanofibres compared to growth on tissue culture plate (c). Merged fluorescence and bright field image of LECs stained with Acridine Orange and Propidium Iodide after 7 days growth on random PLGA (50:50) nanofibres (700nm diameter), colours in gray scale, scale bar 50µm (d)

5.3.2 Topography of aligned fibres influences cellular tube-like formations and morphology

Tube-like formations of LECs were induced by deposition of collagen type I over a confluent monolayer of cells, which were cultured on glass or collagen gel surfaces with nanofibres. The glass and collagen type I gel surfaces were coated with random and aligned polymer nanofibres of different diameters between 150nm to 1500nm, a spatial distribution of 3 μ m to 50 μ m and aligned parallel to within \pm 30 degrees. The 3D collagen network induced rapid cell migration and reorganisation of the cobblestone-like monolayer. The migrating cells formed a tubular network in a honeycomb shape. The length and width of the honeycomb structures showed a symmetrical distribution (Figure 39, a). The presence of nanofibres influenced the cell organisation and the resulting honeycomb pattern. On flat surfaces and random nanofibres cells adopted a morphology having an equal length to width ratio (Figure 39, a and d), but they become elongated when in contact with aligned nanofibres (Figure 39, b and c), aligning themselves in the direction of the underlying nanofibres. The live/dead staining showed viable LECs on aligned and random fibres (Figure 39, c, d).

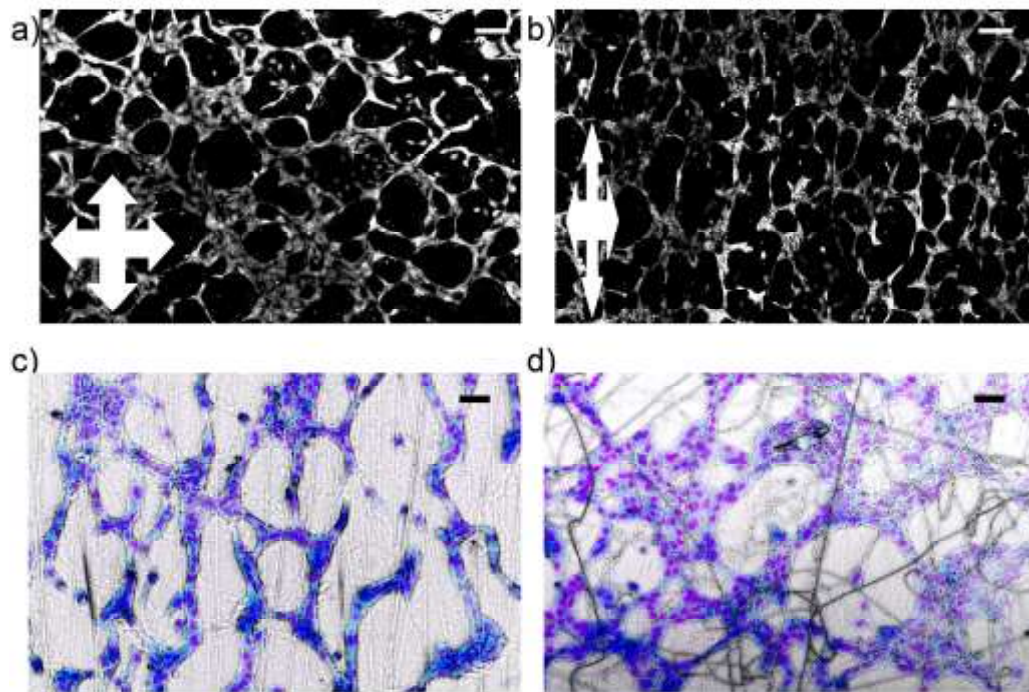


Figure 39 Tube formation of LECs on nanofibres in 3D collagen gels

LECs exhibit a honeycomb pattern on random or flat surfaces after migration and tube-like formation is initiated with collagen deposition (a). The pattern changes on aligned nanofibres, the aspect ratio of the honeycombs becoming elongated in the direction of the fibre alignment (b). LECs were stained with acridine orange, fluorescence images of a 3x3 mosaic (2,64mm x 2mm) were taken and the aspect ratio of the vacuoles was evaluated (results: Figure 42). Images of Live/Dead stain of LECs on aligned fibres (c) and random fibres (d) (PLGL (50:50) with a diameter of >800nm) were taken 24h after collagen deposition by fluorescence microscopy, merged with a phase contrast image. The colours are inverted: a purple cell nucleus indicates viable cells, a dark blue nucleus indicates cell death; straight white-grey lines represent nanofibres and the fine white network between the nanofibres and endothelial cells are collagen type I fibres. The scale bar is 50 μ m.

The morphology of LECs and the actin filament expression as well orientation is influenced by the surface material (Figure 40). On tissue culture plastic LECs showed a distinctive cobblestone pattern with most of the actin filaments expressed at the cell line border. There was no actin orientation. On matrices such as soft collagen gels (1mg/ml) a less obvious cobblestone assembly was observed and the actin filament expression was strongly reduced when compared to cells attached on

hard material such as the tissue culture plate. Cells in tubular formation induced by a layer of collagen gel on top showed weak expression of the actin filaments. The actin filament orientation and expression was directed alongside cell-cell binding contacts, which were randomly orientated. Nanofibre-collagen constructs, with PLDL (50:50) nanofibres of >1000nm diameter orientated the actin filament of attached and tube forming LECs in the direction of the polymer fibres. Actin filaments were more strongly expressed in the images with nanofibres.

Atomic force microscopy showed the size and morphological differences between polymer nanofibres and collagen fibres. The polymer nanofibres showed a smooth surface and a diameter of ~500nm, whereas collagen fibres consisted of a helical structure of <250nm in diameter (Figure 41, a). Collagen fibres overlay the polymer fibers in random patterns. In collagen gel constructs with tube forming LECs, nanofibres and cells were covered completely with helical collagen fibres (Figure 41, b). However, a continuously strong difference in depth (>700nm) in a single direction indicates the position of a polymer fibre covered with collagen fibres and LECs. LEC attachments to the collagen matrix lead to a matrix reorganisation during tube formation. A depth difference between 400-600nm of randomly orientated collagen fibre might indicate tube forming cells and dense cell colonies. The scanned samples are dehydrated; therefore, intact cells are not visible. However, single peaks in the depth profile indicate cellular nuclei. The accumulation of collagen in a random pattern indicates the “ghost tunnels” of dehydrated tube forming LECs.

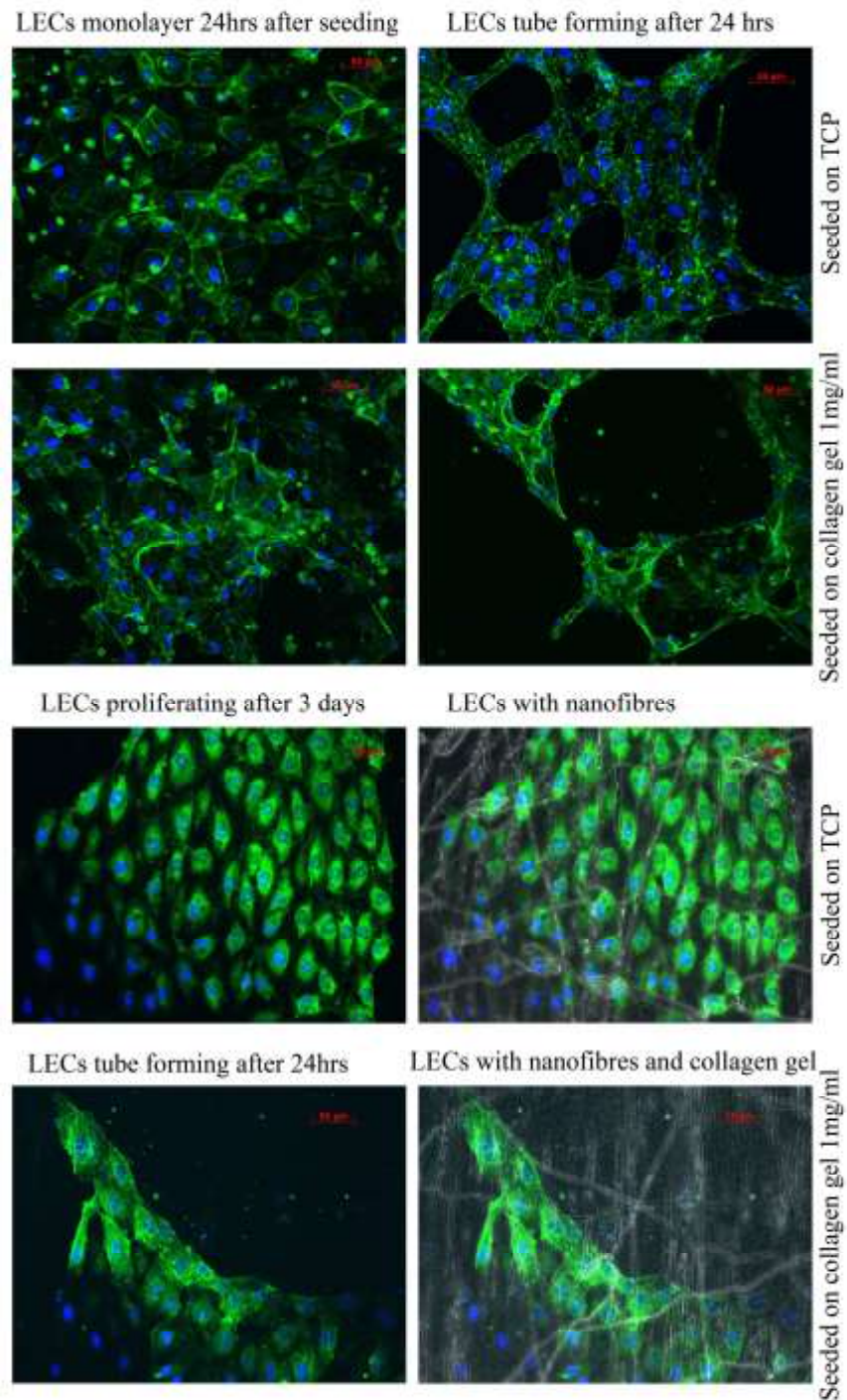


Figure 40 Actin filament of LECs

Images show the staining with Phalloidin-FITC conjugate of the actin filaments (green) and DAPI staining of the cell nucleus (blue) of LECs. The actin filaments of attached LECs are shown on TCP and on soft collagen gel and during tube formation. LECs attachment on nanofibre-collagen gels (PLGL (50:50) with a diameter of >1000nm, collagen gels 1mg/ml) and tube formation in collagen gel sandwiches is shown as fluorescence images and with the

overlaid phase contrast image of the nanofibres. Images were taken with the Zeiss epifluorescence microscope (Zeiss Axio Imager, Zeiss Ltd, UK) at 20x magnification.

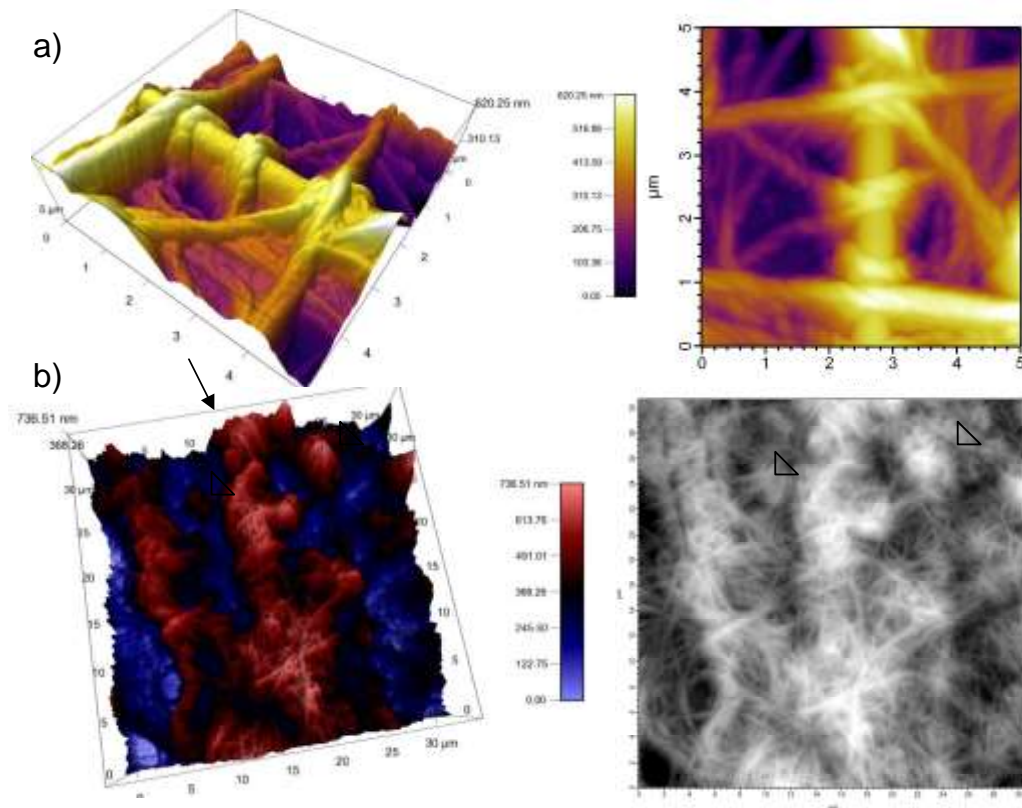


Figure 41 Atomic force microscopy of collagen-nanofibre constructs with LECs
 The image a) shows a nanofibre (white arrow) covered with collagen fibres in 3D (left column) and 2D (right column). The smooth nanofibre of $\sim 400\text{nm}$ surrounded by helical collagen fibres $\sim 200\text{nm}$ visible in image was acquired with the atomic force microscope operating in contact mode and fitted with an Olympus siliconnitride micro-cantilever probe (TR400PB). The surface was scanned at a scan rate of 0.23Hz with 512 data points acquired per line and 512 lines per image. Image size was $5\mu\text{m} \times 5\mu\text{m}$. Image (b) shows the air dried sample of LECs embedded in a nanofibre collagen gel construct. Polymer fibres are overlaid with collagen fibres but the 3D image acquisition (left column) shows the position of an aligned polymer fibre identifiable by a straight line with a strongly increased depth difference of over 600nm (black arrow). LEC nuclei may be identified as rounded structures in the 2D images (right column), and in 3D as peaks of $\sim 300\text{nm}$ size (white arrow head). The position of tube forming cells (white arrow) is indicated by collagen fibre accumulation in continuous non linear patterns with a depth difference of $400\text{--}500\text{nm}$. The image was acquired with the same setting as before. The surface was scanned at a scan rate of 0.23Hz with 1024 data points acquired per line and 1024 lines per image and the size of the image was $40\mu\text{m} \times 40\mu\text{m}$.

The vacuole aspect ratio was calculated from a series of images comparable to Figure 39, a) and b) with variation in fibre alignment, diameter, density as well as matrix surface. A positive aspect ratio in the charts indicates the migration of cells along the nanofibre direction. In the presence of aligned fibres LECs significantly changed their aspect ratio (Figure 42, a). The aspect ratio increased in proportion to the density of the layers of nanofibres (Figure 42, a). However, fibres below 350nm, which had a similar diameter to the collagen type I random fibres of the gels showed no significant difference in their aspect ratio when compared to thicker fibre diameters. LECs were significantly affected in their migration and tube forming process by a minimum coating of 20 fibres per mm (Figure 42, a). The aspect ratio peaked at a distribution of approximately $\sim 5\mu\text{m}$ fibres on glass surfaces and $\sim 10\mu\text{m}$ on collagen gel surfaces (Figure 42, a and b). Flat glass surfaces showed up to 3 fold stretch in the direction of the fibres, whereas in collagen type I gel sandwiches the stretch effect remained under 2 fold. Not only did surface chemistry and compliance influence the cellular migration but it was also influenced by the material properties of the nanofibres. PLGA (10:90), which previously demonstrated advantages for cellular attachment, was less likely to direct cell migration along the fibres compared to PLDL, which previously showed a very low affinity for cellular attachment (Figure 42, c).

Another factor was the alignment of the fibres. On densely packed surfaces with nanofibres, cells exhibited a strong elongation and migration in the direction of the fibre alignment. However, a low fibre alignment greater than 15 degrees eliminated this effect (Figure 42, d). The cellular response on lower densities of nanofibres was less influenced by the alignment of the nanofibres.

Overall this fast migrating 3D assay showed an increased elongation and migration of LECs by fibres of thicker diameter, a spatial fibre distribution slightly below the size of the endothelial cells, less adhesive polymer fibres and a high fibre alignment. Moreover, a compliant matrix, such as collagen hydrogels, reduced the overall effect compared to solid glass surfaces, but cellular elongation and migration was still significant.

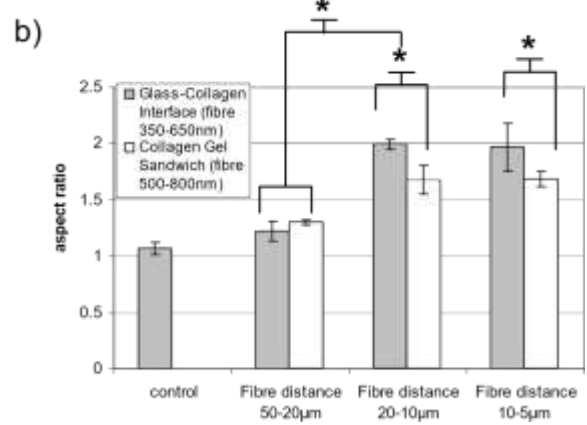
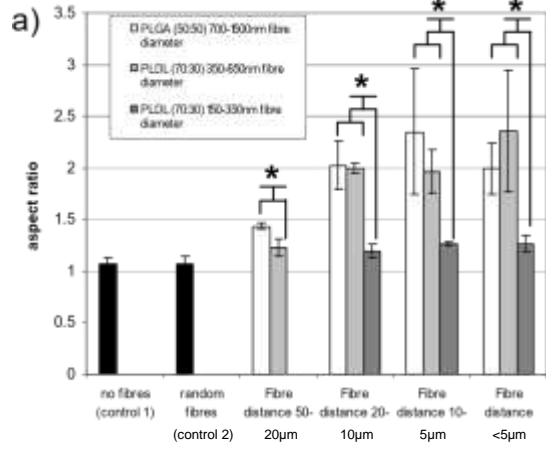
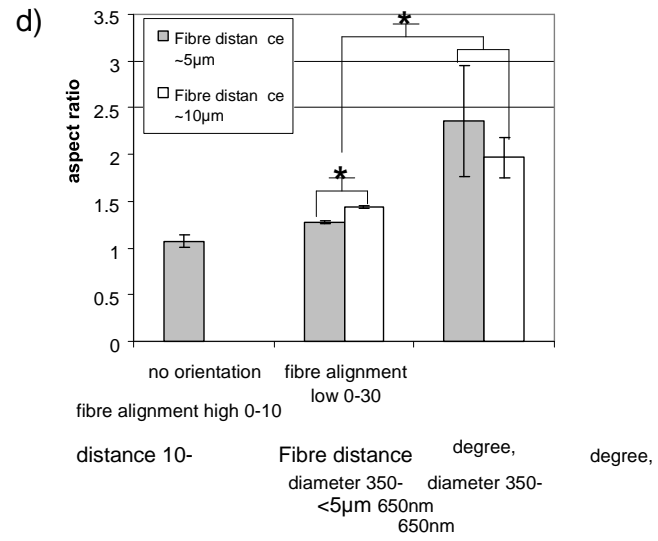
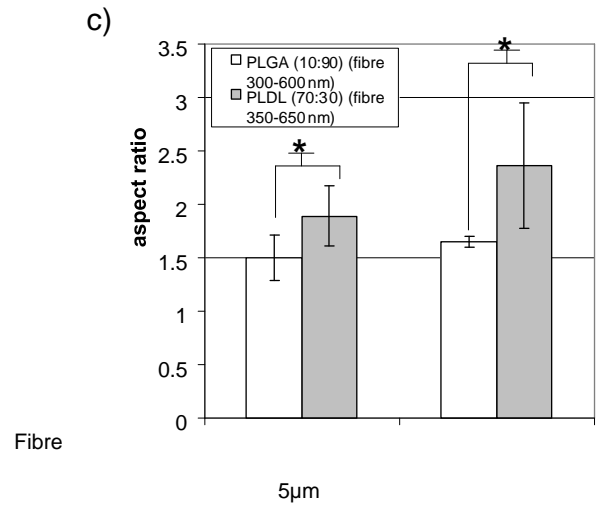


Figure 42 Determination of aspect ratio of tube forming LECs

The aspect ratio changes >1 when fibre diameter is >300nm (a). There is no significant difference in the aspect ratio between PLDL (70:30) nanofibres of 350/650nm and PLGA (50:50) nanofibres of 700/1500nm. The aspect ratio increased with increasing fibre deposition (a-b). Surface materials such as soft collagen gels significantly reduce the aspect ratio when compared to glass surfaces (b). PLDL (70:30) compared to PLGA (10:90) of similar fibre diameter and deposition increased the aspect

ratio of the tube forming LECs significantly (c). Higher fibre alignment correlates with a higher aspect ratio (d).



5.3.3 Migration of LECs on aligned nanofibres

LECs seeded into the well structure show a distinctive outgrowth and migration pattern in response to the underlying topography of nanofibres. The outgrowth of the cells aligned in the direction of the nanofibres and an elliptic pattern was formed after 12-14 days in culture (Figure 43, a). The growth pattern is formed by cone shaped outgrowths of cells from the main body. Moreover, single cells separated, strongly elongated and migrated rapidly along the direction of the nanofibres (Figure 43, c). In general, LECs migrated 2-fold faster in the direction of the aligned nanofibres (Figure 44, b). The aspect ratio, cellular growth and migration speed in the direction of the nanofibres increased with the nanofibre deposition (Figure 44, a and b). However, at very high nanofibre densities cellular growth was significantly reduced. Nevertheless, the aspect ratio of cells growing in the horizontal (with the nanofibre alignment) versus vertical (against the nanofibre alignment) direction increased significantly. A comparison of highly aligned PLLDL nanofibres (>75% of the nanofibres are in the range between 0°-15°) to low aligned nanofibres (>75% of the nanofibres are in the range between 10°-30°) of the same diameter showed similar results as before (Figure 44, d). Low alignment showed an increased aspect ratio, but significantly reduced cellular migration in fibre direction by 50% compared to high alignment. The total growth area was reduced by more than 50% from 612 μm^2 /day at higher fibre alignment to 281 μm^2 /day at lower fibre alignments. LECs were restricted in growth and migration by densely aligned nanofibres and poor alignment. Nanofibre surfaces compared with flat surfaces showed an overall smaller growth, but the difference in growth rate was less significant on low fibre

distribution of $>5\mu\text{m}$. In addition, fibre diameter affected the growth area per day of LECs significantly. Fibre diameter above 500nm reduced the total growth by half, but showed a relatively minor attenuation in the cellular migration and no differences in the aspect ratio (Figure 44, c). LECs were not only restricted in growth by the amount and degree of alignment of the deposited nanofibre, but also by their dimensions in height or diameter.

The nanofibres exhibited two functions: one is to direct and enhance migration of the cells along the fibres; the other is to restrict cells to grow in a direction normal to the surface of each fibre. The nanofibre-coated surfaces of ~ 200 fibres per mm and above successfully combined high cell migration and proliferation with a distinctive cell orientation.

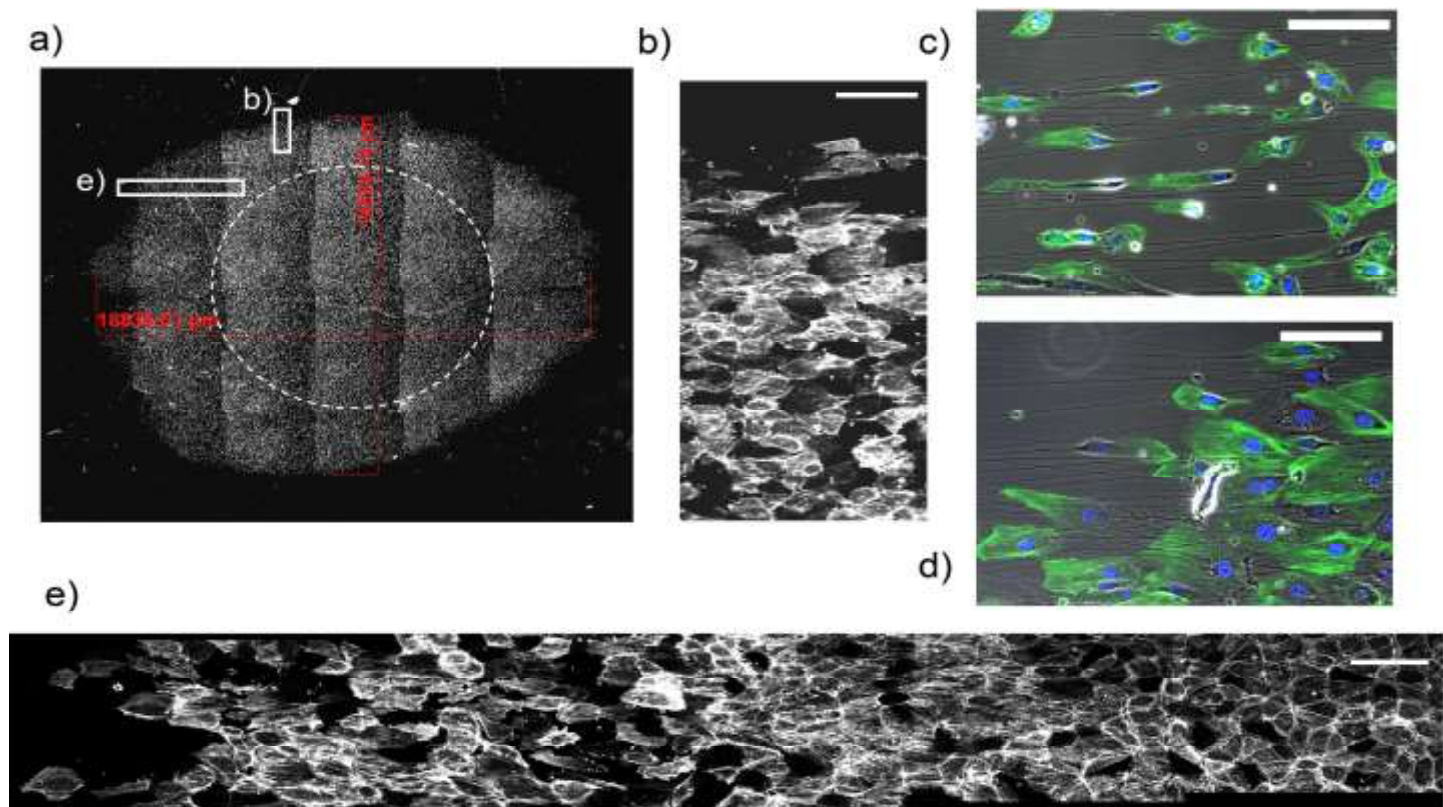


Figure 43 Morphology and actin staining of LECs on aligned nanofibres

LECs seeded within an 11mm circle (dashed line, a) and grown for 12 days on nanofibre structured surfaces show an elliptical outgrowth in the direction of the nanofibres (a). The nuclei of LECs were stained with DAPI (a, c, d). Actin staining was performed with Phalloidin-FITC to show the cytoskeleton (b-e). In the horizontal direction, LECs show cobblestone morphology at the seeding area and an organized cytoskeleton of elongated cells at the growth frontier (e). In the vertical direction cells show a mixture of cobblestone and elongated morphology (b). Phase-contrast images of cells and PLDL (70:30) nanofibres were merged with fluorescent images of the DAPI (blue; cell nucleus) and Phalloidin-FITC (green; cytoskeleton) stain (c, d). The images highlight the difference in cell morphology on low fibre densities (c) and high fibre densities (d)

Actin staining revealed that the mechanism of attachment to the nanofibres is not significantly different to that on flat surfaces (Figure 43, e): while migrating cells adjusted their cytoskeleton in the direction of the nanofibres, resting cells exhibited a cobblestone morphology. Moreover, LECs stretched several fold of their actual cell size when located between two narrow aligned fibres while some cells develop growth cone tips (Figure 43, c). Those LECs that resided between two fibres migrated and elongated into the space between the fibres. On densely populated fibre surfaces LECs stretched over several fibres (Figure 43, d). Despite their aligned actin fibre filaments they show a reduced spindle shape. LECs showed a mixture of cobblestone and aligned cytoskeleton at the outgrowth frontier at right angles to the predominant direction of fibre alignment (Figure 43, b), which was indicative of reduced growth and migration in that direction. The morphology and cytoskeleton analyses demonstrated that cells correlated their shape and actin filament with the alignment of the fibres. Thus, the presence of those fibres appeared to constrain cellular elongation and migration against the direction of those fibres.

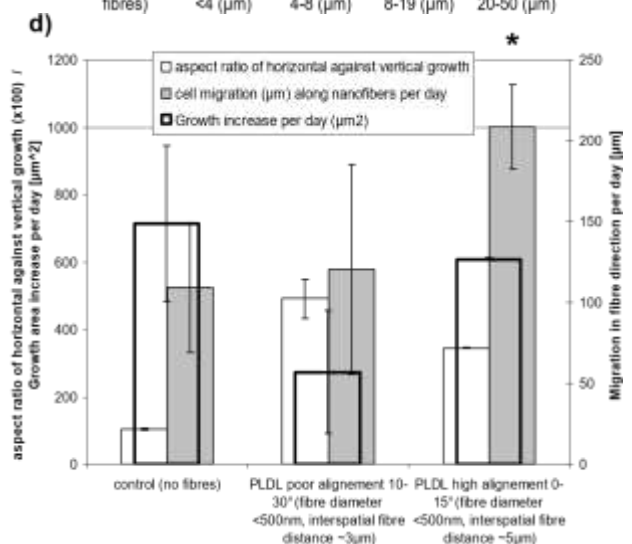
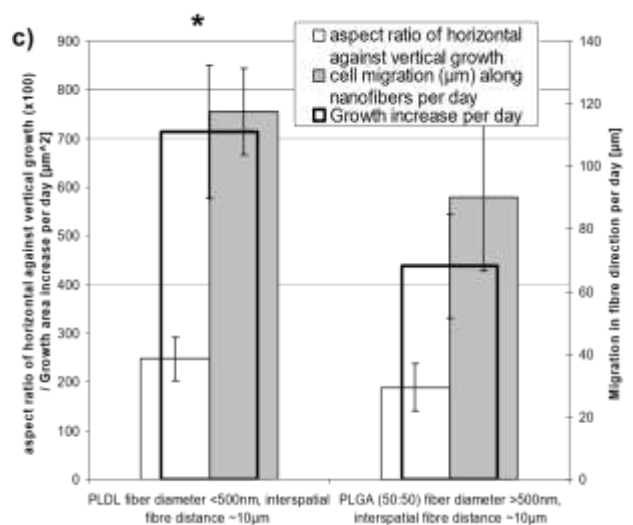
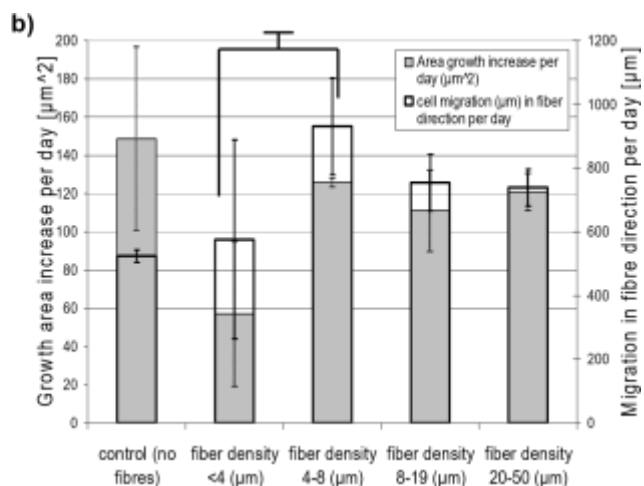
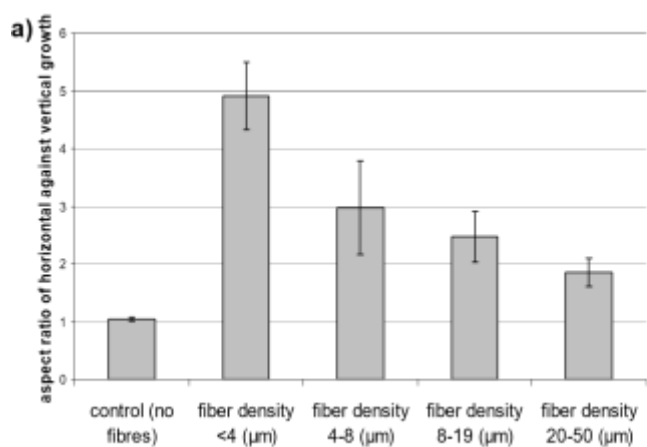


Figure 44 Growth and migration of LECs on 2D aligned nanofibre surfaces

The aspect ratio of endothelial cell outgrowth on different fibre densities of PLDL (70:30) with a 400-600nm diameter was measured and compared (a). LECs growth per day was compared to LEC migration per day on different fibre densities (b). The chart shows an increase in the aspect ratio and migration per day in proportion to fibre density increments. Growth on fibres was significantly reduced, but aspect ratio was the highest on high fibre densities. Image (c) compares fibre diameter of PLDL below 500nm to PLGA (50:50) above 500nm, and Image (d) compares high PLDL fibre alignment to low PLDL fibre alignment on aspect ratio, cell growth area increase per day and cell migration in fibre direction per day. Poor alignment and large fibre diameters reduced migration in fibre direction and decreased total cell growth, but had no effect on aspect ratio, or in the

case of lower alignment increased aspect ratio.

5.4 Discussion

The response of human endothelial cells to the topographical features of nanofibres has been demonstrated in this research. A comprehensive review of the topic is given by Nisbet and colleagues [180]. Briefly, the cellular responses may be summarised as follows: endothelial cells improve their orientation [193], attachment and growth [194] on fibre mats with increasing fibre diameter [195]. They migrate in the direction of an organised surface pattern and elongate significantly [179]. Cellular orientation and migration is subject to surface pattern and geometry [189]. Nanostructures strongly influence gene expression of endothelial cells and can reduce their extracellular matrix protein expression [196]. Endothelial cells prefer flat surfaces for adhesion and growth; the extent of the effect of the surface roughness is still controversial [197,198]; however, rough surfaces such as nanofibre mats, with either aligned or random orientation, do not enhance proliferation or enzymatic activity; growth is significantly reduced [199].

The key challenge here is to direct endothelial cell migration without hampering or disturbing their growth. The combination of a smooth surface with a minimum of topographical signalling such as electrospun nanofibres benefits cellular migration, elongation and proliferation. Overall a spatial distribution of well aligned nanofibres separated by a cell width (5-10 μ m) provides the essential contact guidance and has the least effect on proliferation. The fibre diameter is essential to provide signalling for contact guidance. Despite the fact that endothelial cells recognise a minimum dept of 150nm [41], larger diameter fibres are necessary in order to promote better organisation and migration at collagen gel interfaces.

It has been a challenge to demonstrate contact guidance in 3D hydrogels. Sukmana and Vermette (2009) first demonstrated an *in vitro* model of thick polymer fibres of 100µm diameter in fibrin gels as rigid support for endothelial cells for attachment and migration [182]. In contrast, the present study suggests that nanofibres between 350nm to 1500nm are sufficient to provide a form of contact guidance in 3D hydrogels. Finer fibre diameters do not contribute to the organisation of LECs in collagen gels. The topographical signal can be disturbed by favourable surface chemistry as shown with randomly orientated collagen type I fibres of >250nm. Further, in 3D experiments nano-dimensional polymer structures with a decreasing size of 200nm and below have been shown to increase the binding of endothelial cells when compared to larger structures [200]. It is also known that the surface compliance strongly influences the binding of nanoparticles to endothelial cells. Rigid surfaces such as tissue culture plates dominate cell attachment and growth of micro vascular endothelial cells over collagen gels of different stiffness grades [201]. Nevertheless, it can be assumed that the massive amount of randomly orientated collagen fibres in the hydrogel have a more favourable surface chemistry and specific binding receptors for the LECs. Thus, the collagen matrices provide a higher number of binding sites per cell compared to the integrated polymer fibres. The transduced signalling from the collagen fibres competes with the aligned polymer fibres. Thus, the signalling for cellular guidance is disturbed by the large random collagen fibre network, which results in non-directional growth.

Lymphatic endothelial vessels *in vivo* are connected via a fibrillar network and orientated along elastin fibres of ~1µm diameter, which are surrounded by wave

patterned collagen [90,91]. The *in vitro* model employed here mimics approximately the *vivo* features of elastic fibre orientation in size and shape. Moreover, capillary sprouting of endothelial cells *in vivo* showed that elastic fibres of 180nm to 1400nm are involved in contact guidance during wound healing [202]. The three dimensional AFM images show the “ghost tunnels” of collagen type I fibres. These fibres are incorporated in the LECs-ECM and I believe that they been actively reorganized by the LECs. Although the organisation is random, the embedding of LECs with a layer collagen type I is typical for the initial lymphatic vessel organization as reviewed by Wiig and colleagues [111].

Surface chemistry and topography are both required for contact guidance of endothelial cells. In principle, LECs attach to the surface of the nanofibres via integrins and translate the topographical cues into cytoskeletal migration via the filopodia and growth cones [203]. (Similar behaviour has been observed with neural cells; see review by Cao and colleagues [204].) LECs, however, do not show these growth cones or hyper-extensions when seeded onto densely aligned nanofibre, or random nanofibre, meshes, which suggests that migration in the sequence of “stretch, stick and pull” is disturbed by too many topographical signals, which would explain the reduced elongation and migration on these surfaces. Whereas endothelial cells benefit from nanofibres in terms of contact guidance the presence of these fibres appears to restrict the cell growth and migration.

Apart from topographical features, the migration of endothelial cells was affected also by the surface chemistry, namely the wettability of the fibres. Cells do not adhere

well to hydrophobic materials. Hydrophobicity can be measured by water contact angle: cells will adhere when this angle is 60-70°, but optimal conditions are seen at contact angles ~50° [205,206]. Cellular alignment and migration on more hydrophilic PLGA (90:10) nanofibre surfaces is an example of classic contact guidance. Cell attachment to hydrophobic polymers may be improved by blending with polyglycolic polymers having lower contact angles [207]. Surprisingly, PLDL 70:30 (contact angle >75 degrees [208]) though more hydrophobic than PLGA (90:10) [209], is seen here to give rise to a certain degree of cell orientation despite the cellular attachment to a more hydrophobic material being significantly weaker compared to the flat surface.

5.5 Conclusion

In summary, an electrospinning technique has been used to deposit fibres within collagen hydrogels precisely 1 to 50 micrometer apart and aligned to within +/- 30 degrees. Studies involving these gel-fibre composites have shown the ability of resorbable nanofibres to promote cell guidance without direct cell-fibre contact. Contact guidance and migration operate effectively as long as each endothelial cell is in contact with a single fibre of appropriate size. Equally, hydrophobic nanofibres may be used to direct growth and migration of cells located between fibres 5-10um apart. The diameter of the guiding fibres must be greater than the fibres of the matrix material, such as collagen, in which the cells and fibres are embedded. Fibre alignment is a key parameter to drive the cells in a particular direction. Crossing fibres, such as those present in microfibrinous mats, hamper the motility, elongation and growth of endothelial cells that would otherwise require a flat surface to migrate efficiently. LEC orientation during attachment and migration in 3D and on 2D surfaces is influenced by three factors, surface topography, surface chemistry and differences in material compliance.

The fabricated collagen gel and nanofibre coated gel surfaces with incorporated endothelial cells mimics the native ECM of collagen and elastic fibres. This novel *in vitro* model showed that the dimensional features of elastic fibres *in vivo* are highly likely to contribute to endothelial cell orientation.

My results showed that endothelial cell guidance is possible within nanofibre/collagen-gel constructs that mimic the native ECM in terms of size and orientation of fibrillar components. Thus collagen-fibre composites may prove to be

an effective way to promote contact guidance of human microvascular endothelial cells and directed capillary tube formation.

Chapter VI

Summary

This thesis documents a novel approach for lymphatic tissue regeneration. The first part of the thesis (Chapter 2) investigated how lymphatic endothelial cells (LECs) were influenced by polyglycolide based biomaterials and ECM based hydrogels during *in vitro* culture. In this section, biomarkers were evaluated; co-culture systems with fibroblasts were introduced; and 3D hydrogels were generated. One central question of this section was whether a 3D tissue culture with specific biomaterials or co-culture could sustain lymphatic functionality.

The second part of the thesis (Chapter 3 and 4) illustrated the fabrication of electrospun nanofibres and their precise alignment over specific surfaces. In this section, the fibre properties and electrospinning process parameters were determined to generate reproducible polymer fibres. The focus was on fibre alignment. A dual field electrospinning set up was introduced with a low oscillating frequency to spin fibres across a gap in order to coat surfaces such as culture plates, hydrogels, glass slides and metals. The work in this section described process development and product analyses of aligned polymer fibres with desired properties.

The third part (Chapter 5) combined the findings of parts I and II for a novel approach in lymphatic tissue engineering. Hydrogels with aligned nanofibres were fabricated and the response of lymphatic endothelial cells in those 3D scaffolds evaluated in terms of lymphatic cell attachment, growth and migration. The aim of this work was to generate a nanofibre reinforced hydrogel scaffold that not only sustained lymphatic functionality but also delivered appropriate topographical cues for neo-vessel (tubule) formation.

In part one I first evaluated lymphatic markers. The first part concluded that Prox-1 was the most relevant marker in lymphatic identification. Moreover, not only did Prox-1 identify LECs *in vivo* and *in vitro* with a single marker, it also indicated a physiological and functional aspect of LECs. LEC tube formation was induced with collagen type I and fibrin 3D hydrogels. Lymphatic structures lost their physiology and native morphology; and later viability in all hydrogel cultures without supplementation of vascular endothelial growth factor (VEGF). Although collagen type I based hydrogels led to fast LEC degradation without supplementation of VEGFs, they are a useful tool in creating rapid migration assays where LECs form tube like structures within a few hours after attachment. Moreover, it was observed that while on the one hand fibrin extended lymphatic viability compared to collagen type I, growth, migration and metabolism was enhanced within collagen type I hydrogels. Thesis results lead to the assumption and generation of collagen-fibrin blended hydrogels for a beneficial lymphatic culture. In another approach to improve lymphatic functionality *in vitro* we co-cultured fibroblasts with LECs in collagen type I hydrogels. Fibroblasts interfered with lymphatic attachment but could preserve some LEC tube like formation in collagen type I hydrogels. Nevertheless, the high rate of cellular death of LECs indicated a minor role for fibroblasts in lymphatic tissue engineering.

In the second part, three polylactic-co-polymers were electrospun and their features such as fibre diameter, mesh porosity and scaffold biodegradability under different process parameters were characterised. The second part concluded that polylactic-coglycolic acid at a ratio of 1:1 showed best characteristics for tissue engineering

applications for soft tissue. Polylactic-co-glycolic acid biodegraded within 90 days and was electrospun at dimensions from 150nm to several micrometers in diameter. Further, dual field electrospinning was used to align the polymer fibres. Instead of one collector, two parallel collectors were positioned centrally beneath the extrusion needle with a specific gap distance from each other. The polymer transferred between the two collectors and generated a narrowly aligned fibre sheet over various surfaces, such as glass, plastics, metals and hydrogels, which were positioned in the gap between the two collectors. Specific process parameters such as gap distance, collector geometry, spin duration and voltage were defined to manipulate interspatial fibre distance and alignment. However, alignment was strongly reduced with spinning duration, because residual charges deposited on the surface and interacted with the deposition profile, causing so called “stray fibres”. In order to reduce residual charges we introduced a new, low oscillating electric field between the two collectors. It stabilized the electrospinning process, reduced stray fibres and improved alignment. This technology allowed us to produce polymer fibres of specific diameters, as well as control interspatial distances and alignments. Although a fibre alignment of >80% has not yet been achieved, dual field electrospinning technology is the only technology so far able to coat any desired surface with a layer of polymer fibres of specific characteristics.

The third part used random and aligned polymer fibres on glass and collagen type I hydrogels to investigate LEC migration, tube formation and growth. Aligned fibres provided topographical cues for LECs in single cells as well as tube formation. Contact guidance and migration was directed as long as each endothelial cell was in

contact with a single fibre of $>300\text{nm}$. Contact guidance could be provided effectively with hydrophobic or hydrophilic nanofibres at an interspatial fibre distance of $5\text{-}10\mu\text{m}$. Fibre alignment was a key parameter to drive the cells in a particular direction. Random fibres impaired outgrowth and migration. The results in the third part showed that LEC guidance is possible within nanofibre/collagen type I hydrogel constructs that mimic the native extra cellular matrix in terms of size and orientation of fibrillar components. Thus, hydrogel-fibre composites may prove to be an effective tool in lymphatic regeneration.

This thesis has accomplished several objectives steps in its approach to generate a tissue engineered lymphatic vessel network:

- Evaluation of the lymphatic marker Prox-1 as highly selective tool for lymphatic identification and lymphatic functionality *in vivo* and *in vitro* (Chapter 2.3.1; Figure 3 and Figure 4).
- Comparison of collagen type I and fibrin hydrogels for lymphatic vessel in vitro culture (Chapter 2.3.2)
 - Fibrin hydrogels maintained lymphatic vessel for a longer time without additional growth factors and developed blind ended vessel structures similar to their native structure (Figure 9 and Figure 11)
 - Collagen type I induced high metabolism of LECs and rapid migration into tube like honeycomb structure (Figure 8 and Figure 11)
 - LECs showed a VEGF dependency in hydrogels (Figure 6)
- Exclusion of 3T3 fibroblasts as a potent co-culture partner for lymphatic vessel sustainability and growth in collagen type I hydrogels (Chapter 2.3.3)

- Development of a collagen type I hydrogel scaffold with biodegradable organized polymer nanofibres for directed lymphatic endothelial cell migration, tube formation; and thus cellular guidance (Chapter 3-5)

- Evaluation of electrospun polymer fibre morphology and

biodegradation (Chapter 3.3)

High flow rates, low polymer concentrations and an increased voltage reduced the fibre diameter of PLGA and PLDL

(Figure 18, Figure 19 and Figure 21)

Morphology of fibres is highly influenced by ambient humidity

(Figure 22)

PLGA in contrast to the slowly degradable PLDL degraded about 50% in 90 days. Small fibre diameter (<300nm) accelerated PLGA fibre degradation (Figure 23 and Figure 24).

- Process developments in dual field electrospinning led to a technique, which is able to coat surfaces with polymer nanofibres of specific orientation and interspatial fibres distance (Chapter 4.3)

Fibre distance depended on the spinning duration (Figure 34)

Fibre orientation was influenced by multiple factors, environmental as well process parameters. Mainly, voltage and residual charges decreased fibre orientation (Table 8). The introduction of a novel non static (altering) electric field supported the electrospinning process (Table 8 and Figure 35).

- Identification of essential nanofibre parameters for lymphatic attachment and cellular guidance in collagen hydrogels (Chapter 5.3)
 - LECs rapidly attached to fibres in micrometer dimensions but not in nano-dimensions (Figure 38)
 - Hydrophobic PLDL polymers led to very low cellular attachments, but were able to provide signals for cellular guidance (Figure 38 and Figure 42)
 - Cellular guidance in collagen hydrogels depended on polymer fibre diameter of 350nm and above (Figure 42)
 - High fibre alignment was a critical parameter to accelerate directed migration and tube formation of LECs (Figure 44).

Discussion and Future Recommendations

The lymphatic research field is small. The 2010 Gordon research conference on Molecular Mechanisms in Lymphatic Function & Disease, hosted almost all lymphatic scientists (approx. 180 people) in Lucca, Italy. The area of lymphatic tissue engineering was covered there as well, but only very few research groups within the lymphatic research field have set out to reconstruct lymphatic vessels *in vitro* for medical grafts. Melody Swartz's group in Lausanne, Switzerland, is one of the well-established research groups studying lymphatic vessel networks in a tissue engineering approach. Her group's efforts in constructing lymphatic tissues in perfused bioreactors [33] has contributed much to the understanding of lymphatic fluid and mass transport within the interstitium [210]. However, there has been little progress in lymphatic tissue engineering and no laboratory concentrates primarily on

lymphatic tissue development. There are potentially a few reasons for this lack of progress. A common assumption regarding lymphatic tissue engineering describes lymphatics as a secondary vascular network, a “drainage system” of the body. Further, the importance of the lymphatic system as a vital tissue function seems to be less prominent; therefore there is no need for a tissue engineering approach. This view may be outdated. Therefore, the following section of this chapter will discuss a paradigm shift in lymphatic tissue engineering with regards to the significant findings presented in this thesis.

The lymphatic system is often compared to the vascular system. University text books teach that blood flow is approximately 7200 L/day. Nearly all circulates in the blood vascular system, only 20 L/day are distributed from the capillaries into the interstitial tissues. Almost 80% of it is reabsorbed by the blood capillaries. The rest, approximately 3L/day, is thought to be recycled by the lymphatic system and redistributed into the vascular blood flow. The common conclusion is that the lymphatic system drains and transports 3L/day, which is significant small amount compared to 7200L/day of the vascular system. This perspective may be flawed, and has contributed to a lesser scientific and medical awareness for the lymphatic system. The outflow from the thoracic duct is indeed about 3L/day but the fluid volume processed by the lymphatic network is not necessarily the same and is most likely of much higher magnitude. The out flow from the thoracic duct into the blood vascular system was measured and found to be stable at 2-4L/day independent of blood pressure changes [211]. In an earlier study the lymphatic outflow was blocked by high vascular pressure, which prevents the inflow of new lymph into the blood

system. Elevation of venous pressure also increases the interstitial fluid pressure from the kidneys [212]. However, lymph flow and pressure did not change and interestingly experimental animals did not suffer any oedema conditions [211]. It was assumed that interstitial fluid was recycled by other means. Later it was discovered that the lymphatic network is semipermeable. Lower weight molecules (such as insulin, water) of 6000kD and below can exchange freely through the lymphatics only controlled by the interstitial pressure, whereas high molecular weight compounds (e.g. fats) are concentrated in the lymphatic system [213]. This demonstrates that the balance of lymphatic fluid intake might not be equal to the fluid out flow of the thoracic duct. Hence, the fluid transport between the lymphatics and the interstitium is eventually higher and more dynamic than previously thought. In addition, more than 50% of all macromolecules are recycled through the lymphatic system back to the blood system to keep a balanced tissue homeostasis system [213]. Although, the vital function of the lymphatic system is undeniable at this point many people would still argue that it is not necessary to incorporate lymphatic vessels into engineered tissue in order to generate functional grafts. The argument here is that, the vascular system is the primary system supplying necrotic and injured tissues with nutrition and oxygen, other structures such as the lymphatics can and will arrive from the surrounding healthy tissue in the remodelling process during wound healing (Chapter 1). In general this view is correct, but recently it has been shown computationally [214] and later *in vitro* [215] that vascularized scaffolds also require drainage to maintain interstitial fluid homeostasis. In the absence of lymphatic drainage, endothelial cells detach from tissue engineered scaffolds, which might impair the success of vascularized grafts in future medical applications. Although

vascular grafts have been successfully implanted in children with congenital heart diseases [216], adult patients may encounter different challenges to adapt to larger grafts. The translational vascular field is novel; hence, clinical data about vascularized tissue implants for adults is yet not representative. However, it is likely that the importance of lymphatic vessels in tissue engineered grafts will be recognized in future. Thinking ahead of time, it might be topical to introduce lymphatics into current tissue engineered grafts. A reasonable application for lymphatic networks would be alongside vascular tissue. Vascular graft designs are already tested concepts of translational medicine with a fair amount of success [216]; far ahead of any lymphatic approaches. In this case it is an advantage for the lymphatic tissue engineering. The acquired knowledge in vascular tissue engineering can be easily transferred towards the lymphatics, due to their tissue similarity and shared ancestral origin. Only a few factors have to be considered before both tissue types can be co-grafted. The lymphatic tissue engineering approach should determine a feasible hydrogel platform, importance of extracellular matrix types, essential growth factor supplementation and then test co-culture of lymphatics with vascular and interstitial cells types. This thesis has contributed to some aspects of tissue engineered lymphatics which can be used in future application.

Hydrogels are a class of biomaterials that have great scaffolding potential in many tissue engineering applications due to their high tissue-like water content, high biocompatibility in general, mechanical properties that parallel the properties of soft tissues, efficient transport of nutrients and waste, powerful ability to uniformly encapsulate cells, and ability to be injected as a liquid that gels in situ [217]. A

disadvantage of hydrogels is a poor internal organization and low response to mechanotransduction, which can be critical for cell survival. Although there are more advanced alternatives to generate soft tissues, such as the use of highly advanced 3D tissue printers and composite assembly of 2D cell sheets [218], the hydrogel approach is technically one of the easiest with which to mimic native soft tissue, including lymphatics. Compositions of hydrogel shown in this thesis are ECM based. Although it would be fascinating and scientifically important to introduce polymer hydrogels in lymphatic tissue engineering, only native biomaterials were used in the cell culture studies of this thesis. The reasoning was that the understanding of the mechanism of interaction between cells and their native environment requires only structural proteins of the ECM. Also, at that time, there was not enough scientific data to understand lymphatics and their response to native biomaterials. Although it would be preferable to provide the full ECM for lymphatic tissue engineering it is currently technically impossible to reproduce the level of complexity and organisation of the native ECM *in vitro*. Moreover, lymphatics have been shown to have a specific matrix environment and cell adhesion sites for a group of ECM polymers (Chapter 2.1) Thus, it is argued in Chapter 2 that only a few structural proteins are essential for LECs, to provide the necessary binding cues for lymphatic functionality and tubular assembly. The ECM composition, such as collagen type I and fibrin, distinctively influences the morphology, organization pattern and growth of lymphatic endothelium (Chapter 2.3). In addition it has been shown that hyaluronan hydrogels do not support lymphatic attachment. The strong contrasting responses to different structural EMC proteins with LECs show the importance of the tissue engineering design. From a tissue engineering point, a collagen type I

hydrogel would be of advantage as it induces high cellular metabolism and growth (Chapter

2.3). However, a drawback in the design is high cellular demand for essential vascular growth factor in order to sustain lymphatic vessels in the 3D tissues. Just like vascular grafts, delivery of growth factors is critical for vessel sustainability. The requirement for growth factors is challenging, especially when hydrogels are used as the delivery system. Despite better cell survival in fibrin gels over collagen gels (Chapter 2.3.2); when cultured without growth factors; natural polymer systems are difficult to design, expensive and more difficult to control in terms of drug release, given their tendency to bind growth factors [219]. Thus, introduction of synthetic biomaterials might provide an advantage over native biomaterial. Fully synthetic polymer hydrogels such as polyethylene glycol, which include matrices for controlled drug release are the gold standard for polymers in biomedical application [220]. However, there are many other technical alternatives for controlled drug release (e.g. (Chapter 5) incorporation of electrospun polymer fibres in hydrogels). Polymer fibres fabricated in this thesis can be used for controlled drug release. The electrospun polymer fibres can be either functionalized or specifically designed with “core-shell” electrospinning technology as biodegradable hollow fibres with slow drug release [221]. Although, it has been shown in this research that polymers can be functionalized (blended) with collagen to improve attachment of cells (Chapter 2.3), further polymer fibre functionalizations with critical VEGFs have not been attempted, as this technology has been recently demonstrated by Zhang and colleagues [222]. Nevertheless, an alternative approach was conducted to deliver critical growth factors for lymphatic vessels.

Considering that tissue and cell communications is based on exchange of cytokines and growth factors in a paracrine and juxtacrine fashion from one cell type to another, it would be logical to implement a functional co-culture in tissue engineering designs.

This approach has had great success in skin organ development where fibroblasts of the dermal layer sustain the growth of the epithelium via paracrine exchange of basic fibroblast growth factor and VEGFs [223]. The experiments with fibroblast coculture systems in this thesis (Chapter 2.3.3) indicated beneficial support for lymphatic vessel sustainability in collagen hydrogels. This finding is promising and should be extended in further co-culture systems with cell types known to provide the critical growth factors for lymphatic growth, such as immunological cells and vascular endothelial cells. If paired with the right co-culture system, it might be even more supportive regarding cellular growth and maturation than growth factor drug release by synthetic biomaterials. Changing demand of several growth factors due to cell growth and death are not well addressed by a stable drug release from synthetic material. A balanced co-culture system, such as the skin organ culture, would be able to support growth and development over months *in vitro* with little contribution from external growth factors [223]. Currently, drug release technology is used to provide one or two critical biomolecules for a limited time in order to attract and proliferate desired cells types in tissue engineered scaffolds and hydrogels. Whether this process is enough to achieve effective wound healing and physiological homeostasis cannot be fully answered currently. It is quite likely that the co-culture approach is more sensible as it provides a tissue that is highly functional due to existing cell-cell communication, which provides sustainability in long term culture. Further,

synthetic biomaterials such as PLG, PGA and PLGA mostly undergo biodegeneration (Chapter 3.1, 3.4), which can impair the healing process. A co-culture system embedded in a native hydrogel or scaffold would have a lower chance of failure due to lack of biodegeneration or biomaterial toxicity. Although, it would be reasonable to argue for a tissue model without any synthetic biomaterials to evade tissue developmental complications because of polymer degeneration, hydrophobicity and compliance; one critical aspect of tissue engineering that is difficult to achieve without incorporation of synthetic polymers is tissue organization.

Hydrogels are a poor substitute, especially so in terms of the organisation of structural protein fibres. Although soft tissues have much higher levels of unorganized fibres than hard tissue such as bone and tendon, organized structural fibres such as the anchoring filaments are essential for the tissue lymphatic functionality and lymph transportation (Chapter 1). Cellularized hydrogels do not necessarily develop the distinctive interconnective structures of native tissue. This is due to the lack of mechanotransduction signalling [224]. In order to apply an organizational structure, cellularized hydrogels are mechanically stretched and moulded, thus cells remodel structural proteins of hydrogels with a distinctive orientation along the mechanical stress lines [224]. Tissues such as cartilage, tendon and muscles require a functional ECM organisation. Structural organisation in a specific direction can guide cell migration and growth. Native fibres such as elastin and collagen bundles not only provide structural support, but also chemotactic and topographic guidance for cellular organisation (Chapter 5.1). Regarding wound healing, contact guidance is a desirable feature for tissue engineered designs. It

would drive rapid cell migration within the hydrogels, and increase cell survival within the tissue engineered scaffold. Repopulation of hydrogel structures would be shortened, and it would help to build up structured networks and microchannels similar to a native tissue.

Implementing and mimicking the natural structural fibres in order to provide guidance for LECs was a major aspect of this thesis. Although many approaches stimulate hydrogels mechanically, a different approach was performed in this thesis with constructed electrospun aligned polymer fibres in between hydrogel layers. These polymer fibres conditioned the hydrogel with an organization pattern which provided contact guidance and attachment. Although it would be a native process to provide structural organisational patterns via mechnotransduction, the electrospun polymer fibres delivered better control of the hydrogel environment. Electrospun nanofibrous environments are quite complex, and by changing a dimension such as fibre diameter, interspatial fibre distance or fibre alignment, it automatically influenced cell migration, attachment and growth (Chapter 5). Moreover, the established “one fibre per cell-cell distance” rule in this thesis evidently reduced the amount of incorporated synthetic polymer when compared with any other electrospun tissue engineering models. Currently the polymer-hydrogel model in this thesis is the only full tissue model that demonstrates efficient cellular guidance with a minimum amount of incorporated polymer fibres. One 500nm thick polymer fibre at a spatial distance of 5-10 μ m changed endothelial cell migration, tube formation and growth in tissue engineered hydrogels efficiently. This response, often quoted in literature, has been attributed to similarities of fibre diameter and quantity with the natural ECM environment (Chapter 5.4). Whether this is entirely true or not remains

to be shown, but it is known that endothelial cells respond to ECM components at similar size scale (Chapter 5.4). The underlying mechanisms for enhanced cellular response to nanostructures are only now beginning to be realized by using highly regular and reproducible nanostructured surfaces. Hence, micro- and nanotechnology will play an important part for all tissue engineering constructs and the understanding of tissue functionality. In this regard, electrospinning is an established technology to construct a directional topography in micro- and nano-dimensions. Moreover, the anticipated dual function of electrospun fibres as drug delivery systems, matrix organization and structural support, is one of the most interesting features for tissue engineering to explore in future.

Although electrospinning offers a rapid and convenient way of producing scaffolds and material coatings with features that are aligned and of a micro-nanoscale; and may be utilized across a broad range of polymer systems and tissue engineering endeavours; it is unlikely to reach much beyond the laboratory bench. Poor reproducibility of the electrospinning process and the materials it produces has been a barrier to its commercialisation to date. The dual field electrospinning introduced here, on the other hand, can produce fairly reproducible fibre materials and coatings under stable environmental conditions (Chapter 4). The application of an alternating field can lead to further improvements in quality. Residual charges and environmental factors are the main difficulties in dual field electrospinning (Chapter 4.3). Nevertheless, it is reasonable to say that confinement of residual charges during the electrospinning process and alterations of the electrospinning design will lead to a pro-commercial development in future. However, electrospinning has not achieved commercialisation and the fabrication quality is still inferior to 3D bio-printer and

2D micro patterning technology, both of which have achieved commercial success with a broader spectrum of applications. Nevertheless, dual field electrospinning might be able to acquire a commercial niche such as engineering of simple tissue constructs, which provide cellular guidance and drug delivery. The aforementioned approach of drug delivery by Zhang and colleagues [222] to provide vascular growth factor via “core-shell” electrospinning is critical for new developments in vascular and lymphatic tissue engineering with electrospinning technology. It is therefore likely that a combinatory “core-shell” and dual field electrospinning approach would be able to construct tissue hydrogels which have the possibility to challenge current 3D printing designs in terms of organisation and growth factors delivery.

Nevertheless as a next step, highly engineered functionalised polymer fibre hydrogels or simple constructs, as shown in this thesis, should prove their regenerative potential in a lymphatic oedema tail rodent model. Animal experiments are a critical step in translational medicine, which decide the future of tissue engineered designs. Future experiments should also combine fibrin hydrogels, growth factors and co-culture within the electrospun construct to avoid tissue failure. Once a stable matrix is provided for lymphatic growth and vessel function, further experiments could aim towards tissue maturation and the development of collective vessels and lymphatic ducts. However, the engineering of mature lymphatic tissues is somewhat more daunting than previously thought. Challenges are apparent in the engineering of functional lymphatic vessels that would present an intrinsic pump conduit and the active contraction essential to move lymph fluid forward. While speculative, this type of experimental model system could prove a powerful tool for dissecting molecular and cellular events surrounding tumour invasion of lymphatics,

as well as lymphangiogenesis and several oedema-related diseases. A more fitting and topical medical application would aim towards structured scaffolds seeded with engineered lymphatic and/or vascular cells, and controlled growth factor release which would be implanted post-surgically in order to support the injured tissue area with a functional network, cell guidance and accelerated wound healing. In future, these tissues and organs will prove amenable to tissue-engineering therapies, but, as in all fields of tissue engineering, there is a long way to go before the science can be implemented as a clinical regimen.

All in all, the presented final discussion stresses the necessity of lymphatic tissue engineering, and recommends the combination of vascular and lymphatic tissue development.

References

1. Discher DE, Mooney DJ, Zandstra PW: Growth factors, matrices, and forces combine and control stem cells. *Science* 2009, 324(5935):1673-1677.
2. Hutmacher D, Ekaputra A: Design and Fabrication Principles of Electrospinning of Scaffolds. In *Biomaterials Fabrication and Processing*. Edited by Chu P, Liu X. Boca Raton, FL: CRC Press; 2008:115-139.
3. Choi JS, Lee SJ, Christ GJ, Atala A, Yoo JJ: The influence of electrospun aligned poly(epsilon-caprolactone)/collagen nanofiber meshes on the formation of selfaligned skeletal muscle myotubes. *Biomaterials* 2008, 29(19):2899-2906.
4. Shin'oka T, Matsumura G, Hibino N, Naito Y, Watanabe M, Konuma T, Sakamoto T, Nagatsu M, Kurosawa H: Midterm clinical result of tissue-engineered vascular autografts seeded with autologous bone marrow cells. *J Thorac Cardiovasc Surg* 2005, 129(6):1330-1338.
5. Negrini D, Moriondo A: Lymphatic anatomy and biomechanics. *J Physiol* 2011, 589(12):2927-2934.
6. Banu A, Bontas E, Bartos D, Dragoicea I, Dorobantu Maria, Tanikawa A, Crutescu R: Lymphedema - Up to now. *Mædica - a Journal of Clinical Medicine* 2007, 2(1):25-32.
7. Mäkinen T, Norrmén C, Petrova TV: Molecular mechanisms of lymphatic vascular development. *Cell Mol Life Sci* 2007, 64(15):1915-1929.
8. Hong YK, Shin JW, Detmar M: Development of the lymphatic vascular system: a mystery unravels. *Dev Dyn* 2004, 231(3):462-473.
9. Huxley VH, Scallan J: Lymphatic fluid: exchange mechanisms and regulation. *J Physiol* 2011, 589(12):2935-2943.
10. Alitalo K, Tammela T, Petrova TV: Lymphangiogenesis in development and human disease. *Nature* 2005, 438(7070):946-953.
11. Boardman KC, Swartz MA: Interstitial flow as a guide for lymphangiogenesis. *Circ Res* 2003, 92(7):801-808.
12. Drummond GB: To the interstitial space - and beyond! *J Physiol* 2011, 589(12):2925-2925.

13. Avraham T, Clavin NW, Daluvoy SV, Fernandez J, Soares MA, Cordeiro AP, Mehrara BJ: Fibrosis is a key inhibitor of lymphatic regeneration. *Plast Reconstr Surg* 2009, 124(2):438-450.
14. Maruyama K, Li M, Cursiefen C, Jackson DG, Keino H, Tomita M, Van Rooijen N, Takenaka H, D'Amore PA, Stein-Streilein J, Losordo DW, Streilein JW: Inflammation-induced lymphangiogenesis in the cornea arises from CD11b-positive macrophages. *J Clin Invest* 2005, 115(9):2363-2372.
15. Murugan R, Ramakrishna S: Design strategies of tissue engineering scaffolds with controlled fiber orientation. *Tissue Eng* 2007, 13(8):1845-1866.
16. Zeleny J: The electrical discharge from liquid points, and a hydrostatic method of measuring the electric intensity at their surfaces. *Physical Review* 1914, 3(2):69.
17. Murugan R, Huang ZM, Yang F, Ramakrishna S: Nanofibrous scaffold engineering using electrospinning. *J Nanosci Nanotechnol* 2007, 7(12):4595-4603.
18. Yang J, Zhan S, Wang N, Wang X, Li Y, Li Y, Ma W, Yu H: A Mini Review: Electrospun Hierarchical Nanofibers. *Journal of Dispersion Science and Technology* 2010, 31(6):760-769.
19. Rho KS, Jeong L, Lee G, Seo BM, Park YJ, Hong SD, Roh S, Cho JJ, Park WH, Min BM: Electrospinning of collagen nanofibers: effects on the behavior of normal human keratinocytes and early-stage wound healing. *Biomaterials* 2006, 27(8):1452-1461.
20. Shin HJ, Lee CH, Cho IH, Kim YJ, Lee YJ, Kim IA, Park KD, Yui N, Shin JW: Electrospun PLGA nanofiber scaffolds for articular cartilage reconstruction: mechanical stability, degradation and cellular responses under mechanical stimulation in vitro. *J Biomater Sci Polym Ed* 2006, 17(1-2):103-119.
21. Yoshimoto H, Shin YM, Terai H, Vacanti JP: A biodegradable nanofiber scaffold by electrospinning and its potential for bone tissue engineering. *Biomaterials* 2003, 24(12):2077-2082.
22. Xu CY, Inai R, Kotaki M, Ramakrishna S: Aligned biodegradable nanofibrous structure: a potential scaffold for blood vessel engineering. *Biomaterials* 2004, 25(5):877-886.

23. Zong X, Bien H, Chung CY, Yin L, Fang D, Hsiao BS, Chu B, Entcheva E: Electrospun fine-textured scaffolds for heart tissue constructs. *Biomaterials* 2005, 26(26):5330-5338.
24. Bini TB, Gao S, Xu X, Wang S, Ramakrishna S, Leong KW: Peripheral nerve regeneration by microbraided poly(L-lactide-co-glycolide) biodegradable polymer fibers. *J Biomed Mater Res A* 2004, 68(2):286-295.
25. Katiyar D, Singh LK: Filariasis: Current status, treatment and recent advances in drug development. *Curr Med Chem* 2011, 18(14):2174-2185.
26. Brice, Burt J, White G, Tretbar LL, Morgan CL, Lee BB, Simonian SJ, Blondeau B: *Lymphedema*. Hunter House Publishers; 2005.
27. Petrek JA, Pressman PI, Smith RA: Lymphedema: current issues in research and management. *CA Cancer J Clin* 2000, 50(5):292-307; quiz 308.
28. Furukawa H, Osawa M, Saito A, Hayashi T, Funayama E, Oyama A, Sekido M, Yamamoto Y: Microsurgical lymphaticovenous implantation targeting dermal lymphatic backflow using indocyanine green fluorescence lymphography in the treatment of postmastectomy lymphedema. *Plast Reconstr Surg* 2011, 127(5):1804-1811.
29. Felmerer G, Sattler T, Lohrmann C, Tobbia D: Treatment of various secondary lymphedemas by microsurgical lymph vessel transplantation. *Microsurgery* 2012, 32(3):171-177.
30. Conrad C, Niess H, Huss R, Huber S, von Luetlichau I, Nelson PJ, Ott HC, Jauch KW, Bruns CJ: Multipotent mesenchymal stem cells acquire a lymphendothelial phenotype and enhance lymphatic regeneration in vivo. *Circulation* 2009, 119(2):281-289.
31. Tammela T, Saaristo A, Holopainen T, Lyytikka J, Kotronen A, Pitkonen M, Abo-Ramadan U, Ylä-Herttuala S, Petrova TV, Alitalo K: Therapeutic differentiation and maturation of lymphatic vessels after lymph node dissection and transplantation. *Nat Med* 2007, 13(12):1458-1466.
32. Baker A, Kim H, Semple JL, Dumont D, Shoichet M, Tobbia D, Johnston M: Experimental assessment of pro-lymphangiogenic growth factors in the treatment of post-surgical lymphedema following lymphadenectomy. *Breast Cancer Res* 2010, 12(5):R70.
33. Helm CLE, Zisch A, Swartz MA: Engineered blood and lymphatic capillaries in 3-D VEGF-fibrin-collagen matrices with interstitial flow. *Biotechnol Bioeng* 2007, 96(1):167-176.

34. Laco F, Grant MH, Flint DJ, Black RA: Cellular Trans-Differentiation and Morphogenesis Toward the Lymphatic Lineage in Regenerative Medicine. *Stem Cells Dev* 2011, 20(2):181-195.
35. Baluk P, McDonald DM: Markers for microscopic imaging of lymphangiogenesis and angiogenesis. *Ann N Y Acad Sci* 2008, 1131:1-12.
36. Garrafa E, Trainini L, Benetti A, Saba E, Fezzardi L, Lorusso B, Borghetti P, Bottio T, Ceri E, Portolani N, Bonardlli S, Giulini SM, Annibale G, Corradi A, Imberti L, Caruso A: Isolation, purification, and heterogeneity of human lymphatic endothelial cells from different tissues. *Lymphology* 2005, 38(4):159-166.
37. Lohela M, Bry M, Tammela T, Alitalo K: VEGFs and receptors involved in angiogenesis versus lymphangiogenesis. *Curr Opin Cell Biol* 2009, 21(2):154-165.
38. Ramakrishna S, Fujihara K, Teo WE, Lim TC, Ma Z: *An introduction to electrospinning and nanofibers*. Singapore: World Scientific Pub Co Inc; 2005.
39. Andrady AL (Ed): *Science and technology of polymer nanofibers*. Canada: WileyInterscience; 2008.
40. Teo WE, Ramakrishna S: A review on electrospinning design and nanofibre assemblies. *Nanotechnology* 2006, 17(14):R89-R106.
41. Biela SA, Su Y, Spatz JP, Kemkemer R: Different sensitivity of human endothelial cells, smooth muscle cells and fibroblasts to topography in the nanomicro range. *Acta Biomater* 2009, 5(7):2460-2466.
42. Venugopal J, Low S, Choon AT, Ramakrishna S: Interaction of cells and nanofiber scaffolds in tissue engineering. *J Biomed Mater Res B Appl Biomater* 2008, 84(1):34-48.
43. Barrett T, Choyke PL, Kobayashi H: Imaging of the lymphatic system: new horizons. *Contrast Media Mol Imaging* 2006, 1(6):230-245.
44. Waynforth HB, Flecknell PA: *Experimental and surgical technique in the rat*. Academic Press; 1992.
45. Hebel R, Stromberg MW: *Anatomy of the laboratory rat*. Baltimore, US: The Williams and Wilkins Company; 1976.

46. Tilney NL: Patterns of lymphatic drainage in the adult laboratory rat. *J Anat* 1971, 109(Pt 3):369-383.
47. Bollinger A, Amann-Vesti BR: Fluorescence microlymphography: diagnostic potential in lymphedema and basis for the measurement of lymphatic pressure and flow velocity. *Lymphology* 2007, 40(2):52-62.
48. Leak LV: Electron microscopic observations on lymphatic capillaries and the structural components of the connective tissue-lymph interface. *Microvasc Res* 1970, 2(4):361-391.
49. Wigle JT, Oliver G: Prox1 function is required for the development of the murine lymphatic system. *Cell* 1999, 98(6):769-778.
50. Kulkarni RM, Greenberg JM, Akeson AL: NFATc1 regulates lymphatic endothelial development. *Mech Dev* 2009, 126(5-6):350-365.
51. Johnson N, Dillard M, Baluk P, McDonald D, Harvey N, Frase S, Oliver G: Lymphatic endothelial cell identity is reversible and its maintenance requires Prox1 activity. *Genes Dev* 2008, 22(23):3282-3291.
52. Nakamura J, Shigematsu S, Yamauchi K, Takeda T, Yamazaki M, Kakizawa T, Hashizume K: Biphasic function of focal adhesion kinase in endothelial tube formation induced by fibril-forming collagens. *Biochem Biophys Res Commun* 2008, 374(4):699-703.
53. Rocha SF, Adams RH: Molecular differentiation and specialization of vascular beds. *Angiogenesis* 2009, 12(2):139-147.
54. Goldman J, Rutkowski JM, Shields JD, Pasquier MC, Cui Y, Schmökel HG, Willey S, Hicklin DJ, Pytowski B, Swartz MA: Cooperative and redundant roles of VEGFR-2 and VEGFR-3 signaling in adult lymphangiogenesis. *FASEB J* 2007, 21(4):1003-1012.
55. Wigle JT, Harvey N, Detmar M, Lagutina I, Grosveld G, Gunn MD, Jackson DG, Oliver G: An essential role for Prox1 in the induction of the lymphatic endothelial cell phenotype. *EMBO J* 2002, 21(7):1505-1513.
56. Gordon EJ, Gale NW, Harvey NL: Expression of the hyaluronan receptor LYVE1 is not restricted to the lymphatic vasculature; LYVE-1 is also expressed on embryonic blood vessels. *Dev Dyn* 2008, 237(7):1901-1909.

57. Oliver G: Lymphatic vasculature development. *Nat Rev Immunol* 2004, 4(1):3545.
58. Podgrabinska S, Braun P, Velasco P, Kloos B, Pepper MS, Skobe M: Molecular characterization of lymphatic endothelial cells. *Proc Natl Acad Sci U S A* 2002, 99(25):16069-16074.
59. Schacht V, Ramirez MI, Hong YK, Hirakawa S, Feng D, Harvey N, Williams M, Dvorak AM, Dvorak HF, Oliver G, Detmar M: T1alpha/podoplanin deficiency disrupts normal lymphatic vasculature formation and causes lymphedema. *EMBO J* 2003, 22(14):3546-3556.
60. Cueni LN, Detmar M: Galectin-8 interacts with podoplanin and modulates lymphatic endothelial cell functions. *Exp Cell Res* 2009, 315(10):1715-1723.
61. Martín-Villar E, Megías D, Castel S, Yurrita MM, Vilaró S, Quintanilla M: Podoplanin binds ERM proteins to activate RhoA and promote epithelialmesenchymal transition. *J Cell Sci* 2006, 119(Pt 21):4541-4553.
62. Navarro A, Perez RE, Rezaiekhaliq M, Mabry SM, Ekekezie II: T1alpha/podoplanin is essential for capillary morphogenesis in lymphatic endothelial cells. *Am J Physiol Lung Cell Mol Physiol* 2008, 295(4):L543-L551.
63. Norrmen C, Vandevelde W, Ny A, Saharinen P, Gentile M, Haraldsen G, Puolakkainen P, Lukanidin E, Dewerchin M, Alitalo K, Petrova TV: Liprin {beta}1 is highly expressed in lymphatic vasculature and is important for lymphatic vessel integrity. *Blood* 2009,
64. Wick N, Saharinen P, Saharinen J, Gurnhofer E, Steiner CW, Raab I, Stokic D, Giovanoli P, Buchsbaum S, Burchard A, Thurner S, Alitalo K, Kerjaschki D: Transcriptomal comparison of human dermal lymphatic endothelial cells ex vivo and in vitro. *Physiol Genomics* 2007, 28(2):179-192.
65. Rodriguez-Niedenführ M, Papoutsi M, Christ B, Nicolaidis KH, von Kaisenberg CS, Tomarev SI, Wilting J: Prox1 is a marker of ectodermal placodes, endodermal compartments, lymphatic endothelium and lymphangioblasts. *Anat Embryol (Berl)* 2001, 204(5):399-406.
66. Lavado A, Oliver G: Prox1 expression patterns in the developing and adult murine brain. *Dev Dyn* 2007, 236(2):518-524.
67. Papoutsi M, Dudas J, Becker J, Tripodi M, Opitz L, Ramadori G, Wilting J: Gene regulation by homeobox transcription factor Prox1 in murine hepatoblasts. *Cell Tissue Res* 2007, 330(2):209-220.

68. Partanen TA, Arola J, Saaristo A, Jussila L, Ora A, Miettinen M, Stacker SA, Achen MG, Alitalo K: VEGF-C and VEGF-D expression in neuroendocrine cells and their receptor, VEGFR-3, in fenestrated blood vessels in human tissues. *FASEB J* 2000, 14(13):2087-2096.
69. Kubo H, Fujiwara T, Jussila L, Hashi H, Ogawa M, Shimizu K, Awane M, Sakai Y, Takabayashi A, Alitalo K, Yamaoka Y, Nishikawa SI: Involvement of vascular endothelial growth factor receptor-3 in maintenance of integrity of endothelial cell lining during tumor angiogenesis. *Blood* 2000, 96(2):546-553.
70. Sebzda E, Hibbard C, Sweeney S, Abtahian F, Bezman N, Clemens G, Maltzman JS, Cheng L, Liu F, Turner M, Tybulewicz V, Koretzky GA, Kahn ML: Syk and Slp76 mutant mice reveal a cell-autonomous hematopoietic cell contribution to vascular development. *Dev Cell* 2006, 11(3):349-361.
71. Florez-Vargas A, Vargas SO, Debelenko LV, Perez-Atayde AR, Archibald T, Kozakewich HPW, Zurakowski D: Comparative analysis of D2-40 and LYVE-1 immunostaining in lymphatic malformations. *Lymphology* 2008, 41(3):103-110.
72. Jackson DG: The lymphatics revisited: new perspectives from the hyaluronan receptor LYVE-1. *Trends Cardiovasc Med* 2003, 13(1):1-7.
73. Birke K, Lütjen-Drecoll E, Kerjaschki D, Birke MT: Expression of podoplanin and other lymphatic markers in the human anterior eye segment. *Invest Ophthalmol Vis Sci* 2010, 51(1):344-354.
74. Williams MC, Cao Y, Hinds A, Rishi AK, Wetterwald A: T1 alpha protein is developmentally regulated and expressed by alveolar type I cells, choroid plexus, and ciliary epithelia of adult rats. *Am J Respir Cell Mol Biol* 1996, 14(6):577-585.
75. Ramirez MI, Millien G, Hinds A, Cao Y, Seldin DC, Williams MC: T1alpha, a lung type I cell differentiation gene, is required for normal lung cell proliferation and alveolus formation at birth. *Dev Biol* 2003, 256(1):61-72.
76. Hata M, Ueki T, Sato A, Kojima H, Sawa Y: Expression of podoplanin in the mouse salivary glands. *Arch Oral Biol* 2008, 53(9):835-841.
77. Kaddu S, Leinweber B: Podoplanin expression in fibrous histiocytomas and cellular neurothekeomas. *Am J Dermatopathol* 2009, 31(2):137-139.
78. Kalof AN, Cooper K: D2-40 immunohistochemistry--so far! *Adv Anat Pathol* 2009, 16(1):62-64.

79. Martín-Villar E, Yurrita MM, Fernández-Muñoz B, Quintanilla M, Renart J: Regulation of podoplanin/PA2.26 antigen expression in tumour cells. Involvement of calpain-mediated proteolysis. *Int J Biochem Cell Biol* 2009, 41(6):1421-1429.
80. Leak LV, Jones M: Lymphangiogenesis in vitro: formation of lymphatic capillary-like channels from confluent monolayers of lymphatic endothelial cells. *In Vitro Cell Dev Biol Anim* 1994, 30A(8):512-518.
81. Amatschek S, Kriehuber E, Bauer W, Reininger B, Meraner P, Wolpl A, Schweifer N, Haslinger C, Stingl G, Maurer D: Blood and lymphatic endothelial cellspecific differentiation programs are stringently controlled by the tissue environment. *Blood* 2007, 109(11):4777-4785.
82. Farnsworth RH, Achen MG, Stacker SA: Lymphatic endothelium: an important interactive surface for malignant cells. *Pulm Pharmacol Ther* 2006, 19(1):51-60.
83. Matsuo M, Koizumi K, Yamada S, Tomi M, Takahashi RI, Ueda M, Terasaki T, Obinata M, Hosoya KI, Ohtani O, Saiki I: Establishment and characterization of conditionally immortalized endothelial cell lines from the thoracic duct and inferior vena cava of tsA58/EGFP double-transgenic rats. *Cell Tissue Res* 2006, 326(3):749758.
84. Baluk P, Fuxe J, Hashizume H, Romano T, Lashnits E, Butz S, Vestweber D, Corada M, Molendini C, Dejana E, McDonald DM: Functionally specialized junctions between endothelial cells of lymphatic vessels. *J Exp Med* 2007, 204(10):2349-2362.
85. Zöltzer H: Initial lymphatics--morphology and function of the endothelial cells. *Lymphology* 2003, 36(1):7-25.
86. Kriehuber E, Breiteneder-Geleff S, Groeger M, Soleiman A, Schoppmann SF, Stingl G, Kerjaschki D, Maurer D: Isolation and characterization of dermal lymphatic and blood endothelial cells reveal stable and functionally specialized cell lineages. *J Exp Med* 2001, 194(6):797-808.
87. Aukland K, Reed RK: Interstitial-lymphatic mechanisms in the control of extracellular fluid volume. *Physiol Rev* 1993, 73(1):1-78.
88. Petreaca M, Martins-Green M: Cell-ECM Interactions in Repair and Regeneration. *In Principles of Regenerative Medicine*. 1 edition. Edited by Atala A, Lanza R, Thomson J, Nerem R. US: Academic Press; 2008:66-99.

89. Sobocinski GP, Toy K, Bobrowski WF, Shaw S, Anderson AO, Kaldjian EP: Ultrastructural localization of extracellular matrix proteins of the lymph node cortex: evidence supporting the reticular network as a pathway for lymphocyte migration. *BMC Immunol* 2010, 11:42.
90. Gerli R, Ibba L, Fruschelli C: A fibrillar elastic apparatus around human lymph capillaries. *Anat Embryol (Berl)* 1990, 181(3):281-286.
91. Arkill KP, Moger J, Winlove CP: The structure and mechanical properties of collecting lymphatic vessels: an investigation using multimodal nonlinear microscopy. *J Anat* 2010, 216(5):547-555.
92. Paupert J, Sounni NE, Noël A: Lymphangiogenesis in post-natal tissue remodeling: lymphatic endothelial cell connection with its environment. *Mol Aspects Med* 2011, 32(2):146-158.
93. Garmy-Susini B, Varner JA: Roles of integrins in tumor angiogenesis and lymphangiogenesis. *Lymphat Res Biol* 2008, 6(3-4):155-163.
94. Garmy-Susini B, Makale M, Fuster M, Varner JA: Methods to study lymphatic vessel integrins. *Methods Enzymol* 2007, 426:415-438.
95. Bazigou E, Xie S, Chen C, Weston A, Miura N, Sorokin L, Adams R, Muro AF, Sheppard D, Makinen T: Integrin-alpha9 is required for fibronectin matrix assembly during lymphatic valve morphogenesis. *Dev Cell* 2009, 17(2):175-186.
96. Gerli R, Solito R, Weber E, Aglianó M: Specific adhesion molecules bind anchoring filaments and endothelial cells in human skin initial lymphatics. *Lymphology* 2000, 33(4):148-157.
97. Hong YK, Lange-Asschenfeldt B, Velasco P, Hirakawa S, Kunstfeld R, Brown LF, Bohlen P, Senger DR, Detmar M: VEGF-A promotes tissue repair-associated lymphatic vessel formation via VEGFR-2 and the alpha1beta1 and alpha2beta1 integrins. *FASEB J* 2004, 18(10):1111-1113.
98. Doyle DA, Yamada MK: Interactions with the Extracellular Matrix. *In Cellular Mechanotransduction*. Edited by Mofrad M, Kamm R. Cambridge Univ Press; 2010:120-130.
99. Ji RC: Lymphatic endothelial cells, lymphangiogenesis, and extracellular matrix. *Lymphat Res Biol* 2006, 4(2):83-100.

100. Smith S: Effect of novel electronic sterilisation methods on the components of hybrid collagen-based biomaterials. *PhD*. Strathclyde University, Bioengineering; 2009.
101. Wiesmann H, Meyer U: Biomaterials. *In Fundamentals of Tissue Engineering and Regenerative Medicine*. 1 edition. Edited by Meyer U, Handschel J, Meyer T, Handschel J, Wiesmann HP. Germany: Springer Verlag; 2009:457-467.
102. Liu NF: Trafficking of hyaluronan in the interstitium and its possible implications. *Lymphology* 2004, 37(1):6-14.
103. MOSESSON MW: Fibrinogen and fibrin structure and functions. *J Thromb Haemost* 2005, 3(8):1894-1904.
104. Cheresh DA, Berliner SA, Vicente V, Ruggeri ZM: Recognition of distinct adhesive sites on fibrinogen by related integrins on platelets and endothelial cells. *Cell* 1989, 58(5):945-953.
105. Janmey PA, Winer JP, Weisel JW: Fibrin gels and their clinical and bioengineering applications. *Journal of The Royal Society Interface* 2009, 6(30):1-10.
106. Potts JR, Campbell ID: Fibronectin structure and assembly. *Curr Opin Cell Biol* 1994, 6(5):648-655.
107. Leiss M, Beckmann K, Girós A, Costell M, Fässler R: The role of integrin binding sites in fibronectin matrix assembly in vivo. *Curr Opin Cell Biol* 2008, 20(5):502-507.
108. Hwang DS, Sim SB, Cha HJ: Cell adhesion biomaterial based on mussel adhesive protein fused with RGD peptide. *Biomaterials* 2007, 28(28):4039-4046.
109. Durbeej M: Laminins. *Cell Tissue Res* 2010, 339(1):259-268.
110. Saito N, Hamada JI, Furukawa H, Tsutsumida A, Oyama A, Funayama E, Saito A, Tsuji T, Tada M, Moriuchi T, Yamamoto Y: Laminin-421 produced by lymphatic endothelial cells induces chemotaxis for human melanoma cells. *Pigment cell & melanoma research* 2009, 22(5):601-610.
111. Wiig H, Keskin D, Kalluri R: Interaction between the extracellular matrix and lymphatics: consequences for lymphangiogenesis and lymphatic function. *Matrix Biol* 2010, 29(8):645-656.

112. Matsuo M, Koizumi K, Yamada S, Tomi M, Takahashi RI, Ueda M, Terasaki T, Obinata M, Hosoya KI, Ohtani O, Saiki I: Establishment and characterization of conditionally immortalized endothelial cell lines from the thoracic duct and inferior vena cava of tsA58/EGFP double-transgenic rats. (1). *Cell Tissue Res* 2006, 326(3):749-758.
113. Taylor-Papadimitriou J, Shearer M, Stoker MG: Growth requirements of human mammary epithelial cells in culture. *Int J Cancer* 1977, 20(6):903-908.
114. Laco F, Kun M, Weber HJ, Ramakrishna S, Chan CK: The dose effect of human bone marrow-derived mesenchymal stem cells on epidermal development in organotypic co-culture. *J Dermatol Sci* 2009, 55(3):150-160.
115. Inzunza J, Gertow K, Strömberg MA, Matilainen E, Blennow E, Skottman H, Wolbank S, Ahrlund-Richter L, Hovatta O: Derivation of human embryonic stem cell lines in serum replacement medium using postnatal human fibroblasts as feeder cells. *Stem Cells* 2005, 23(4):544-549.
116. Gashev AA, Davis MJ: Long-distance transportation of live isolated lymphatic vessels. *Lymphat Res Biol* 2010, 8(4):189-192.
117. Elsdale T, Bard J: Collagen substrata for studies on cell behavior. *J Cell Biol* 1972, 54(3):626-637.
118. Zhao H, Ma L, Zhou J, Mao Z, Gao C, Shen J: Fabrication and physical and biological properties of fibrin gel derived from human plasma. *Biomedical materials (Bristol, England)* 2008, 3(1):015001.
119. Lee YB, Polio S, Lee W, Dai G, Menon L, Carroll RS, Yoo SS: Bio-printing of collagen and VEGF-releasing fibrin gel scaffolds for neural stem cell culture. *Exp Neurol* 2010, 223(2):645-652.
120. Control of basic fibroblast growth factor release from fibrin gel with heparin and concentrations of fibrinogen and thrombin. *Journal of Controlled Release* 2005, 105(3):249-259.
121. Mäkinen T, Adams RH, Bailey J, Lu Q, Ziemiecki A, Alitalo K, Klein R, Wilkinson GA: PDZ interaction site in ephrinB2 is required for the remodeling of lymphatic vasculature. *Genes Dev* 2005, 19(3):397-410.
122. Petrova TV, Mäkinen T, Mäkelä TP, Saarela J, Virtanen I, Ferrell RE, Finegold DN, Kerjaschki D, Ylä-Herttuala S, Alitalo K: Lymphatic

- endothelial reprogramming of vascular endothelial cells by the Prox-1 homeobox transcription factor. *EMBO J* 2002, 21(17):4593-4599.
123. Nisato RE, Harrison JA, Buser R, Orci L, Rinsch C, Montesano R, Dupraz P, Pepper MS: Generation and characterization of telomerase-transfected human lymphatic endothelial cells with an extended life span. *Am J Pathol* 2004, 165(1):1124.
124. Oh SJ, Jeltsch MM, Birkenhäger R, McCarthy JE, Weich HA, Christ B, Alitalo K, Wilting J: VEGF and VEGF-C: specific induction of angiogenesis and lymphangiogenesis in the differentiated avian chorioallantoic membrane. *Dev Biol* 1997, 188(1):96-109.
125. Solis MA, Chen YH, Wong TY, Bittencourt VZ, Lin YC, Huang LLH: Hyaluronan regulates cell behavior: a potential niche matrix for stem cells. *Biochemistry research international* 2012, 2012:346972.
126. Johnson LA, Clasper S, Holt AP, Lalor PF, Baban D, Jackson DG: An inflammation-induced mechanism for leukocyte transmigration across lymphatic vessel endothelium. *J Exp Med* 2006, 203(12):2763-2777.
127. Weber E, Rossi A, Gerli R, Lamponi S, Magnani A, Pasqui D, Barbucci R: Micropatterned hyaluronan surfaces promote lymphatic endothelial cell alignment and orient their growth. *Lymphology* 2004, 37(1):15-21.
128. Detry B, Bruyère F, Erpicum C, Paupert J, Lamaye F, Maillard C, Lenoir B, Foidart JM, Thiry M, Noël A: Digging deeper into lymphatic vessel formation in vitro and in vivo. *BMC Cell Biol* 2011, 12:29.
129. Cursiefen C, Maruyama K, Jackson DG, Streilein JW, Kruse FE: Time course of angiogenesis and lymphangiogenesis after brief corneal inflammation. *Cornea* 2006, 25(4):443-447.
130. Goldman J, Conley KA, Raehl A, Bondy DM, Pytowski B, Swartz MA, Rutkowski JM, Jaroch DB, Ongstad EL: Regulation of lymphatic capillary regeneration by interstitial flow in skin. *Am J Physiol Heart Circ Physiol* 2007, 292(5):H2176-H2183.
131. Montesano R, Pepper MS, Orci L: Paracrine induction of angiogenesis in vitro by Swiss 3T3 fibroblasts. *J Cell Sci* 1993, 105 (Pt 4):1013-1024.
132. Eisenbarth E: Biomaterials for Tissue Engineering. *Advanced Engineering Materials* 2007, 9(12):1051-1060.

133. Chen G, Ushida T, Tateishi T: Scaffold design for tissue engineering. *Macromol Biosci* 2002, 2(2):67-77.
134. Kim K, Yu M, Zong X, Chiu J, Fang D, Seo YS, Hsiao BS, Chu B, Hadjiargyrou M: Control of degradation rate and hydrophilicity in electrospun nonwoven poly(D,L-lactide) nanofiber scaffolds for biomedical applications. *Biomaterials* 2003, 24(27):4977-4985.
135. Vance RJ, Miller DC, Thapa A, Haberstroh KM, Webster TJ: Decreased fibroblast cell density on chemically degraded poly-lactic-co-glycolic acid, polyurethane, and polycaprolactone. *Biomaterials* 2004, 25(11):2095-2103.
136. Grad S, Zhou L, Gogolewski S, Alini M: Chondrocytes seeded onto poly (L/DL-lactide) 80%/20% porous scaffolds: a biochemical evaluation. *J Biomed Mater Res A* 2003, 66(3):571-579.
137. Ohkawa K, Cha D, Kim H, Nishida A, Yamamoto H: Electrospinning of Chitosan. *Macromolecular Rapid Communication* 2004, 25:1600-1605.
138. Deitzel J, Kleinmeyer J, Harris D, Tan N, Beck C: The effect of processing variables on the morphology of electrospun nanofibers and textiles. *Polymer* 2001, 42:261-272.
139. Mit-uppatham C, Nithitanakul M, Supaphol P: Ultrafine Electrospun Polyamide-6 Fibers: Effect of Solution Conditions on Morphology and Average Fiber Diameter. *Macromolecular Chemistry and Physics* 2004, 205(17):2327-2338.
140. Kulkarni A, Bambole VA, Mahanwar PA: Electrospinning of Polymers, Their Modeling and Applications. *Polymer-Plastics Technology and Engineering* 2010, 49(5):427-441.
141. Zong X, Kim K, Fang D, Ran S, Hsiao B, Chu B: Structure and process relationship of electrospun bioabsorbable nanofiber membranes. *Polymer* 2002, 43(10):4403-4412.
142. Zuo W, Zhu M, Yang W, Yu H, Chen Y, Zhang Y: Experimental study on relationship between jet instability and formation of beaded fibers during electrospinning. *Polymer Engineering & Science* 2005, 45(5):704.
143. Ndreu A: Electrospun Nanofibrous Scaffolds for Tissue Engineering. *Master of Science*. Middle East Technical University, the Graduate School of Natural and Applied Sciences; 2007.
144. Gupta P, Elkins C, Long TE, Wilkes GL: Electrospinning of linear homopolymers of poly(methyl methacrylate): exploring relationships between

- fiber formation, viscosity, molecular weight and concentration in a good solvent. *Polymer* 2005, 46(13):4799-4810.
145. Pham QP, Sharma U, Mikos AG: Electrospinning of polymeric nanofibers for tissue engineering applications: a review. *Tissue Eng* 2006, 12(5):1197-1211.
146. Singh Nalwa H (Ed):*Handbook of Nanostructured Biomaterials and Their Applications in Nanobiotechnology*. US: American Scientific Publishers; 2005.
147. Casper C, Stephens J, Tassi N, Chase D, Rabolt J: Controlling Surface Morphology of Electrospun Polystyrene Fibers: Effect of Humidity and Molecular Weight in the Electrospinning Process. *Macromolecules* 2004, 37(2):573-578.
148. Kotaki M, Huang Z, Ramakrishna S: Polymer Nanofibers and Their Applications in Bioengineering. In *Handbook of Nanostructured Biomaterials and Their Applications in Nanobiotechnology*. Edited by Hari Singh Nalwa. US: American Scientific Publishers; 2005:1002.
149. Subbiah T, Bhat GS, Tock RW, Parameswaran S, Ramkumar SS: Electrospinning of nanofibers. *Journal of Applied Polymer Science* 2005, 96(2):557569.
150. Shin Y, Hohman M, Brenner M, Rutledge G: Experimental characterization of electrospinning: the electrically forced jet and instabilities. *Polymer* 2001, 42(25):09955-09967.
151. Hohman MM, Shin M, Rutledge G, Brenner MP: Electrospinning and electrically forced jets. I. Stability theory. *Physics of Fluids* 2001, 13(8):2201.
152. HONG Y, SHANG T, LI Y, WANG L, WANG C, CHEN X, JING X: Synthesis using electrospinning and stabilization of single layer macroporous films and fibrous networks of poly(vinyl alcohol). *Journal of Membrane Science* 2006, 276(1-2):1-7.
153. Kidoaki S, Kwon IK, Matsuda T: Mesoscopic spatial designs of nano- and microfiber meshes for tissue-engineering matrix and scaffold based on newly devised multilayering and mixing electrospinning techniques. *Biomaterials* 2005, 26(1):3746.
154. Patlolla A, Collins G, Livingston Arinze T: Solvent-dependent properties of electrospun fibrous composites for bone tissue regeneration. *Acta Biomater* 2010, 6(1):90-101.

155. Demir M, Yigor I, Yilgor E, Erman B: Electrospinning of polyurethane fibers. *Polymer* 2002, 43(11):3303-3309.
156. Dong Y, Liao S, Ngiam M, Chan CK, Ramakrishna S: Degradation behaviors of electrospun resorbable polyester nanofibers. *Tissue engineering. Part B, Reviews* 2009, 15(3):333-351.
157. You Y, Min BM, Lee SJ, Lee TS, Park WH: In vitro degradation behavior of electrospun polyglycolide, polylactide, and poly(lactide-co-glycolide). *Journal of Applied Polymer Science* 2005, 95:193-200.
158. Shum AW, Mak AF: Morphological and biomechanical characterization of poly(glycolic acid) scaffolds after in vitro degradation. *Polymer Degradation and Stability* 2003, 81(1):141-149.
159. Matthews JA, Wnek GE, Simpson DG, Bowlin GL: Electrospinning of collagen nanofibers. *Biomacromolecules* 2002, 3(2):232-238.
160. Dabirian F, Sarkeshik S, Kianiha A: Production of Uniaxially Aligned Nanofibers Using a Modified Electrospinning Method: Rotating Jet. *Current Nanoscience* 2009, 5(3):318-323.
161. Yang D, Zhang J, Zhang J, Nie J: Aligned electrospun nanofibers induced by magnetic field. *Journal of Applied Polymer Science* 2008, 110(6):3368-3372.
162. Li D, Wang Y, Xia Y: Electrospinning of Polymeric and Ceramic Nanofibers as Uniaxially Aligned Arrays. *Nano Lett* 2003, 3(8):1167-1171.
163. Acharya M, Arumugam G, Heiden P: Dual electric field induced alignment of electrospun nanofibers. *Macromolecular Materials and Engineering* 2008, 293(8):666-674.
164. Pokorny M, Niedoba K, Velebny V: Transversal electrostatic strength of patterned collector affecting alignment of electrospun nanofibers. *Applied Physics Letters* 2010, 96(19):193111.
165. Rafique J, Yu J, Yu J, Fang G, Wong KW, Zheng Z, Ong HC, Lau WM: Electrospinning highly aligned long polymer nanofibers on large scale by using a tip collector. *Applied Physics Letters* 2007, 91(6):063126.
166. Liu Y, Zhang X, Xia Y, Yang H: Magnetic-field-assisted electrospinning of aligned straight and wavy polymeric nanofibers. *Advanced materials (Deerfield Beach, Fla.)* 2010, 22(22):2454-2457.

167. Yin Z, Chen X, Chen JL, Shen WL, Hieu Nguyen TM, Gao L, Ouyang HW: The regulation of tendon stem cell differentiation by the alignment of nanofibers. *Biomaterials* 2010, 31(8):2163-2175.
168. Xie J, Macewan MR, Ray WZ, Liu W, Siewe DY, Xia Y: Radially aligned, electrospun nanofibers as dural substitutes for wound closure and tissue regeneration applications. *ACS nano* 2010, 4(9):5027-5036.
169. Jha BS, Colello RJ, Bowman JR, Sell SA, Lee KD, Bigbee JW, Bowlin GL, Chow WN, Mathern BE, Simpson DG: Two pole air gap electrospinning: Fabrication of highly aligned, three-dimensional scaffolds for nerve reconstruction. *Acta Biomater* 2011, 7(1):203-215.
170. Tamura T, Kawakami H: Aligned Electrospun Nanofiber Composite Membranes for Fuel Cell Electrolytes. *Nano Lett* 2010, 10(4):1324.
171. Yin K, Zhang L, Lai C, Zhong L, Smith S, Fong H, Zhu Z: Photoluminescence anisotropy of uni-axially aligned electrospun conjugated polymer nanofibers of MEH-PPV and P3HT. *Journal of Materials Chemistry* 2011, 21(2):444-448.
172. Ayres CE, Jha BS, Meredith H, Bowman JR, Bowlin GL, Henderson SC, Simpson DG: Measuring fiber alignment in electrospun scaffolds: a user's guide to the 2D fast Fourier transform approach. *J Biomater Sci Polym Ed* 2008, 19(5):603621.
173. Park SH, Yang DY: Fabrication of aligned electrospun nanofibers by inclined gap method. *Journal of Applied Polymer Science* 2011, 120(3):1800-1807.
174. Li D, Wang Y, Xia Y: Electrospinning Nanofibers as Uniaxially Aligned Arrays and Layer-by-Layer Stacked Films. *Advanced Materials* 2004, 16(4):316-366.
175. Teo WE, Ramakrishna S: Electrospun fibre bundle made of aligned nanofibres over two fixed points. *Nanotechnology* 2005, 16(9):1878-1884.
176. Liu L: Studies of deposition and alignment of electrospun nanofibers assemblies. *PhD*. University of Nebraska-Lincoln, 2007.
177. Liu L, Dzenis YA: Analysis of the effects of the residual charge and gap size on electrospun nanofiber alignment in a gap method. *Nanotechnology* 2008, 19(35):355307.

178. Pokorny M, Velebny V: Collection method for extra aligned nanofibers deposited by electrospinning. *Rev Sci Instrum* 2011, 82(5):055112.
179. Han Z, Kong H, Meng J, Wang C, Xie S, Xu H: Electrospun aligned nanofibrous scaffold of carbon nanotubes-polyurethane composite for endothelial cells. *J Nanosci Nanotechnol* 2009, 9(2):1400-1402.
180. Nisbet D, Forsythe J, Shen W, Finkelstein D, Horne M: Review paper: a review of the cellular response on electrospun nanofibers for tissue engineering. *J Biomater Appl* 2009, 24(1):7-29.
181. Hadjizadeh A, Doillon CJ: Directional migration of endothelial cells towards angiogenesis using polymer fibres in a 3D co-culture system. *J Tissue Eng Regen Med* 2010, 4(7):524-531.
182. Sukmana I, Vermette P: Polymer fibers as contact guidance to orient microvascularization in a 3D environment. *Journal of Biomedical Materials Research Part A* 2009, 9999A:NA-NA.
183. Krzysiek-Maczka G, Korohoda W: Surface anisotropy orients cell divisions in contact guided cells. *Folia Biol (Krakow)* 2008, 56(1-2):13-19.
184. Mills CA, Martinez E, Errachid A, Engel E, Funes M, Moormann C, Wahlbrink T, Gomila G, Planell J, Samitier J: Nanoembossed polymer substrates for biomedical surface interaction studies. *J Nanosci Nanotechnol* 2007, 7(12):4588-4594.
185. Dusseiller MR, Schlaepfer D, Koch M, Kroschewski R, Textor M: An inverted microcontact printing method on topographically structured polystyrene chips for arrayed micro-3-D culturing of single cells. *Biomaterials* 2005, 26(29):5917-5925.
186. Steketee MB, Tosney KW: Three functionally distinct adhesions in filopodia: shaft adhesions control lamellar extension. *J Neurosci* 2002, 22(18):8071-8083.
187. Eichmann A, Noble FL, Autiero M, Carmeliet P: Guidance of vascular and neural network formation. *Curr Opin Neurobiol* 2005, 15(1):108-115.
188. Doiron AL, Clark B, Rinker KD: Endothelial nanoparticle binding kinetics are matrix and size dependent. *Biotechnol Bioeng* 2011, 108(12):2988-2998.
189. Liliensiek S, Wood J, Yong J, Auerbach R, Nealey P, Murphy C: Modulation of human vascular endothelial cell behaviors by nanotopographic cues. *Biomaterials* 2010, 31(20):5418-5426.

190. Hoffman-Kim D, Mitchel JA, Bellamkonda RV: Topography, cell response, and nerve regeneration. *Annu Rev Biomed Eng* 2010, 12:203-231.
191. Lamoureux P, Buxbaum RE, Heidemann SR: Direct evidence that growth cones pull. *Nature* 1989, 340(6229):159-162.
192. Xu C, Yang F, Wang S, Ramakrishna S: In vitro study of human vascular endothelial cell function on materials with various surface roughness. *J Biomed Mater Res A* 2004, 71(1):154-161.
193. Bashur CA, Dahlgren LA, Goldstein AS: Effect of fiber diameter and orientation on fibroblast morphology and proliferation on electrospun poly(D,Llactic-co-glycolic acid) meshes. *Biomaterials* 2006, 27(33):5681-5688.
194. Rubenstein D, Han D, Goldgraben S, El-Gendi H, Gouma PI, Frame MD: Bioassay chamber for angiogenesis with perfused explanted arteries and electrospun scaffolding. *Microcirculation* 2007, 14(7):723-737.
195. Keun Kwon I, Kidoaki S, Matsuda T: Electrospun nano- to microfiber fabrics made of biodegradable copolyesters: structural characteristics, mechanical properties and cell adhesion potential. *Biomaterials* 2005, 26(18):3929-3939.
196. Gasiorowski JZ, Liliensiek SJ, Russell P, Stephan DA, Nealey PF, Murphy CJ: Alterations in gene expression of human vascular endothelial cells associated with nanotopographic cues. *Biomaterials* 2010, 31(34):8882-8888.
197. Chung TW, Liu DZ, Wang SY, Wang SS: Enhancement of the growth of human endothelial cells by surface roughness at nanometer scale. *Biomaterials* 2003, 24(25):4655-4661.
198. Shah A, Shah S, Mani G, Wenke J, Agrawal M: Endothelial cell behaviour on gas-plasma-treated PLA surfaces: the roles of surface chemistry and roughness. *J Tissue Eng Regen Med* 2011, 5(4):301-312.
199. Heath DE, Lannutti JJ, Cooper SL: Electrospun scaffold topography affects endothelial cell proliferation, metabolic activity, and morphology. *J Biomed Mater Res A* 2010, 94(4):1195-1204.
200. Doiron AL, Clark B, Rinker KD: Endothelial nanoparticle binding kinetics are matrix and size dependent. (1). *Biotechnol Bioeng* 2011, 108(12):2988-2998.
201. Wood JA, Shah NM, McKee CT, Hughbanks ML, Liliensiek SJ, Russell P, Murphy CJ: The role of substratum compliance of hydrogels on vascular endothelial cell behavior. *Biomaterials* 2011, 32(22):5056-5064.

202. Anderson CR: Immunohistochemical identification of an extracellular matrix scaffold that microguides capillary sprouting in vivo. *J Histochem Cytochem* 2004, 52(8):1063-1072.
203. Eichmann A, Le Noble F, Autiero M, Carmeliet P: Guidance of vascular and neural network formation. *Curr Opin Neurobiol* 2005, 15(1):108-115.
204. Cao H, Liu T, Chew SY: The application of nanofibrous scaffolds in neural tissue engineering. *Adv Drug Deliv Rev* 2009, 61(12):1055-1064.
205. Arima Y, Iwata H: Effect of wettability and surface functional groups on protein adsorption and cell adhesion using well-defined mixed self-assembled monolayers. *Biomaterials* 2007, 28(20):3074-3082.
206. Solouk A, Cousins BG, Mirzadeh H, Solati-Hashtjin M, Najarian S, Seifalian AM: Surface modification of POSS-nanocomposite biomaterials using reactive oxygen plasma treatment for cardiovascular surgical implant applications. *Biotechnol Appl Biochem* 2011, 58(3):147-161.
207. Mehdiavaz R, Najarian S, Emami H: In vitro evaluation of biodegradable poly(E-caprolactone)-based blended nanofibrous scaffold for soft tissue engineering. *International Journal of Academic Research* 2011, 3(1):477-478.
208. Cai Q, Wang Y, Yang F, Shen H, Yang X, Wang S: Phase separation of polyphosphazene/poly(lactide-co-glycolide) blends prepared under different conditions. *Polymers for Advanced Technologies* 2010, :n/a-n/a.
209. Lee SJ, Khang G, Lee YM, Lee HB: Interaction of human chondrocytes and NIH/3T3 fibroblasts on chloric acid-treated biodegradable polymer surfaces. *J Biomater Sci Polym Ed* 2002, 13(2):197-212.
210. Rutkowski JM, Swartz MA: A driving force for change: interstitial flow as a morphoregulator. *Trends Cell Biol* 2007, 17(1):44-50.
211. Onizuka M, Flatebø T, Nicolaysen G: Lymph flow pattern in the intact thoracic duct in sheep. *J Physiol* 1997, 503 (Pt 1):223-234.
212. Rohn DA, Stewart RH, Elk JR, Laine GA, Drake RE: Renal lymphatic function following venous pressure elevation. *Lymphology* 1996, 29(2):67-75.
213. Scallan J, Huxley VH, Korhuis RJ: Granger ND, Granger J (Ed): *Capillary Fluid Exchange Regulation, Functions, and Pathology*. San Rafael (CA): Morgan & Claypool Life Sciences; 2010.

214. Truslow JG, Price GM, Tien J: Computational design of drainage systems for vascularized scaffolds. *Biomaterials* 2009, 30(26):4435-4443.
215. Wong KHK, Truslow JG, Khankhel AH, Chan KLS, Tien J: Artificial lymphatic drainage systems for vascularized microfluidic scaffolds. *Journal of Biomedical Materials Research Part A* 2012, :n/a-n/a.
216. Udelsman BV, Maxfield MW, Breuer CK: Tissue engineering of blood vessels in cardiovascular disease: moving towards clinical translation. *Heart* 2013, 99(7):454-460.
217. Slaughter BV, Khurshid SS, Fisher OZ, Khademhosseini A, Peppas NA: Hydrogels in regenerative medicine. *Advanced materials (Deerfield Beach, Fla.)* 2009, 21(32-33):3307-3329.
218. Nemen-Guanzon JG, Lee S, Berg JR, Jo YH, Yeo JE, Nam BM, Koh YG, Lee JI: Trends in Tissue Engineering for Blood Vessels. *Journal of Biomedicine and Biotechnology* 2012, 2012(6):1-14.
219. Park JE, Keller GA, Ferrara N: The vascular endothelial growth factor (VEGF) isoforms: differential deposition into the subepithelial extracellular matrix and bioactivity of extracellular matrix-bound VEGF. *Mol Biol Cell* 1993, 4(12):1317-1326.
220. Knop K, Hoogenboom R, Fischer D, Schubert US: Poly(ethylene glycol) in drug delivery: pros and cons as well as potential alternatives. *Angew Chem Int Ed Engl* 2010, 49(36):6288-6308.
221. Tiwari SK, Tzezana R, Zussman E, Venkatraman SS: Optimizing partition-controlled drug release from electrospun core-shell fibers. *Int J Pharm* 2010, 392(12):209-217.
222. Zhang H, Jia X, Han F, Zhao J, Zhao Y, Fan Y, Yuan X: Dual-delivery of VEGF and PDGF by double-layered electrospun membranes for blood vessel regeneration. *Biomaterials* 2013, 34(9):2202-2212.
223. Sorrell JM, Caplan AI: Fibroblasts-a diverse population at the center of it all. *International review of cell and molecular biology* 2009, 276:161-214.
224. Tibbitt MW, Anseth KS: Hydrogels as extracellular matrix mimics for 3D cell culture. *Biotechnol Bioeng* 2009, 103(4):655-663.

Annex

SOP Electrospinning

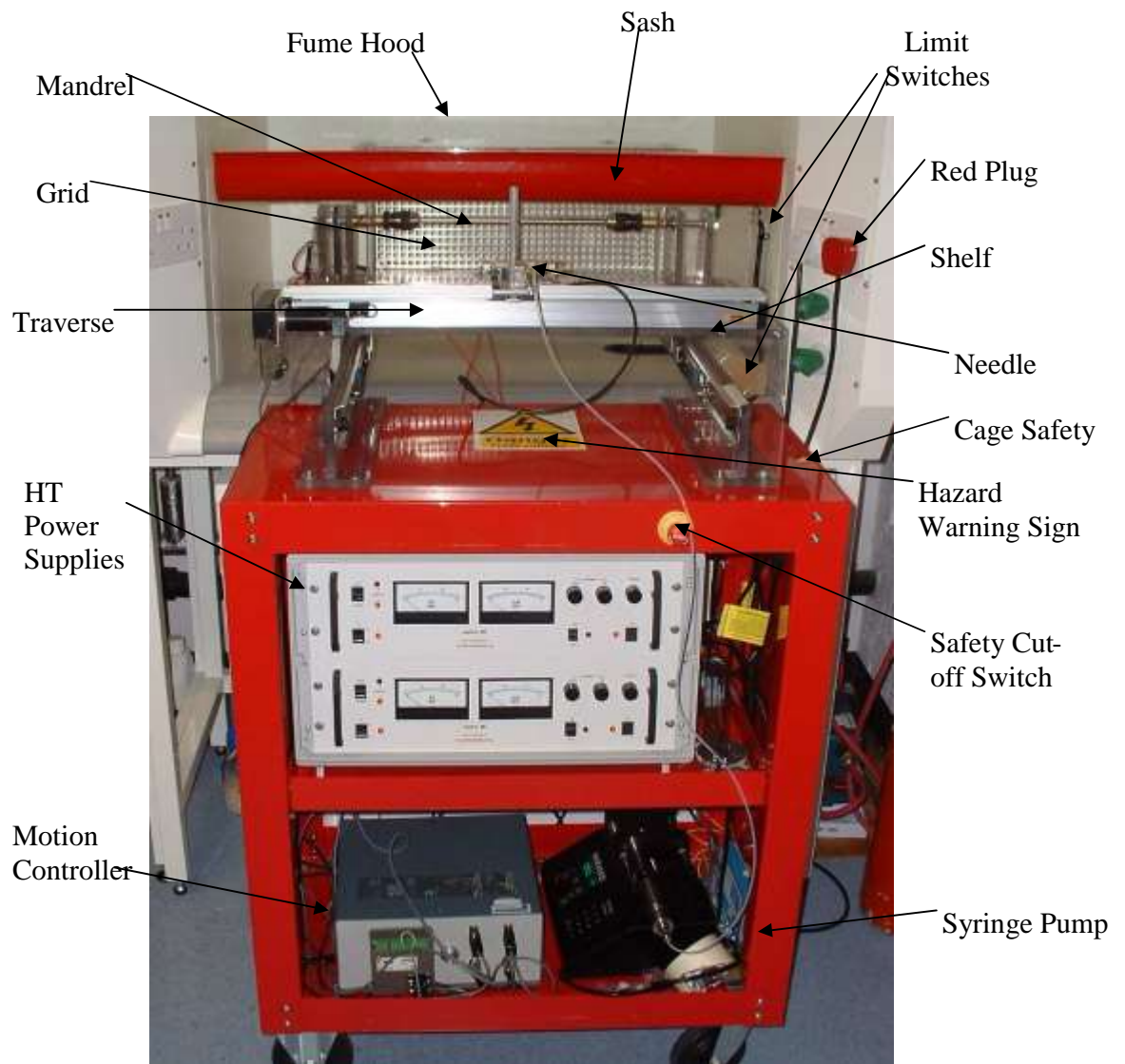
Electrostatic Polymer Spinning Apparatus

Instructions for Safe Operation in 'Local and Remote' Mode (Front Panel Operation)

Contents:

- 1) Brief description of apparatus (incl. labelled photograph)
- 2) Wiring diagram (HT circuit only)
- 3) Start-up and shutdown procedures (normal operation)

1) Description of Apparatus



This apparatus is used to create electrospun fibrous sheets from a polymer solution. Polymer in solution is delivered from a syringe pump through a tube and out of a needle. The polymer solution is drawn from the needle tip towards a charged target and the solvent evaporates during the travel. The needle and target part of the apparatus are housed in a fume cupboard to remove the evaporated solvent.

In the **default setup** the target consists of a rotating mandrel and the needle is mounted on a reciprocating traverse. This produces a polymer tube around the mandrel.

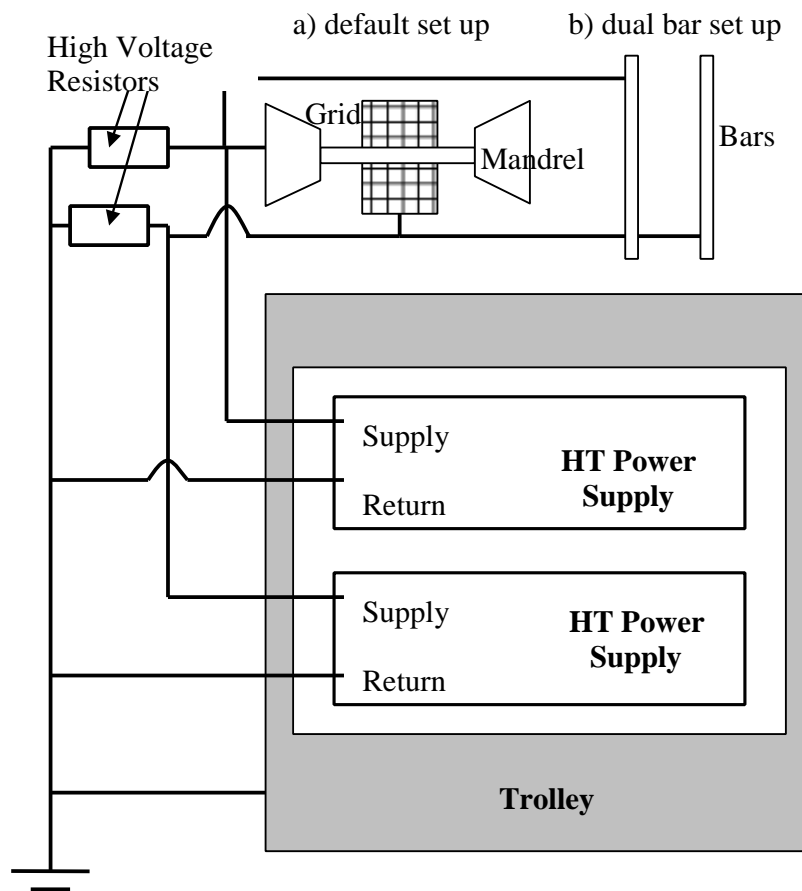
The mandrel and adjacent grid are charged by two separate high tension power supplies. Both of the supplies are connected to ground through a resistance to maintain a small current. This allows the supply to cut out in the event of an increase in current due to contact with any charged surfaces.

Mandrel and grid of the default set up has been dismantled and replaced with the dual bars which are wired in the same way. In the **dual bar set up** the target consists of two parallel bars and the needle is mounted above the centre of these two bars.

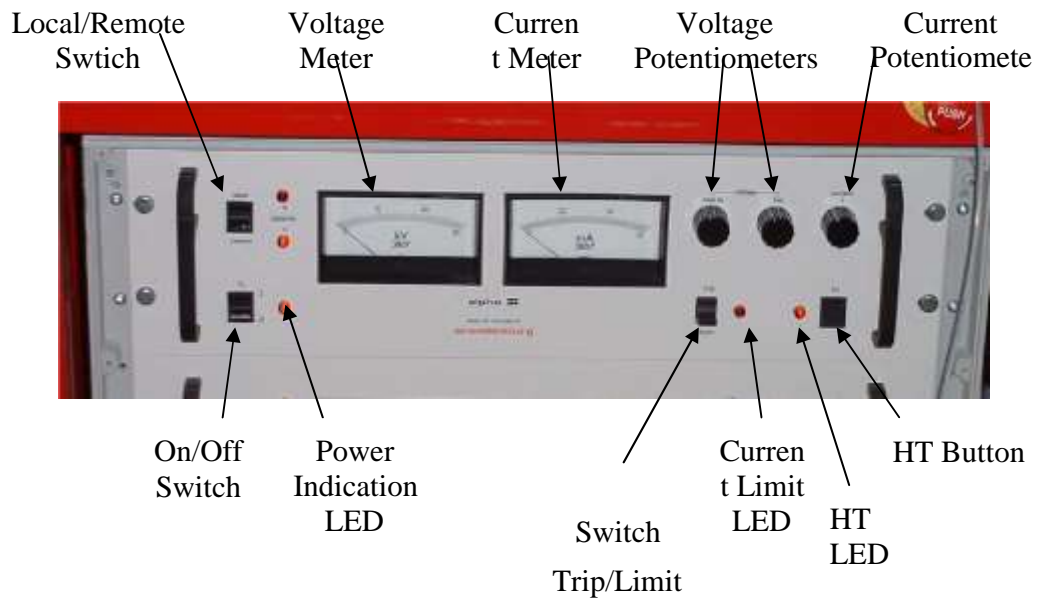
To prevent access to the charged surfaces the sash of the fume cupboard is lowered. Two safety switches are used to only allow power to be supplied to the system when the unit's shelf is fully extended into the fume cupboard and the sash is adequately lowered.

To prevent access to charged surfaces by random persons while the operator is not present, a safety cage is placed around the electrospinning rig holding down a third safety switch

2) Wiring Diagram



3a) Start-up Procedure



Preparation for computer assisted remote control (optional): Connect both power supplies with the LabView interface according to the manufactures description to operate in remote mode Preparation of trolley:

- remove all loose items from target area on top shelf
- position trolley in front of fume hood ensuring that cables do not snag
- Lift sash of fume hood and extend top shelf inside fume hood to full extent
- Lower sash so that it engages with and activates limit switch
- Connect needle with tubing to the polymer solution system

Ensure all potentiometers on front panel are rotated fully anticlockwise
Ensure power supply is in limit mode

Ensure that Local/Remote switch is in desired position either remote or local mode
Bridge safety cage limit switch (push the button down, or tape it down)

Switch on mains supply: electrical power on the trolley is supplied via a single distribution board connected to the mains (red-coloured plug)

Switch on power supply: switch on left of front panel

Activate HT output: push button on right of front panel, HT light will illuminate Only for local mode:

- Turn current potentiometer approximately $\frac{1}{2}$ turn clockwise
- Set desired voltage using voltage potentiometers
- Turn current potentiometer anticlockwise until current limit LED illuminates, then clockwise just enough for LED to go out Only for remote mode:
- Set desired values (e.g. voltage, current,...) via LabView program and run program

Switch unit from 'Limit' to 'Trip' Mode (Comment for remote mode: Depending on the LabView program switch unit to 'Limit' mode to avoid power trip during the experiment)

Only during 'Trip' mode the electrospinning trolley can be leaved unattended by placing the safety cage around it and enable the safety cage limit switch

During 'Limit' mode the operator has to be present at any time while the power supply is activated!

3b) Shut down procedure

Press HT button
Turn current and voltage potentiometers fully anticlockwise
Turn off power supply
Change from Trip to Limit mode

Emergency Shutdown:

Power to the trolley may be isolated by striking the yellow emergency shut-off button (see picture)



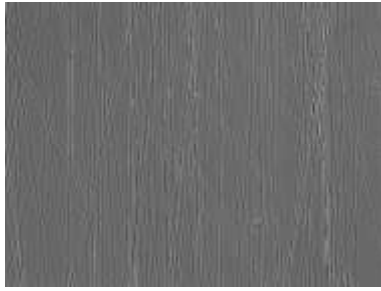
Good Working Practices:

Limit switches must not be defeated, when operator is not around
Target area must be kept clear of clutter
Safety warning signs must not be obscured
Cage safety switch and cage has to be in place when operator is not around

Appendices:

Responsible person:
Dr Richard Black, Senior Lecturer, Department of Bioengineering
Email: richard.black@strath.ac.uk;
Telephone: JA ext. 4568;

Polymer fibre alignment quantification



Original Microscope Image in xxx.tif format
Open image with ImageJ® or import stack of
images to process several images at the same time

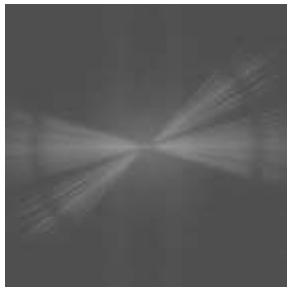


1036 pixel)

Image > Crop

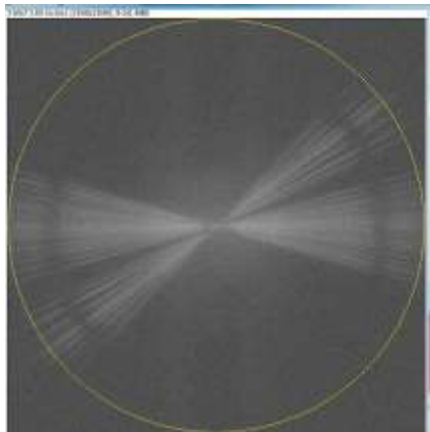
Crop Image with ImageJ® to 6.91 by
6.91 inches (1036 by

Use selection tool square and do it by
hand after selection



Fast Fourier Transformation Image with
ImageJ

Process > FFT > FFT

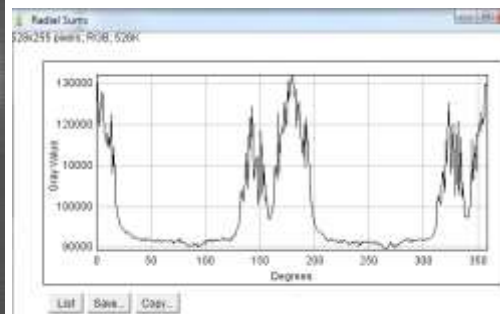
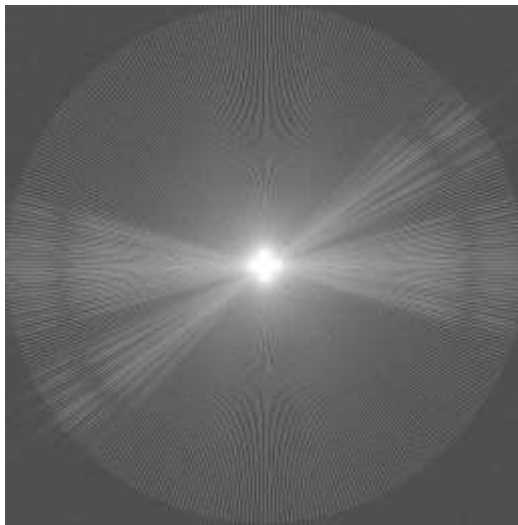
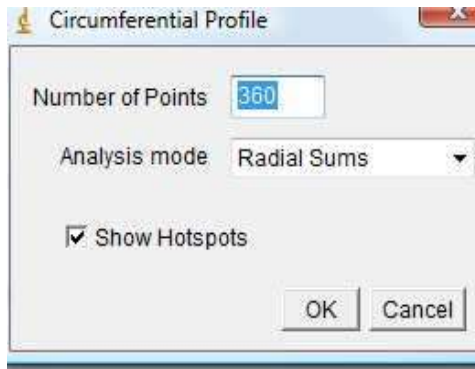


Draw a circle selection with the circular
selection tool over the whole area

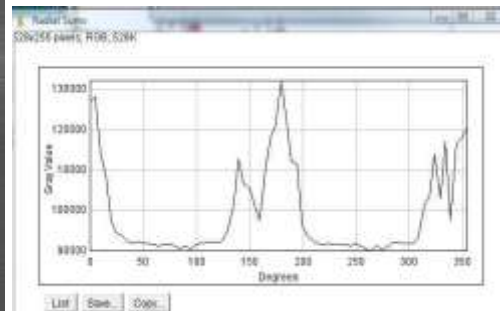
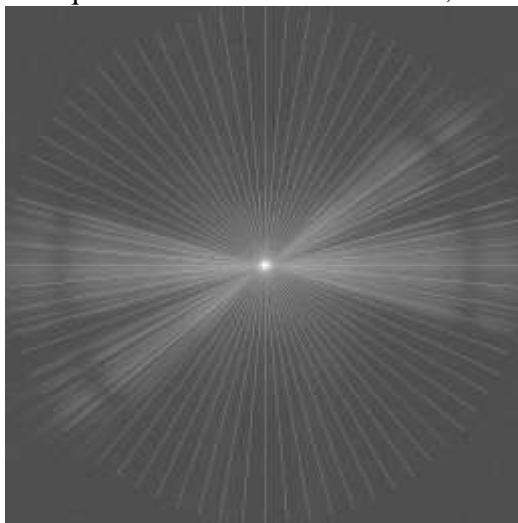
Analyse the pixel Intensity of the lines in
radial direction

Plug-in from OVAL PROFIL down loaded
from ImageJ plug-in

Plug-in > Analyse >Oval Profile > 360 or 72 points > Radial Sum



360° quantification with 1° intervals, 360 data points



360° quantification with 5° intervals, 72 data points

Select List and the graph and save the data in an excel sheet
Important note: The acquired graph and values is shifted by 90 degree.

Data evaluation are done with Microsoft Excel ®
(Fig.: Data evaluation with MS Excel with 72 data points from FFT image)

Table: Data evaluation with Excel with 72 data points from FFT image Intensity values are displayed at row 2, degree at row 1. Background (value at 90 degree) is subtracted in row 3. Negative values converted to zero (row 4). Percentage is calculated in row 5. Simplified values are displayed in row 7 and 9, only 50% or 25% of the total results are used to the alignment spectrum per image. In this example evaluation of only one image is shown. In general, simplified values are grouped together from a minimum of 5 images per electrospinning setting.

Degree	Pixel Intensity	Pixel Intensity		Intensity after normalization in percentage	Values simplified from -90 to 90 degree		Values simplified from -45 to 45 degree	
		- Background (value at 90 values degree)	Elimination of negative		degree	degree	degree	degree
				6.3%	-90	0.0%	-45	3.6%
0	128829	37649	37649	5.4%	-85	0.0%	-40	9.0%
5	123530.3828	32350.38281	32350.38281	4.2%	-80	0.2%	-35	5.9%
10	116191.7422	25011.74219	25011.74219	3.3%	-75	0.2%	-30	6.4%
15	111296.1172	20116.11719	20116.11719	1.2%	-70	0.2%	-25	3.2%
20	98305.28125	7125.28125	7125.28125	0.6%	-65	0.2%	-20	2.4%
25	94577.26563	3397.265625	3397.265625	0.3%	-60	0.2%	-15	5.1%
30	93240.35938	2060.359375	2060.359375	0.1%	-55	0.6%	-10	9.9%
35	91863.02344	683.0234375	683.0234375	0.1%	-50	1.3%	-5	12.1%
40	92056.49219	876.4921875	876.4921875	0.1%	-45	3.5%	0	13.5%
45	91789.78906	609.7890625	609.7890625	0.1%	-40	8.7%	5	10.3%
50	91945.17188	765.171875	765.171875	0.1%	-35	5.7%	10	7.5%
55	91767.80469	587.8046875	587.8046875	0.1%	-30	6.2%	15	7.9%
60	91889.14844	709.1484375	709.1484375	0.1%	-25	3.1%	20	1.5%
65	91543.02344	363.0234375	363.0234375	0.1%	-20	2.4%	25	0.7%
70	92042.32813	862.328125	862.328125	0.1%	-15	5.0%	30	0.6%
75	91542.83594	362.8359375	362.8359375	0.1%	-10	9.6%	35	0.2%
80	91441.07031	261.0703125	261.0703125	0.0%	-5	11.7%	40	0.1%
85	90705.17969	-474.8203125	0	0.0%	0	13.1%	45	0.1%
90	91180	0	0	0.0%	5	10.0%	SUM	100.0%
95	90382.60938	-797.390625	0	0.0%	10	7.3%		
100	91806.84375	626.84375	626.84375	0.0%	15	7.7%		
105	91734.17188	554.171875	554.171875	0.1%	20	1.4%		
110	91878.63281	698.6328125	698.6328125	0.1%	25	0.6%		
115	91684.13281	504.1328125	504.1328125	0.1%	30	0.6%		
120	91903.77344	723.7734375	723.7734375	0.1%	35	0.2%		
125	92958.14844	1778.148438	1778.148438	0.1%	40	0.1%		
130	95102.63281	3922.632813	3922.632813	0.1%	45	0.1%		
135	101595.7109	10415.71094	10415.71094	0.1%	50	0.1%		
140	116844.4844	25664.48438	25664.48438	0.3%	55	0.0%		
145	107912.1797	16732.17969	16732.17969	0.7%	60	0.0%		
150	109369.4844	18189.48438	18189.48438	1.7%	65	0.0%		
155	100274.6016	9094.601563	9094.601563	2.8%	70	0.1%		
160	98129.25781	6949.257813	6949.257813	3.0%	75	0.0%		
165	105839.7188	14659.71875	14659.71875	4.3%				
				1.5%				
				1.2%				
				2.4%				

170	119604.6563	28424.65625	28424.65625	4.7%	80	0.0%
175	125637.9766	34457.97656	34457.97656	5.7%	85	0.0%
180	129778	38598	38598	6.4%	90	0.0%
185	120647.3516	29467.35156	29467.35156	4.9%	SUM	100.0%
190	112624.1172	21444.11719	21444.11719	3.6%		
195	113901.1094	22721.10938	22721.10938	3.8%		
200	95458.78906	4278.789063	4278.789063	0.7%		
205	93098	1918	1918	0.3%		
210	92924.5625	1744.5625	1744.5625	0.3%		
215	91662.55469	482.5546875	482.5546875	0.1%		
220	91537.35156	357.3515625	357.3515625	0.1%		
225	91509.85938	329.859375	329.859375	0.1%		
230	91430.60156	250.6015625	250.6015625			
235	91074.58594	-105.4140625	0			
240	90774.73438	-405.265625	0			
245	90739.85938	-440.140625	0			
250	91333.10938	153.109375	153.109375			
255	90816.23438	-363.765625	0			
260	90243.41406	-936.5859375	0			
265	89378.64844	-1801.351563	0			
270	91011	-169	0	0.0%		
275	89585.45313	-1594.546875	0	0.0%		0.0%
				0.0%		
280	90833.57813	-346.421875	0	0.0%		0.0%
				0.0%		
285	91537.89844	357.8984375	357.8984375	0.0%		0.1%
				0.0%		
290	91266.19531	86.1953125	86.1953125	0.0%		0.0%
295	91363.91406	183.9140625	183.9140625	0.0%		
300	91752.20313	572.203125	572.203125	0.1%		
305	91804.82813	624.828125	624.828125	0.1%		
310	92615.48438	1435.484375	1435.484375	0.2%		
315	101400.9922	10220.99219	10220.99219	1.7%		
320	103309.1484	12129.14844	12129.14844	2.0%		
325	116614.2969	25434.29688	25434.29688	4.2%		
330	103649.6563	12469.65625	12469.65625	2.1%		
335	115780.7266	24600.72656	24600.72656	4.1%		
340	97072.02344	5892.023438	5892.023438	1.0%		
345	111919.1641	20739.16406	20739.16406	3.4%		
350	117605.7422	26425.74219	26425.74219	4.4%		
355	122366.5469	31186.54688	31186.54688	5.2%		
			SUM	100.0%		

Calculation of Decay / Half life of Cell populations

Nuclei are counted manually with Image J software from the acquired microscopic samples.

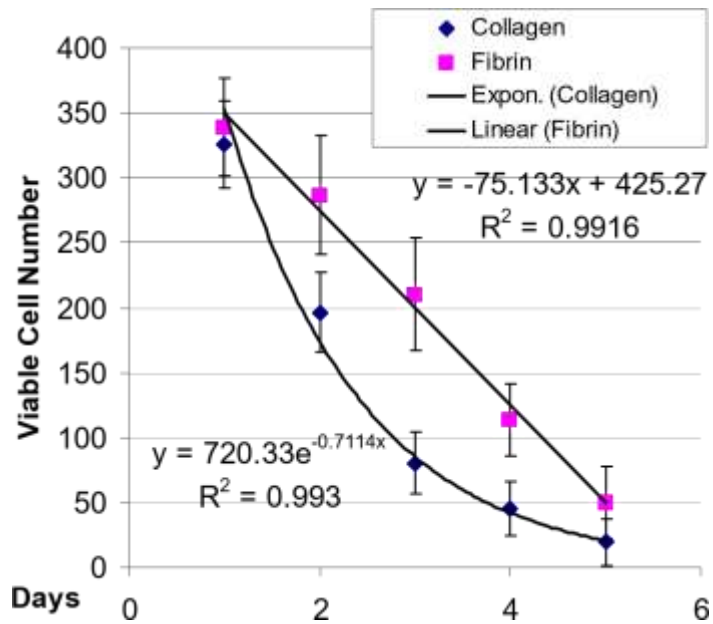
Table below shows the Cell counts over five days in two different conditions

- a) LECs coated with fibrin gels on TCP
- b) LECs coated with collagen gel type I on TCP

TCP	Cell counts				
Fibrin	Sample 1	Sample 2	Sample 3	Average	STD
Day 1	376	301	340	339	37.51
Day 2	332	240	288	286.6667	46.01449
Day 3	211	166	253	210	43.50862
Day 4	102	94	146	114	28
Day 5	40	28	81	49.66667	27.79089
Collagen	Sample 1	Sample 2	Sample 3	Average	STD
Day 1	350	287	340	325.6667	33.85754
Day 2	222	162	205	196.3333	30.92464
Day 3	82	56	103	80.33333	23.54428
Day 4	40	28	68	45.33333	20.52641
Day 5	0	23	35	19.33333	17.78576

Values are graphically displayed in an excel chart (see below) Apply a trend line (curve fit) with MS Excel ®.

Either a linear or exponential curve can be chosen. In general the exponential curve is selected. However, if the R^2 value is too low (<95) try a linear curve fit. Display the equations of the curve fit/ trend line.



Exponential Curve: To calculate the half life of the cell population the native Logarithms $\ln(2)$ is divided by exponential factor of the exponential curve equation. $\ln(2)/-0.7114 = \text{Day to half the population}$

Linear Curve: Calculate the Day 1 population from the linear equation (initial population) $x=1$. Divide the initial population by 2 (half population). Calculate from the linear equation the day to half the population $y = \text{half population}$ $x = \text{half life}$. Result is the difference between day 0 and starting day, here +1 for Day1.

Table below show the values and calculation for the half life from the previous equations (chart above)

Cell decay on TCP with Fibrin and Collagen hydrogels		
Collagen	(exponential approach)	
growth/ decay frequency		Half life of the Cell Population in days
-0.7114		-0.97434
Fibrin	(linear approach)	
Day 1	50% of population	Half life of the Cell Population in days
350	175	-2.33333